

15305

NATIONAL LIBRARY  
OTTAWA



BIBLIOTHÈQUE NATIONALE  
OTTAWA

NAME OF AUTHOR.... *John Donald Payzant*....  
 TITLE OF THESIS... *Studies... of... the... kinetics... and*  
*equilibria... of... selected... ion-...*  
*molecule... reactions.....*  
 UNIVERSITY..... *Alberta*.....  
 DEGREE FOR WHICH THESIS WAS PRESENTED... *Ph. D.*.....  
 YEAR THIS DEGREE GRANTED..... *1973*.....

Permission is hereby granted to THE NATIONAL LIBRARY  
 OF CANADA to microfilm this thesis and to lend or sell copies  
 of the film.

The author reserves other publication rights, and  
 neither the thesis nor extensive extracts from it may be  
 printed or otherwise reproduced without the author's  
 written permission.

(Signed) *John D. Payzant*

PERMANENT ADDRESS:

*55 Alexander St.,*  
*New Glasgow,*  
*Nova Scotia*

DATED *4 May* ..... 19 *73*

NL-91 (10-68)

THE UNIVERSITY OF ALBERTA

STUDIES OF THE KINETICS AND EQUILIBRIA OF  
SELECTED ION-MOLECULE REACTIONS

BY



JOHN DONALD PAYZANT

A THESIS

SUBMITTED TO THE FACULTY OF GRADUATE STUDIES AND RESEARCH  
IN PARTIAL FULFILMENT OF THE REQUIREMENTS FOR THE DEGREE

OF

DOCTOR OF PHILOSOPHY

DEPARTMENT OF CHEMISTRY

EDMONTON, ALBERTA

SPRING 1973

THE UNIVERSITY OF ALBERTA

FACULTY OF GRADUATE STUDIES AND RESEARCH

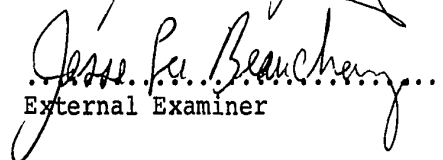
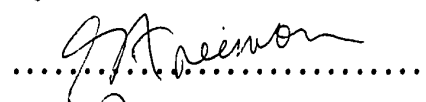
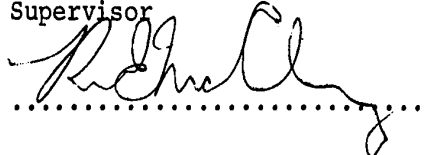
The undersigned certify that they have read, and recommend to the Faculty of Graduate Studies and Research for acceptance, a thesis entitled

"STUDIES OF THE KINETICS AND EQUILIBRIA OF  
SELECTED ION-MOLECULE REACTIONS"

submitted by JOHN DONALD PAYZANT in partial fulfilment of the requirements for the degree of Doctor of Philosophy.



.....  
Supervisor



.....  
External Examiner

Date *27 April 1973*.....

iv

TO MOTHER



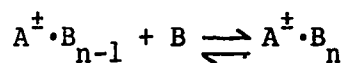
Even when I carry out *scientific work*, etc., an activity which I can seldom conduct in direct association with other men - I perform a *social*, because *human* act. It is not only the material of my activity - like the language itself which the thinker uses - which is given to me as a social product. My *own* existence *is* a social activity. For this reason, what I myself produce, I produce for society and with the consciousness of acting as a social being.

Karl Marx, Economic and Philosophical Manuscripts (1844).

A B S T R A C T

A pulsed high pressure mass spectrometer constructed for the measurement of the rate constants and equilibria of ion-molecule reactions at thermal energies is described. The mass spectrometer could be operated with ion source pressures up to 10 torr. High speed electrical circuits involving a multichannel scaler were constructed which permitted the observation of the temporal behaviour of the ions in the ion source. The instrument was applied to the study of ionic reactions which are believed to be of importance in the D region of the earth's ionosphere and also to the hydration of various ions in the gas phase. Both positive and negative ions were studied. The studies were conducted over the temperature range 90° - 850°K.

The study of the variation of the equilibrium constant with temperature in the reaction

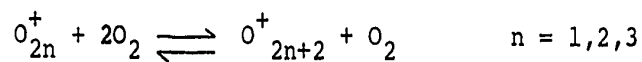


permitted the evaluation of  $\Delta G_{n-1,n}$ ,  $\Delta S_{n-1,n}$  and  $\Delta H_{n-1,n}$  for this reaction. Results are presented for the cases where  $A = N_2^+$ ,  $B = N_2$  and  $n = 1$ ;  $A = O_2^+$ ,  $B = O_2$  and  $n = 1, 2$ ;  $A = O_2^-$ ,  $B = CH_3OH$ , and  $n = 1, 2, 3$ ;  $A = NO_3^-$ ,  $B = H_2O$ , and  $n = 1$ ;  $A = NO_2^-$ ,  $B = H_2O$  and  $n = 1, 2, 3$ ; and  $A = H^+$ ,  $B = H_2O$  and  $n = 2, 3, 4$ . The thermodynamic parameters for the formation of the ions  $NH_4^+(NH_3)_n(H_2O)_w$ ,  $n + w = 1, 2, 3, 4$  are also presented along with estimates for the electron affin-

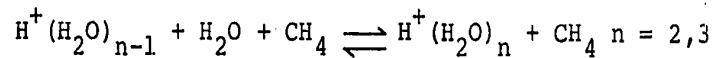
ities of  $\text{NO}_2$  and  $\text{NO}_3$ .

The kinetics of the attachment of water to  $\text{NO}_2^-$ ,  $\text{NO}_3^-$  and  $\text{H}_3\text{O}^+$  were also studied as well as the negative ion-molecule reactions occurring in moist oxygen.

The temperature dependence of the forward rate of the reactions



and



was studied. It was found that the temperature dependence of the forward rate constant could be expressed in the form  $k_f \propto T^{-n}$  where  $n$  is from 3.2 to 5.1 depending on the reaction.

A C K N O W L E D G E M E N T S

I wish to express my sincere appreciation to Prof. P. Kebarle for his advice and encouragement throughout the course of this work.

The projects described in Chapters 5, 8, 9 and 10 were done in collaboration with Dr. A. J. Cunningham who contributed approximately half of the material contained therein.

The author would like to thank the members of the Chemistry Department Machine Shop. Special thanks are due to Mr. H. Hoffman for his skill in constructing the low temperature ion source and for his ability to repair the author's blunders. The assistance of the members of the Chemistry Department Electronics Shop is acknowledged. Mr. R. Kadlec and Mr. T. Nord greatly assisted the author in the design and maintenance of the electronics of the apparatus.

The author wishes to thank Mrs. M. Waters for her care in typing the manuscript and her patience in reading the author's writing.

The assistance of other members of the mass spectrometry group, in particular Dr. R. Yamdagni, is gratefully acknowledged.

The financial assistance provided by the University of Alberta and the National Research Council of Canada is acknowledged.

T A B L E O F C O N T E N T S

	<u>Page</u>
ABSTRACT . . . . .	vi
ACKNOWLEDGEMENTS . . . . .	viii
LIST OF TABLES . . . . .	xiv
LIST OF FIGURES . . . . .	xvii
I Introduction . . . . .	1
1.1 Types of Ion-Molecule Reactions . . . . .	1
1.2 Progress of Ion-Molecule Reaction Studies . . . . .	5
A Studies at Low Pressures . . . . .	5
B Other Studies at High Pressures . . . . .	11
a High Pressure Mass Spectrometry . . . . .	11
b Chemical Ionization . . . . .	12
c Flowing Afterglow . . . . .	12
d Stationary Afterglow . . . . .	13
e Ion Drift Tube Experiments . . . . .	14
1.3 The Present Study . . . . .	15
1.4 Ion Chemistry of the D Region . . . . .	16
1.5 Ion-Solvent Interactions. . . . .	19
II Experimental. . . . .	23
2.1 Requirements of the Apparatus . . . . .	23
2.2 Improvements in the Present Apparatus . . . . .	24
2.3 Vacuum Chamber. . . . .	25
2.4 Gas Handling System . . . . .	28
2.5 High Temperature Ion Source . . . . .	31

	<u>Page</u>
2.6 Low Temperature Ion Source . . . . .	34
2.7 The Electron Gun and the Pulsing Circuitry	34
2.8 Time of Flight . . . . .	41
2.9 Physical Conditions in the Ion Source . .	43
A Number of Collisions of the Ions. . . .	43
B Ion Sampling. . . . .	44
C Charged Particle Recombination . . . .	45
D Temporal Behaviour of the Ions. . . . .	47
2.10 Normalization of the Data. . . . .	56
2.11 Determination of Thermodynamic Parameters from the Equilibrium Constants . . . . .	57
III The Clustering Equilibrium $N_2^+ + 2N_2 \rightleftharpoons N_4^+ + N_2$ and the Bond Dissociation Energy of $N_4^+$ . . . . .	59
3.1 Previous work on $N_4^+$ . . . . .	59
3.2 Method of Measurement . . . . .	60
3.3 Materials Used . . . . .	61
3.4 Results and Discussion . . . . .	61
IV Kinetics of Reactions Leading to $O_2^-(H_2O)_n$ in Moist Oxygen . . . . .	68
4.1 Introduction . . . . .	68
4.2 Experimental . . . . .	68
4.3 Results and Discussion . . . . .	75
A Ion Production . . . . .	75

	<u>Page</u>
B Reactions Leading to $O_2^-(H_2O)_n$ in Moist Oxygen . . . . .	76
C Determination of $k_1$ , $k_2$ and $k_{-1}$ . . .	99
D Computer Calculation of $k_3$ to $k_5$ . . .	102
4.4 The Reaction $O^- + 2O_2 \rightarrow O_3^- + O_2$ . . . .	112
V Kinetics and Rate Constants Leading to Hydration of $NO_2^-$ and $NO_3^-$ . . . . .	120
5.1 Introduction. . . . .	120
5.2 Experimental. . . . .	120
A Production of Ions . . . . .	120
B Measurement of Water Pressure. . . . .	127
5.3 Results and Discussion. . . . .	128
VI The Thermodynamics of the Hydration of $NO_2^-$ and $NO_3^-$ . . . . .	157
6.1 Introduction . . . . .	157
6.2 Experimental . . . . .	158
6.3 Results and Discussion . . . . .	160
A Calculation of Total Single Ion Heats of Hydration . . . . .	160
B Determination of $EA(NO_2)$ and $EA(NO_3)$ . . . .	164
VII Solvation of $O_2^-$ and $Cl^-$ with $H_2O$ , $CH_3OH$ and $CH_3CN$ . . . . .	172
7.1 Introduction . . . . .	172
7.2 Experimental Results . . . . .	172
7.3 Discussion of Results . . . . .	173

	<u>Page</u>
VIII The Competitive Solvation of $\text{NH}_4^+$ by $\text{H}_2\text{O}$	
and $\text{NH}_3$ . . . . .	185
8.1 Introduction . . . . .	185
8.2 Experimental Results . . . . .	186
A Pure Ammonia. . . . .	186
B The Ammonia-Water System . . . . .	187
C The Competitive Solvation of $\text{NH}_4^+$ by	
Water and Ammonia . . . . .	191
8.3 Discussion of Results. . . . .	197
A The $\text{NH}_4^+(\text{NH}_3)_n$ and $\text{NH}_4^+(\text{H}_2\text{O})_n$ Systems	197
B The Mixed Clusters $\text{NH}_4^+(\text{H}_2\text{O})_w(\text{NH}_3)_n$ . .	204
IV The Proton Hydrates . . . . .	208
9.1 Introduction . . . . .	208
9.2 Experimental Method . . . . .	210
9.3 Ion Production and Data Analysis . . . . .	211
9.4 Experimental Results . . . . .	213
A Kinetic Measurements . . . . .	213
B Equilibria Measurements . . . . .	235
C Temperature Dependence of Diffusion . .	243
D Temperature Measurement . . . . .	244
E Effect of Repeller. . . . .	246
9.5 Discussion of Results. . . . .	251



	<u>Page</u>
X The Temperature Dependence of Selected Termolecular Reactions . . . . .	260
10.1 Introduction . . . . .	260
10.2 Experiments in Oxygen . . . . .	264
10.3 Experiments in Argon . . . . .	266
10.4 Results and Discussion . . . . .	269
REFERENCES . . . . .	297
APPENDIX I . . . . .	309
APPENDIX II . . . . .	313

---

L I S T O F T A B L E S

<u>Table</u>	<u>Page</u>
2.1 Typical Operating Voltages	36
3.1 Thermodynamic Parameters for the Reaction $N_2^+ + 2N_2 \rightleftharpoons N_4^+ + N_2$	65
4.1 Calculated Values of Rate Coefficients for Reactions Leading to $O_2^-(H_2O)_n$ in Moist Oxygen	94
4.2 Rate Constants Leading to $O_2^-(H_2O)_n$ in Moist Oxygen	95
4.3 Measured Rate Coefficients for the Reaction $O^- + 2O_2 \longrightarrow O_3^- + O_2$	116
5.1 Selected Thermodynamic Data	123
5.2 Rate Constants of Reactions Leading to $NO_x^-(H_2O)_n$	139
5.3 Comparison of Apparent First Order Rate Coefficients for $NO_2^- + H_2O + O_2 \rightarrow NO_2^- \cdot H_2O +$ $O_2$ Calculated by Graphical and Computer Methods	142
5.4 Rate Constants for $NO_2^- + H_2O + M \rightarrow NO_2^- \cdot H_2O +$ M	146
5.5 Summary of Kinetic Data	147
5.6 Equilibrium Constants for $NO_2^-(H_2O)_{1,2}$ and $NO_3^- \cdot H_2O$	154

<u>Table</u>	<u>Page</u>
6.1 Thermodynamic Values for the Hydration of $\text{NO}_2^-$ and $\text{NO}_3^-$	162
6.2 Total and Partial Enthalpies of Hydration of some Single Negative Ions	163
6.3 Heats of Hydration	165
6.4 Electron Affinities of $\text{NO}_2$ and $\text{NO}_3$	169
7.1 Thermodynamic Data for the Reaction $\text{A}^-\cdot\text{B}_{n-1} + \text{B} \rightleftharpoons \text{A}^-\cdot\text{B}_n$	178
8.1 Thermodynamic Values for the Reactions $\text{NH}_4^+(\text{NH}_3)_{n-1} + \text{NH}_3 \rightleftharpoons \text{NH}_4^+(\text{NH}_3)_n$	190
8.2 Thermodynamic Values for the Reactions $\text{NH}_4^+(\text{H}_2\text{O})_{n-1} + \text{H}_2\text{O} \rightleftharpoons \text{NH}_4^+(\text{H}_2\text{O})_n$	194
8.3 Thermodynamic Parameters for the Addition of Successive Ligands to $\text{NH}_4^+$	200
9.1 Rate Constants of Reactions Leading to $\text{H}^+(\text{H}_2\text{O})_n$	216
9.2 Temperature Dependence of the Proton Hydration Reactions $\text{H}^+(\text{H}_2\text{O})_{n-1} + \text{H}_2\text{O} + \text{CH}_4 \rightleftharpoons$ $\text{H}^+(\text{H}_2\text{O})_n + \text{CH}_4$	232
9.3 Thermochemical Data for $\text{H}^+(\text{H}_2\text{O})_{n-1} + \text{H}_2\text{O} \rightleftharpoons$ $\text{H}^+(\text{H}_2\text{O})_n$ Equilibria	242
10.1 Calculated Values of Rate Coefficients for Positive Ion-Molecule Reactions in Pure Oxygen	284

<u>Table</u>		<u>Page</u>
10.2	The Temperature Dependence of $k_f$ for Selected Ion-Molecule Reactions	295

---

LIST OF FIGURES

<u>Figure</u>	<u>Page</u>
2.1 Schematic Diagram of Apparatus	27
2.2 Schematic Diagram of Gas Flow System	30
2.3 Block Schematic of Experimental Apparatus	37
2.4 Time Dependence of Total Ionization of and 2.5 Positive and Negative Ions	48-49
3.1 Plot of the Equilibrium Constant K for the Reaction $N_2^+ + N_2 \rightleftharpoons N_4^+$ as a Function of Nitrogen Pressure	62
3.2 van't Hoff Plots of the Data of Figure (3.1) for the Reaction $N_2^+ + N_2 \rightleftharpoons N_4^+$	64
4.1 Determination of the Value of the Equilibrium Constant $K_{2,3}$ for the Reaction $O_2^-(H_2O)_2 +$ $H_2O \rightleftharpoons O_2(H_2O)_3$ at 300.5°K	73
4.2 to 4.18 Time Dependence of Normalized Ion Intensities	77-93
4.19 Plots of $\log[O_2^-]$ <u>versus</u> Time	98
4.20 Plot of $v_T/[O_2][H_2O]$ <u>versus</u> $[O_2]/[H_2O]$	101
4.21 Plot of $v_4/[H_2O]$ <u>versus</u> $P_{O_2}$	105
4.22 Plot of $v_{-4}/[H_2O]$ <u>versus</u> $P_{O_2}$	106
4.23 Plots of the Apparent Rate of $O_2^-(H_2O)_2 +$ $H_2O + O_2 \rightleftharpoons O_2(H_2O)_3 + O_2$	107
4.24 Logarithmic Plots of the Decay of the Nor- malized $O^-$ Intensity with Time	113

<u>Figure</u>	<u>Page</u>
4.25 Plot of $v_6 = k_6 [O_2]^n$ <u>versus</u> the Square of the Oxygen Pressure for the Data of Figure (4.24)	115
4.26 Plots of Normalized $O^-$ Ion Intensities <u>versus</u> Time for Various Conditions	117
4.27 Arrhenius Type Plot of the Rate of the Reaction $O^- + 2O_2 \rightarrow O_3^- + O_2$	118
5.1 to 5.10 Time Dependence of Normalized Ion Intensities	129-138
5.11 Logarithmic Plots of Normalized $I_{NO_2^-}$ $I_{NO_2^-}$ (eq) <u>versus</u> Time	141
5.12 Dependence of $v_1/[H_2O]$ on $P_M$	143
5.13 Dependence of $v_2/[H_2O]$ on $P_{O_2}$	144
5.14 Dependence of $v_{-1}$ on $P_{O_2}$	148
5.15 Dependence of $v_{-2}$ on $P_{O_2}$	149
5.16 Logarithmic Plots of Normalized $I_{NO_3^-}$ $I_{NO_3^-}$ (eq) <u>versus</u> Time	151
5.17 Dependence of $v_3/[H_2O]$ on $P_{O_2}$	152
5.18 Dependence of $v_{-3}$ on $P_{O_2}$	153
6.1 Time Dependence of $NO_2^-$ and $NO_2^- \cdot H_2O$ Escaping from the Ion Source	159
6.2 van't Hoff Plots of Equilibrium Constants $K_{n-1,n}$ for Reactions $A^-(H_2O)_{n-1} + H_2O \rightleftharpoons$ $A^-(H_2O)_n$	161

<u>Figure</u>	<u>Page</u>
6.3 Plot of Heat of Hydration for Negative Ions $A^-$ <u>versus</u> $-\Delta H_{0,1}$	166
6.4 Plot of $\Delta H_{0,1}$ for the Reaction $A^- + H_2O \rightarrow A^- \cdot H_2O$ <u>versus</u> the Heterolytic Bond Dissociation Energy	168
6.5 Plot of $\Delta H(OH^-,HX)$ for the Reaction $OH^- + HX \rightarrow OH^- \cdot HX$ <u>versus</u> the Heterolytic Bond Dissociation Energy	171
7.1 Plot of the Equilibrium Constant $K_{0,1}$ for the Reaction $O_2^- + CH_3OH \rightleftharpoons O_2^- \cdot CH_3OH$ as a Function of the Partial Pressure of Methanol	174
7.2 Plot of the Equilibrium Constant $K_{1,2}$ for the Reaction $O_2^- \cdot CH_3OH + CH_3OH \rightleftharpoons O_2^- (CH_3OH)_2$ as a Function of the Partial Pressure of Methanol	175
7.3 Plot of the Equilibrium Constant $K_{2,3}$ for the Reaction $O_2^- (CH_3OH)_2 + CH_3OH \rightleftharpoons O_2^- (CH_3OH)_3$ as a Function of the Partial Pressure of Methanol	176
7.4 van't Hoff Plot of the Data of Figures (7.1-7.3) for the Reaction $O_2^- (CH_3OH)_{n-1} + CH_3OH \rightleftharpoons O_2^- (CH_3OH)_n$	177

<u>Figure</u>	<u>Page</u>	
7.5	Plot of $-\Delta H_{n-1,n}$ <u>versus</u> $n-1,n$ for the Reaction $A^{\cdot}B_{n-1} + B \rightleftharpoons A^{\cdot}B_n$	181
8.1	Equilibrium Constant $K_{0,1}$ for the Reaction $NH_4^+ + NH_3 \rightleftharpoons NH_4^+ \cdot NH_3$ at Several Tempera- tures Plotted <u>versus</u> Ammonia Pressure	188
8.2	van't Hoff plots of Equilibrium Constants $K_{n-1,n}$ for the $NH_4^+(NH_3)_{n-1} + NH_3 \rightleftharpoons$ $NH_4^+(NH_3)_n$	189
8.3	Equilibrium Constant $K_{0,1}$ for the Reaction $NH_4^+ + H_2O \rightleftharpoons NH_4^+ \cdot H_2O$ at Several Tempera- tures Plotted <u>versus</u> the Water Pressure	192
8.4	van't Hoff Plots of the Equilibrium Constants $K_{n-1,n}$ for the $NH_4^+(H_2O)_{n-1} + H_2O \rightleftharpoons$ $NH_4^+(H_2O)_n$ Equilibria	193
8.5	van't Hoff Plots of Equilibrium Constants for the Formation of $NH_4^+(NH_3)_n(H_2O)_w$ where $n + w = 2$	196
8.6	van't Hoff Plots of Equilibrium Constants for the formation of $NH_4^+(NH_3)_n(H_2O)_w$ where $n + w = 3$	198
8.8	$-\Delta H$ Values (kcal/mole) for the Addition of Successive Ligands to $NH_4^+$	205



<u>Figure</u>	<u>Page</u>
9.1 Time Dependence of Ion Counts as Observed with the Multiscaler	214
9.2 Results of Figure (9.1) but Presented as Percent Total Ionization	215
9.3 to 9.13 Time Dependence of Normalized Ion Intensities	217-227
9.14 Logarithmic Plots of Normalized $\text{H}_3\text{O}^+$ Inten- sity with Time	228
9.15 Dependence of Apparent First Order Rate Constant $v_1 = k_1[\text{H}_2\text{O}][\text{CH}_4]$ on Water Con- centration	229
9.16 Dependence of the $v_1/[\text{CH}_4]$ on $[\text{H}_2\text{O}]$	230
9.17 Dependence of $v_1/[\text{CH}_4]$ on $[\text{H}_2\text{O}]$	231
9.18 Temperature Dependence of Third Order Rate Constant $k_1$ for the Reaction $\text{H}_3\text{O}^+ + \text{H}_2\text{O} + \text{M}$ $\text{H}^+(\text{H}_2\text{O})_2 + \text{M}$	234
9.19 Time Dependence of Ion Counts with Rapid Achievement of $\text{H}_3\text{O}^+ + \text{H}_2\text{O} \rightleftharpoons \text{H}^+(\text{H}_2\text{O})_2$ Equilibrium	236
9.20 Time Dependence of Normalized Ion Inten- sities	237
9.21 Equilibrium Constant $K_{0,1}$ for the Reaction $\text{H}_3\text{O}^+ + \text{H}_2\text{O} \rightleftharpoons \text{H}^+(\text{H}_2\text{O})_2$ at several tem- peratures <u>versus</u> Water Pressure	239
9.22 van't Hoff Plots for the Reaction $\text{H}^+(\text{H}_2\text{O})_{n-1} +$ $\text{H}_2\text{O} \rightleftharpoons \text{H}^+(\text{H}_2\text{O})_n$	241

<u>Figure</u>	<u>Page</u>
9.23 Effect on the Equilibrium Constant $K_{1,2}$ of Varying the Temperature of Portions of the Ion Source	245
9.24 Effect of Repeller Voltage on the Temporal Behavior of the Ion Signal	247
9.25 Relative Concentrations of Proton Hydrates as a Function of Repeller Voltage	249
9.26 Relative Concentrations of Proton Hydrates as a Function of Repeller Voltage	250
9.27 Time Dependence of Ion Counts Observed with Multiscaler	252
9.28 Comparison of van't Hoff Plots from Present Work with those Obtained by Field	253
10.1 to 10.13 Time Dependence of Normalized Ion Intensities	271-283
10.14 to 10.16 Plot of the Normalized $O_2^+$ Intensity <u>versus</u> Time	286-288
10.17 Plot of $v$ <u>versus</u> the Square of the Oxygen Pressure	289
10.18 van't Hoff Plot for the Reactions $O_{2n}^+ + O_2 \rightleftharpoons$ $O_{2n+2}^+$	292
10.19 Plot of the Log of the Third Order Rate Constant <u>versus</u> the Log of Temperature	294

<u>Figure</u>		<u>Page</u>
A1.1	Analogue Computer Programme	310
A1.2	Analogue Computer Programme	312

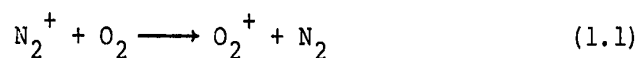
---

I N T R O D U C T I O N

This study was directed toward the examination of the kinetics and thermodynamics of selected ion-molecule reactions in gases at pressures in the torr range. Reactions were investigated over the temperature range 85° to 850°K. The temporal behaviour of the ions in the ion source of a mass spectrometer was measured with the aid of a pulsing technique involving a multichannel scaler. The present method permits the rapid evaluation of the rates of ion-molecule reactions and the measurement of ionic equilibria.

1.1 Types of Ion-Molecule Reactions

Perhaps the simplest of ion-molecule reactions is charge transfer. For example the reaction



proceeds rapidly with a rate of  $1.1 \times 10^{-10} \text{ cm}^3 \text{ molecule}^{-1} \text{ s}^{-1}$ . The reaction is exothermic by the difference in the ionization potentials of nitrogen and oxygen.

$$-\Delta H = I_p(\text{N}_2) - I_p(\text{O}_2) = 15.6 - 12.0 = 3.6 \text{ eV} \quad (1.2)$$

In general if a bimolecular ion-molecule reaction is exothermic then the reaction proceeds at the collision frequency (1). Exceptions may be found for complex re-

2.

actions in which extensive rearrangements of atoms in the colliding species may be involved. Bimolecular reactions usually proceed with large ( $\sim 10^{20} \text{A}^2$ ) cross sections (1). In 1958 Giomousis and Stevenson (2) proposed a theory to explain these exceptionally large cross sections. In the theory the attractive forces between the colliding particles are visualized as being electrostatic in nature. As the colliding particles approach each other, a dipole moment is induced in the neutral by the electric field of the ion (this may add to any contribution from a permanent dipole moment) drawing the particles together. This attractive force becomes significant (i.e.  $\sim kT$ ) at intermolecular separation in the order of several angstroms. At these distances van der Waals' repulsive forces due to the interaction of the electron clouds of the particles in question are negligible. Giomousis and Stevenson (2) were able to show that the rate coefficient for the reaction,  $k$ , could be expressed in the form

$$k = 2\pi e \left(\frac{\alpha}{\mu}\right)^{\frac{1}{2}} \quad (1.3)$$

where  $e$  is the electronic charge,  $\alpha$  the polarizability of the neutral and  $\mu$  the reduced mass of the system. Since the cross section  $Q$  is given by

$$Q = k/v \quad (1.4)$$

where  $v$  is the velocity of approach of the particles it

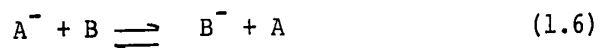
3.

follows that

$$Q = \frac{2\pi e}{v} \left( \frac{\alpha}{\mu} \right)^{\frac{1}{2}} \quad (1.5)$$

This expression predicts the observed large cross sections. Furthermore the theory predicts that  $Q$  will be independent of temperature for moderate temperatures. Thus reactions such as (1.1) proceed without any activation energy. This prediction has been largely confirmed by experimental observation (3).

The corresponding charge transfer reaction with a negative ion would be



the direction of this reaction being determined by the relative electron affinities of A and B.

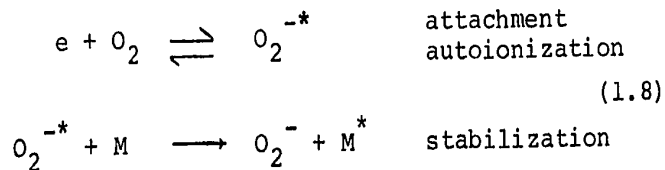
Negative ions may be produced by electron capture, electron attachment or pair production. In an electron capture reaction the neutral molecule encounters an electron which may have thermal or greater kinetic energy. The molecule then dissociates to form an ion and a neutral fragment.



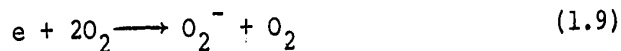
The electron attachment process is where the electron is captured by the molecule, and the resulting excited ion may either autoionize or be collisionally stabilized. The

4.

fragmentation process (1.7) not being favoured in this case.

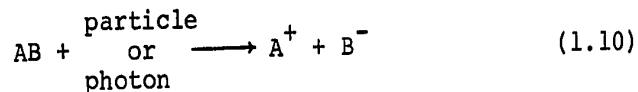


An example of this is the attachment of the electron to  $O_2$

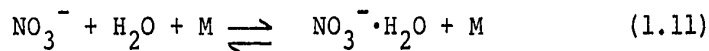


which proceeds at a rate of  $2.0 \pm 0.2 \times 10^{-30} \text{ cm}^6 \text{ molecule}^{-2} \text{ s}^{-1}$  (4).

Negative ions may also be produced by the interaction of an energetic particle or photon with the appropriate neutral in a "pair production" process. This is when both a negative ion and a positive ion are produced.

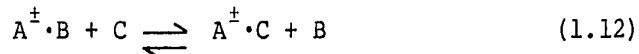


The reactions mentioned above may all be regarded as primary reactions in the sense that they produce only simple ions from neutrals. More complex reactions may occur between ions and neutrals. One example is the condensation or attachment reaction. This type of reaction is similar to the electron attachment reaction (1.8). An example of an attachment reaction is the clustering of water about  $NO_3^-$  to form  $NO_3^- \cdot H_2O$

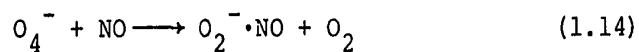
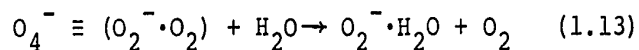


where M is a stabilizing third body.

Another type of ion-molecule reaction involves the exchange of a molecule attached to the ion for another neutral molecule. Such reactions have been called "switching" reactions (5)



These reactions are in general fast proceeding at near the Langevin orbiting limit (15) in the preferred direction. Whether this reaction proceeds from left to right in (1.11) or vice versa depends on the free energy change involved. Examples of switching reactions are



## 1.2 Progress of Ion-Molecule Reaction Studies

### A Studies at Low Pressure

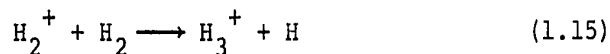
In the conventional analytical mass spectrometer, the ion source and in particular the mass analysis sections of the instrument are maintained at as low a pressure as possible. This is done so that the probability of an ion striking a neutral gas molecule, either in the ion source or during mass analysis is reduced to a minimum. If the



6.

pressure in the ion source is raised, the primary ions produced by electron bombardment may undergo reactive collisions with the neutral gas in the chamber. This represents a serious problem in the determination of isotopic abundances and is undesirable in qualitative analysis studies.

Early in this century J. J. Thompson (6) described the first mass spectrometer and reported the observation of an ion of  $m/e = 3$  as a product from an electrical discharge in hydrogen. Dempster (7) repeated this observation and showed the ion to be  $H_3^+$ . The presence of this ion was later explained (8,9) as coming from the reaction



Research with mass spectrometers at this time was largely devoted to the study of isotopic abundances and processes such as (1.15) were regarded as undesirable. Improved vacuum technology and increased ion current detection capabilities eliminated the difficulty.

It was not until several decades later in the early 1950's that systematic studies of ion-molecule reactions were undertaken. Tal'rose and Lyubimova (10), Stevenson and Schissler (11,12) and Gutbier (13) were early workers in the field. The technique involved raising the pressure in the ion source of a mass spectrometer of conventional design to  $10^{-3}$  to  $10^{-4}$  torr. At these pressures a small

fraction of the primary ions will undergo collisions with the neutral gas to produce secondary ions. From the study of the quantity of secondary ions produced as a function of ion source pressure, cross sections for ion molecule reactions could be deduced (1).

The early work in the study of ion-molecule reactions involved the use of an ion source which had a small but constant electric field gradient across it, designed to repel ions into the mass analysis section of the instrument. In order to calculate the cross section and subsequently the rate constant for an ion-molecule reaction assumptions were made concerning the translational energy dependence of the cross section (1). The Gimousis-Stevenson equation (1.3) may be extended to

$$Q = \frac{2\pi e}{v} \left( \frac{\alpha}{\mu} \right)^{\frac{1}{2}} = 2\pi e \left( \frac{2\alpha m_p}{\mu e E_r l} \right)^{\frac{1}{2}} \quad (1.16)$$

where  $m_p$  is the mass of the primary ion,  $l$  is total path length of the ion and  $E_r$  is the voltage of the repeller electrode. The above expression is valid for many simple reactions, however several examples were found where the  $Q \propto E_r^{-\frac{1}{2}}$  relationship was not obeyed (1).

The difficulty of determining the energy dependence of the cross section and therefore the rate constant was overcome by using a pulsing technique in which the ions react under field free conditions. The method consisted of switching the electron beam in the ion source on for a

8.

brief period of time ( $\sim 10^{-7}$  sec) after which the ion source was maintained under equipotential conditions. After a variable but known delay time a brief pulse was applied to the repeller electrode to expel the ions from the ion source. Tal'rose (14,15) showed that

$$\frac{I_s}{I_p} = kn t_d + f(t_e, t_r) \quad (1.17)$$

where  $I_s/I_p$  is the ratio of secondary to primary ions,  $k$  is the rate constant,  $n$  is the number density of neutrals,  $t_d$  is the delay time and  $f(t_e, t_r)$  is a function of the time the electron beam is on  $t_e$ , and the width of the repeller pulse  $t_r$ . For a given  $t_e$  and  $t_r$ ,  $f(t_e, t_r)$  is a constant. Since the early work of Tal'rose, the pulsing technique has been used by other workers notably Harrison et al (16) and Ryan and Futrell (17).

The conventional or pulsed low pressure techniques possess a number of limitations in terms of the types of ion-molecule reactions which may be studied. The low pressure in the ion source ( $\sim 10^{-4}$  torr) coupled with the short reaction times ( $\sim 10^{-6}$  sec) are such that only bimolecular reactions possessing large ( $\sim 10^{-9}$  cm<sup>3</sup> molecule<sup>-1</sup> s<sup>-1</sup>) rate coefficients may be studied (i.e. reactions which occur at the collision frequency).

The difficulties centering about short reaction times were largely overcome by various trapping techniques

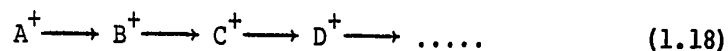
(18-21). Harrison et al (19-21) have developed a technique whereby the ions in the ion source are trapped in the space charge of an electron beam. A low energy electron beam (~5 eV) is passed continuously through the ion source trapping the ions in the space charge. The ions are then extracted by applying a suitable pulse to the repeller electrode. Using this method, ions may be retained in the ion source for several milliseconds.

Another approach is ion cyclotron resonance. This method involves capturing the ions in crossed electric and magnetic fields. Reactions may be observed over time periods as long as 100 milliseconds. The technique was pioneered by Baldeschwieler et al (22) and extensive studies have been conducted in recent years by Beauchamp et al (23,24), Brauman et al (25) and others (26).

Both ion cyclotron resonance and the conventional low pressure techniques possess some disadvantages and limitations. The ions are usually produced by electron bombardment and may be generated in an internally or translationally excited state. Thus the energy state of the reactant ion may be unknown. Reactions which require third body stabilization cannot usually be studied by these methods because the maximum pressure which may be used is  $\sim 10^{-3}$  torr.

The utilization of ion source pressures in the torr range overcomes many of the difficulties of the low pres-

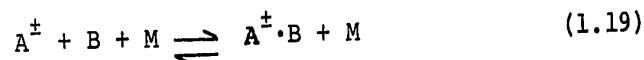
sure technique and greatly expands the types of reactions which may be investigated. The increased pressure slows down the movement of the ions to the walls since the ions must diffuse to the walls as opposed to an almost unimpeded flight in the case of the low pressure instrument. This means that ions may be retained in the ion source for several milliseconds without specific trapping arrangements. The long retention time of ions permits the study of complex reaction sequences of the form



The ions undergo many thousands of collisions while they are in the ion source. This number of collisions should quench most excited ionic species to the ground state and thus reactions of thermal species may be studied.

In the high pressure ion source, ions escape through a small orifice to the mass analysis system of the instrument by a combination of mass flow and diffusion. Thus the presence of an electric field gradient across the ion source to "push" the ions out as is the case with the low pressure design is not essential. The absence of any externally applied field ensures that the translational energies of the ions under examination reflect the temperature of the gas in which they are carried. The high pressures permit the occurrence of multiple collisions of individual ions and thus termolecular reactions such as

11.

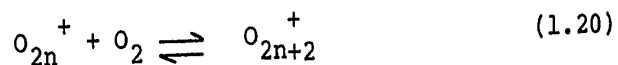


which require "third body" stabilization may be investigated. The work to be described later in this thesis is largely a study of termolecular reactions.

## B. Other Studies at High Pressures

### (a) High Pressure Mass Spectrometry

Conway and coworkers (27-30) have studied the thermodynamics of several clustering reactions. Yang and Conway (28) have studied the equilibrium in the reaction



where  $n = 1, 2, 3, 4$ . They found a general decrease in  $\Delta H$  for the reaction with increasing  $n$ . Other equilibrium reactions such as

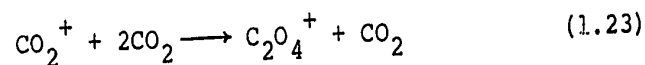


and



have been investigated by Conway et al (27,29,30).

Franklin and coworkers (31-34) have conducted studies of the kinetics of termolecular reactions such as



which occurs in carbon dioxide. The positive ion-molecule reactions in CO (31), and other compounds (32-34) have also

been investigated by these workers.

(b) Chemical Ionization

The chemical ionization method developed by Field et al (35-44) is one of the most widely used high pressure mass spectrometric techniques. The chemical ionization method involves the electron bombardment of a carrier gas (usually  $\text{CH}_4$ ) containing small amounts of substrate. The primary ions formed are rapidly converted to  $\text{CH}_5^+$  and  $\text{C}_2\text{H}_5^+$  which then proton transfer to the substrate. The method is widely used as an analytical tool. The major difference between the chemical ionization method of Field et al and the present approach is that a repeller electrode is retained in the ion source in the chemical ionization experiment to "push" ions out of the high pressure ion source. Field et al have undertaken extensive studies of the equilibria and kinetics of ion-molecule clustering reactions (39-44).

(c) Flowing Afterglow

The flowing afterglow technique developed by Ferguson, Fehsenfeld and Schmeltpopf (45) is one of the most powerful techniques available today for the study of ion-molecule reactions. In this technique, a carrier gas (usually He) which has been weakly ionized by electron impact or a microwave discharge is flowed down a tube at a pressure of about 0.5 torr. Reactant gases are injected downstream from

the excitation region. The helium ions and excited helium atoms ionize the reactant gas molecules. At some point downstream a second gas whose reactions with the primary ions are to be studied is added. At the end of the tube the ions are sampled mass spectrometrically. The reaction time and therefore the rate constant may be calculated from the knowledge of the fluid dynamics of the flowing plasma.

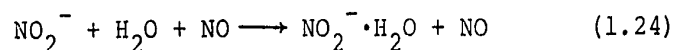
The technique is quite flexible. Reactions involving unstable neutral species, such as reactive atoms, have been undertaken. Ferguson and coworkers have performed extensive studies of clustering reactions and a compilation of the reactions they have investigated is available (1, 46). The technique has been used to measure electron affinities (47) and proton affinities (48,49) as well as reaction kinetics.

(d) Stationary Afterglow

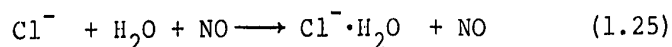
The stationary afterglow technique involves exciting the gas in a cell (usually at pressures in the torr range) by various means (microwave discharge or photon absorption) and then mass spectrometrically observing the temporal behaviour of the ionic species in the decaying plasma. Fite et al (50) and Sayers and Smith (51) were early workers in the field who applied the technique to the study of aeronomically important reactions. Recently



Lineberger and Puckett (52) have applied the method to the study of negative-ion hydration reactions such as



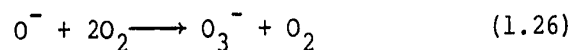
and



reporting values of  $1.3 \pm 0.3 \times 10^{-28}$  and  $3.4 \pm 1.3 \times 10^{-29}$   $\text{cm}^6 \text{ molecule}^{-2} \text{ s}^{-1}$  for the respective forward rate constants.

(e) Ion Drift Tube Experiments

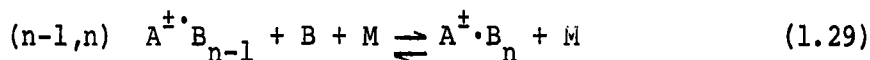
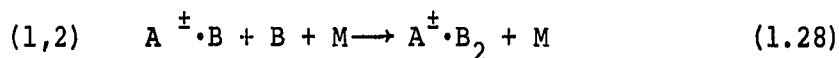
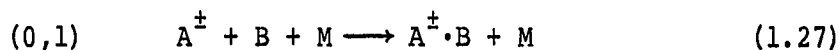
In the mass spectrometric drift tube experiments, a short burst of ions enters a tube containing gas at pressures in the torr range where there is a uniform axial electric field gradient. The ions then drift down the tube under the influence of the electric field and are then sampled with a mass spectrometer at the end of the tube. At sufficiently low field gradients, thermal or near thermal conditions are approached. McDaniel et al (53,54) have used this technique to measure diffusion coefficients and mobilities of various ions. They have also applied the method to the study of ion-molecule reactions such as



for which a value of  $k = 1.0 \pm 0.2 \times 10^{-30} \text{ cm}^6 \text{ molecule}^{-2} \text{ s}^{-1}$  was reported (53).

### 1.3 The Present Study

Classically in the study of chemical kinetics, the experimentalist observes the variation in concentration of the reactants and/or products of a reaction as a function of time. Such studies have been extremely valuable in the investigation of reaction mechanisms and have made a major contribution to the understanding of the processes of chemical transformations as a whole. The present work deals with a study of selected reactions of the type



where A is a positive or negative ion which may be a single atom or a molecule, and B and M are either atoms or small molecules (Ar, O<sub>2</sub>, N<sub>2</sub>, H<sub>2</sub>O, CH<sub>4</sub> etc.).

In the present experiments the ionic species A<sup>±</sup> is generated by high energy electron bombardment in the ion source of the mass spectrometer. The temporal behaviour of the ion A<sup>±</sup> and its subsequent reactions products A<sup>±</sup>·B<sub>n</sub> are observed experimentally. From the time dependence of the concentrations of the various ionic species the rates of the reactions may be determined.

The reverse process in many termolecular reactions such as (1.29) is negligible. That is under normal conditions the reverse processes in (1.29) are negligible. However,

under suitable conditions many reactions of this type are reversible and thermodynamic equilibrium may be achieved between the reacting species. The studies which will be described in subsequent chapters in this thesis are directed to the investigation of the kinetics and thermodynamics of reversible ionic reactions.

The apparatus used in the present experiments is similar to that developed in these laboratories by Durden (55) and Arshadi (56). Arshadi's apparatus was modified so that the time dependence of the various ionic species in the ion source could be followed.

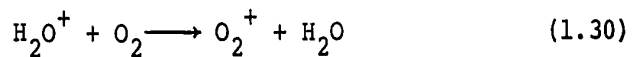
Techniques were also developed in the present experiment to permit the study of reactions over a wide temperature range (85-850°K). Such apparatus permits the investigation of the temperature dependence of the rates of reactions such as (1.29). The experimental observations may then be compared to the predictions of various theoretical models. Some of the problems to which studies as those above may be directed are described in the following sections.

#### 1.4 Ion Chemistry of the D Region

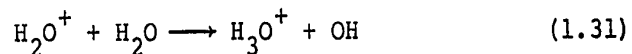
The so called D region of the earth's ionosphere extends from an altitude of 50 km to 85 km and has been the subject of intense study over the last decade. It is in this region where much of the high energy radiation

17.

from the sun is absorbed and also the region from which many radio waves are reflected. In 1965 Narcisi and Bailey (57) reported the first observations of the ionic constituents of the D region. Sampling with a rocket launched mass spectrometer travelling at supersonic speeds they observed that the ions  $\text{H}_3\text{O}^+$  ( $m/e = 19$ ) and  $\text{H}^+(\text{H}_2\text{O})_2$  ( $m/e = 37$ ) were dominant in much of the region (57). The result was initially a theoretical stumbling block as no satisfactory explanation for the observation could be made. The D region contains only trace amounts of water, the major gases being nitrogen, oxygen, argon and small amounts of nitric oxide. Only a very small amount of  $\text{H}_2\text{O}^+$  is expected to be formed by direct absorption of solar radiation due to the low concentration of water at these altitudes. Furthermore any  $\text{H}_2\text{O}^+$  formed is expected to be rapidly removed via the fast ( $2 \times 10^{-10} \text{ cm}^3 \text{ molecule}^{-1} \text{ s}^{-1}$  (58)) reaction



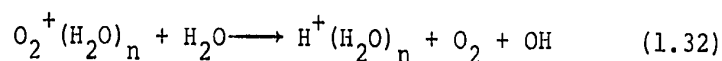
Thus the reaction sequence leading to  $\text{H}^+(\text{H}_2\text{O})_n$  cannot start via the well known reaction



It was postulated (59,60) and demonstrated in the laboratory (61,62,63) that the formation of the proton hydrates may occur via the initial clustering of water

18.

molecules about the ion  $O_2^+$ . The hydrate  $O_2^+(H_2O)_n$  was found to react with a water molecule yielding the proton hydrates in a reaction of the form



A similar mechanism has been proposed for the nitric oxide hydrates  $NO^+(H_2O)_n$  (64-67).

The negative ion chemistry of the D region is however somewhat unclear. Reid (68) has said (1971) that "Our ignorance of the negative ion chemistry of the ionosphere remains so complete that the major problems cannot even be formulated yet". Narcisi et al (69) and Arnold et al (70) have performed rocket measurements of the negative ions present in the D region. Although their results are conflicting quantitatively they suggest qualitatively that the terminal negative ions in this region will be hydrated. Apparently ions of the form  $NO_3^-(H_2O)_n$  are dominant (69) although the species  $CO_3^-(H_2O)_n$  was reported by Arnold et al (70) to be significant.

Recently Ferguson et al (47) have reported a model system for the reactions of negative ions in the D region. The model postulates that some ten ions are involved as well as a number of neutral species. However, complexities which may arise due to clustering reactions involving water were not considered.

In order to determine rate coefficients for reactions

which may be of importance in the negative ion chemistry of the ionosphere several studies were undertaken. Chapter 5 describes an investigation of the negative ion-molecule reactions in moist oxygen leading to the formation of  $O_2^-(H_2O)_n$ . In Chapters 6 and 7 is presented a study of the thermodynamics and kinetics of hydration of the ionospherically important ions  $NO_2^-$  and  $NO_3^-$ .

### 1.5 Ion-Solvent Interactions

Central to the study of ionic solutions is the nature of the interaction of the ions in the solution with the solvent. The interaction of the ions with their immediate solvating molecules is considered to be of greatest importance. In the examination of ion solvent interactions it is natural to consider first the isolated ion and then the effects of adding solvent molecules to this isolated species. Clearly after the addition of a sufficient number of solvent molecules the completely solvated ionic species will be obtained. This approach from the isolated ion to the solvated species is central to many theoretical as well as experimental treatments.

Traditionally the interaction of the ion with its immediate solvating molecules has been examined in terms of electrostatic forces namely ion-dipole and ion-induced dipole forces. From the study of gaseous ionic equilibria it is possible to obtain the thermodynamic parameters for

the addition of solvent molecules to the isolated ion. It is common to discuss ions in solution as if they had a certain number of solvating molecules surrounding them. These immediate solvating molecules are regarded as being in an "inner sphere" or "inner solvation shell" and these ligands are believed to determine the behaviour of the ion in solution. Usually the number of such ligands is proposed to be an even number i.e. 4 or 6. This belief stems perhaps from studies of crystals where the three dimensional array may place constraints on the number and position of coordinated species.

If there is an "inner solvation shell" then if one examines the enthalpies for the successive addition of ligand molecules a discontinuity may be expected in the data at the completion of the solvation shell. For example Searles and Kebarle (71), Hogg and Kebarle (82) and Hogg, Haynes and Kebarle (73) have found that the addition of the fifth molecule of ammonia to  $\text{NH}_4^+(\text{NH}_3)_4$  was characterized by a considerable drop in the enthalpy for this addition compared to the general trend which was observed for the addition of the first four ammonia molecules. The authors (71-73) ascribed this to the non-spherical nature of the central ammonium ion. They suggested that the first four ammonia molecules are tetrahedrally arranged about the ammonium ion thus completing the "inner solvation shell". The fifth molecule was then

visualized as occupying a position external to the four central ammonia molecules and thus was more weakly bound.

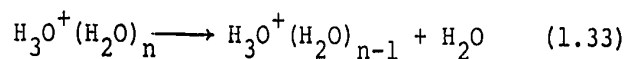
Similar results using a spherical central ion and a polyatomic ligand were observed by Yamdagni and Kebarle (74) in their study of the solvation of the negative halide ions with acetonitrile. The spatial charge distribution in the acetonitrile molecule ( $\text{CH}_3\overset{\delta^+}{\text{C}}\overset{\delta^-}{\text{N}}$ ) causes the acetonitrile molecules to "crowd" each other when attached to a negative halide ion. This causes "solvation shells" to be formed. The number of acetonitrile molecules in each shell depends on the nature of the central atom.

The results using acetonitrile as the solvent differ considerably from the results using water as the solvent. Arshadi, Yamdagni and Kebarle (75) have studied the solvation of the negative halide ions with water. In this case the authors (75) report that the enthalpy of addition of successive water molecules varied smoothly with increasing number of water molecules thus suggesting that a discrete "solvent ion shell" is not formed. Džidić and Kebarle (76) conducted a similar study on the solvation of the alkali metal positive ions with water. They found in this system, as in the halide system, that there was a smooth decrease in the enthalpy of addition of successive water molecules, indicating again that there was not any special "solvation shell".

A decade or so ago it was believed (77-82) that the



species  $H^+(H_2O)_4$  was of exceptional stability in aqueous solution. The four water molecules were visualized as being rather tightly bound to the proton and that this species behaved as a unit in solution. Kebarle et al (82) found that the  $+\Delta H^\circ_{n-1,n}$  for the reaction



decreased regularly from 36 kcal/mole for  $n = 1$  to 12 kcal/mole for  $n = 7$  demonstrating that  $H^+(H_2O)_4$  was not of exceptional importance (82).

The work presented in this thesis is a continuation of the previous studies from this laboratory on ionic solvation which were described above. Chapter 4 presents a study of the solvation of  $O_2^-$  with methanol and a comparison of this system with several other systems which have been investigated in this laboratory. A study of the hydration of  $NO_2^-$  and  $NO_3^-$  is given in Chapter 7. Chapter 8 is an investigation of the competitive solvation of the  $NH_4^+$  ion with water and ammonia and Chapter 9 is a re-investigation of the equilibria involved in the formation of the proton hydrates. The rate constants leading to the formation of the proton hydrates  $H^+(H_2O)_n$  ( $n = 1, 2, 3, 4$ ) were also determined. A discussion of the literature relevant to each system will be given with the individual chapter.

E X P E R I M E N T A L2.1 Requirements of the Apparatus

Considerable modification is necessary to a conventional mass spectrometer in order to prepare the instrument for studies of reactions at high ion source pressures. For the study of ionic equilibria, the ion source must be maintained at a constant, accurately known and uniform temperature for a prolonged period of time.

The high pressure in the ion source requires that the ionizing particles used be of high energy so as to deeply penetrate the gas sample. In these experiments 2 kV electrons were found to be suitable. In order to maintain a uniform temperature over the ion source the incandescent filament which produces the electrons must be mounted sufficiently distant from the ion source so that heating effects from the filament will be negligible. In the present apparatus the filament was mounted some 30 cm from the ion source and the high energy electrons were directed to the ion source by an electrostatic focussing electron gun. The design of this gun is similar to that found in a cathode ray tube.

In order that the high pressure of gas in the ion source does not interfere with the performance of the mass spectrometer a high capacity pumping system is required. It is necessary to maintain a vacuum in the

mass analysis section of the instrument such that the mean free path is much greater than the dimensions of the apparatus. The techniques involved are described in the subsequent sections of this Chapter.

## 2.2 Improvements in the Present Apparatus

The study of the kinetics of ion-molecule reactions using a high pressure mass spectrometer were initiated in this laboratory by Durden, Kebarle and Good (83). In the Durden (55) experiment a short (10  $\mu$ s) burst of high energy electrons was delivered to the ion source and then the ions which came out of the ion source were electronically gated as a function of time after this initial pulse before being permitted to enter the mass analysis section of the apparatus. The gate width was typically of 10  $\mu$ s. After 2 ms it was found that the concentration of ions in the ion source had decayed by a factor of  $10^2 - 10^3$ . This was approximated as zero concentration, and the electron gun was pulsed again.

The difficulty with this experiment is that when a 10  $\mu$ s electron pulse is used with a 10  $\mu$ s ion gate and a 2 ms repetition rate, one may expect a reduction in signal intensity of a factor of 40,000 over that which would be observed with continuous electron bombardment and ion sampling. Such a reduction in signal intensity is almost a mortal blow to the experiment and necessitates the per-

formance of the measurement at the limits of sensitivity. This problem and several others arising from this approach (drifting signal, excessive time required to perform the experiment, and laborious data manipulation) were overcome in the present apparatus by utilizing ion counting and a signal accumulation technique. Briefly, the method consists of collecting ions of different arrival times after the electron pulse in separate channels of a multi-channel scaler.

### 2.3 Vacuum Chamber

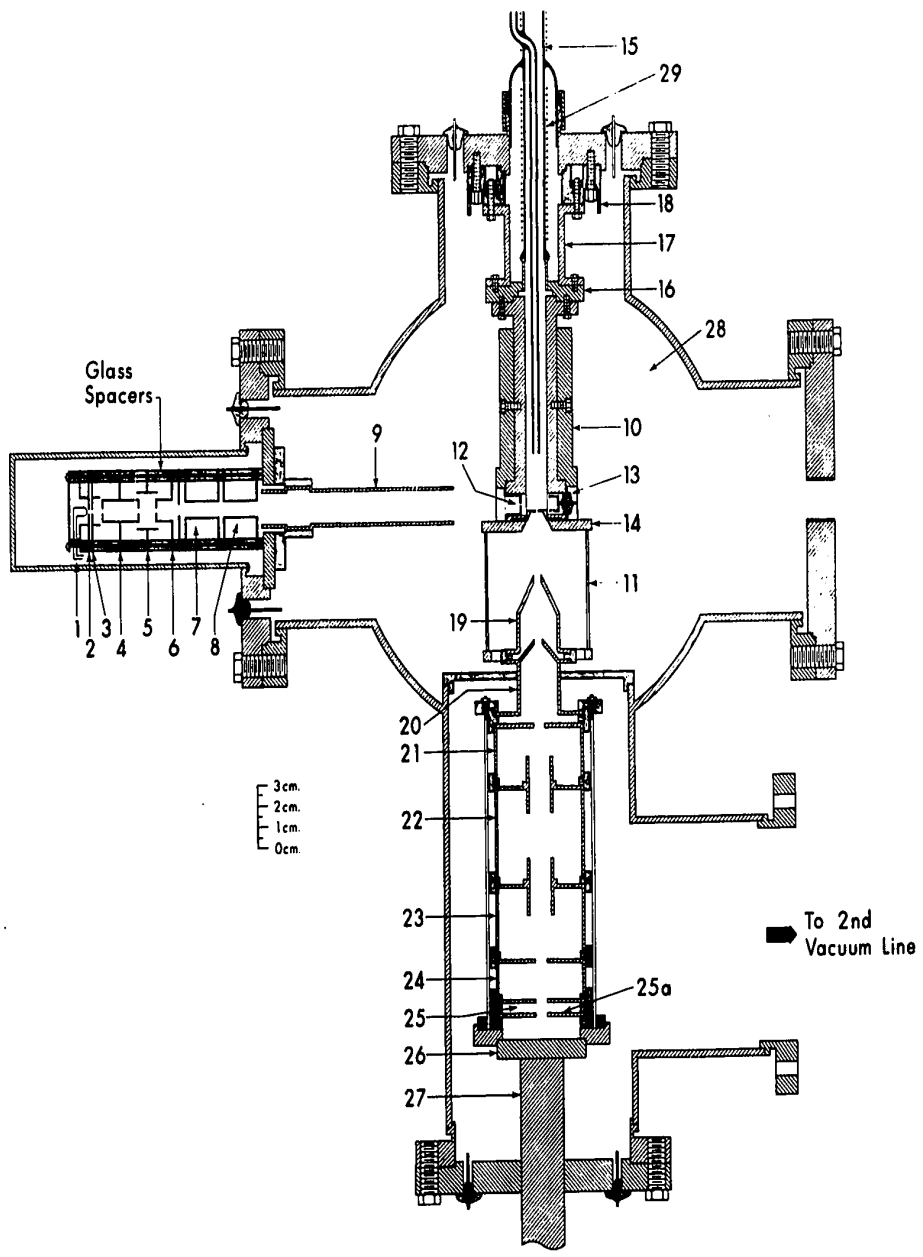
A schematic diagram of the apparatus is shown in Figure (2.1). The apparatus has been described previously in detail by Arshadi (56) and therefore only a brief outline will be presented here. The main vacuum chamber consisted of an 8 inch diameter stainless steel tube which supported four ports. These ports at right angles to each other, carried the ion source, electron gun and ion acceleration system. The fourth port, a spare, usually supported an ion gauge. The main chamber was pumped by a large oil diffusion pump through a water-cooled optical baffle which provided a pumping speed in the plane of the ion source of some  $550 \text{ ls}^{-1}$  (56).

The second chamber which contained the ion acceleration tower was pumped independently by a second large oil diffusion pump. This chamber was connected to the main

FIGURE 2.1

Schematic Diagram of Apparatus

<u>Electrode Number</u>	<u>Description</u>
1	Filament
2	Draw out
3	Extractor
4	} Einzel lens
5	
6	
7	} Deflection plates
8	
9	Shielding cylinders
10	Heating (cooling) jacket
11	Electrostatic shield
12	Electron entrance slit
13	Electron trap
14	Ion exit slit cone
15	Gas inlet
16	Kovar seal flange
17	Stainless steel support
18	Ceramic spacer
19	First cone
20	Second cone
21	Cylinder entrance
22	First cylinder
23	Second cylinder
24	Cylinder exit
25,25a	Ion beam deflection plates
26	Mass analysis slit flange
27	Mass analyzer tube



chamber only via the opening in the first electrode of the ion acceleration system. The third section of the apparatus, the mass analysis section, was also pumped independently by a small oil diffusion pump. The only opening between this chamber and the ion acceleration chamber was the entrance slit of the mass spectrometer itself. The slits in the ion source were typically of dimensions  $1 \times 0.01$  mm. It was found that with apertures of these dimensions and with 3 torr of air in the ion source the pressure in the main chamber was  $\sim 1 \times 10^{-4}$  torr, in the ion acceleration chamber  $\sim 1 \times 10^{-5}$  torr, and in the mass analysis section  $\sim 1.5 \times 10^{-6}$  torr. Ultimate vacuum in the apparatus was typically 1 to  $3 \times 10^{-7}$  torr depending on the history of the system.

#### 2.4 Gas Handling System

The gas handling system used in the present experiments has been described previously in detail by Arshadi (56). The main body of the system consisted of an asbestos box ( $\sim 80 \times 80 \times 80$  cm) which enclosed the valves and the main vacuum manifold. The system was constructed of glass and stainless steel. The box could be heated electrically to  $\sim 150^\circ\text{C}$  for degassing purposes. All valves in the system possessed elastomer seals and this presented some difficulty as the elastomer would absorb polar substances such as water and ammonia and degas them only slowly even at  $150^\circ\text{C}$ .

The system was evacuated by two independent mercury diffusion pumps one of which pumped the system itself and the other was used to maintain a vacuum on the reference side of the manometer. Total pressure was measured with an Atlas-Breman MCT capacitance manometer which could also be "baked out" for purposes of degassing. The calibration of this capacitance manometer was checked from time to time against an oil manometer. The flowing gas mixture or pure gas used in the experiments was prepared as follows. The appropriate major gas from a cylinder was first flowed through a drying tower ( $P_2O_5$ ) to remove any large amounts of water which might be present. The gas then passed through a flowmeter at a pressure of one atmosphere and then through a needle valve where the pressure was reduced to the desired value (usually several torr). The gas then passed through a coil immersed in liquid nitrogen to remove traces of water and other condensable impurities. Reactant gases needed at much lower concentrations were added to the major gas through one or more capillaries, the tips of which reached into the flowing stream of the major gas. A schematic diagram of the gas flow system is displayed in Figure (2.2). The mixture then flowed through the main gas handling system where the pressure was monitored and from there to the ion source. The glass tubes leading to the ion source were wrapped with heating tape for degassing purposes. After passing through the ion source the gas



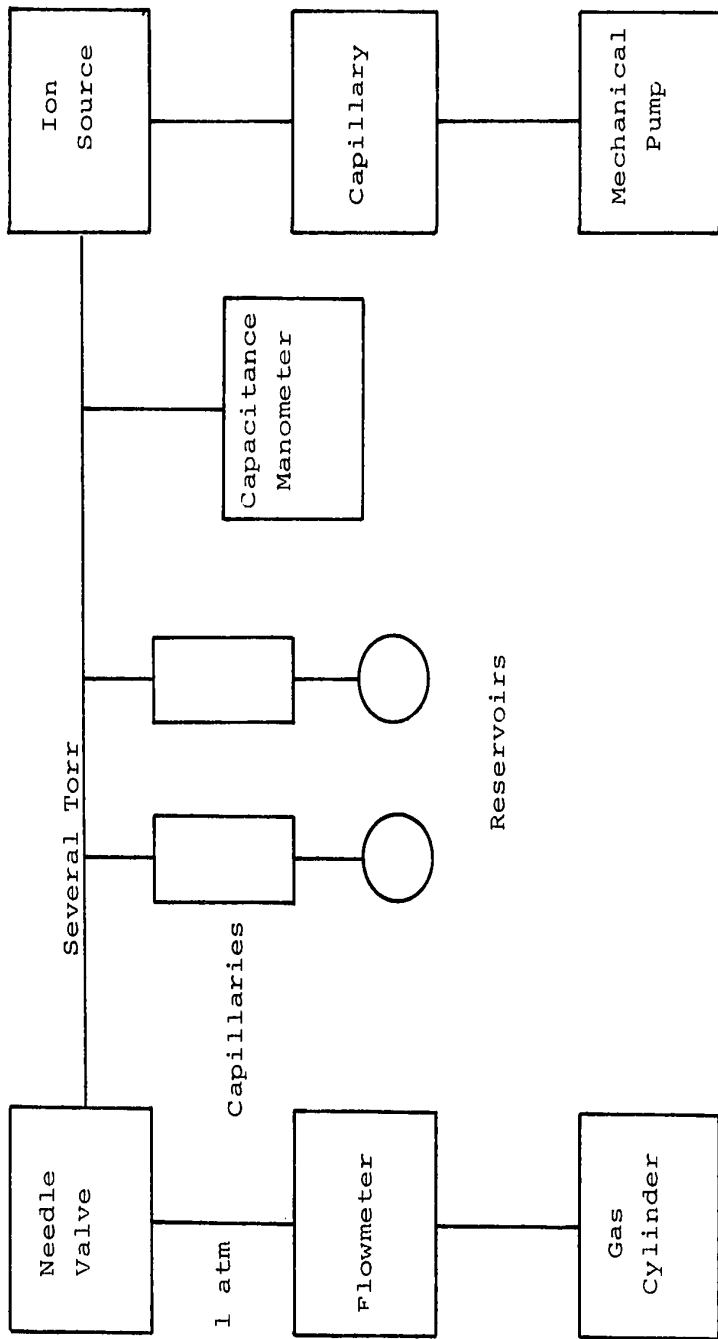


FIGURE 2.2. Schematic Diagram of Gas Flow System

flowed via a capillary which controlled the flow to a mechanical pump.

The valves and tubing used to bring the gas to the ion source were large (>1/2" i.d.) so that there would be a negligible pressure gradient between the manometer and the ion source. The pressure gradient may be calculated from Poiseuille's Law (84)

$$n_M = \frac{\pi a^4 (P_2^2 - P_1^2)}{16\eta \ell RT} \quad (2.1)$$

where  $n_M$  is the flow (moles/sec) through a tube of length  $\ell$  and radius  $a$ ,  $R$  is the gas constant,  $T$  is the temperature and  $\eta$  the viscosity of the gas.  $P_2$  is the inlet pressure and  $P_1$  the outlet pressure. The flow rate at 4 torr pressure in the present apparatus was  $\sim 30 \text{ cm}^3 \text{ atm min}^{-1}$ . Taking the length of the tube as 1 m, the radius as 0.7 cm and the viscosity (air) as 182 micropoise it may be calculated from equation (2.1) that the pressure difference between the manometer and ion source was <0.5%. The pressure reading of the manometer was therefore taken as the pressure in the ion source in the present studies.

### 2.5 High Temperature Ion Source

The ion source which was used for the studies at room temperature and above is shown in Figure (2.1). It was machined from non-magnetic stainless steel. In the lower part of the one-half inch inside diameter cylindrical chamber was bored a channel perpendicular to the main

axis. A small "hat shaped" flange which carried the electron entrance slit [12] was mounted on one side. On the opposite side was mounted the electron trap which also supported a small repeller plate [13]. The ions escaped through a slit which was supported by a demountable flange at the bottom of the ion source. The slits were typically 1-2 mm in length and  $\sim 0.010$  mm in width. They were constructed by spot welding under a microscope two stainless steel razor blades into position. All flanges were sealed with gold wire gaskets.

The ion source was incased in a copper heating mantle [10] in which were inbedded "pencil" wire wound electric heaters. A current of some four amperes at fifty volts would produce a temperature of roughly  $600^{\circ}\text{C}$ . The temperature of the ion source was monitored by a thermocouple mounted deep in the stainless steel block. Thermocouples were also mounted in the heater block [10] and in the copper plate [14] which carried the shielding screen [11].

At the highest obtainable experimental temperatures ( $\sim 600^{\circ}\text{C}$ ) one may question whether or not the ion source thermocouple accurately reflects the gas temperature. At these temperatures the ion source glows a beautiful cherry red and the major source of heat loss from the ion source is radiation rather than conduction through the supporting mounts. This is indicated by the fact that it is necessary

to double the power input to the heaters to achieve a temperature rise from 500°C to 600°C. Also the radiation causes considerable heating of the main vacuum housing necessitating cooling by several fans in order to maintain the instrument at an acceptable temperature.

The ion exit slits are made of razor blades and consequently are very thin at the edges. It may be argued that the rate of heat loss from the slits by radiation is greater than the rate at which heat is supplied to the edges by conduction through the razor blades. If, in fact, the edges of the slits are cooler than the ion source, then the gas near the slits will be correspondingly cooler and as a consequence considerable error in temperature determination may result. To test this hypothesis, heaters were mounted in the copper plate [14]. A stainless steel ring  $\sim 3\frac{1}{2}$ " in diameter and with a  $1\frac{1}{2}$ " hole was mounted at the bottom of the electrostatic shield [11]. This ring could be heated and its temperature monitored independently from the ion source. The ring could be heated to temperatures greater than the ion source so that radiation could reach the ion exit slit from below. The argument being that this should compensate for radiative losses from the slit. The equilibrium position of a clustering reaction is very sensitive to temperature. Thus altering the temperature of this ring relative to the ion source while monitoring a particular equilibrium should provide a sen-

sitive test of whether radiative loss from the region of the slit is significant. Within experimental error the results were negative. The experimental data are presented in detail in the chapter on the proton hydrates. Considerable care was exercised to ensure that the thermocouples were in intimate thermal contact with the ion source. The thermocouples used were iron-constantan, and the potential was measured relative to a junction maintained at 0°C. The temperature was determined by reference to standard tables and the thermocouples were used without further calibration.

## 2.6 Low Temperature Ion Source

A second ion source was constructed in which the heating jacket [10] was replaced by a cooling jacket through which could be flowed a suitably cooled fluid. This source was used to study the positive ion-molecular reaction in oxygen over a wide range of low temperatures. It was found by passing cooled nitrogen gas through the jacket that it was possible to achieve controlled temperatures in the range 85° - 300°K.

## 2.7 The Electron Gun and the Pulsing Circuitry

A schematic diagram of the electron gun is shown in Figure (2.1). The design of this gun is similar to that found in a TV tube and has been discussed in detail by

Arshadi (56). For operation with positive ions the filament was maintained at approximately ground potential and the ion source at +2kV. For operation with negative ions the filament was maintained at -4kV and the ion source at -2kV. Thus electrons of 2kV energy were used in both experiments and the ions were subjected to 2kV acceleration before magnetic mass analysis in a 90°, 15 cm radius field. Typical voltage settings for the various electrodes are given in Table 2.1. The filament in the gun was constructed of thoriated iridium and was found to be quite resistant to attack by all of the gases used in the present experiments and in particular oxygen.

Pulsing of the electron gun was accomplished by applying a suitable potential to the drawout electrode (number 2 in Figure (2.1)). A block diagram of the circuits and instrument is given in Figure (2.3). A battery powered pulse generator which could be floated to the potential of the drawout plate (-4kV in the case of negative ions) was used. The drawout electrode was maintained some 90 volts negative with respect to the filament. Upon receiving an electrical pulse from a master pulse generator the floating pulse generator would alter the potential on plate 2 until it was positive with respect to the filament for the desired time (4-180  $\mu$ s). This permitted electrons to pass from the filament into the focussing and accelerating region of the electron gun. After the preset period

TABLE 2.1Typical Operating Voltages

<u>Electrode</u> <sup>a</sup>	<u>Positive Ions</u>	<u>Negative Ions</u>
1 Filament	0	-4000
2 Drawout	3	-3997
3 Extractor	275	-3725
4 )	2000	-2000
5 ) Einzel lens	260	-3740
6 )	2000	-2000
7 )		
8 ) Deflection plates	2000	-2000
<u>Ion Source</u>		
19 First Cone	1775	-1775
20 Second Cone	1730	-1730
21 Cylinder entrance	1640	-1640
22 First cylinder	1160	-1160
23 Second cylinder	1050	-1050
24 Cylinder exit	900	- 900
25 Deflection plate	0	0
27 Mass analyzer tube	0	0

<sup>a</sup>  
Number refers to Figure (2.1).

---

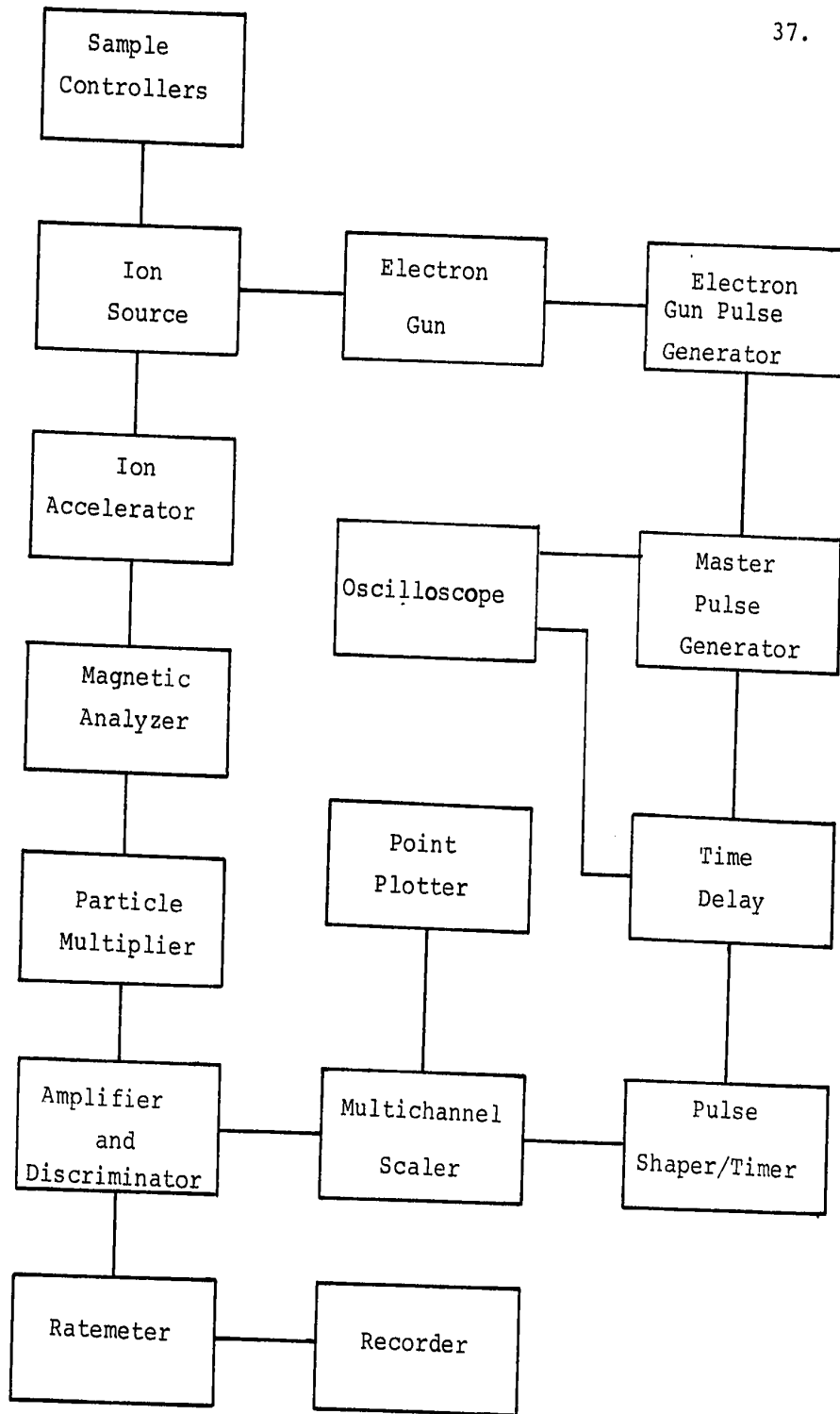


FIGURE 2.3 Block Schematic of Experimental Apparatus.



of time had elapsed the floating pulse generator would return the drawout plate to its original potential negative with respect to the filament. In this way pulses of electrons of known time duration could be delivered to the ion source. The frequency of the pulsing could be controlled by the master pulse generator and the intensity of the pulse by the current passing through the filament as well as the settings of the other electrodes of the electron gun. The dimensions of the pulse output (time and intensity) were controlled independently of the master pulse generator and could be adjusted for optimum conditions.

When the electron gun was not pulsed the electron beam striking the ion source generally had an intensity of several microamperes. The current measured at the electron trap in the ion source was some  $3 \times 10^{-8}$  ampere under these conditions. It may therefore be calculated that in a  $10 \mu\text{s}$  pulse roughly  $2 \times 10^6$  electrons entered the ion source.

Focussing of the electron beam was facilitated by a small plate mounted in front of the electron entrance slit of the ion source. This plate contained a hole of suitable dimensions to permit the passage of the electron beam to the ion source. The outer surface of this plate was coated with a phosphor (Type P-31 Sylvania) imbedded in water glass. The electron beam could be deflected

onto this screen and focussed to the desired spot size.

It was found that the magnetic field of the analysing magnet would significantly deflect the electron beam. Thus ions of different mass would be resulting from different electron intensities such that their signals would not be comparable. To overcome this problem the electron gun and the magnet were incased in a magnetic shield. The use of this shielding reduced the perturbing effect of the magnetic field on the electron beam to a negligible level except at the very highest experimentally accessible magnetic fields which were not required for the present measurements.

The ions, after magnetic mass analysis, were detected by a Spiraltron electron multiplier obtained from Bendix Corp. The multiplier was so operated that per input ion a pulse of  $\sim 10^6$  electrons was delivered to the pulse amplifier. With a new spiraltron this necessitated a voltage of  $\sim 2500$  V across the multiplier and corresponded to the manufacturer's specifications. The output pulses, according to the manufacturer, were of extremely narrow width ( $\sim 3$  ns) and furthermore the pulses were of a fairly uniform size. This has been attributed to space charge saturation of the pulse of electrons as it moves through the tubes of the multiplier (85). This is to be contrasted with multipliers of the conventional dynode structure whose output pulses are of rather variable height. Uniform

pulse heights allow one to set the gate of amplifier discriminator such that almost all multiplier pulses are accepted while low level noise is rejected.

The detection efficiency of this type of multiplier is expected to be high (86-88). The multiplier detects with roughly unit efficiency negative ions which impact on the multiplier with energy greater than  $\sim 500$  eV (88). Apparently it also detects positive ions with  $\sim 90\%$  efficiency (87). The high efficiency for negative ions was explained (88) as being due to the ease of the detachment on impact of the loosely held electron of the negative ion as contrasted with the more strongly bound electrons of a positive ion.

The pulse amplifier package consisted of a preamplifier, amplifier and discriminator unit. This amplification package would deliver a four volt  $0.25 \mu\text{s}$  pulse into 50 ohms for each triggering input signal. The amplified pulses were then counted with a ratemeter and/or delivered to a multichannel scaler (Northern Scientific model NS-630). After attention to electrical shielding the background noise was reduced to approximately 0.5 count per second.

The time dependence of a particular ion was observed in the following manner. The triggering of the electron gun and the sweep of multichannel scaler were synchronized. In a typical experiment, the dwell time per channel in the

multichannel scaler was set at  $10 \mu\text{s}$  and  $2^7 = 128$  channels were selected. The number of ions which arrived at the detector in the first  $10 \mu\text{s}$  after the pulse was stored in the first channel of the multichannel scaler. The number of ions which arrived from  $10$  to  $20 \mu\text{s}$  after the pulse was stored in channel 2 and so on for 128 channels or in this case  $1280 \mu\text{s}$ . After a period of say  $5 \text{ ms}$  the signal had decayed by a factor of  $10^3 - 10^4$  and the electron gun was pulsed again and the process repeated. This time the signal was added to that already stored in the multichannel scaler. In most experiments counting times of 1-5 minutes were found to be sufficient to afford a statistically meaningful signal.

## 2.8 Time of Flight

The time required for the flight of the ions from the ion source to the detector is finite, thus a correction was made. A delay circuit was introduced between the master pulse generator and the multichannel scaler. This circuit would delay the triggering pulse to the multichannel scaler by an amount equivalent to the flight time of the ion under examination. To calculate the flight time, some simplifying assumptions were made. It was assumed that the electric field gradient from electrode to electrode in the ion accelerating tower was uniform and was the quotient of the voltage difference between the electrodes and the interelectrode spacing. Using this assumption and the

42.

geometry and potential of the electrodes (see Figure (2.1) and Table 2.1)) the flight time was calculated using the following expression.

$$x_{ij} = v_i t_{ij} + \frac{eE_{ij}}{2m} t_{ij}^2 \quad (2.2)$$

where  $x_{ij}$  is the distance between the  $i$  and  $j^{\text{th}}$  electrode,  $v_i$  is the velocity of the particle at the  $i^{\text{th}}$  electrode,  $E_{ij}$  is the potential difference between electrodes  $i$  and  $j$ ,  $m$  is the mass of the particle,  $e$  the electric charge and  $t_{ij}$  the time of flight from electrode  $i$  to electrode  $j$ .

Since

$$v_i = v_{i-1} - \frac{eE_{ij}}{m} t_{ij} \quad (2.3)$$

we may solve the quadratic equation (2.2) to obtain  $t_{ij}$ .

The time of flight  $t_f$  is then the sum of the  $t_{ij}$  namely

$$t_f = \sum_{j=i+1}^n t_{ij} \quad (2.4)$$

It was found that

$$t_f = 1.68 \sqrt{m} \quad (2.5)$$

where  $t_f$  is in microseconds and  $m$  is the mass of the ion in amu. The time of flight of  $m/e = 32$  is only  $9.5 \mu\text{s}$ . This may be compared to the minimum time resolution of the multichannel scaler, which is  $10 \mu\text{s}$ . Thus the time of flight correction is almost negligible and the approximations made in its calculation should not lead to serious error. The time of flight correction was made in all

studies.

## 2.9 Physical Conditions in the Ion Source

### A Number of Collisions of the Ions

The number of collisions of a molecule per second (z) in a gas is given by

$$z = \sqrt{2} n \bar{v} \pi d^2 \quad (2.6)$$

where n is the gas number density,  $\bar{v}$  is the average velocity, and d is the diameter of the molecule (89, p.40). The quantity  $\pi d^2$  is thus the collision cross section. For oxygen ( $d = 3.6 \times 10^{-8}$  cm) at a pressure of 1 torr at 300°K the molecule will suffer about 7,000 collisions in a millisecond.

A charged particle will suffer a somewhat greater number of collisions since its collision cross section is larger than that of a neutral molecule. The Giomousis-Stevenson (2) cross section for the collision of an ion with a neutral is given in equation (1.5). This expression predicts collisional cross sections for ions at room temperature typically in the order of several hundred square angstroms. Using a value of  $\sim 10^2 \text{ \AA}^2$ , it is calculated that an ion will undergo some  $10^5$  collisions in a millisecond for a gas pressure of 1 torr at 300°K. After such a number of quenching collisions the ion should be in the ground state.

In most equilibria measurements, conditions were so selected that the ion ratios became constant after some 100  $\mu$ s and were observed not to change up to reaction times in the millisecond range. The ion ratios should therefore reflect the thermodynamic equilibrium ionic population of thermal energy species because of the number of collisions that an ion may undergo in this time interval.

The kinetic measurements which are described in later chapters in this thesis were usually determined some 100  $\mu$ s after the initial electron pulse. Since the ions may be expected to undergo some  $10^4$  collisions in 100  $\mu$ s these species should also be in the ground state.

#### B. Ion Sampling

Previous experience in this laboratory (71, 72, 73, 90) has shown that serious problems may arise when sampling from a high pressure ion source. Using high pressures (20 torr) and large orifices (0.1 mm) flow through the orifice becomes non-molecular and serious distortions of the ionic population may result from cooling effects and collisions in the expanding jet of gas. The cooling in the jet will cause the growth of large clustered ions while collision of the ions during acceleration into the mass spectrometer will dissociate larger clusters into smaller ones. Previous experience in this laboratory has shown that molecular flow is best suited (90).

This means that the dimensions of the orifice (1 x 0.010 mm) must be comparable to the mean free path, that is, the average distance a molecule travels between successive collisions. The mean free path  $\lambda$ , is given by

$$\lambda = \frac{1}{\sqrt{2}n\pi d^2} \quad (2.7)$$

where  $n$  is the gas number density and  $d$  is the diameter of the gas molecules in question (89, p.40). The mean free path in oxygen ( $d = 3.6 \times 10^{-8}$  cm) at 4 torr and 300°K is 0.015 mm. Thus flow through the orifice (1 x 0.010 mm) should be near molecular.

### C. Charged Particle Recombination

The sum of all positive ions in the ion source may be depleted by diffusion to the walls and by charged particle recombination. The most important type of charged particle recombination for positive ions is ion-electron recombination. The half life for recombination may be calculated from the expression

$$t_{1/2} \approx (\alpha n_e)^{-1} \quad (2.8)$$

where  $\alpha$  is the ion-electron recombination coefficient and  $n_e$  is the density of electrons. For the ion  $O_2^+$ ,  $\alpha = 1.7 \times 10^{-7} \text{ cm}^3 \text{ molecule}^{-1} \text{ s}^{-1}$  (89, p.610). The parameter  $n_e$  is somewhat more difficult to estimate.

The number of primary ions per electron is given by



46.

$$I_p/I_e = Qnl \quad (2.9)$$

where  $Q$  is the ionization cross section, and  $l$  is the electron path length. The distance from the electron beam entrance slit to the electron trap  $l$  is  $\sim 1$  cm in the present apparatus. At a pressure of 4 torr and  $300^\circ\text{K}$ ,  $n = 12 \times 10^{16}$  molecules  $\text{cm}^{-3}$ . The ionization cross section of  $\text{O}_2$  for 2000 eV electrons may be taken as  $5 \times 10^{-17} \text{ cm}^2$  (91). Thus from equation (2.9)  $\sim 6$  ions should be produced by the primary electron beam, assuming that the electron energy remains constant. Assuming that some 100 eV are lost per ionizing collision (92), one would expect that the final electron energy will be around 1400 eV. At this energy the cross section is larger but not significantly so. However for each ion a secondary electron will also be produced. The average energy imparted to these electrons is about 70 eV and each electron is expected to generate about two extra ions before being degraded to low energies (92). Thus each high energy electron which enters the ion source should produce about 15 ions (at 4 torr). In a  $10 \mu\text{s}$  electron pulse  $\sim 2 \times 10^6$  electrons enter the ion source and therefore  $\sim 3 \times 10^7$  ions should be generated.

To calculate the initial density of ions, assumptions must be made concerning the volume in which they are generated. The total volume of the ion source is about  $1 \text{ cm}^3$ ,

however the ions are not generated uniformly over this volume but instead along the path of the high energy electron beam. The distance from the electron entrance slit to the electron trap is 1 cm and the dimensions of the electron entrance slit is  $1 \times 0.010$  mm as was mentioned previously. If the volume in which the ions are generated is taken to be  $1.0 \times 0.2 \times 0.1 \text{ cm}^3 = 2 \times 10^{-2} \text{ cm}^3$  then the initial density of ions is  $\sim 1.5 \times 10^9 \text{ cm}^{-3}$ . This is a maximum density because the volume of generation is increased as the second electrons ionize. From equation (2.8) the half life for ion-electron recombination in oxygen is calculated to be  $\sim 4$  milliseconds. The half life for disappearance of the positive ions in the system may be seen from Figure (2.4) to be about 0.2 milliseconds. Thus ion-electron recombination should not be a significant loss mechanism in the present experiments.

#### D. Temporal Behaviour of the Ions

Figures (2.4, 2.5) show the temporal profiles of the major positive ion ( $\text{H}^+(\text{H}_2\text{O})_n$ ) and the major negative ion ( $\text{NO}_2^-$ ) observed in a mixture of 4.17 torr methane and 40 mtorr water containing variable amounts of ethyl nitrate at  $127^\circ\text{C}$ . The clustering reactions of water about the ions in question under these conditions are sufficiently rapid that the given profiles are a good approximation to the behaviour of the total positive and negative ion signals. The results

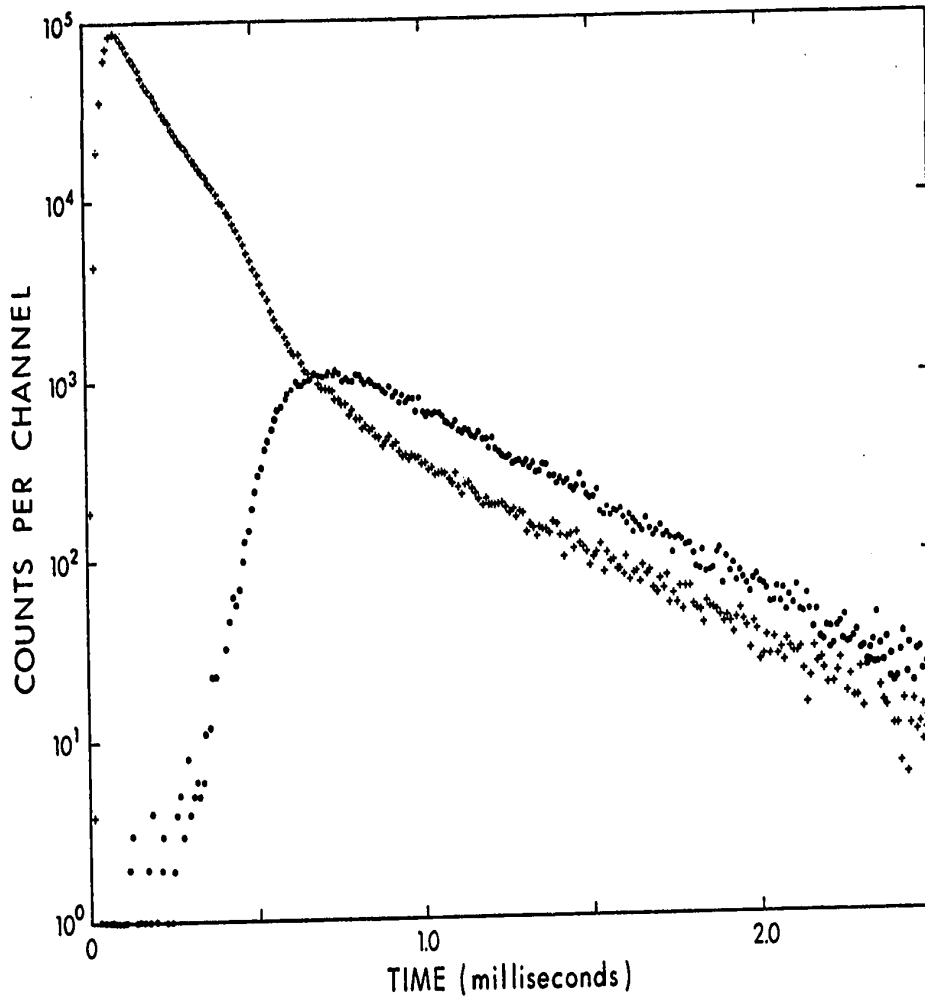


FIGURE 2.4. Time dependence of total ionization of positive and negative ions in 4.17 torr  $\text{CH}_4$  containing 40 mtorr  $\text{H}_2\text{O}$  and trace amounts of  $\text{C}_2\text{H}_5\text{ONO}_2$ ,  $T = 127^\circ\text{C}$ , + positive ions ( $\text{H}^+(\text{H}_2\text{O})_4$ ), • negative ions ( $\text{NO}_2^-$ ).

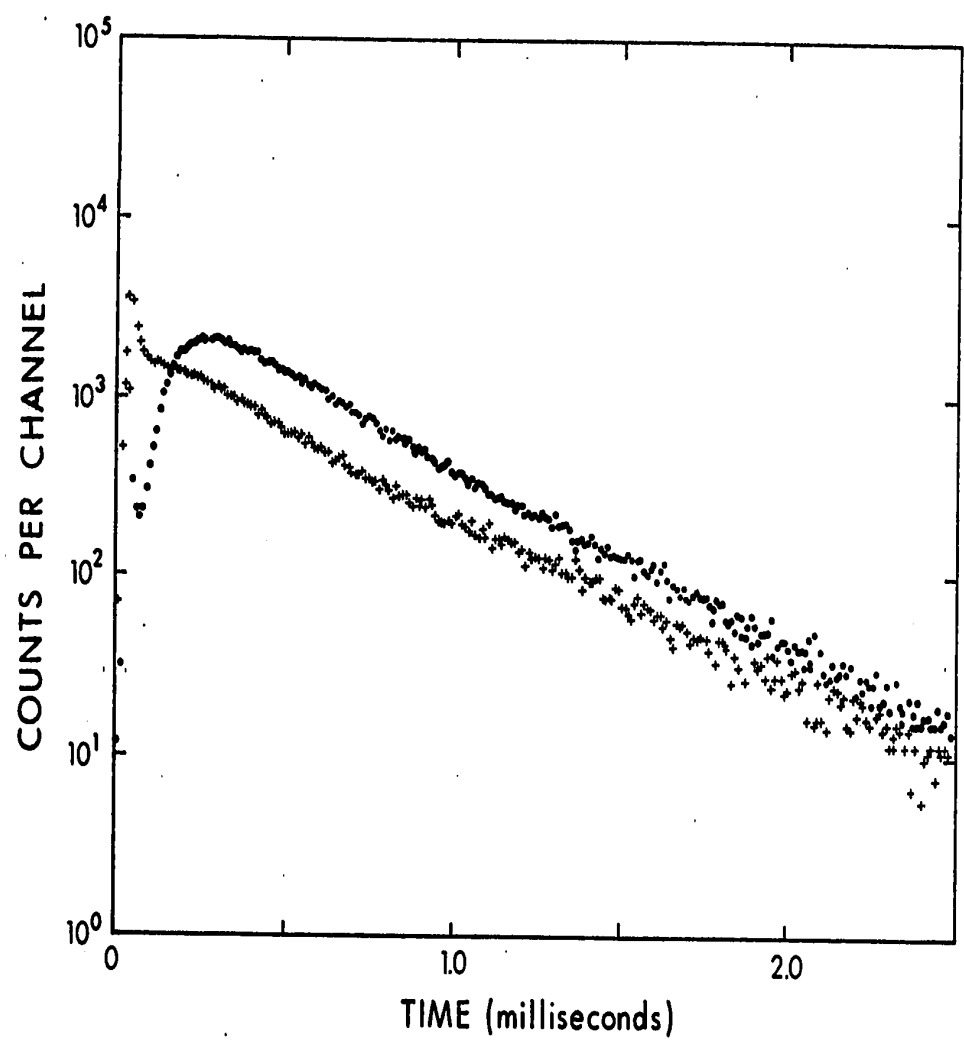


FIGURE 2.5 Time dependence of total ionization of positive and negative ions in 4.17 torr CH<sub>4</sub> containing 40 mtorr H<sub>2</sub>O and a few mtorr of C<sub>2</sub>H<sub>5</sub>ONO<sub>2</sub>, T = 127°C, + positive ions (H<sup>+</sup>(H<sub>2</sub>O)<sub>4</sub>), ● negative ions (NO<sub>2</sub><sup>-</sup>).

displayed in Figures (2.4,2.5) were obtained by first observing the positive ion signal and then altering the instrument for the observation of negative ions. This procedure requires roughly one half hour. In Figure (2.4) the positive and negative ions decay at nearly the same rate but not exactly. This is believed to be caused by a slight drift in the total pressure in the ion source during the time interval required to change from the observation of positive to negative ions.

The relative intensities of the two signals are qualitatively comparable. Thus the area under the curves approximately reflects the observed ratios of the ion signals. As can be seen the two signals are similar when substantial amounts of ethyl nitrate are added, but the negative ion signal is much less when only trace amounts of the nitrate are present. Qualitatively this is to be expected, however, one should not attach too much significance to the absolute intensities, as they may be greatly influenced by unknown instrumental factors involved in switching from the observation of positive ions to negative ions. In Figure (2.4) the positive ion signal is observed to decay initially quite rapidly and then at ~500  $\mu$ s there is a break after which the positive ion signal decays much more slowly. The negative ion signal on the other hand exhibits a completely different temporal behaviour. The negative ion signal is initially zero and

then at the transition point (of the positive signal) rises to a maximum in intensity and afterwards decays at the same rate as the positive ion signal.

Figures (2.4, 2.5) show the effect on the temporal profile of the addition of small amounts of ethyl nitrate. Ethyl nitrate has a large cross section for the capture of thermal electrons (93). As the concentration of ethyl nitrate is raised the transition occurs earlier in the decay of the plasma.

Qualitatively the observations may be explained in the following manner. The high energy electron beam when passing through the gas in the ion source initially creates mainly positive ions and the corresponding secondary electrons. These electrons will then cause further ionization and will be degraded by inelastic collisions to near thermal energies. Very few negative ions would be formed initially as the cross sections for the capture of a high energy electron to form a negative ion, and for the formation of negative ions by pair production processes are expected to be small (89, p.382). In the initial stages then the plasma consists mainly of positive ions and electrons.

Electrons have a mobility which is much greater than that of the ions (89, p.512). Consequently the electrons move rapidly to the walls of the container. However, as the electrons move away the positive ions are left behind.

This creates a "self field" in the plasma which restrains the movement of the electrons, and any negative ions. The positive ions and electrons then diffuse together under the influence of their mutual electric fields. The diffusion of charged particles through a gas which is controlled by electrical forces between the particles is referred to as ambipolar diffusion. Ambipolar diffusion becomes important for charge densities greater than about  $10^7 \text{ cm}^{-3}$  (89, p.512). Below this level, the charged particles are sufficiently distant from each other that their mutual electrical forces are small compared to thermal energies.

The ambipolar diffusion coefficient  $D_a$  is defined (89, p.513) by the equation

$$D_a = \frac{D^+K^- + D^-K^+}{K^+ + K^-} \quad (2.10)$$

where  $D^+$  and  $D^-$  are the diffusion coefficients of the positive ions and electrons respectively, and  $K^+$  and  $K^-$  are the mobilities of the respective species. Using the Einstein relationship (89, p.514)

$$\frac{D}{K} = \frac{kT}{e} \quad (2.11)$$

and assuming that  $K^- \gg K^+$  we find that

$$D_a \approx 2D^+ \quad (2.12)$$

when  $T^+ = T^- = T_{\text{gas}}$

During the period of electron-positive ion ambipolar diffusion one may expect that the positive ions reaching the exit slit will be abundant while the negative ions will be restrained by the electric field and be of low abundance. With time more electrons and ions will be discharged at the walls until eventually the number density of electrons is no longer sufficient to maintain the electric field. This collapse of the electric field is evident in Figure (2.4) at  $\sim 500 \mu\text{s}$ . At this point the negative ion signal rises very sharply and afterwards the negative and positive ion signals decay exponentially with the same frequency. After the transition point diffusion is presumably dominated by negative-ion-positive-ion ambipolar diffusion (94). At this point the ion density is expected to be rather low so that free diffusion may be dominant.

The addition of ethyl nitrate moves the transition point to earlier times in the afterglow (Figure (2.5)). The addition of ethyl nitrate will cause a rapid conversion of the electrons to negative ions, since ethyl nitrate has a large cross section for the dissociative capture of thermal electrons (93). The electron density is rapidly depleted and thus the transition point moves to earlier times in the afterglow.

There are, however, two observations which are not completely consistent with this simplistic analysis.



First, the diffusive loss frequency before the transition point is expected to be twice the loss frequency after the transition since  $D_a \approx 2D^+$ . In Figure (2.4), the slope of the positive ion signal before the transition point should be twice the slope afterward. The ratio is however  $\sim 3.5$ . The value of the ratio is greater than two for all experiments which have been done with this apparatus. The ratio appears to be somewhat pressure dependent but the determination of the slope is a rather subjective process, particularly before the transition. The diffusion coefficients for the positive ions in the two regions should differ by a factor of two and consequently a discontinuity in the positive ion profile is expected (94). This discontinuity is somewhat "smeared" in the present experiments.

The inconsistencies mentioned above are not serious but reflect the non-ideality of the present system. The discussion concerning the ion transport in the plasma and in particular the ratio of the loss frequencies before and after the transition is predicated by two conditions. First the electron, gas and ion temperatures are assumed to be equivalent. The variation of the positive-ion-electron ambipolar diffusion coefficient with the electron temperature is given by (89, p.513)

$$D_a = D^+ \left( 1 + \frac{T_e}{T_i} \right) \quad (2.13)$$

where  $T_e$  and  $T_i$  are the electron and ion temperatures respectively. As can be seen from (2.13) an elevated electron temperature will lead to an accelerated decay of the ion concentration before the transition. It may be that the electrons have had insufficient time to relax before the transition and thus the ambipolar diffusion coefficient is larger than would be expected when  $T_e = T_i = T_{\text{gas}}$ .

The second assumption involved in the treatment of the ion transport phenomena is that the charged particles are "smoothly" distributed over the volume of the ion source. However, the ionizing electron beam enters the chamber through a narrow slit and may be expected to produce initially a thin "sheet" of ionization. The time required for the distribution of ions to relax should be roughly the average time required for the ions to diffuse to the walls which is given by (89,p.493)

$$t \sim x^2/D \quad (2.14)$$

The distance over which the ions are to diffuse,  $x$ , may be taken as the distance from the plane of the electron beam to the ion exit slit which is about 1 mm. Taking  $D = 10 \text{ cm}^2 \text{ s}^{-1}$ , a typical value for a diatomic ion at 4 torr pressure at 300°K,  $t$  is calculated to be roughly a millisecond. It may be that the relaxation of the initial distribution of ions contributes to the anomalously high rate of decay of the positive ion signal before the transi-

tion point.

## 2.10 Normalization of the Data

As can be seen from Figures (2.4-2.5) the total ion signal varies with time. To facilitate data analysis, the ion intensities were "normalized". That is the ion intensity of a given ion at some time  $t$  was expressed as a percentage or a fraction of the total ion intensity. Thus the normalized ion intensities appear as if they represented ion changes in an ion source in which the total number of ions remained constant. Without this simplification, it is almost impossible to analyse the experimental data for kinetic parameters. This assumption is not involved in the determination of equilibrium constants.

The normalization procedure involves some approximations however. It is assumed that all loss mechanisms other than ion-molecule reactions affect all ions equally. Charged particle recombination phenomena are a negligible loss mechanism in the present experiments as has been shown previously in this chapter. Diffusion is not a negligible process and the normalization procedure assumes that the diffusion coefficients for all ions are equal. This is incorrect as diffusion coefficients are dependent on mass as given below (89, p.435)

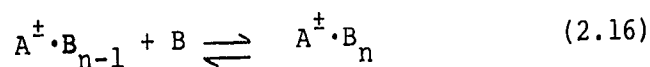
$$D \propto \left(\frac{1}{\mu}\right)^{\frac{1}{2}} \quad (2.15)$$

where  $\mu$  is the reduced mass of the ion and neutral gas molecules. Diffusion coefficients are probably not greatly different for the ions which were studied in the present experiments (89,p.435).

In most of the experiments in the present study the rate of depletion of a particular ion by ion-molecule reactions is much faster than the rate of loss by diffusion. Thus diffusion in many cases is a minor contribution to the all over loss frequency when compared to ion-molecule reactions. It is concluded that the normalization procedure does not introduce serious error into the experiment.

### 2.11 Determination of the Thermodynamic Parameters from the Equilibrium Constants.

Consider the equilibrium reaction



After the achievement of equilibrium in (2.16) the equilibrium constant for the (n-1,n) reaction  $K_{n-1,n}$  is given by

$$K_{n-1,n} = \frac{P_{A^{\pm} \cdot B_n}}{P_{A^{\pm} \cdot B_{n-1}} \cdot P_B} \quad (2.17)$$

where  $P_X$  is the partial pressure of X. It is assumed in this study that the ratio of the partial pressures of

58.

the ionic species may be approximated by the ratio of the observed ion intensities at equilibrium. That is

$$\frac{P_{A^{\pm} \cdot B_n}}{P_{A^{\pm} \cdot B_{n-1}}} \approx \frac{I_{A^{\pm} \cdot B_{n-1}}}{I_{A^{\pm} \cdot B_n}} \quad (2.18)$$

so that equation (2.17) becomes

$$K_{n-1,n} = \frac{I_{A^{\pm} \cdot B_n}}{I_{A^{\pm} \cdot B_{n-1}} \cdot P_B} \quad (2.19)$$

The free energy of reaction (n-1,n) is then given by

$$\Delta G_{n-1,n} = -RT \ln K_{n-1,n} \quad (2.20)$$

where R is the gas constant and T the absolute temperature.

The expression

$$\Delta G_{n-1,n} = \Delta H_{n-1,n} - T \Delta S_{n-1,n} \quad (2.21)$$

when combined with (2.20) yields

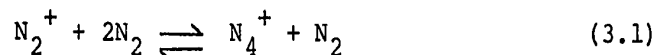
$$\log_{10} K_{n-1,n} = - \frac{\Delta H_{n-1,n}}{2.303 \cdot R} \cdot \frac{1}{T} + \frac{\Delta S_{n-1,n}}{2.303 \cdot R} \quad (2.22)$$

which is a form of van't Hoff's relationship. Thus from a study of the dependence of the equilibrium constant  $K_{n-1,n}$  on temperature one may deduce the thermodynamic parameters  $\Delta H_{n-1,n}$ ,  $\Delta S_{n-1,n}$ , and from (2.20)  $\Delta G_{n-1,n}$ .

III The Clustering Equilibrium  $N_2^+ + 2N_2 \rightleftharpoons N_4^+ + N_2$   
and the Bond Dissociation Energy of  $N_4^+$

3.1 Previous Work on  $N_4^+$

The clustering of nitrogen molecules about the  $N_2^+$  ion in the reaction



has been extensively studied with regard to the magnitude of the forward rate constant (95). Values of  $5$  to  $8 \times 10^{-29}$   $\text{cm}^6 \text{ molecule}^{-2} \text{ s}^{-1}$  were obtained by several authors. Thus the magnitude of the forward rate constant has been established with some certainty. This is not the case for the reverse reaction, or the position of the equilibrium. Knewstubb (96) has reported an equilibrium constant

$$K = \frac{P_{N_4^+}}{P_{N_2^+} \cdot P_{N_2}} = 75 \quad (3.2)$$

$T = 298^\circ\text{K}$ , standard state = 1 torr

However, previous work in this laboratory by Durden, Kebarle and Good (83) has demonstrated that the value of Knewstubb must be too low by several orders of magnitude.

The literature reports considerable disagreement as to the bond energy of  $N_4^+$ . Varney (97,98) has studied the mobility of  $N_2^+$  and  $N_4^+$  in nitrogen using a drift tube

60.

apparatus. He calculated the extent of dissociation of  $N_4^+$  from the change of ionic mobility with the variation in  $E/P_0$  (E being the electric field strength and  $P_0$  the reduced pressure of  $N_2$ ,  $P_0 = P_{\text{observed}} \times 273/T$ ). From the extent of the dissociation he deduced an equilibrium constant K. Varney also proposed a relationship between the ion temperature  $T_i$  and the  $E/P_0$  ratio of the form

$$T_i = T_{\text{gas}} + aE/P_0 \quad (3.3)$$

where a is a constant. A van't Hoff like plot ( $\ln K$  vs  $1/T_i$ ) was used to calculate a value for the dissociation energy  $D(N_2^+ - N_2) \cong -\Delta H$ . However two successive applications (97,98) of this technique lead to values of  $D(N_2^+ - N_2)$  of 11.5 and 20 kcal/mole. Conway (99) on the basis of an approximate SCF-MO treatment obtained  $D(N_2^+ - N_2) \sim 35$  kcal/mole. In order to determine  $D(N_2^+ - N_2)$  and to put the previous measurements from this laboratory on somewhat firmer ground a study of reaction (3.1) was undertaken.

### 3.2 Method of Measurement

The experiments in nitrogen were done before the development of the pulsing circuitry described in the experimental section. In this experiment the gas in the ion source was irradiated continuously with high energy electrons and ions were sampled continuously from the

system. It was assumed that the ratio of the measured ion intensities reflected the ratio of the partial pressures of the ions in the ion source. The equilibrium constant for reaction (3.1) was calculated using equation (2.19). Van't Hoff's relationship (see section 2.11) permits the evaluation of  $-\Delta H \sim D(N_2^+ - N_2)$  from the variation of the equilibrium constant with temperature.

### 3.3 Materials Used

The nitrogen used in the experiment was 99.998% pure (Matheson, Prepurified) and was passed through a liquid nitrogen trap to remove any water or other condensable impurities before being flowed through the ion source. A small ( $\leq 5\%$  in all experiments)  $O_2^+$  signal was observed. This impurity is not believed to significantly perturb the results.

### 3.4 Results and Discussion

As a test that the measured  $I_{N_4^+}/I_{N_2^+}$  reflected the equilibrium ratio at a given temperature a study of the variation of the equilibrium constant  $K$  with pressure of nitrogen gas was made at each experimental temperature. The results of this study are shown in Figure (3.1). As can be seen the equilibrium constants are independent of the pressure of nitrogen within the scatter of the experimental data over the pressure range 2.5 to 6.0 torr.



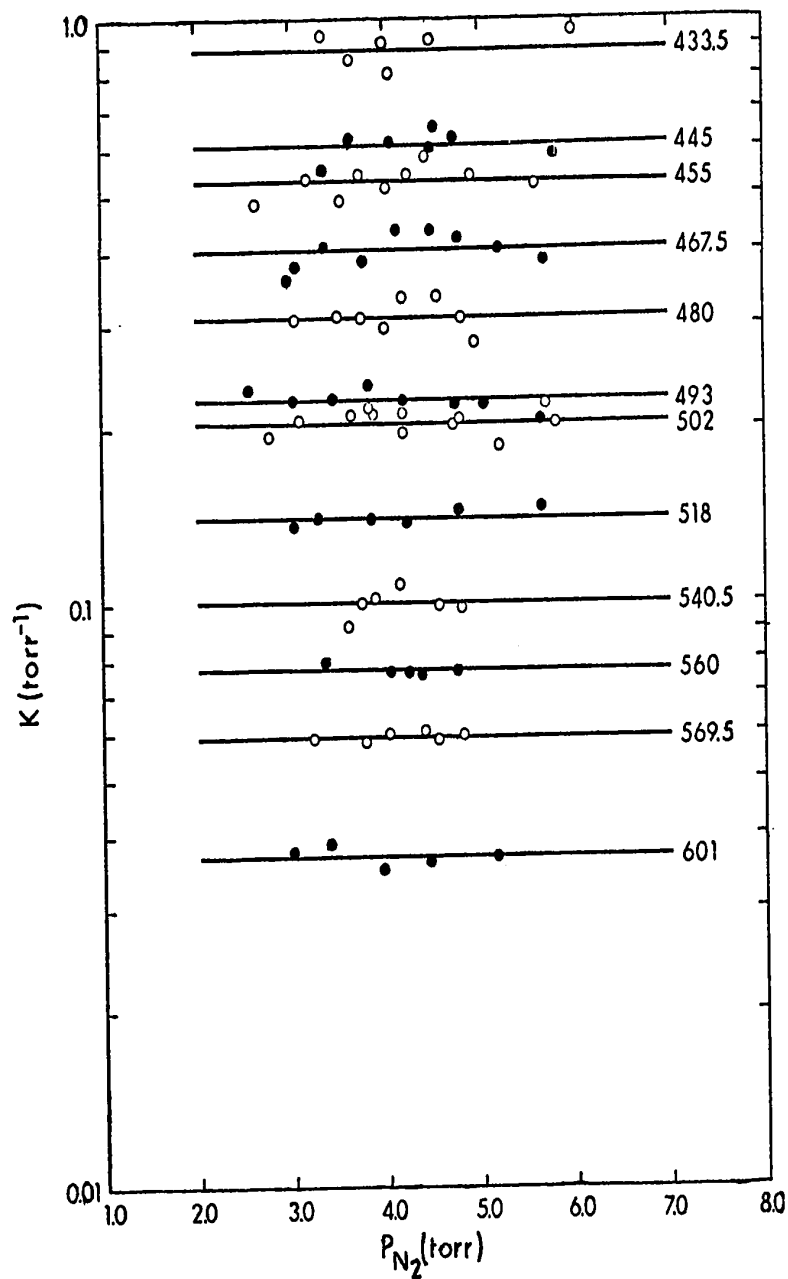
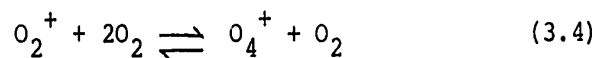


FIGURE 3.1. Plot of the equilibrium constant  $K$  for the reaction  $N_2^+ + N_2 \rightleftharpoons N_4^+$  as a function of nitrogen pressure. As may be seen  $K$  is independent of the nitrogen pressure at the various experimental temperatures ( $^{\circ}C$ ).

Shown in Figure (3.2) is a van't Hoff plot of the data which leads to the thermodynamic values for reaction (3.1) as presented in Table 3.1.

It is the paramount assumption in this study that the measured ion ratios reflect the equilibrium ion concentrations. In this experiment this assumption may be subject to considerable question specifically because the measurements were done at high temperatures (450°-600°C) where the forward reaction is slow but ionic diffusion to the walls is fast.

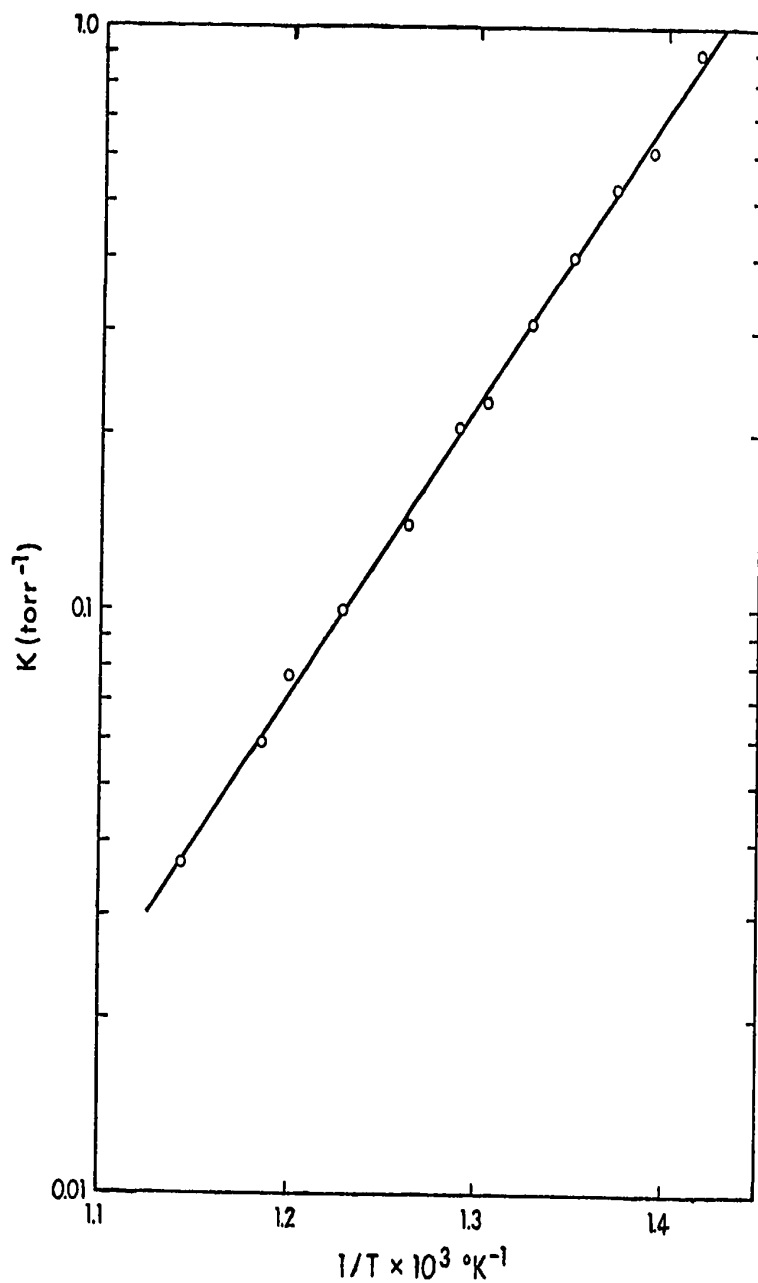
In a later chapter in this thesis there will be presented a study of the kinetics of the clustering reaction



in the temperature range 90-350°K. It was found in this study that the temperature dependence of the forward rate coefficient could be adequately expressed in the empirical form .

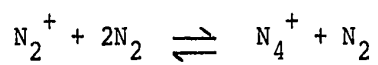
$$k_f \propto T^{-3.2} \quad (3.5)$$

Assuming this as a reasonable form of the temperature dependence of (3.1) and using Durden's (83) value of  $8 \times 10^{-29} \text{ cm}^6 \text{ molecule}^{-2} \text{ s}^{-1}$  for the forward rate of (3.1) at 300°K, a half life of the forward reaction of (3.1) at ~500°C and 4 torr of nitrogen may be calculated to be ~50  $\mu\text{s}$ . In the study of the  $\text{H}^+(\text{H}_2\text{O})_n$  system (to be pre-



**FIGURE 3.2.** van't Hoff plots of the data of Figure (3.1) for the reaction  $\text{N}_2^+ + \text{N}_2 \rightleftharpoons \text{N}_4^+$ . The thermodynamic data from this plot is summarized in Table 3.1.

TABLE 3.1

Thermodynamic Parameters for the Reaction

$-\Delta H \sim D(N_2^+ - N_2)^a$	$-\Delta S^{b,c}$	$-\Delta G^{a,c}$	$K^d$	Ref.
22.8	19.5	17.1	$\sim 4 \times 10^9$	present work
			75	Knewstubb (96)
11.5				Varney (1959) (97)
20				Varney (1965) (98)
$\sim 35$				Conway (99)

a In kcal/mole

b In entropy units

c Standard state 1 atmosphere, T = 298°K

d Standard state 1 torr, T = 298°K.

sented later) which was done at temperatures comparable to the nitrogen study and which had the benefit of the pulsing circuitry it was found that the total ion signal decays very fast at these high temperatures - much faster than had been believed at the time when the nitrogen study was performed. From the ion decay curves in the proton hydrate system it may be estimated that in the nitrogen system the average ion was probably in the ion source for only some 200  $\mu$ s. This exceeds the estimated half life of the forward reaction of (3.1) by only a factor of four. Thus not too safe a margin is left for the establishment of equilibrium particularly considering that the estimate of the half life may be regarded as rather questionable.

However, the values of K displayed in Figure (3.1) correspond to reaction (3.1) going only partially to completion. Thus after one or two half lives the reaction may be quite close to equilibrium. On the basis of this argument and the experimentally observed pressure independence of K, it is concluded that the reported value for  $\Delta H$  is not seriously in error.

The value of  $D(N_2^+ - N_2) \approx -\Delta H = 22.8$  kcal/mole compares favourably with the latest determination by Varney (98). The value of  $\Delta S = -19.5$  e.u. for reaction (3.1) may be compared to the value of  $-20.6$  e.u. obtained by Durden, Kebarle and Good (83) for reaction (3.4).

Thus the thermodynamic values presented here appear reasonable. The  $\Delta G(298) = -17.1$  kcal/mole (standard state 1 atm) leads to  $K(298) \sim 4 \times 10^9$  (standard state 1 torr). Thus the value of  $K(298) = 75$  reported by Knewstubb (96) appears to be in error. The  $N_2^+$  observed by Knewstubb presumably arose from non-equilibrium sources.

IV Kinetics of Reactions Leading to  $O_2^-(H_2O)_n$  in Moist  
Oxygen

4.1 Introduction

The reaction of  $O_2^-$  with water is probably of importance in the negative ion chemistry in the earth's lower ionosphere, particularly in the D region. The low temperatures ( $\sim 200^\circ K$ ) moderate pressures (torr range), and presence of trace amounts of water at these altitudes ensure that any stable positive or negative ion will be hydrated (100).

In this laboratory, Good, Durden and Kebarle (61) performed a study of the kinetics and mechanism of the formation of  $H^+(H_2O)_n$  in moist oxygen. It was thought that a study of the negative ion-molecule reactions in moist oxygen would not only complement the study of Good et al (61) but would be of interest in the ion chemistry of the D region.

4.2 Experimental

In order to determine the kinetics of the clustering reactions of water about the ion  $O_2^-$ , it is necessary to introduce oxygen into the ion source containing small but accurately known amounts of water. Water, because of its polar nature is readily absorbed and desorbed from the walls of any container. Consequently an attempt to prepare a static mixture containing known trace amounts

of water will fail. This difficulty necessitates the preparation of such mixtures in a flowing system. The flowing system has two distinct advantages. First by continuously renewing the gas in the ion source with a fresh sample, problems related to the accumulation of impurities in the ion source are largely eliminated. These impurities could result from degassing from the ion source walls, or from the ejection of impurities from the metal walls of the ion source upon electron bombardment. Second, the flowing system permits an equilibrium to be established between water being absorbed onto and being desorbed from the walls of the apparatus.

The partial pressure of water in the stream could be determined by measuring the moles/sec of  $H_2O$  added to the major (carrier) gas  $O_2$  whose flow rate was also measured. The partial pressure of water in the ion source was obtained from the following considerations. Equation (4.1) based on the ideal gas law

$$p = \frac{gRT}{MV} \quad (4.1)$$

relates  $P$ , the partial pressure of water,  $R$  the gas constant,  $T$  the absolute temperature,  $M$  the molecular weight of water,  $V$  the total volume of gas swept through the system in some time interval and  $g$  the weight of water introduced into the flowing stream during this time interval.



The volume  $V$  of gas passing through the system is then given by

$$V = \frac{760 \text{ ft}}{P_{\text{total}}} \quad (4.2)$$

where  $f$  is the flow rate of oxygen measured at 1 atmosphere,  $t$  is the time and  $P_{\text{total}}$  is the pressure of the major gas ( $O_2$ ) in the ion source. In all determinations the content of water in the major gas was  $\lesssim 1\%$ , thus its contribution to the flow is negligible compared to that of the major gas. Combining equations (4.1) and (4.2) we have

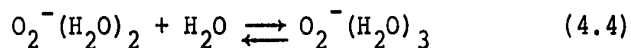
$$P = \frac{gRTP_{\text{total}}}{760 \text{ M ft}} \quad (4.3)$$

Equation (4.3) assumes that the minor component ( $H_2O$ ) and the carrier gas ( $O_2$ ) travel at the same speed. This is the usual assumption made for viscous flow.

As mentioned in the experimental chapter, water was added by a capillary from a small thermostated bulb of liquid water. In order to reproduce experimental results it was necessary to warm (with heating tape) the jacket which surrounded the capillary to a temperature which was above the highest temperature to which the water in the bulb was to be heated. Without this precaution the water vapour would condense in the capillary or the tubing leading to the capillary. This would result in meaningless weight loss measurements. Also the rate of water

introduction would be highly erratic as small droplets of water would be forced through the capillary.

When the partial pressure of water in the carrier gas was desired to be less than 10 mtorr it was found that the rate at which water was lost from the thermostated bulb was prohibitively slow. Furthermore, trace amounts of water  $\sim 0.2$  mtorr were always found in the gas passing through the ion source even after careful baking out of the apparatus at  $150^\circ\text{C}$ . This was attributed to outgassing from the elastomer seals of the valves of the gas handling system. These difficulties necessitated the use of an alternative method for measuring the partial pressure of water at low water concentrations. In almost all of the determinations performed in oxygen the achievement of equilibrium in the reaction



could be clearly observed. The measured intensity ratio of the clustered ions could be related to the partial pressure of water as follows:

$$K_{2,3} = \frac{I_{\text{O}_2^-(\text{H}_2\text{O})_3}}{I_{\text{O}_2^-(\text{H}_2\text{O})_2} \cdot P_{\text{H}_2\text{O}}} = 20 \quad (4.5)$$

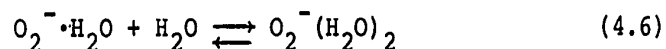
$T = 300.5^\circ\text{K}$ , standard state 1 torr.

The value of 20 for  $K_{2,3}$  was determined in a number of calibration runs where the partial pressure of water was known from weight loss measurements. The results of

72.

these calibration runs is shown in Figure (4.1). The dashed line at  $K_{2,3} = 20$  represents the value of the equilibrium constant measured earlier in these laboratories by Arshadi and Kebarle (101). Since the agreement between the presently observed value of  $K_{2,3}$  and the previous determination was satisfactory, the value of  $K_{2,3} = 20$  was adopted in the present work. It is gratifying to note that the experimentally determined equilibrium constant remains essentially independent of water pressure over a factor of  $\sim 500$ . The observation that the equilibrium constant was invariant over such a wide pressure range is taken as evidence that it is reasonable to assume that the measured equilibrium constant is independent of experimental artifacts. It was then assumed that the equilibrium constant method of determining water pressure will remain valid as the water pressure is lowered to the mtorr range, and that equation (4.5) will permit the evaluation of the partial pressure of water.

In experiments in which very small amounts of water ( $< 1$  mtorr) were used it was found that the position of the equilibrium in reaction (4.4) was so far to the left that the intensity of  $O_2^-(H_2O)_3$  could not be satisfactorily measured. However the equilibrium



could be observed clearly under these conditions. Using

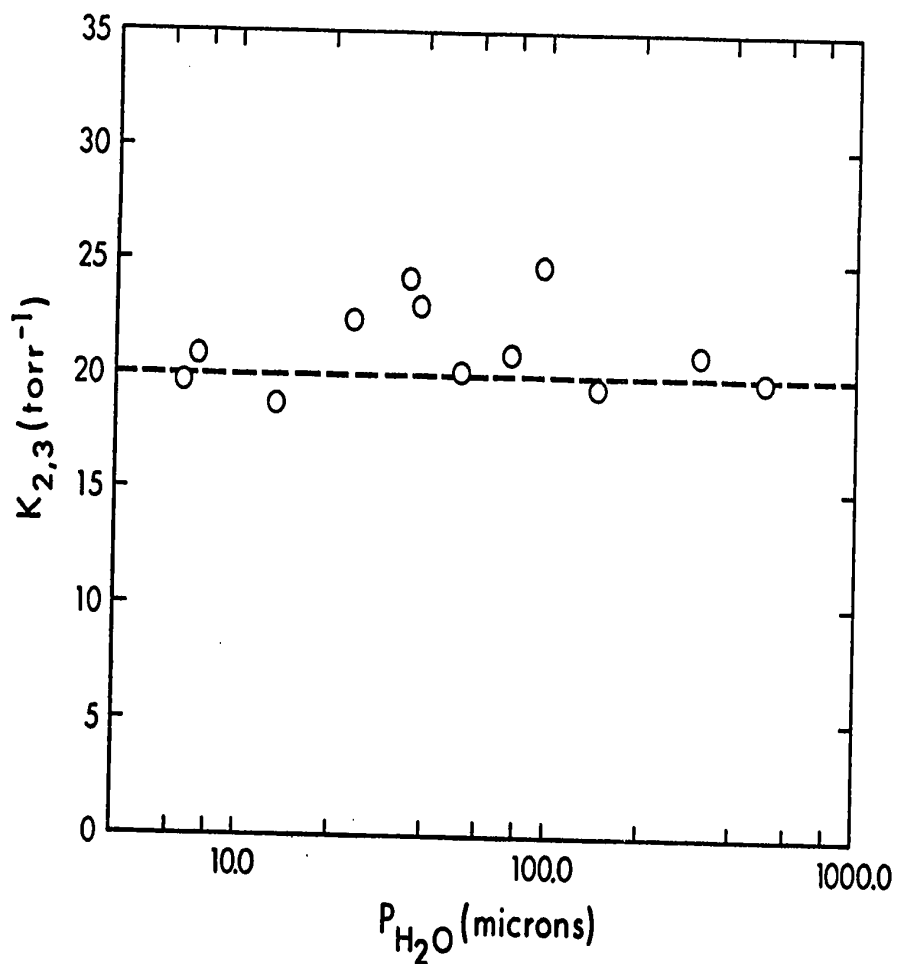


FIGURE 4.1. Determinations of the value of the equilibrium constant  $K_{2,3}$  for the reaction  $O_2^-(H_2O)_2 + H_2O \rightleftharpoons O_2^-(H_2O)_3$  at 300.5°K. Experimental points are the present results. Dashed line obtained from van't Hoff plots in earlier measurements in this laboratory (56,75) at higher water pressures.

the expression

$$K_{1,2} = \frac{I_{O_2^-(H_2O)_2}}{I_{O_2^-\cdot H_2O \cdot P_{H_2O}}} = 1600 \quad (4.7)$$

$T = 300.5^\circ K$ , standard state 1 torr, one could evaluate the partial pressure of water. The value of  $K_{1,2} = 1600$  was determined from measurements at higher water pressures when either the species  $O_2(H_2O)_n$ ,  $n = 1, 2, 3$  were clearly observed, and thus the partial pressure of water was determined from equation (4.5), or the partial pressure of water was known directly from weight loss measurements.

All of the experiments which were performed in the study of the hydration of  $O_2^-$  were conducted at ambient temperatures, that is without applying any power to the ion source heaters. Under these conditions the ion source would remain at  $300.5^\circ K$  for prolonged periods of time if suitable care was exercised to ensure a constant room temperature.

In order to ensure that the water pressure in the ion source had reached a stable equilibrium value, the gas mixture was flowed through the apparatus for at least a few hours before any measurements were undertaken. After roughly an hour the relative ratios of the clustered species at equilibrium remained constant indicating that a stable water pressure had been achieved.

For most of the experiments performed in this study the ion signal when the electron beam was pulsed was

$10^3 - 10^4$  counts/sec. This signal intensity permitted a satisfactory temporal profile of an ion to be accumulated in the multichannel scales in some 3 minutes. The time dependence of the signals was recorded as rapidly as possible so as to minimize error due to drifting of the overall signal intensity. If the total signal intensity drifted significantly, i.e.  $\gtrsim 10\%$ , during the course of an experiment, the data were discarded, the instrumental problem rectified and the experiment repeated.

In these experiments the duration of the electron pulse delivered to the ion source was  $\sim 10 \mu\text{s}$ . The repetition rate was some 6 ms except for some runs at low total pressures where diffusion of ions to the walls is rapid. Under these conditions a pulse repetition rate of 2 to 3 ms was used to enhance the signal intensity. For most runs the dwell time per channel in the multichannel scaler was set at  $20 \mu\text{s}$ , although in cases of slow reactions (low water pressure) a dwell time of  $30 \mu\text{s}$  was used.

#### 4.3 Results and Discussion

##### A Ion Production

The dominant ion initially in moist oxygen is  $\text{O}_2^-$  which constitutes  $\sim 90\%$  of the total ionization. The  $\text{O}_2^-$  ion is presumably produced by the electron attachment reaction (4.8).



The electrons involved in reaction (4.8) are presumably secondary electrons which have been degraded to thermal energies. The small (~10%) amount of  $O_2^-$  which is initially produced presumably arises from the dissociative attachment process



The electrons involved in reaction (4.9) must have greater than thermal energies since (4.9) is endothermic (102).

It was found that the reaction sequence involving  $O_2^-$  did not convert to the reaction sequence involving  $O^-$ . The reaction products of both ions were found to behave independently of each other with time, demonstrating the absence of interconversion. The results of the  $O_2^-$  reactions will be considered first and then the reactions of  $O^-$ .

B Reactions Leading to  $O_2^-(H_2O)_n$  in Moist Oxygen

In Figures (4.2 - 4.18) are shown the normalized ion intensities for the seventeen runs in moist oxygen. The solid curves connecting the experimental points are the calculated ion intensity profiles based on the measured rate coefficients (which are summarized in Tables 4.1 and 4.2) and the proposed reaction mechanism. For simplicity

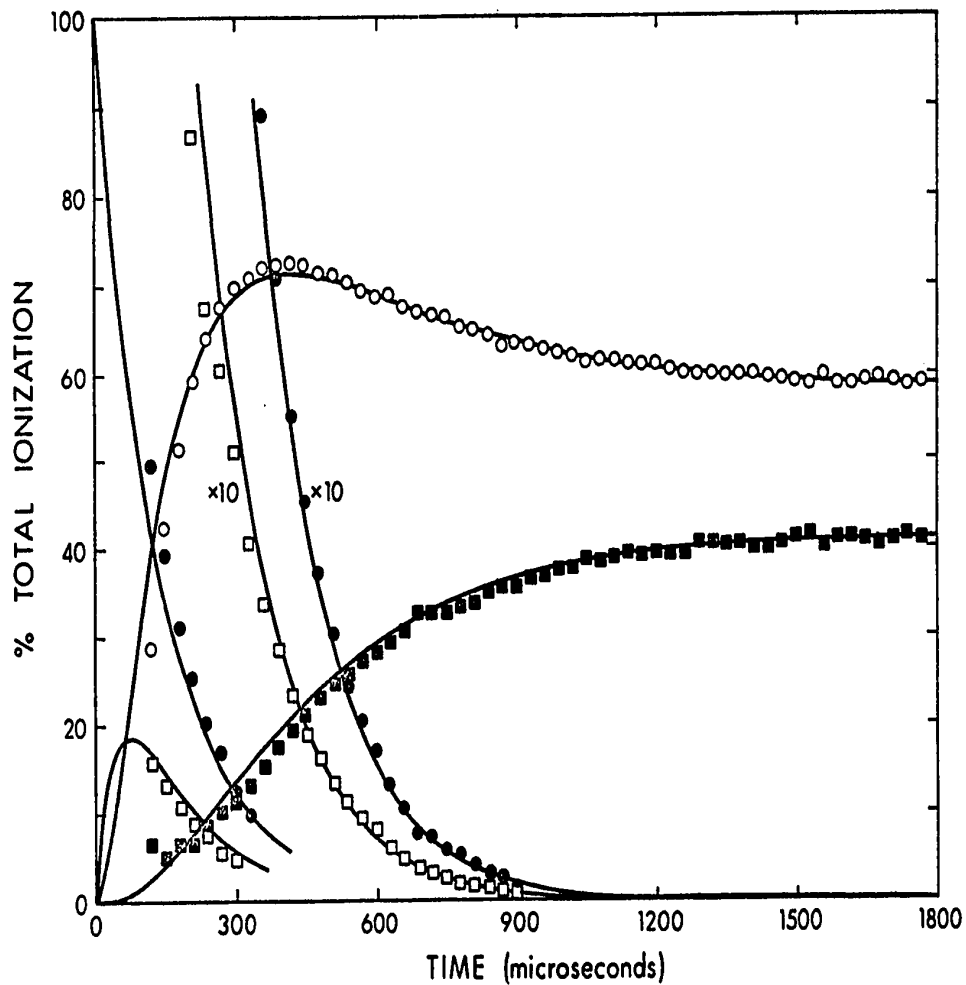


FIGURE 4.2. Time dependence of normalized ion intensities. The curves are the calculated time dependence for the rate parameters summarized in Table 4.1.  $P_{O_2} = 3.98$  torr,  $P_{H_2O} = 0.41$  mtorr, ●  $O_2^-$ , □  $O_4^-$ , ○  $O_2^- \cdot H_2O$ , and ■  $O_2^-(H_2O)_2$ . The  $O_4^-$  maybe clearly seen at this low water pressure.



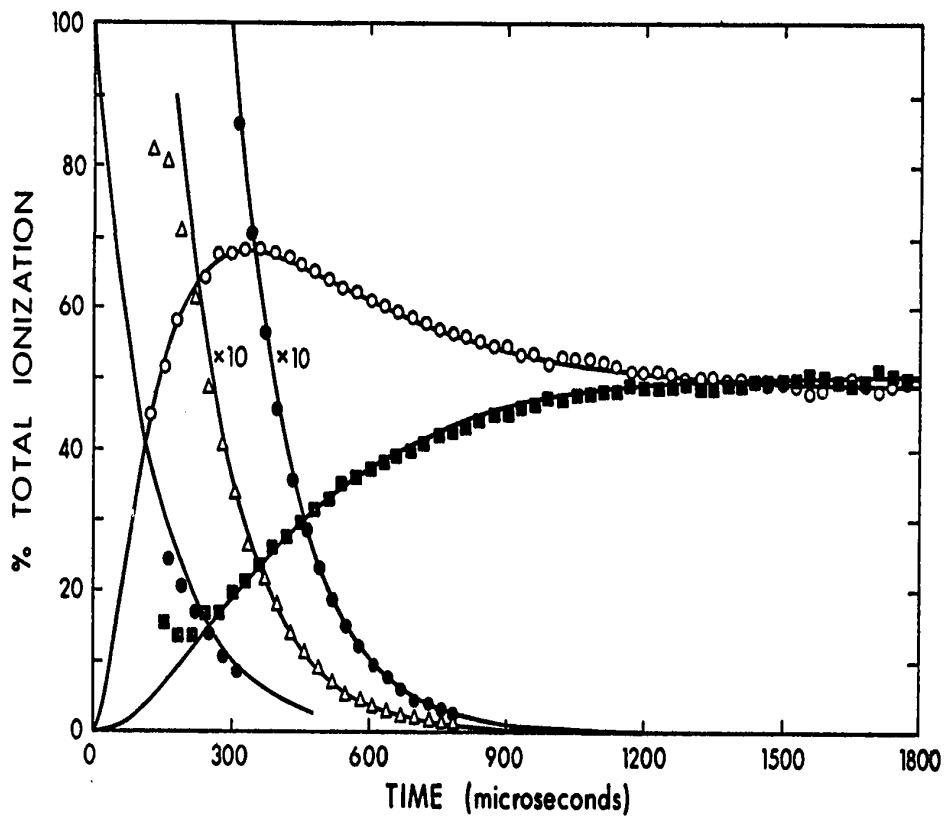
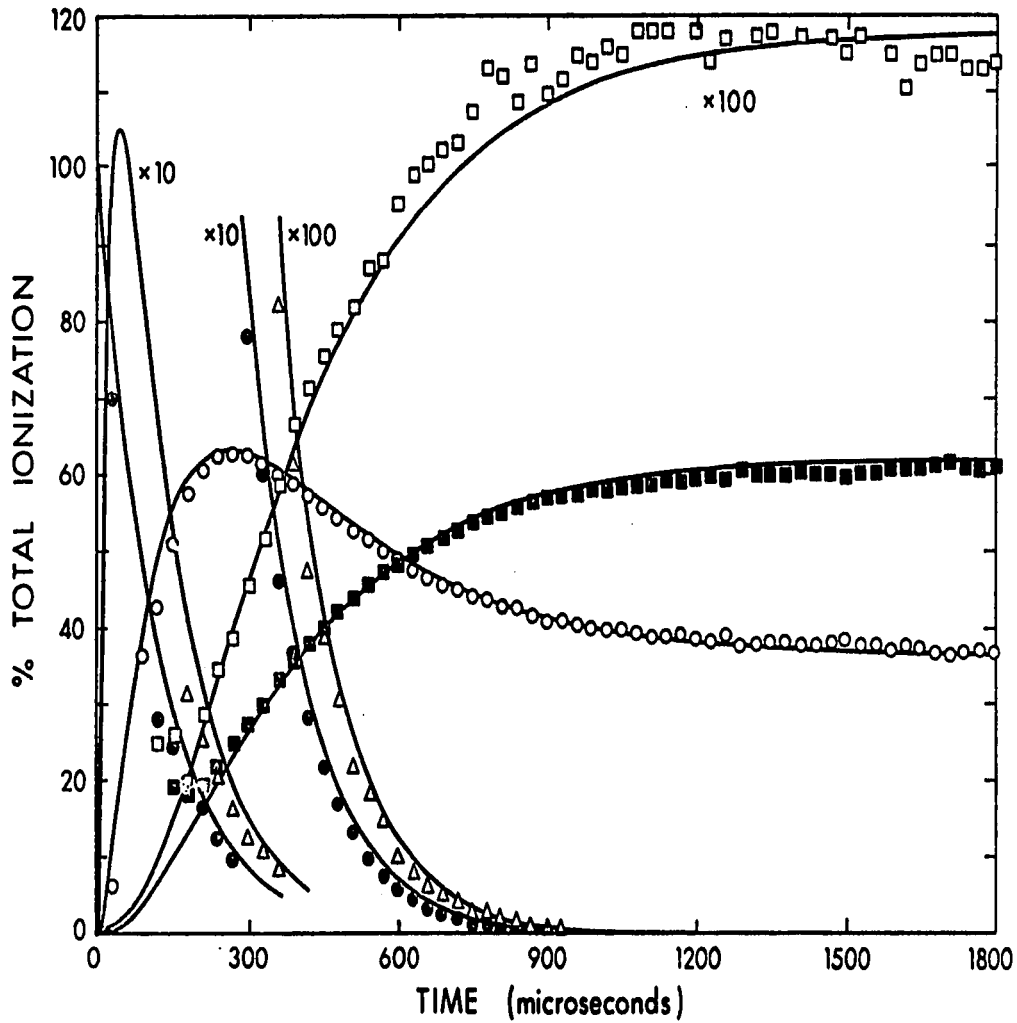


FIGURE 4.3. Time dependence of normalized ion intensities for the rate parameters summarized in Table 4.1.  $P_{O_2} = 3.95$  torr,  $P_{H_2O} = 0.65$  mtorr,  $\bullet$   $O_2^-$ ,  $\Delta$   $O_4^-$ ,  $\circ$   $O_2^- \cdot H_2O$ , and  $\blacksquare$   $O_2^-(H_2O)_2$ . The  $O_4^-$  may be clearly seen at this low water pressure



**FIGURE 4.4.** Time dependence of normalized ion intensities for the rate parameters summarized in Table 4.1.  $P_{O_2} = 3.92$  torr,  $P_{H_2O} = 1.00$  mtorr, ●  $O_2^-$ , △  $O_4^-$ , ○  $O_2^-\cdot H_2O$ , ■  $O_2^-(H_2O)_2$ , and □  $O_2^-(H_2O)_3$ . The  $O_4^-$  may be clearly seen at this low water pressure.

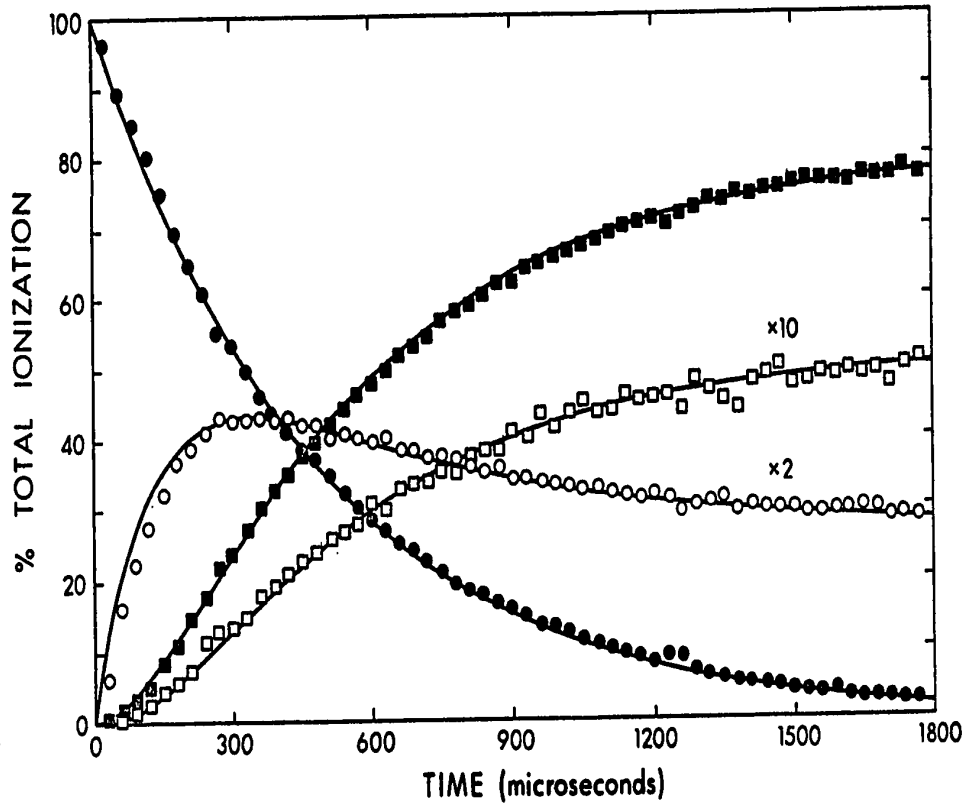


FIGURE 4.5. Time dependence of normalized ion intensities for the rate parameters summarized in Table 4.1.  $P_{O_2} = 1.68$  torr,  $P_{H_2O} = 3.39$  mtorr. ●  $O_2^-$ , ○  $O_2^- \cdot H_2O$ , ■  $O_2^-(H_2O)_2$ , and □  $O_2^-(H_2O)_3$ .

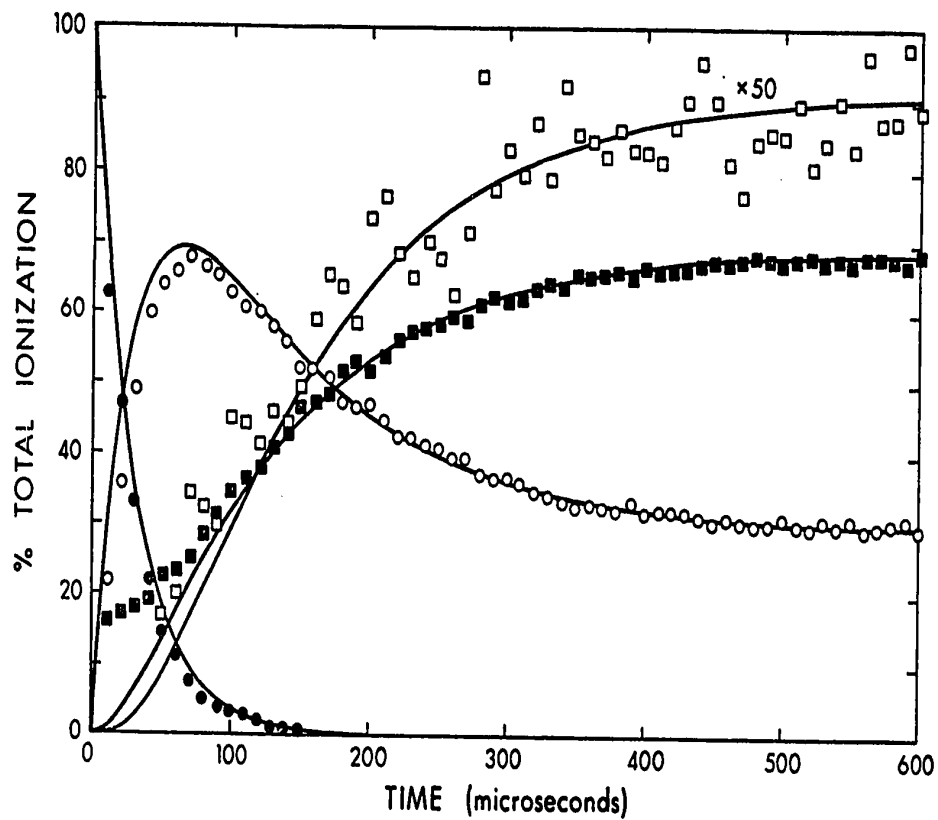


FIGURE 4.6. Time dependence of normalized ion intensities for the rate parameters summarized in Table 4.1.  $P_{O_2} = 7.85$  torr,  $P_{H_2O} = 1.40$  mtorr,  $\bullet$   $O_2^-$ ,  $\circ$   $O_2^-\cdot H_2O$ ,  $\blacksquare$   $O_2^-(H_2O)_2$ , and  $\square$   $O_2^-(H_2O)_3$ .

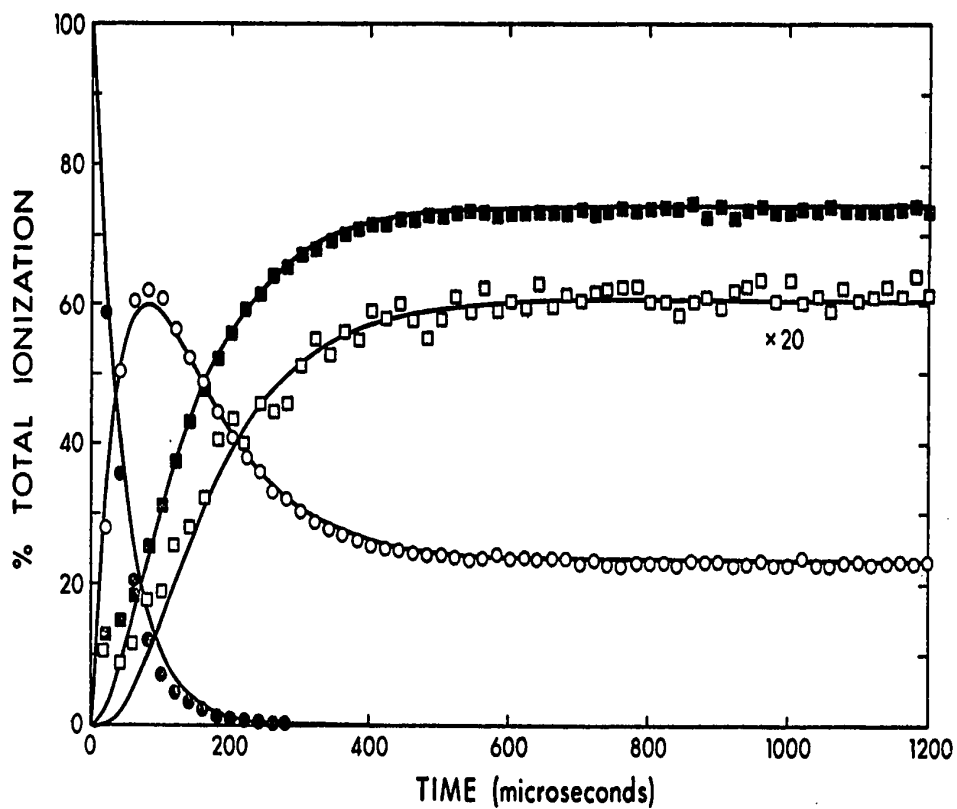


FIGURE 4.7. Time dependence of normalized ion intensities for the rate parameters summarized in Table 4.1.  $P_{O_2} = 6.20$  torr,  $P_{H_2O} = 2.13$  mtorr,  $\bullet$   $O_2^-$ ,  $\circ$   $O_2^-(H_2O)$ ,  $\blacksquare$   $O_2(H_2O)_2$ , and  $\square$   $O_2^-(H_2O)_3$ .

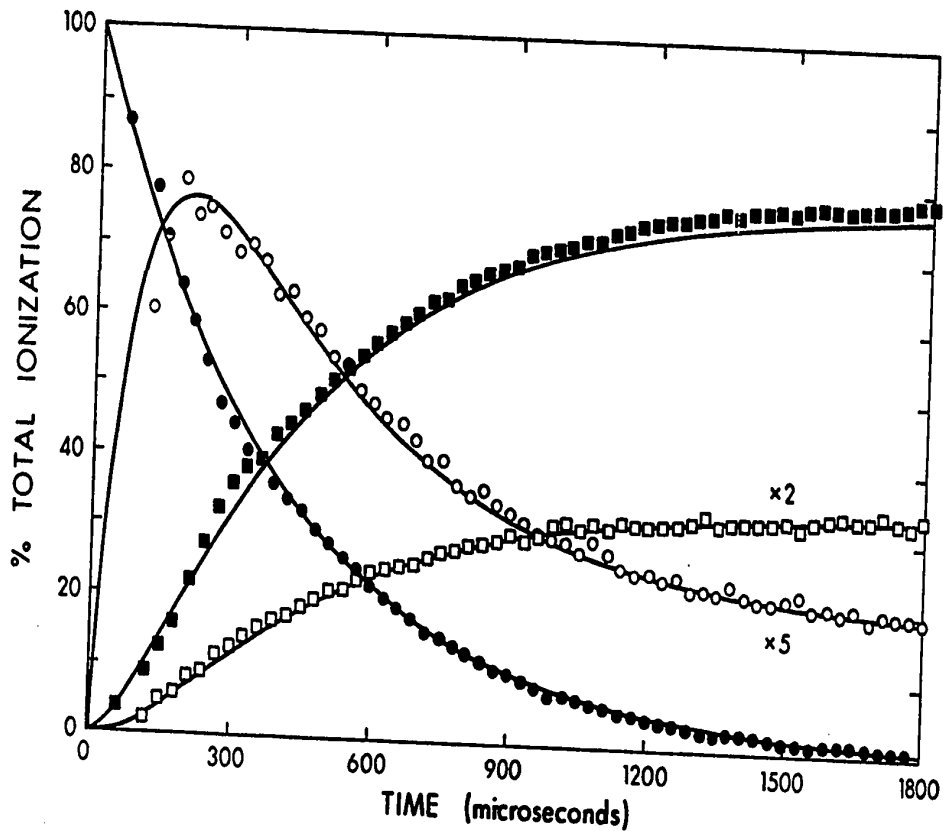


FIGURE 4.8. Time dependence of normalized ion intensities for the rate parameters summarized in Table 4.1.  $P_{O_2} = 0.96$  torr,  $P_{H_2O} = 11.8$  mtorr,  $\bullet$   $O_2^-$ ,  $\circ$   $O_2^-\cdot H_2O$ ,  $\blacksquare$   $O_2^-(H_2O)_2$ , and  $\square$   $O_2^-(H_2O)_3$ .

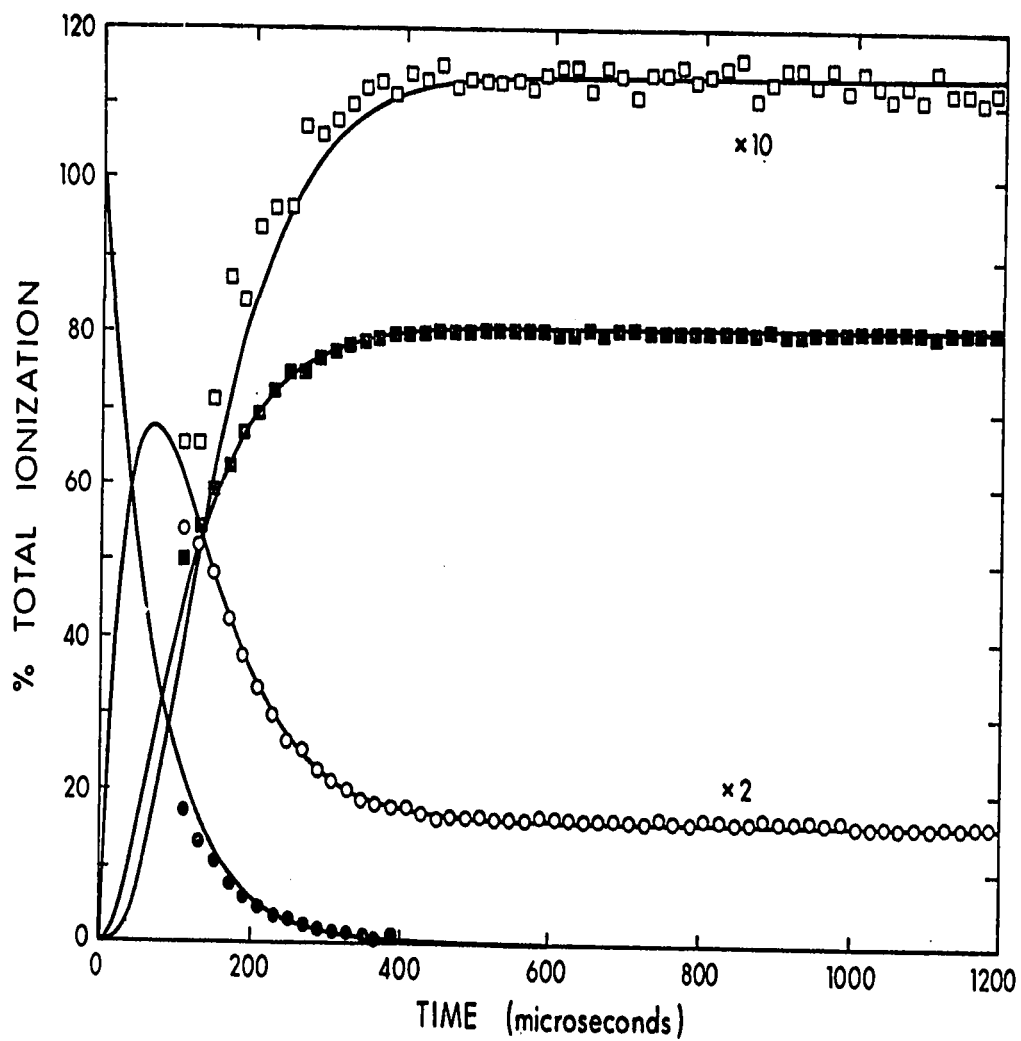


FIGURE 4.9. Time dependence of normalized ion intensities for the rate parameters summarized in Table 4.1.  $P_{O_2} = 4.42$  torr,  $P_{H_2O} = 6.63$  mtorr,  $\bullet$   $O_2^-$ ,  $\circ$   $O_2^-\cdot H_2O$ ,  $\blacksquare$   $O_2^-(H_2O)_2$ , and  $\square$   $O_2^-(H_2O)_3$ .

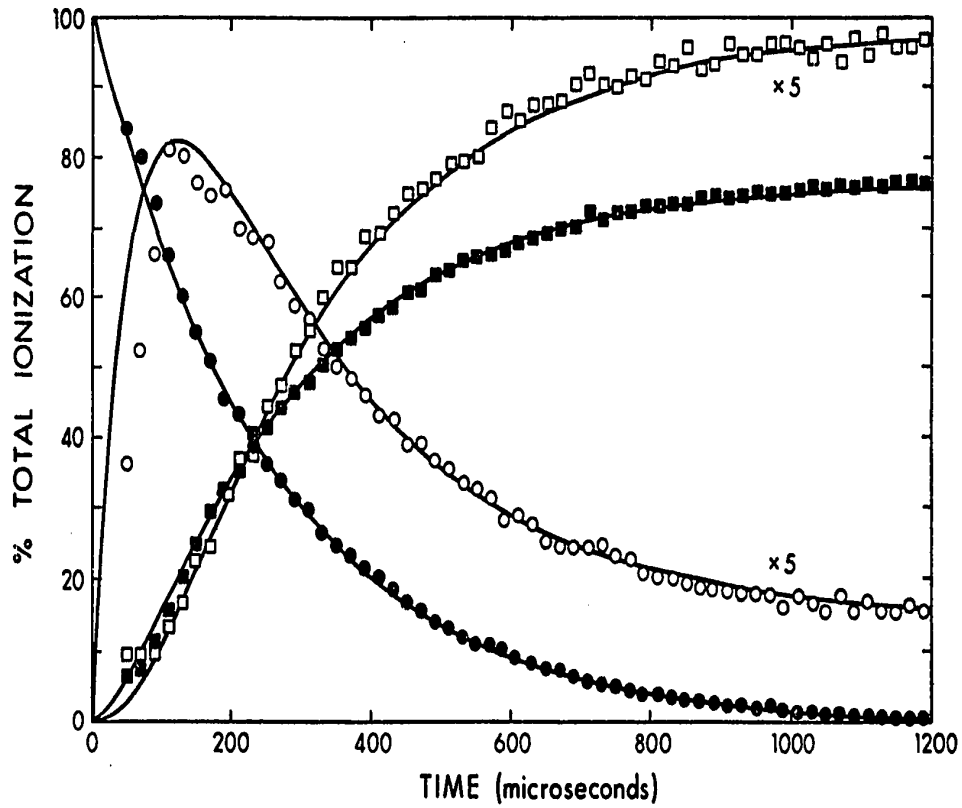


FIGURE 4.10. Time dependence of normalized ion intensities for the rate parameters summarized in Table 4.1.  $P_{O_2} = 1.34$  torr,  $P_{H_2O} = 13.0$  mtorr,  $\bullet$   $O_2^-$ ,  $\circ$   $O_2^-\cdot H_2O$ ,  $\blacksquare$   $O_2^-(H_2O)_2$ , and  $\square$   $O_2^-(H_2O)_3$ .



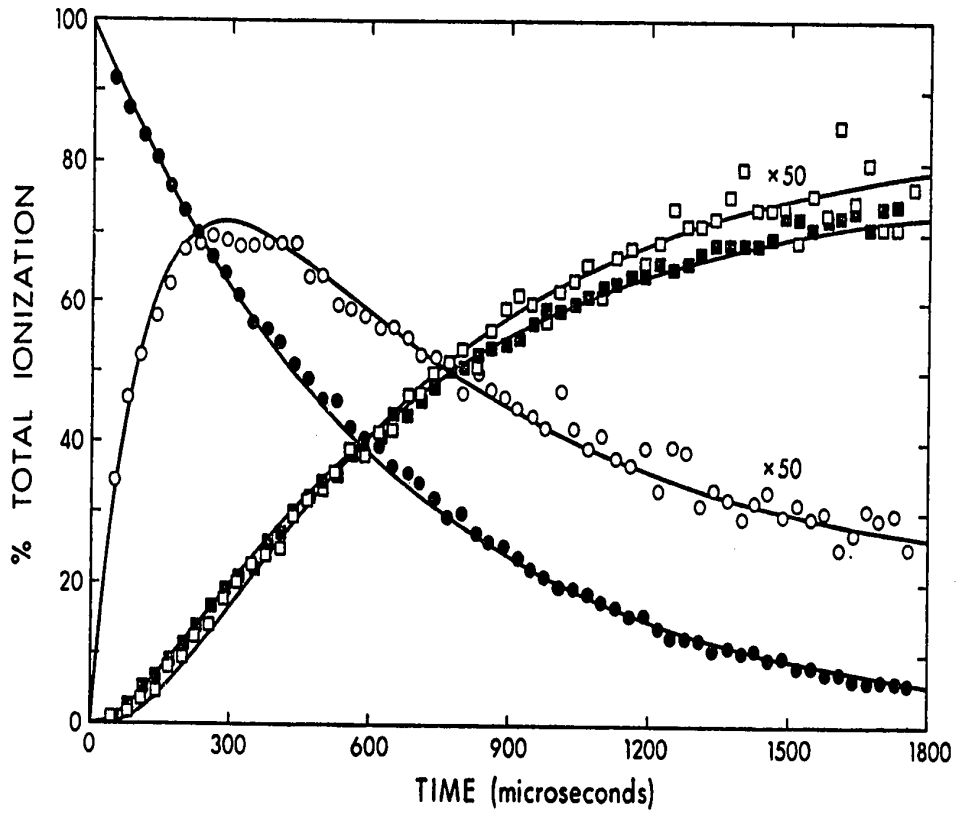


FIGURE 4.11. Time dependence of normalized ion intensities for the rate parameters summarized in Table 4.1.  $P_{O_2} = 0.64$  torr,  $P_{H_2O} = 10.0$  mtorr.  
 ●  $O_2^-$ , ○  $O_2^-\cdot H_2O$ , ■  $O_2^-(H_2O)_2$  and □  $O_2^-(H_2O)_3$ .

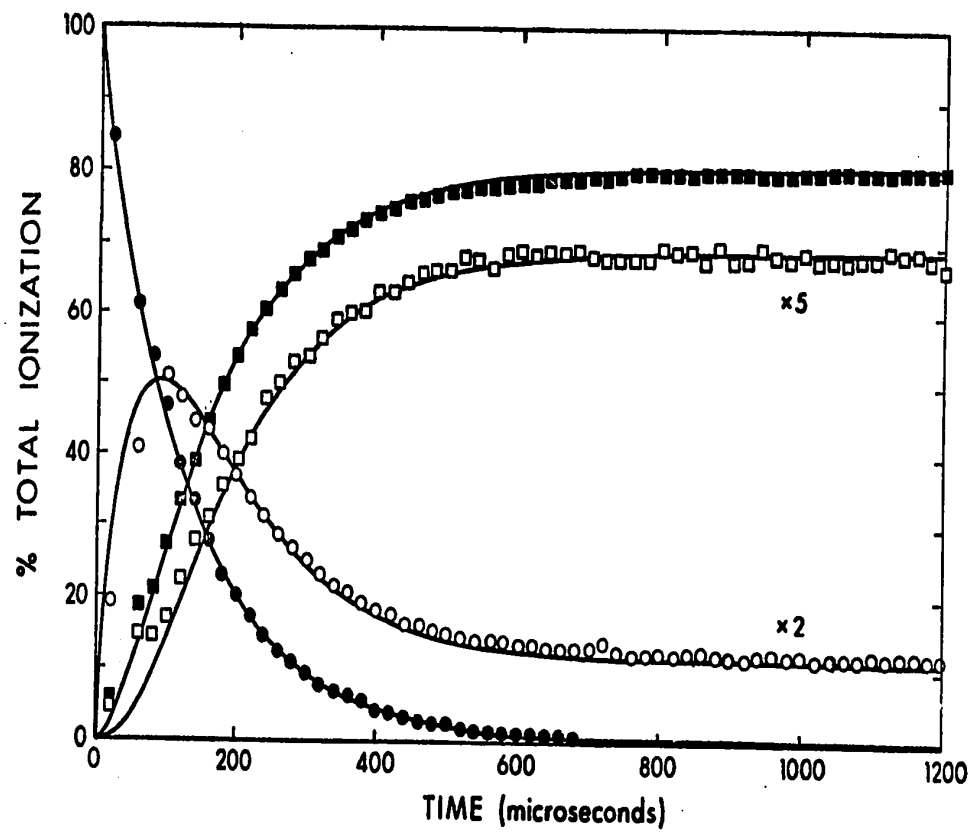


FIGURE 4.12. Time dependence of normalized ion intensities for the rate parameters summarized in Table 4.1.

$P_{O_2} = 2.82$  torr.  $P_{H_2O} = 8.21$  mtorr. ●  $O_2^-$ , ○  $O_2^-\cdot H_2O$ ,  
■  $O_2^-(H_2O)_2$  and □  $O_2^-(H_2O)_3$ .

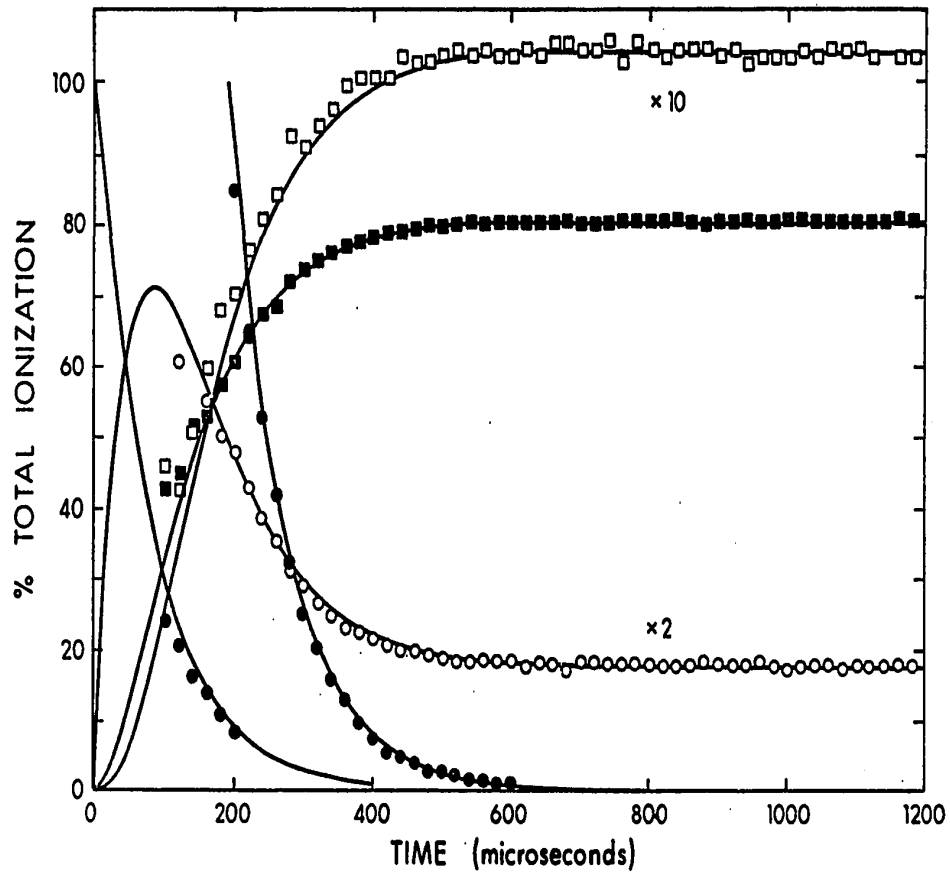


FIGURE 4.13. Time dependence of normalized ion intensities for the rate parameters summarized in Table 4.1.  $P_{O_2} = 3.96$  torr,  $P_{H_2O} = 6.06$  mtorr,  $\bullet$   $O_2^-$ ,  $\circ$   $O_2^- \cdot H_2O$ ,  $\blacksquare$   $O_2^-(H_2O)_2$ , and  $\square$   $O_2^-(H_2O)_3$ .

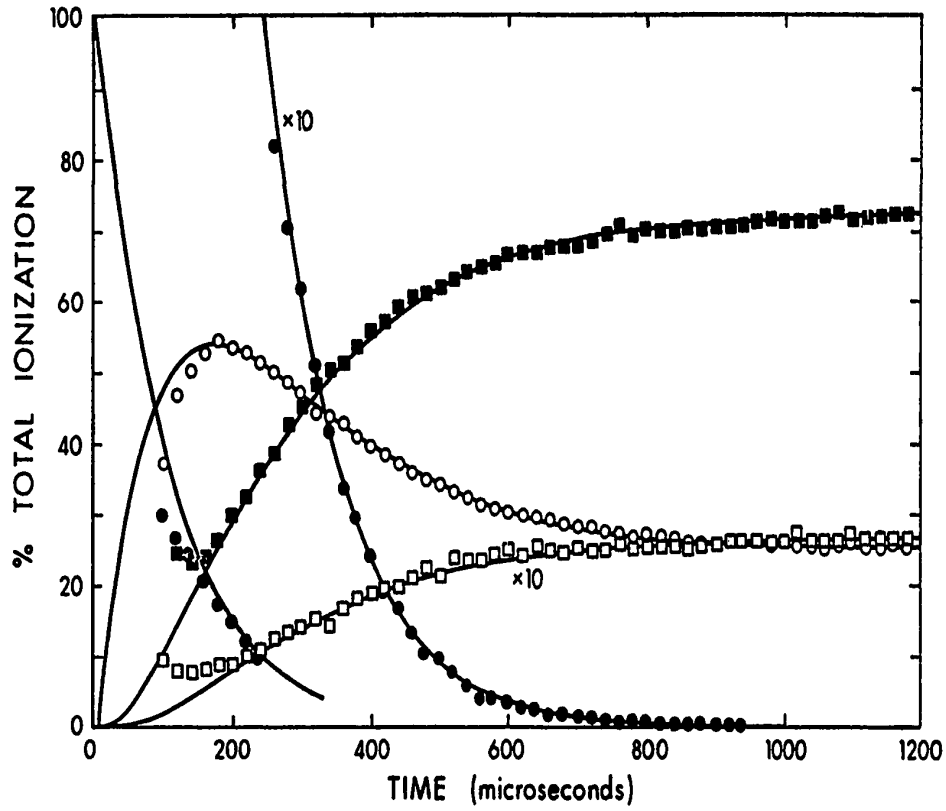


FIGURE 4.14. Time dependence of normalized ion intensities for the rate parameters summarized in Table 4.1.

$P_{O_2} = 3.92$  torr,  $P_{H_2O} = 1.78$  mtorr, ●  $O_2^-$ , ○  $O_2 \cdot H_2O$ , ■  $O_2^-(H_2O)_2$ , and □  $O_2^-(H_2O)_3$ .

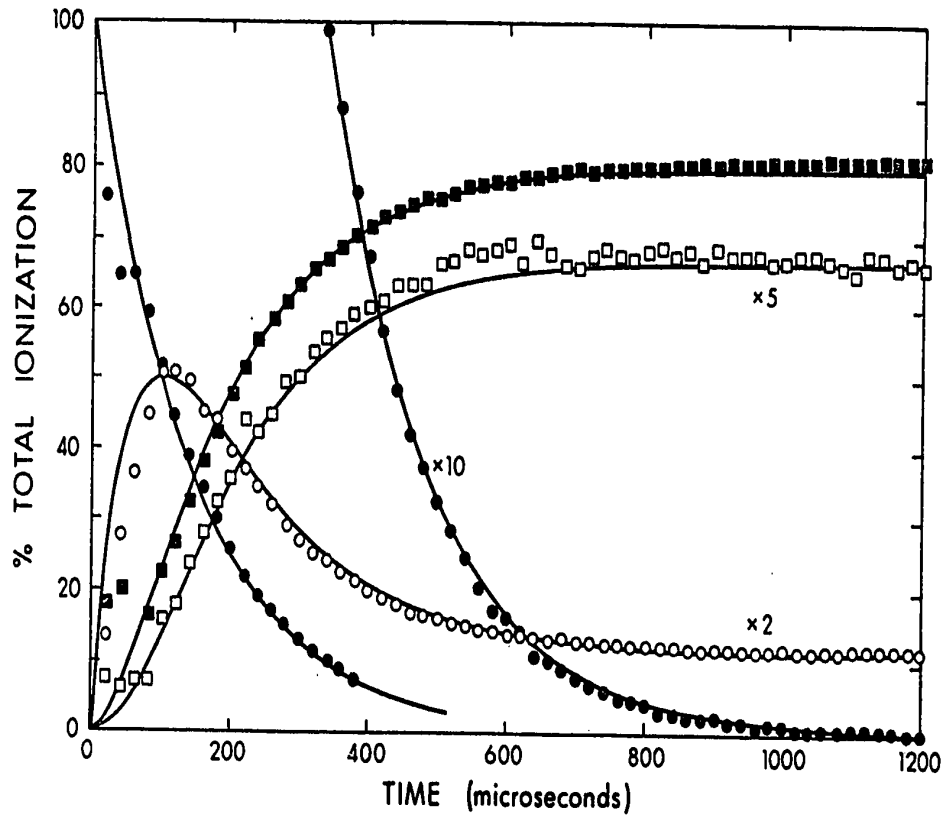


FIGURE 4.15. Time dependence of normalized ion intensities for the rate parameters summarized in Table 4.1.  $P_{O_2} = 2.55$  torr,  $P_{H_2O} = 8.58$  mtorr,  $\bullet$   $O_2^-$ ,  $\circ$   $O_2^-\cdot H_2O$ ,  $\blacksquare$   $O_2^-(H_2O)_2$ , and  $\square$   $O_2^-(H_2O)_3$ .

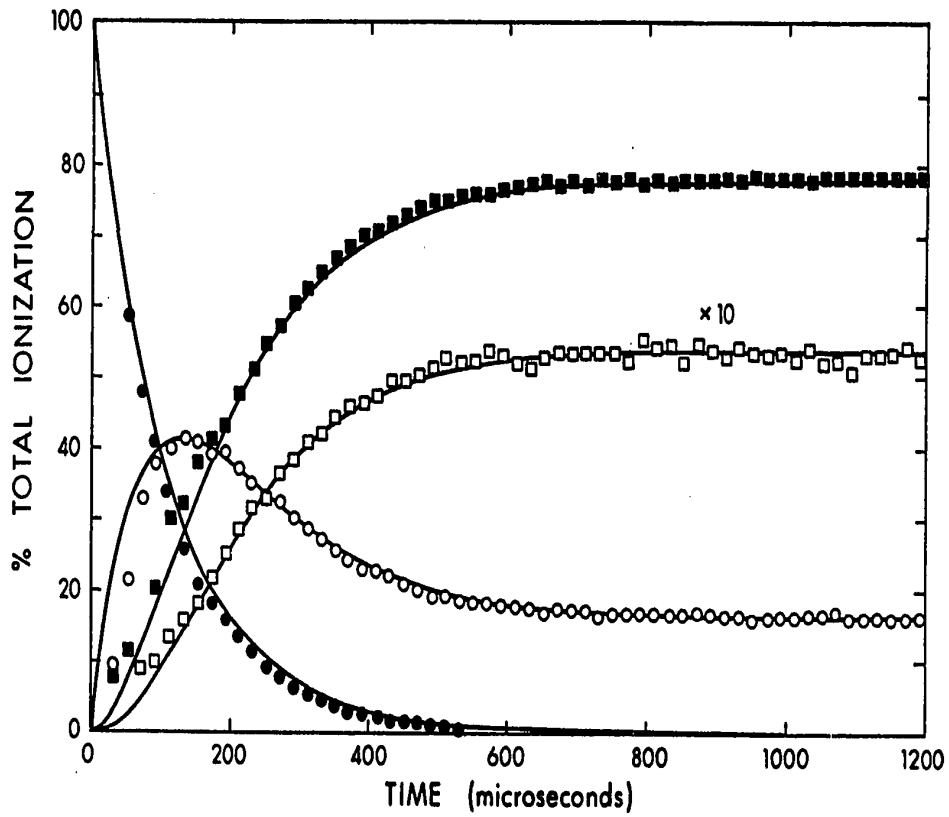


FIGURE 4.16. Time dependence of normalized ion intensities for the rate parameters summarized in Table 4.1.  $P_{O_2} = 3.29$  torr,  $P_{H_2O} = 3.63$  mtorr,  $\bullet$   $O_2^-$ ,  $\circ$   $O_2^-\cdot H_2O$ ,  $\blacksquare$   $O_2^-(H_2O)_2$ , and  $\square$   $O_2^-(H_2O)_3$ .

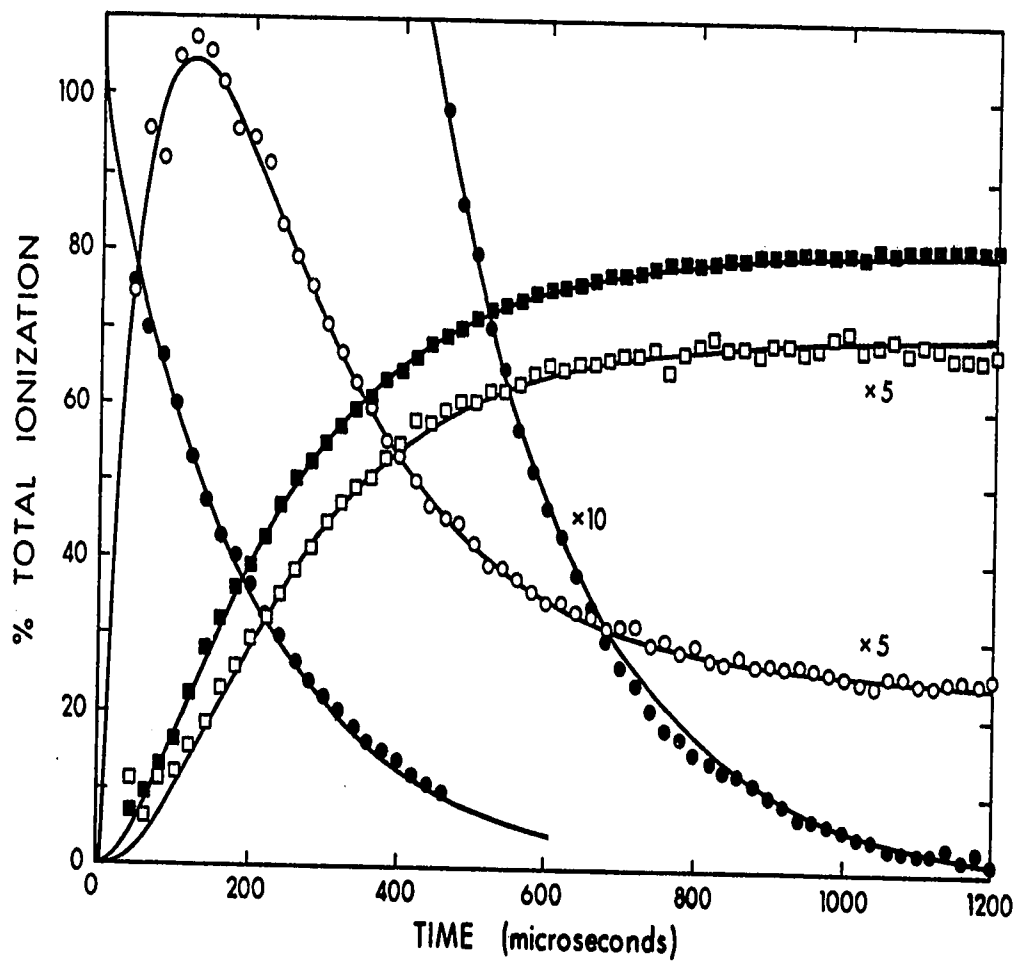


FIGURE 4.17. Time dependence of normalized ion intensities for the rate parameters summarized in Table 4.1.  $P_{O_2} = 2.12$  torr,  $P_{H_2O} = 8.13$  mtorr,  $\bullet$   $O_2^-$ ,  $\circ$   $O_2^-\cdot H_2O$ ,  $\blacksquare$   $O_2^-(H_2O)_2$ , and  $\square$   $O_2^-(H_2O)_3$ .

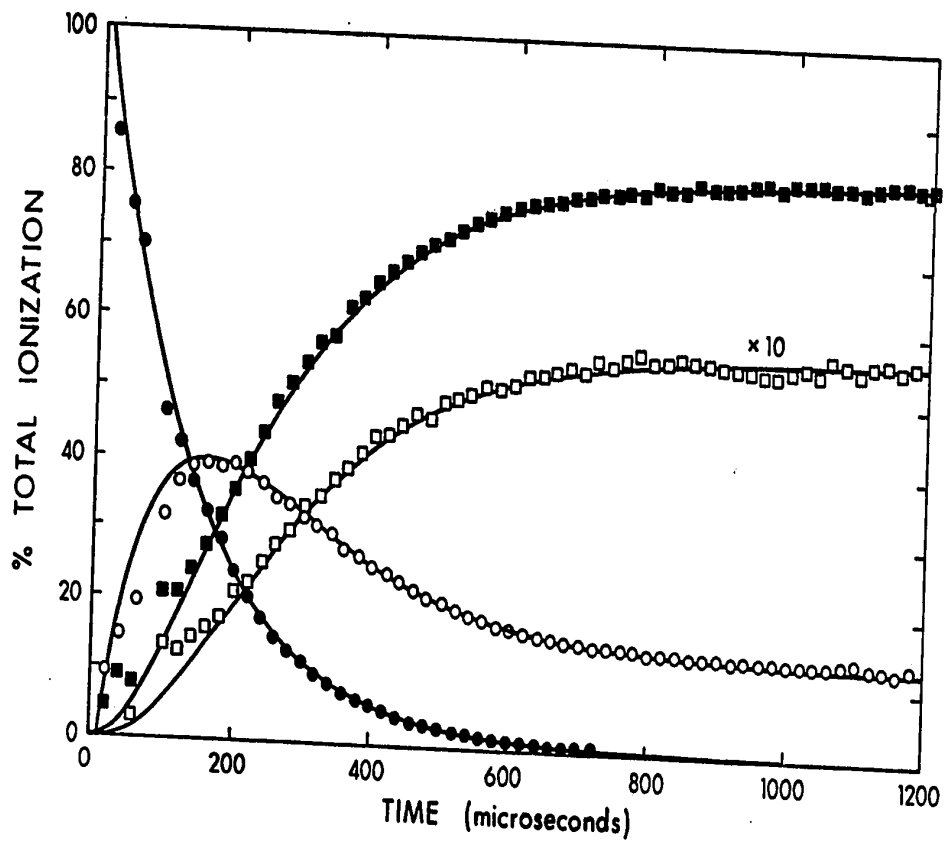


FIGURE 4.18. Time dependence of normalized ion intensities for the rate parameters summarized in Table 4.1.  $P_{O_2} = 3.90$  torr,  $P_{H_2O} = 3.19$  mtorr, ●  $O_2^-$ , ○  $O_2^-\cdot H_2O$ , ■  $O_2^-(H_2O)_2$ , and □  $O_2^-(H_2O)_3$ .



TABLE 4.1

Calculated Values of Rate Coefficients for Reactions Leading  
to  $O_2^-(H_2O)_n$  in Moist Oxygen<sup>a</sup>

Fig. <sup>b</sup>	$P_{O_2}$ <sup>c</sup>	$P_{H_2O}$ <sup>d</sup>	$v_1^e$	$v_{-1}^e$	$v_2^e$	$v_3^e$	$v_4^e$	$v_{-4}^e$	$v_5^e$	$v_{-5}^e$
4.2	3.98	0.41	7.50	2.05	0.667	21.2	1.39	1.97		
4.3	3.95	0.65	8.25	2.06	0.578	27.8	1.78	1.69		
4.4	3.92	1.00	8.25	2.11	0.888	55.6	2.39	1.47	0.583	38.9
4.5	1.68	3.39		2.28			6.62	1.14	2.00	28.0
4.6	7.85	1.40		30.5			6.66	2.83	1.09	36.7
4.7	6.20	2.13		24.1			7.92	2.50	1.36	27.1
4.8	0.96	11.8		2.69			10.0	0.528	6.03	21.3
4.9	4.42	6.63		15.5			18.9	1.89	4.16	26.5
4.10	1.34	13.0		4.35			16.9	0.706	6.21	24.2
4.11	0.64	10.0		1.69			8.19	0.47	4.81	18.9
4.12	2.82	8.21		8.54			17.4	1.21	5.75	29.1
4.13	3.96	6.06		13.1			14.5	1.58	4.21	28.8
4.14	3.92	1.78		9.38			4.18	1.46	1.02	27.1
4.15	2.55	8.58		7.32			15.6	1.14	6.67	39.5
4.16	3.29	3.63		7.32			6.64	1.06	1.95	27.8
4.17	2.12	8.13		5.58			15.3	0.936	6.84	39.4
4.18	3.90	3.19		10.0			9.08	1.79	2.91	38.4

<sup>a</sup> T = 300°K

<sup>b</sup> Figure in which data is displayed

<sup>c</sup> Pressure in torr

<sup>d</sup> Pressure in mtorr

<sup>e</sup> v's in units of  $10^3 s^{-1}$

TABLE 4.2

Rate Constants Leading to  $O_2^-(H_2O)_n$  in Moist Oxygen

Reaction	Present <sup>a</sup>	Pack & Phelps <sup>b</sup>	Others
$O_2^- + 2O_2 \rightleftharpoons O_4^- + O_2$	5.1	4	$3^c, 3.5^d$ $\times 10^{-31e}$
$O_4^- + H_2O \longrightarrow O_2^- H_2O + O_2$	1.6 <sup>f</sup>	1.8	$2.7^c, 2.8^d$ $\times 10^{-14g,f}$
$O_2^- + H_2O + O_2 \longrightarrow O_2^- H_2O + O_2$	1.5	1.3	$\times 10^{-9f,h}$
$O_2^- H_2O + H_2O + O_2 \rightleftharpoons O_2^-(H_2O)_2 + O_2$	1.6	3	$\times 10^{-28e,h}$
	5.4	4	$\times 10^{-28e}$
	1.1	0.71	$\times 10^{-14f}$
$O_2^-(H_2O)_2 + H_2O \rightleftharpoons O_2^-(H_2O)_3$	$2.2 \times 10^{-11}$ f,i		
	$3.5 \times 10^3$ s <sup>-1</sup> , i		

<sup>a</sup> All measurements done at 300.5°K. Other authors are for ~300°K.

<sup>b</sup> Ref. 108, J. L. Pack and A. V. Phelps, Bull. Am. Phys. Soc., 16, 214 (1971).

<sup>c</sup> Ref. 110, L. G. McKnight and J. M. Sawina, Bull. Am. Phys. Soc., 15, 434 (1970).

<sup>d</sup> C. Sharer, Ph.D. Thesis, University of Colorado (1970), as quoted in footnote h.

<sup>e</sup> In units of cm<sup>6</sup> molecule<sup>-2</sup> s<sup>-1</sup>.

<sup>f</sup> In units of cm<sup>3</sup> molecule<sup>-1</sup> s<sup>-1</sup>

(continued.....)

Footnotes to Table 4.2 continued

<sup>g</sup> Calculated assuming  $K = k_1/k_{-1} = 3.1 \times 10^{17}$  cm<sup>3</sup> molecule (30).

<sup>h</sup> Phelps (A.V. Phelps, Aeronomy Report #48, COSPAR Symposium on D and E

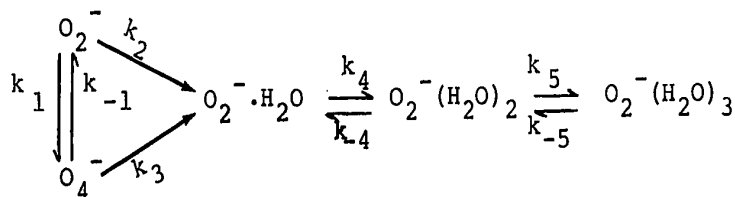
Region Ion Chemistry, Urbana, Illinois, July 1971) has reanalysed the data of ref.(108) and concludes that the reaction  $O_2^- \cdot H_2O \longrightarrow O_2^- \cdot H_2O$  is second order with  $k = 1.7 \times 10^{-11}$  cm<sup>3</sup> molecule<sup>-1</sup> s<sup>-1</sup>. However, the data is quite scattered ref.(109).

<sup>i</sup> Probably valid only for oxygen pressures greater than ~2 torr.

97.

the ions of the reaction sequence involving  $O_2^-$  are not expressed as a percent of the total ions but as a percentage of the total ionization arising from  $O_2^-$ .

An examination of Figures (4.2-4.4) shows that the  $O_2^-$  ion decays rapidly with time followed by the appearance of  $O_2^- \cdot H_2O$  and  $O_4^-$ . The  $O_4^-$  could only be satisfactorily observed at low water pressures. The increase in intensity of the ions  $O_2^-(H_2O)_2$  and  $O_2^-(H_2O)_3$  and the equilibrium between them occur at later times. On the basis of these observations the following reaction mechanism is proposed for the hydration of  $O_2^-$  in moist oxygen.



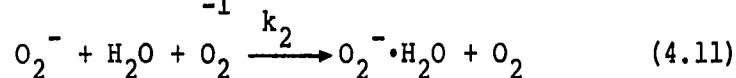
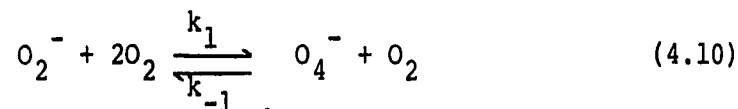
Scheme I

The density of neutral molecules in the ion source ( $\sim 10^{17} \text{ cm}^{-3}$ ) is vastly greater than the estimated maximum density of ions ( $\sim 10^9 \text{ cm}^{-3}$ ). Consequently the density of neutrals is not significantly perturbed in the course of a reaction. Therefore the reaction of the various ions are first order in ion and zero order in neutral concentration for a given experimental determination. In order to determine the order of a reaction it is necessary

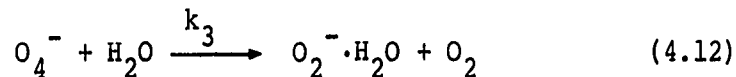
to perform the experiment at a variety of neutral concentrations and to examine the dependence of the apparent first order rate coefficient on these concentrations.

C. Determination of  $k_1$ ,  $k_2$  and  $k_{-1}$

The  $O_2^-$  ion disappears by two competing reactions



The  $O_4^-$  ion is rapidly converted to  $O_2^- \cdot H_2O$  via



The observation that the ions  $O_2^-$  and  $O_4^-$  decay below the limits of detection at long reaction times demonstrates that the reverse of reactions (4.11) and (4.12) are not significant under the present conditions. The rates of the reverse of (4.11) and (4.12) were approximated as zero in subsequent calculations.

The normalized  $O_2^-$  ion intensity was observed to decay exponentially over several decades in all experiments. Some examples of these decays are shown in Figure (4.19). From the measured values of  $k_1$ ,  $k_{-1}$  and  $k_3$  it can be shown that in most of the present experiments  $\nu_3 > 10^2 \nu_{-1}$  where the  $\nu_i$  are the apparent first order reaction frequencies. The apparent first order rate coefficient,  $\nu_T$ , for the disappearance of  $O_2^-$  may be

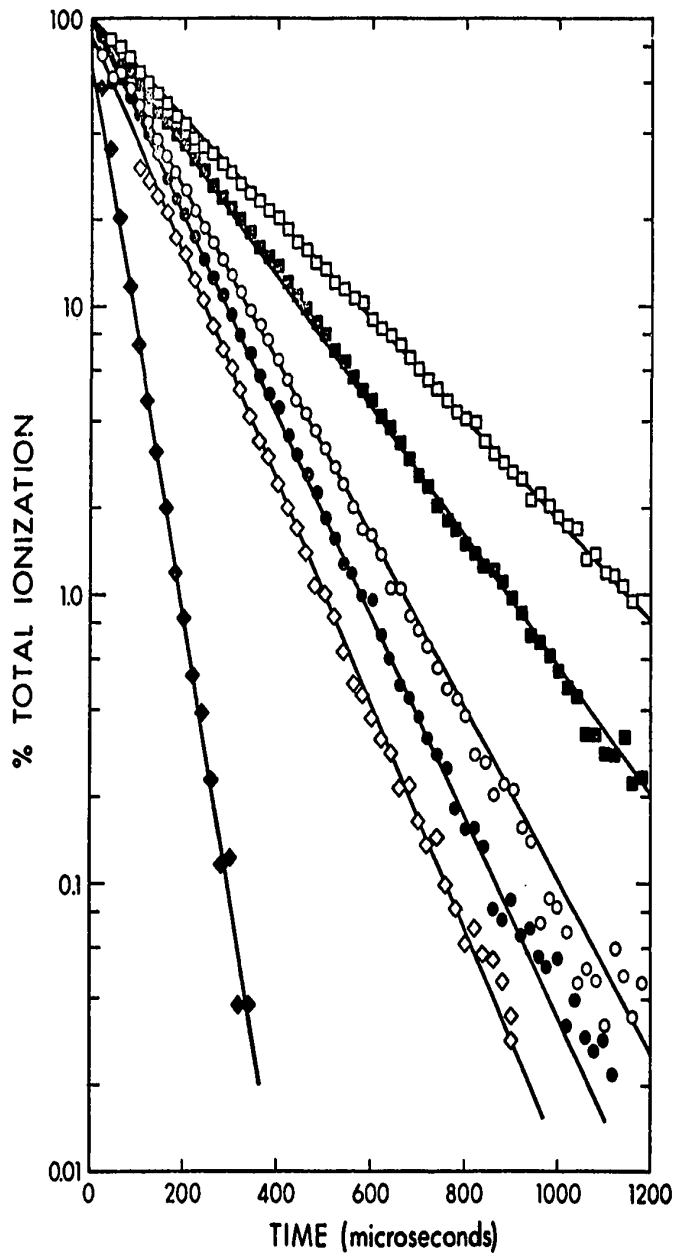


FIGURE 4.19. Plots of  $\log [O_2^-]$  versus time. Slope gives  $v_T$  the apparent rate of disappearance of  $O_2^-$  (see equation (4.14) at different reaction conditions. First number given is  $P_{O_2}$  in torr, number in brackets is  $P_{H_2O}$  in mtorr, and third number is  $v_T$  in units of  $10^3 s^{-1}$ . 0 2.55 (8.58) 7.32,  $\square$  1.34 (12) 4.35,  $\blacksquare$  2.12 (8.13) 5.58,  $\bullet$  2.82 (8.21) 8.54,  $\diamond$  3.92 (1.78) 9.38 and  $\blacklozenge$  6.2 (2.13) 24.1.

expressed as

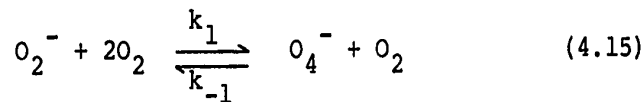
$$v_T = k_1 [O_2]^2 + k_2 [H_2O][O_2] \quad (4.13)$$

where the  $k_i$  are the termolecular rate coefficients and [A] symbolizes the concentration or partial pressure of A. The resulting  $v_T$  may be used to evaluate  $k_1$  and  $k_2$ . Dividing equation (4.13) by  $[O_2][H_2O]$  expression (4.14) is obtained.

$$\frac{v_T}{[H_2O][O_2]} = k_1 \frac{[O_2]}{[H_2O]} + k_2 \quad (4.14)$$

Thus a plot of  $\frac{v_T}{[H_2O][O_2]}$  vs  $\frac{[O_2]}{[H_2O]}$  should yield a straight line of slope  $k_1$  and intercept  $k_2$ . A plot of this type is displayed in Figure (4.20). From this plot values of  $k_1 = 5.1 \times 10^{-31} \text{ cm}^6 \text{ molecule}^{-2} \text{ s}^{-1}$  and  $k_2 = 1.6 \times 10^{-28} \text{ cm}^6 \text{ molecule}^{-2} \text{ s}^{-1}$  were determined.

The equilibrium constant K for the reaction



may be expressed as

$$K = \left\{ \frac{[O_4^-]}{[O_2^-][O_2]} \right\} \text{ at equilibrium} = \frac{k_1}{k_{-1}} \quad (4.16)$$

The equilibrium constant K was not directly determined

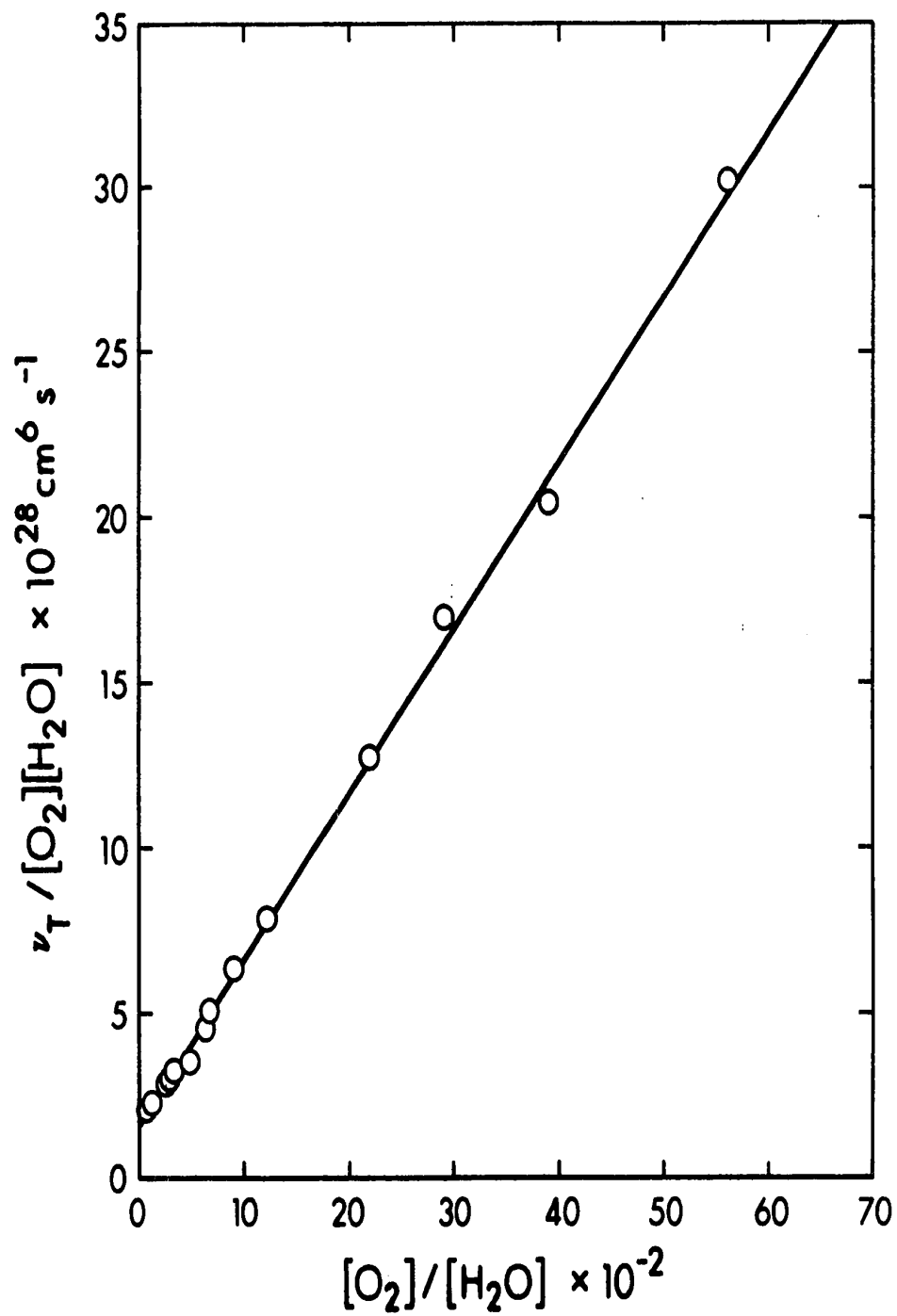


FIGURE 4.20. Plot of  $v_T / [O_2][H_2O]$  versus  $[O_2] / [H_2O]$ . Slope leads to  $k_1 = 5.1 \times 10^{-31} \text{ cm}^6 \text{ molecule}^{-2} \text{ s}^{-1}$  and intercept to  $k_2 = 1.6 \times 10^{-28} \text{ cm}^6 \text{ molecule}^{-2} \text{ s}^{-1}$ .



in this work owing to the inability to remove traces of water from the system. However, Conway and Nesbitt (30) report a value of  $K = 3.1 \times 10^{-17} \text{ cm}^3 \text{ molecule}^{-1}$  at  $300^\circ\text{K}$ . Using the present value of  $k_1 = 5.1 \times 10^{-31} \text{ cm}^6 \text{ molecule}^{-2} \text{ s}^{-1}$  a value of  $k_{-1} = 1.6 \times 10^{-14} \text{ cm}^3 \text{ molecule}^{-1} \text{ s}^{-1}$  was calculated using equation (4.16).

#### D. Computer Calculation of $k_3$ to $k_5$

The values of the  $\nu_i$  ( $i = \pm 1, \dots, \pm 5$ ) may be determined by calculating the temporal profile of the normalized ion intensities for various values of the  $\nu_i$ . The  $\nu_i$  may then be treated as variables and adjusted until optimum agreement is achieved between the observed and calculated intensity profiles. Utilizing the numbering sequence shown in Scheme I the set of differential equations which describe the system is

$$\frac{d[\text{O}_2^-]}{dt} = -(k_1 + k_2)[\text{O}_2^-] + k_{-1}[\text{O}_4^-] \quad (4.17)$$

$$\frac{d[\text{O}_4^-]}{dt} = k_1[\text{O}_2^-] - (k_{-1} + k_3)[\text{O}_4^-] \quad (4.18)$$

$$\frac{d[\text{O}_2^- \cdot \text{H}_2\text{O}]}{dt} = -k_4[\text{O}_2^- \cdot \text{H}_2\text{O}] + k_2[\text{O}_2^-] + k_3[\text{O}_4^-] + k_{-4}[\text{O}_2^- (\text{H}_2\text{O})_2] \quad (4.19)$$

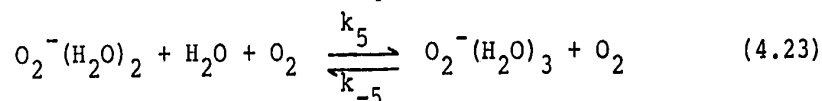
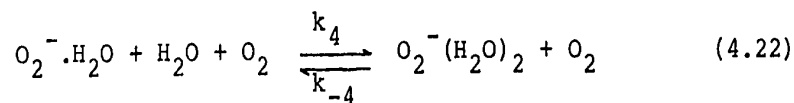
$$\frac{d[\text{O}_2^- (\text{H}_2\text{O})_2]}{dt} = -(k_5 + k_{-4})[\text{O}_2^- \cdot \text{H}_2\text{O}] + k_{-5}[\text{O}_2^- (\text{H}_2\text{O})_3] + k_4[\text{O}_2^- \cdot \text{H}_2\text{O}] \quad (4.20)$$

$$\frac{d[\text{O}_2^-(\text{H}_2\text{O})_3]}{dt} = k_5 [\text{O}_2^-(\text{H}_2\text{O})_2] - k_{-5} [\text{O}_2^-(\text{H}_2\text{O})_3] \quad (4.21)$$

with boundary conditions  $t = 0$ ,  $[\text{O}_2^-] = 1$  and [all other species] = 0.

Such a set of equations undoubtedly possesses a solution in a closed analytical form (103). However, the equations may be readily solved using an analogue computer. An analogue computer (Yokogawa Electronic Works Type 3302) will rapidly generate solutions to the above equations to an accuracy of better than 1%. The analogue computer programme is given in Appendix I. The solid curves connecting the experimental points in Figures (4.2-4.18) are the analogue computer calculated ion intensities based on the  $v_i$  which are summarized in Table 4.1. In practice it was found that the curves could be fitted with a precision better than 10%. However, as the calculations proceeded on in the reaction sequence, the error increased and is estimated to be ~20% for  $v_{\pm 5}$ . The increased error is caused by the dependency of the final rate constants on those which preceded them and because the shape of the curves at the end of the reaction sequence is not very sensitive to the selected values of  $v_{\pm i}$ .

Reactions (4.22) and (4.23) might well be expected to exhibit an all over third order dependence while the reverse reactions would be expected to exhibit a second order dependence .



It follows that if the above equations are correct

$$v_i = k_i [\text{H}_2\text{O}] [\text{O}_2] \quad i = 4, 5 \quad (4.24)$$

and

$$v_{-i} = k_{-i} [\text{O}_2] \quad (4.25)$$

Thus a plot of  $v_i/[\text{H}_2\text{O}]$  vs  $[\text{O}_2]$  should yield a straight line of slope  $k_i$ . A plot of  $v_4/[\text{H}_2\text{O}]$  vs  $[\text{O}_2]$  is shown in Figure (4.21) from which it may be seen that reaction (4.22) indeed displays a dependence on the total gas pressure. From Figure (4.21) a value of  $k_4 = 5.4 \times 10^{-28} \text{ cm}^6 \text{ molecule}^{-2} \text{ s}^{-1}$  may be calculated. A plot of  $v_{-4}$  vs  $[\text{O}_2]$  is shown in Figure (4.22). The line corresponds to  $k_{-4} = 1.1 \times 10^{-14} \text{ cm}^3 \text{ molecule}^{-1} \text{ s}^{-1}$ .

The plots of  $v_5/[\text{H}_2\text{O}]$  and  $v_{-5}$  vs  $[\text{O}_2]$  do not exhibit a dependence on  $[\text{O}_2]$  as did the corresponding plots for reaction (4.22). It appears from Figure (4.23) that the rate constants,  $k_{\pm 5}$ , are independent of  $[\text{O}_2]$  for pressures of oxygen in excess of  $\sim 2$  torr. There are at least two explanations for this rather unusual experimental observation. One is that the result is an experimental artifact. This possibility cannot be dismissed unambiguously. A second possibility is that the observation

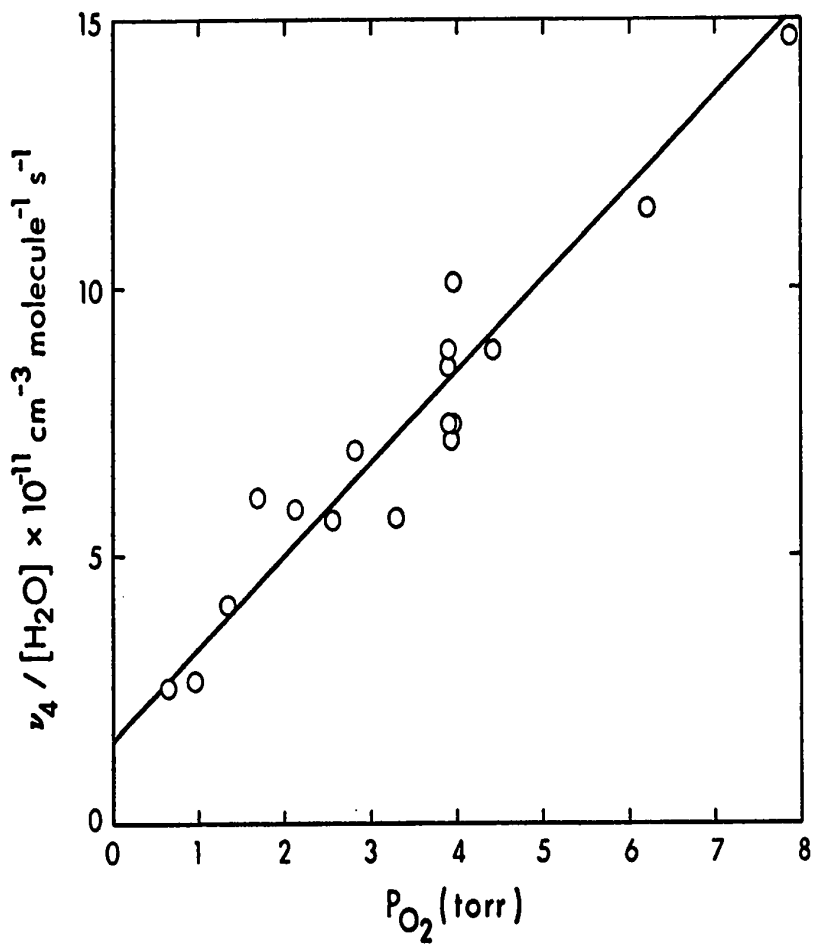


FIGURE 4.21. Plot of  $v_4/[H_2O]$  versus  $P_{O_2}$ . Plot shows that the reaction  $O_2^{\cdot-} \cdot H_2O + H_2O + O_2 \longrightarrow O_2^{\cdot-}(H_2O)_2 + O_2$  depends on the first power of the concentration of oxygen. Slope of line leads to  $k_4 = 5.4 \times 10^{-28} \text{ cm}^6 \text{ molecule}^{-1} \text{ s}^{-1}$ .

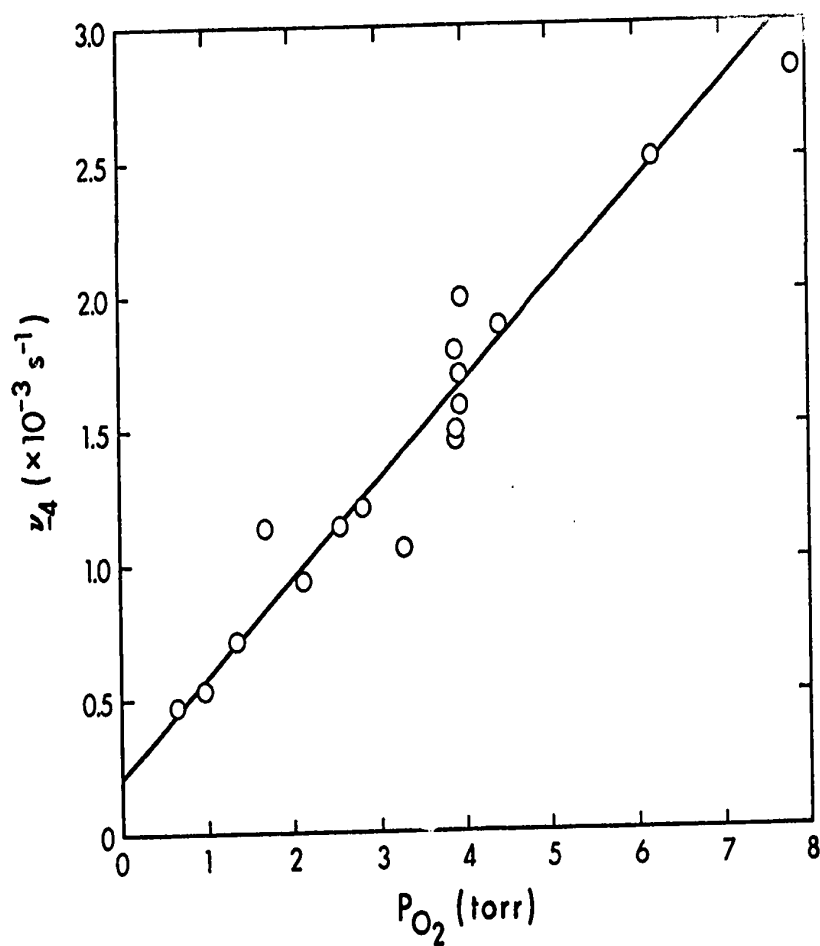


FIGURE 4.22. Plot of  $v_{-4}/[\text{H}_2\text{O}]$  versus  $P_{\text{O}_2}$ . Plot shows that the reaction  $\text{O}_2^-(\text{H}_2\text{O})_2 + \text{O}_2 \longrightarrow \text{O}_2^-\cdot\text{H}_2\text{O} + \text{H}_2\text{O} + \text{O}_2$  depends on the first power of the concentration of oxygen. Slope of line leads to  $k_{-4} = 1.1 \times 10^{-14} \text{ cm}^3 \text{ molecule}^{-1} \text{ s}^{-1}$ .

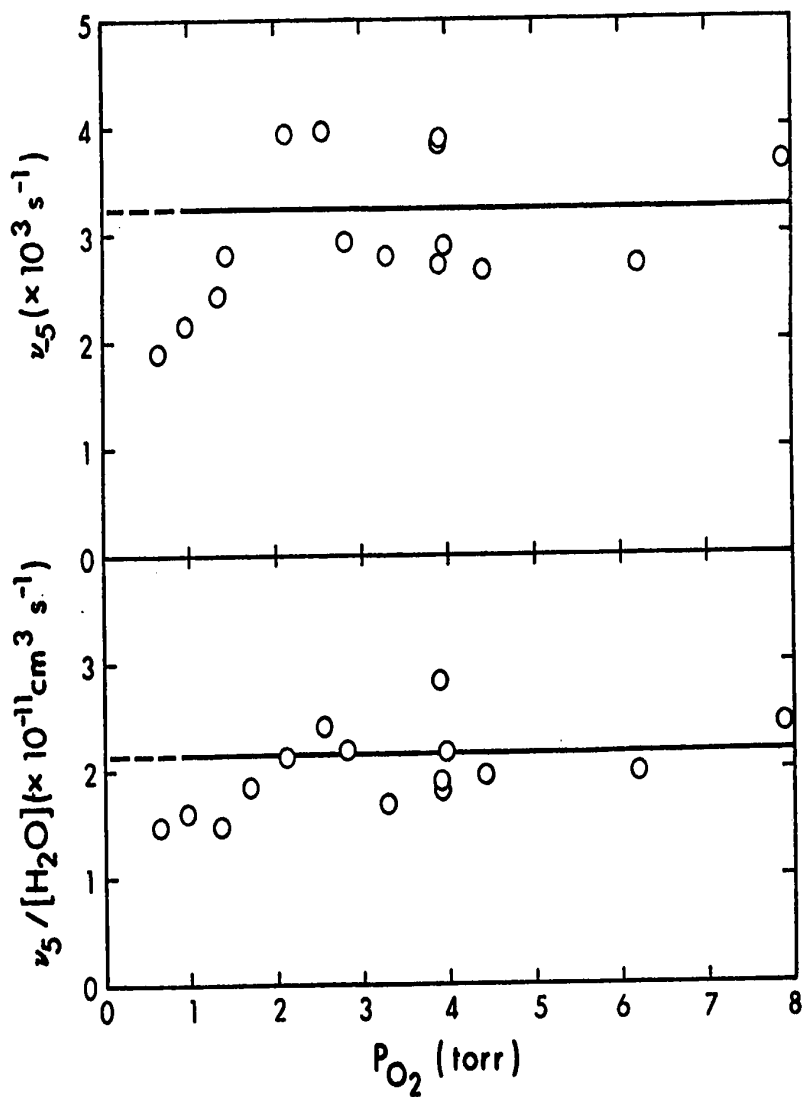
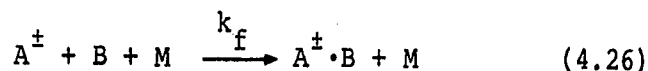


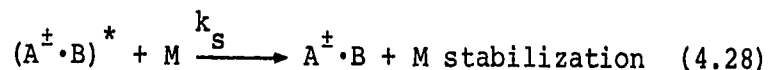
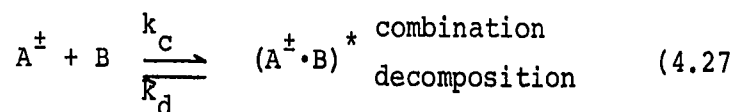
FIGURE 4.23. Plots of the apparent rate of  $O_2^-(H_2O)_2 + H_2O + O_2 \rightleftharpoons O_2^-(H_2O)_3 + O_2$ . Plots show that this reaction is independent of the partial pressure of oxygen for  $P_{O_2} \geq 2$  torr.

reflects the fundamental nature of the system.

Consider the general ion-molecule association reaction



The reaction may be visualized as being composed of three separate reactions (83,104,105).



and the all over forward rate coefficient in the steady state approximation being given by (106)

$$k_f = \frac{k_c k_s}{k_d} \quad (4.29)$$

If the lifetime of the species  $(A^{\pm} \cdot B)^*$  is short with respect to the average time between collisions, i.e. if  $k_d \gg k_s [M]$ , then the reaction will exhibit a dependence on  $[M]$ . If however the species  $(A^{\pm} \cdot B)^*$  is long lived, i.e. its lifetime is greater than or comparable to the time between collisions, then the dependence of  $k_f$  on  $[M]$  will be quite shallow. The time between collisions of neutral oxygen molecules at 2 torr and 300°K is  $\sim 10^{-8}$  s. Thus a

possible explanation of the results is that the lifetime of the intermediate species  $O_2^-(H_2O)_3^*$  is long.

The rate constant  $k_d$  for the decomposition of  $(A^\ddagger \cdot B)^*$  in (4.27) may be approximated by the Rice-Ramsperger-Kassel model. The simplest form of the RRK equation is (102)

$$k_d = Z \left( \frac{E-E^*}{E} \right)^{s-1} \quad (4.30)$$

The RRK model assumes that the molecule under consideration contains  $s$  coupled oscillators. The term  $\left( \frac{E-E^*}{E} \right)^{s-1}$  expresses the probability that the total energy  $E$  of  $(A^\ddagger \cdot B)^*$  may be transferred to one of the oscillators which has a critical energy  $E^*$  with respect to rupture. The  $Z$  factor is a proportionality constant related to the frequency of the coupled oscillators. Using the approximation that the critical energy  $E^*$  required for bond rupture is equal to the bond energy of  $A^\ddagger \cdot B$ , the total energy  $E$  may be approximated as  $E^*$  plus a contribution from the thermal energies of the reactant species. Thus  $E$  is given by

$$E = D(A^\ddagger - B) + rRT \quad (4.31)$$

where  $R$  is the gas constant and  $T$  the temperature. The term  $rRT$  may be difficult to assign a value to but if translational energy is considered then  $r = 3/2$ . Substituting equation (4.31) into (4.30), we have



$$k_d = Z \left( \frac{rRT}{D + rRT} \right)^{s-1} \quad (4.32)$$

Noting that  $D \gg rRT$  the above may be approximated as

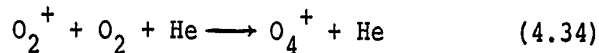
$$k_d \approx Z \left( \frac{rRT}{D} \right)^{s-1} \quad (4.33)$$

Thus the larger  $D$  and the greater the number of oscillators the smaller  $k_d$  will be, and therefore the longer the lifetime of the intermediate excited species. Reaction (4.23) is exothermic by 15.4 kcal/mole while reaction (4.22) is exothermic by 17.2 kcal/mole (101). The species  $O_2^-(H_2O)_2$  has 18 ( $3N-6$ ) vibrational degrees of freedom while  $O_2^-(H_2O)_3$  has 27. The difference in reaction enthalpies is small while the difference in the number of possible oscillators is substantial. Thus it may not be unreasonable to argue that the intermediate species  $O_2^-(H_2O)_3^*$  is long lived compared to  $O_2^-(H_2O)_2^*$ .

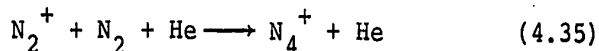
If the intermediate species is long lived compared to the average time between collisions, and if every collision of this intermediate stabilizes the species then the overall rate coefficient for the bimolecular association reaction will be given by the Gioumouisis-Stevenson equation (1.5). This expression predicts a value of  $\sim 10^{-9} \text{ cm}^3 \text{ molecule}^{-1} \text{ s}^{-1}$  for the bimolecular coefficient of reaction (4.23). The apparent bimolecular rate coefficient of (4.23) saturates at  $2.2 \times 10^{-11} \text{ cm}^3 \text{ molecule}^{-1} \text{ s}^{-1}$  as is shown in Figure (4.23).

Conway (104) has argued that the collision between an excited intermediate and some third body does not necessarily have to lead to stabilization but can lead to decomposition of the intermediate to the starting species. He considers the probability of the excited species being stabilized as small (a few percent). Thus the experimentally observed value may be reasonable for a saturated reaction.

The only other reported observation of such a phenomenon was by Ferguson et al (105) who observed saturation in the clustering reactions



and



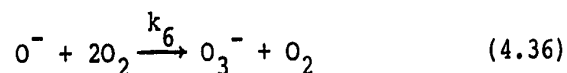
at 82°K. They observed that the apparent bimolecular rate coefficient for (4.34) saturated at a helium pressure of 0.6 torr at a value of  $7.1 \times 10^{-12} \text{ cm}^3 \text{ molecule}^{-1} \text{ s}^{-1}$  and that (4.35) saturated at 1.6 torr of helium at a value of  $5.3 \times 10^{-12} \text{ cm}^3 \text{ molecule}^{-1} \text{ s}^{-1}$ . It therefore appears that present rate constant for reaction (4.23) is reasonable.

Pack and Phelps (108) have examined the negative ion-molecule reactions in moist oxygen using a drift tube attached to a mass spectrometer. The present results are compared to those of Pack and Phelps and other workers in

Table 4.2. As can be seen the agreement between the present data and that initially reported by Pack and Phelps (108) is good. Phelps (109) has reanalyzed the data however, and concludes that reaction (4.22) is second order for oxygen pressures in the torr range. This is not in agreement with the present data. However, Phelps (109) considers the data somewhat unreliable and therefore the disagreement is not considered serious.

#### 4.4 The Reaction $O^- + 2O_2 \longrightarrow O_3^- + O_2$

As was mentioned previously in this Chapter ~10% of the primary ions produced on electron bombardment in oxygen were  $O^-$ . In dry oxygen the reaction



was observed. A brief study was made of this reaction and its temperature dependence. Upon the addition of water to this system the cluster ions  $O_3^-(H_2O)_n$ ,  $n = 1, 2$  were observed. However, no attempt was made to study the kinetics of formation of  $O_3^-(H_2O)_n$ .

In Figure (4.24) is shown a plot of the normalized  $O^-$  intensity ( $[O^-]/([O^-] + [O_3^-])$ ) versus time for various pressures of oxygen at 340°K. As can be seen the  $O^-$  signal decays exponentially over several decades. If equation (4.36) is the correct representation of the order

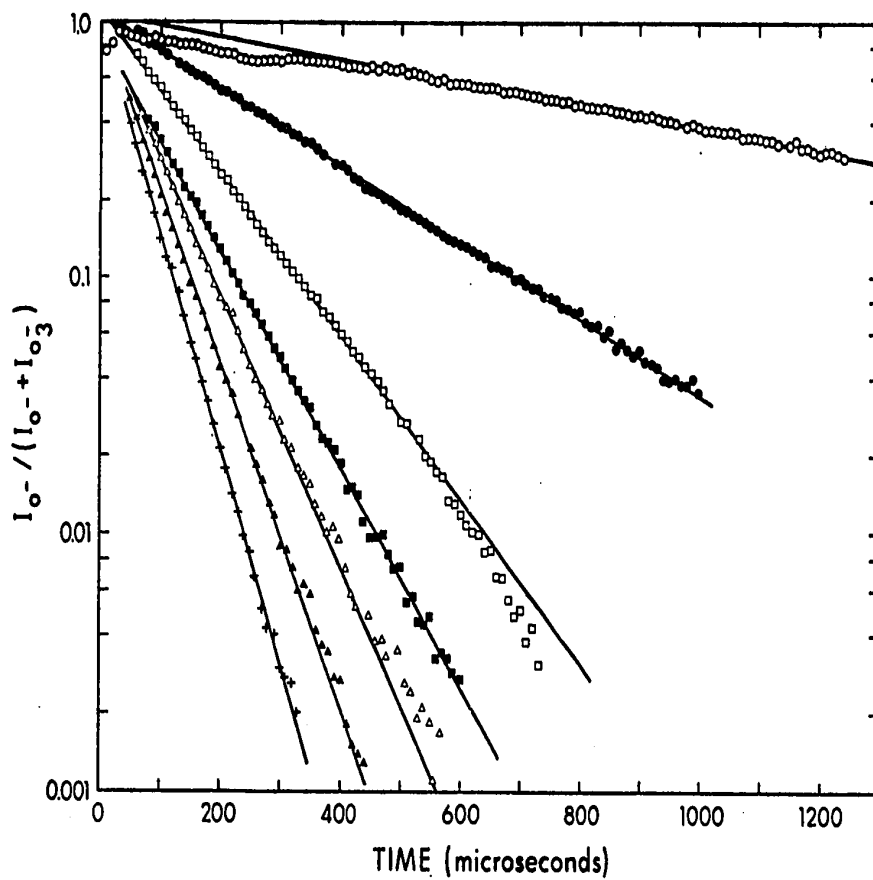


FIGURE 4.24. Logarithmic plots of the decay of the normalized  $O^-$  intensity with time lead to rate constant for  $O^- + 2O_2 \rightarrow O_3^- + O_2$ . Pressure of oxygen in torr: 0 1.1, ● 2.0, □ 3.0 ■ 3.5, Δ 4.0, Δ 4.5, + 5.0.  $T = 340^\circ K$ .

of the reaction then a plot of the pseudo first order rate coefficients obtained from Figure (4.24) versus the square of the oxygen pressure should yield a straight line of slope  $k_6$ . Such a plot is shown in Figure (4.25) for the data of Figure (4.24). The slope of the line leads to a value of  $k_6 = 1.0 \times 10^{-30} \text{ cm}^6 \text{ molecule}^{-2} \text{ s}^{-1}$  at  $340^\circ\text{K}$ . Displayed in Figure (4.26) are plots similar to Figure (4.24) for different temperatures. The data is summarized in Table 4.3 along with some previous measurements.

The rate of reaction (4.36) was investigated at several temperatures, the results of which are summarized in Table 4.3 and in Figure (4.27). Figure (4.27) shows a plot of  $\log k_6$  versus  $1/T$  in the classical Arrhenius fashion. The plot shown leads to an "activation" energy of  $-1.9 \text{ kcal/mole}$ . This is not to imply that this "activation" energy has any meaning in terms of a model for the reaction. Instead this type of plot is merely a convenient method of expressing the temperature dependence of the rate. The small negative temperature coefficient of (4.36) is easily expressed in this fashion. The variation of the observed rate coefficient is small in the temperature range over which data were taken. This difficulty combined with the scatter in the data is such that almost any temperature function would be consistent with the data.

In the previous section of this chapter concerning

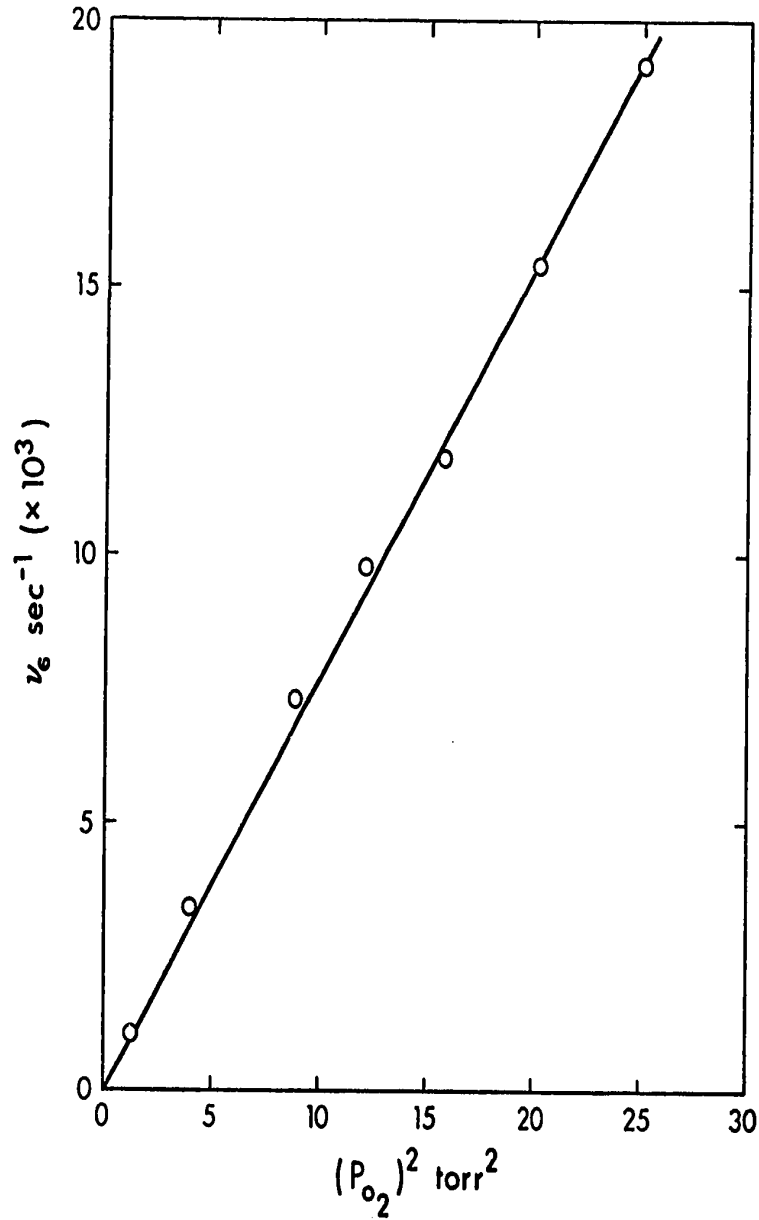
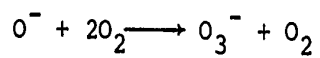


FIGURE 4.25. Plot of  $v_6 = k_6 [O_2]^n$  versus the square of the oxygen pressure for the data of Figure (4.24). Plot shows that  $n=2$  and the slope of the line leads to  $k_6 = 1.0 \times 10^{-30} \text{ cm}^6 \text{ molecule}^{-2} \text{ s}^{-1}$ .  $T = 340^\circ\text{K}$ .

TABLE 4.3Measured Rate Coefficients for the Reaction

<u><math>k_6^a</math></u>	<u>T (°K)</u>	<u>Reference</u>
14	300	Present work
11.1	329	Present work
10	340	Present work
7.9	367	Present work
6.6	395	Present work
12	Extrapolated to E/N = 0 T~300°K	(109)
10 ± 2	Extrapolated to E/N = 0 T~300°K	(53)
5	Extrapolated to E/N = 0 T~300°K	(111)
9	Extrapolated to E/N = 0 T~300°K	(112)
9	Extrapolated to E/N = 0 T~300°K	(113)

<sup>a</sup> In units of  $10^{-30} \text{ cm}^6 \text{ molecule}^{-2} \text{ s}^{-1}$ .

---

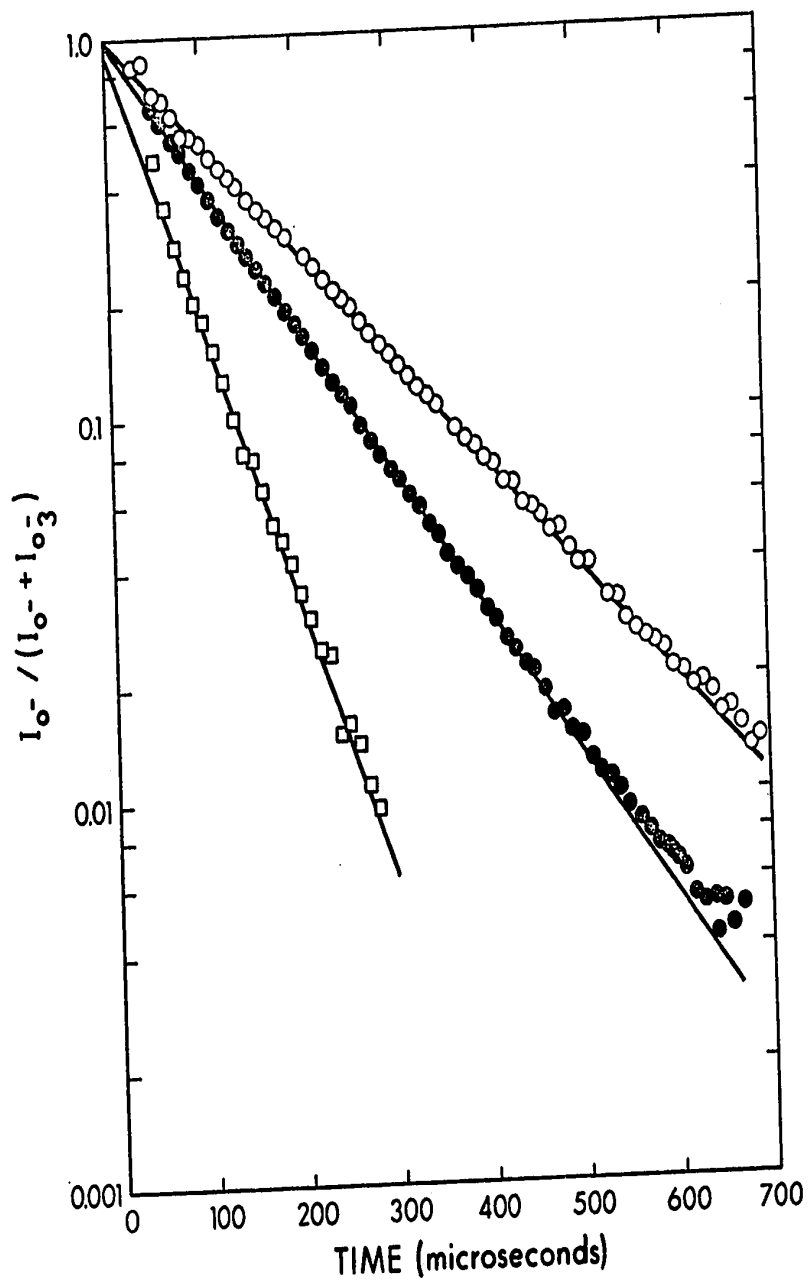


FIGURE 4.26. Plots of normalized  $O^-$  ion intensities versus time for various conditions. First number is  $P_{O_2}$  in torr, number in brackets is the rate in units of  $10^3 \text{ s}^{-1}$  and the third number is the temperature in  $^\circ\text{C}$ .  $\circ$  4.03 (6.05) 122,  $\bullet$  3.97 (8.68) 94, and  $\square$  4.0 (12.3) 56.



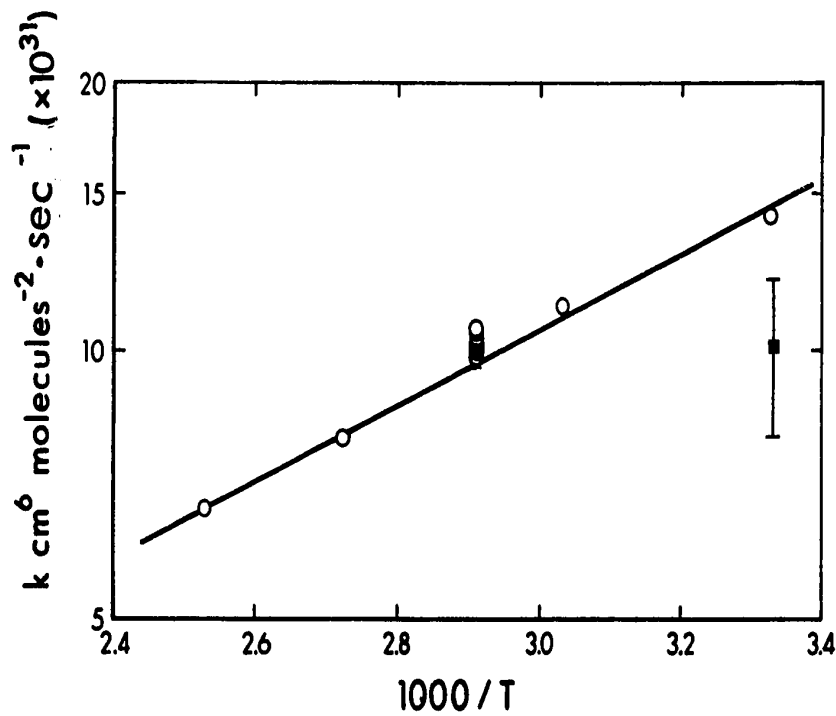
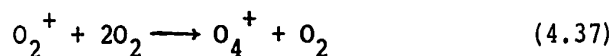


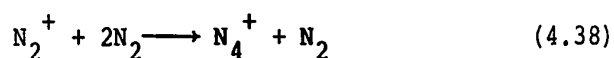
FIGURE 4.27. Arrhenius type plot of the rate of the reaction  $\text{O}^- + 2\text{O}_2 \longrightarrow \text{O}_2^- + \text{O}_2$ . Slope of line leads to an apparent "activation energy"  $E_a = -1.9$  kcal/mole. O present work, ■ data of McDaniel et al (53).

the kinetics of the hydration of  $O_2^-$ , a consideration of a general termolecular reaction resulted in the conclusion that  $k_d$  (the rate constant for the decomposition of the excited intermediate  $(A^\ddagger \cdot B)^*$ ) could be adequately represented by equation (4.33). All else remaining equal it can be seen from equation (4.33) that as the temperature increases the rate of decomposition of the excited intermediate  $(A^\ddagger \cdot B)^*$  will increase. The shortened lifetime of  $(A^\ddagger \cdot B)^*$  will mean that its chances of suffering a stabilizing collision are reduced. Thus a decrease in the termolecular rate coefficient with increasing temperature is expected.

Durden, Kebarle and Good (83) studied the temperature dependence of the reaction



and



They found that reaction (4.37) had a negative temperature coefficient corresponding to an "activation" energy of -1.5 kcal/mole. For reaction (4.38) the authors (83) reported that " $E_a$ " = -2 kcal/mole. The present temperature data for reaction (4.36) thus appear to be reasonable.

V Kinetics and Rate Constants of Reactions Leading to  
Hydration of  $\text{NO}_2^-$  and  $\text{NO}_3^-$

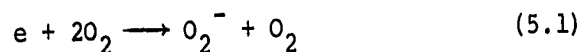
5.1 Introduction

The hydrates of the nitrite and nitrate ions are of particular interest since they are both believed to be involved in the negative ion chemistry of the earth's ionosphere (47). Rocket borne mass spectrometer measurements performed by Narcisi et al (69) and by Arnold et al (70) have indicated that the terminal negative ion in the D region is  $\text{NO}_3^-$ . Narcisi et al (69) report that  $\text{NO}_3^-(\text{H}_2\text{O})_3$  is the dominant negative ion at altitudes below 90 km. The present study was undertaken to determine the kinetics of formation of the hydrated  $\text{NO}_2^-$  and  $\text{NO}_3^-$  ions.

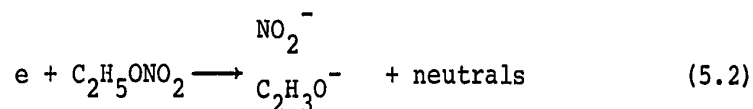
5.2 Experimental

A Production of Ions

In these experiments the pressure of the carrier gas was varied over the range 1.5 to 6.5 torr while the water pressure was in the range 8 to 35 mtorr. All kinetic measurements were done at 300°K. In some experiments argon and helium were used. The addition of trace amounts (~1 mtorr) of ethyl nitrate produced the ions  $\text{NO}_2^-$ ,  $\text{C}_2\text{H}_3\text{O}^-$  and  $\text{NO}_3^-$  in abundance. These ions were formed in addition to the  $\text{O}_2^-$  ion which is generated in oxygen by the third body electron capture reaction



Kriemler and Butrill (93) have studied, by ion cyclotron resonance, the negative ions formed by electron impact in ethyl nitrate. They have also investigated some of the secondary ions produced by ion-molecule reactions of the initially generated ions in ethyl nitrate. They reported that the major ions produced by low energy electron bombardment were  $\text{NO}_2^-$ ,  $\text{C}_2\text{H}_3\text{O}^-$  and small amounts of  $\text{OH}^-$  and  $\text{C}_2\text{H}_5\text{O}^-$ . These ions were presumably formed by the dissociative electron capture reaction (5.2)



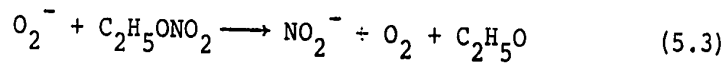
Kriemler and Butrill also noted that the relative yields of the different ions varied sharply with electron energy. They reported that  $\text{C}_2\text{H}_3\text{O}^-$ ,  $\text{OH}^-$  and  $\text{C}_2\text{H}_5\text{O}^-$  react with ethyl nitrate to produce  $\text{NO}_3^-$ . Presumably the  $\text{NO}_2^-$  and  $\text{C}_2\text{H}_3\text{O}^-$  observed in the present experiments are due to dissociative electron capture while the  $\text{NO}_3^-$  results from ion-molecule reactions as suggested by Kriemler and Butrill (93).

It was observed that the ratio of the different ions in the present system varied with the pressure of ethyl nitrate, the nature of the carrier gas and temperature. The addition of large amounts (~50 mtorr) of ethyl nitrate to the oxygen virtually completely suppressed the  $\text{O}_2^-$  signal. This presumably occurred because the dissociative electron capture reaction (5.2) competed efficiently with the  $\text{O}_2^-$

production reaction (5.1) at high ethyl nitrate concentration.

The addition of small amounts of ethyl nitrate to oxygen generated  $O_2^-$ ,  $NO_2^-$ ,  $C_2H_3O^-$  and  $NO_3^-$  in the ratio 100 : 65 : 50 : 20. In argon and helium the ratio was altered to 0 : 65 : 100 : 5. The small amount of  $NO_3^-$  produced in the rare gases precluded any study of the  $NO_3^-$  reactions in this case. Using water as the carrier gas, and large (~50 mtorr) amounts of ethyl nitrate at high temperatures ( $T > 100^\circ C$ ) only  $NO_2^-$  and  $NO_3^-$  were produced and in roughly equal amounts. As the temperature was lowered the ratio  $NO_2^-/NO_3^-$  increased and  $C_2H_3O^-$  appeared.

Using oxygen as the carrier gas containing small amounts of water and ethyl nitrate, it was noted that the hydrated  $O_2^-$ ,  $NO_2^-$ ,  $NO_3^-$  and  $C_2H_3O^-$  ions remained a constant fraction of the total ions with time. This was taken as evidence that these ions do not interconvert, or do so very slowly. This seems surprising since the reaction

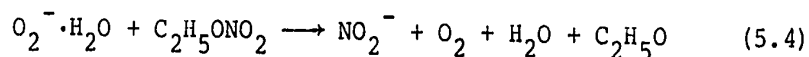


is exothermic. The thermodynamic parameters used in this calculation are given in Table 5.1. Thus it is to be expected that  $O_2^-$  would convert to the  $NO_2^-$  system. However,  $O_2^-$  is rapidly depleted to form  $O_2^-(H_2O)_n$ . The reaction

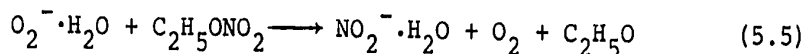
TABLE 5.1Selected Thermodynamic Data

<u>Parameter</u>	<u>Value</u>	<u>Reference</u>
EA(O <sub>2</sub> )	0.43 eV	(4)
EA(NO <sub>2</sub> )	2.4 eV	See Table 6.3
D(C <sub>2</sub> H <sub>5</sub> O-NO <sub>2</sub> )	36.4 kcal/mole	(114)
D(O <sub>2</sub> <sup>-</sup> - H <sub>2</sub> O)	18.4 kcal/mole	(56)
D(NO <sub>2</sub> <sup>-</sup> - H <sub>2</sub> O)	14.3 kcal/mole	See Table 6.2

---

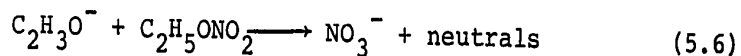


is endothermic. However the reaction



is calculated to be exothermic. A reaction such as (5.5) implies a rather substantial rearrangement and may be slow due to steric factors. Nevertheless it is not observed. Alternatively the thermodynamic parameters given in Table 5.1 may be incorrect and reaction (5.5) may be endothermic. For example the value of  $\text{EA}(\text{NO}_2)$  given in Table 5.1 may be regarded as questionable.

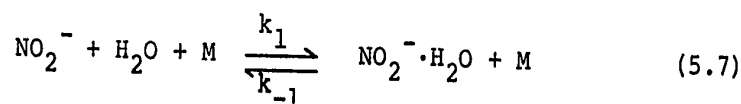
The  $\text{C}_2\text{H}_3\text{O}^-$  and hydrates did not react to any appreciable extent with the ethyl nitrate in the present system to form  $\text{NO}_3^-$ . This is in contradiction with the observation of Kriemler and Butrill (93). It may be that in the experiment of Kriemler and Butrill the  $\text{C}_2\text{H}_3\text{O}^-$  was vibrationally and/or electronically excited and was thus capable of reacting with ethyl nitrate. The  $\text{C}_2\text{H}_3\text{O}^-$  in the present experiments should be in the ground state because of the number of collisions it could be expected to make with the carrier gas before encountering an ethyl nitrate molecule. Alternatively the present experiment involves ions which have thermal ( $T_{\text{ion}} \sim 300^\circ\text{K}$ ) translational energies. In the ICR experiment the ions are translationally excited and it may be that the cross section of the reaction



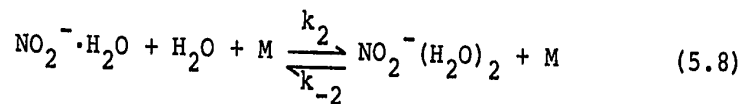
is sharply dependent on translational energy. These reactions have not been studied sufficiently to permit any definitive conclusion.

The identity of the  $\text{NO}_2^-$ ,  $\text{NO}_3^-$  and  $\text{O}_2^-$  and their hydrates was deduced purely on the basis of their m/e ratios. It was found that by using propyl nitrate instead of ethyl nitrate that the ion at m/e = 43 ( $\text{C}_2\text{H}_3\text{O}^-$ ) disappeared and a new ion appeared at m/e = 58 corresponding to  $\text{C}_3\text{H}_6\text{O}^-$ . It was therefore concluded that the m/e = 43 observed with ethyl nitrate was indeed  $\text{C}_2\text{H}_3\text{O}^-$ .

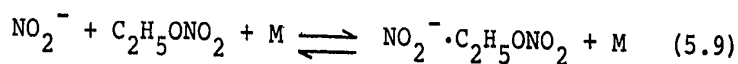
At high ethyl nitrate concentrations it was observed that the rate of  $\text{NO}_2^-$  disappearance became dependent on the ethyl nitrate concentration. This appears anomalous since  $\text{NO}_2^-$  was presumed to be removed by the reactions



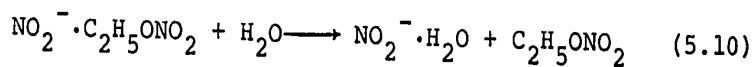
and



It is believed that this anomalous rate dependence was caused by the reactions



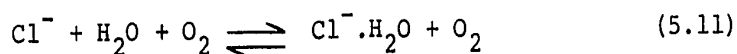
and





Reaction (5.9) is expected to proceed at a rate compatible to reaction (5.7). The presence of substantial amounts (~50 mtorr) of ethyl nitrate compared to water (~10 mtorr) will cause (5.9) to be the preferred mode of removal of  $\text{NO}_2^-$ . It is to be expected that the switching reaction (5.10) proceeds at collision frequency (5) i.e.  $k \approx 10^{-9} \text{ cm}^3 \text{ molecule}^{-1} \text{ s}^{-1}$ . If the mechanism (5.9) and (5.10) is operative then the apparent rate of conversion of  $\text{NO}_2^-$  to  $\text{NO}_2^- \cdot \text{H}_2\text{O}$  will be enhanced and will vary with the pressure of ethyl nitrate as was observed. This difficulty was overcome by lowering the partial pressure of ethyl nitrate until no effect was observed on the rate. The ion  $\text{NO}_2^- \cdot \text{C}_2\text{H}_5\text{ONO}_2$  was not detected. This does not defeat the proposed mechanism as the concentration of the  $\text{NO}_2^- \cdot \text{C}_2\text{H}_5\text{ONO}_2$  ion is predicted to be small since (5.10) is expected to be faster than (5.9).

A similar difficulty was encountered in earlier work where it was attempted to study the reaction



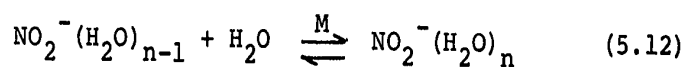
In this case the apparent rate of conversion of  $\text{Cl}^-$  to  $\text{Cl}^- \cdot \text{H}_2\text{O}$  led to a rate constant for (5.11) which was unreasonably large. Furthermore the rate depended on the pressure of carbon tetrachloride which was used to produce the  $\text{Cl}^-$ . However, the ion  $\text{CCl}_5^-$  was observed in this case

and it was found that a reduction of the concentration of carbon tetrachloride overcame the problem. The reactions of  $O_4^-$  in the hydration of  $O_2^-$  which were presented in the preceding chapter is another example of such a rate increase by a parallel branch involving a switching reaction.

#### B. Measurement of Water Pressure

The measurement of the rates of reactions leading to  $NO_2^-(H_2O)_n$  and  $NO_3^-.H_2O$  were performed in a manner similar to that described in the  $O_2^-$  hydration system. In most of these experiments, oxygen was used as the carrier gas and in this case the ions  $O_2^-(H_2O)_2$  and  $O_2^-(H_2O)_3$  could be seen as well as the establishment of the equilibrium between them. Knowledge of the equilibrium concentration of the oxygen hydrates permitted the determination of the water pressure as was described in Chapter 4.

Reactions such as



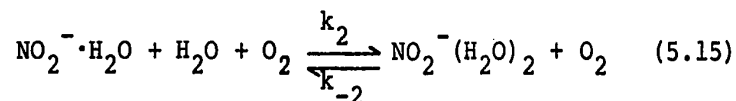
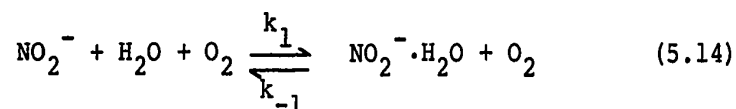
could be observed to reach equilibrium in the system, therefore the  $K_{n-1,n}(NO_2^-)$  for these reactions could be evaluated. In the experiments in which argon and helium were used as carrier gases, the ions  $O_2^-(H_2O)_n$  were of course absent. Water pressures were evaluated in these cases by the observation of the equilibrium in (5.12) and the expression

$$K_{n-1,n}(NO_2^-) = \frac{I_{NO_2^-(H_2O)_n}}{I_{NO_2^-(H_2O)_{n-1}} \cdot P_{H_2O}} \quad (5.13)$$

The  $K_{n-1,n}(\text{NO}_2^-)$  having been previously determined from the experiments using oxygen as carrier gas.

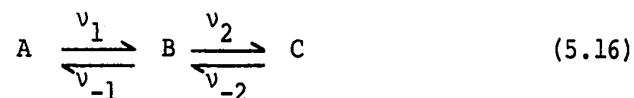
### 5.3 Results and Discussion

Seventeen measurements were conducted in which the partial pressures of water and carrier gas were varied. Ten measurements were made using oxygen as the carrier gas, four with helium and three with argon. All experiments were done at 300°K. The normalized data for the reactions



are summarized in Figures (5.1-5.10). As before the solid lines through the experimental points are the analogue computer calculated temporal profiles based on the above mechanism and the reaction frequencies summarized in Table 5.2. The analogue computer programme is given in Appendix I.

An alternative graphical technique was also used for some of the rate constant determinations. For a first order reaction scheme of the form



with boundary conditions at  $t = 0$ ,  $A = 1$ ,  $B = C = 0$ , it may be shown (Appendix II) that

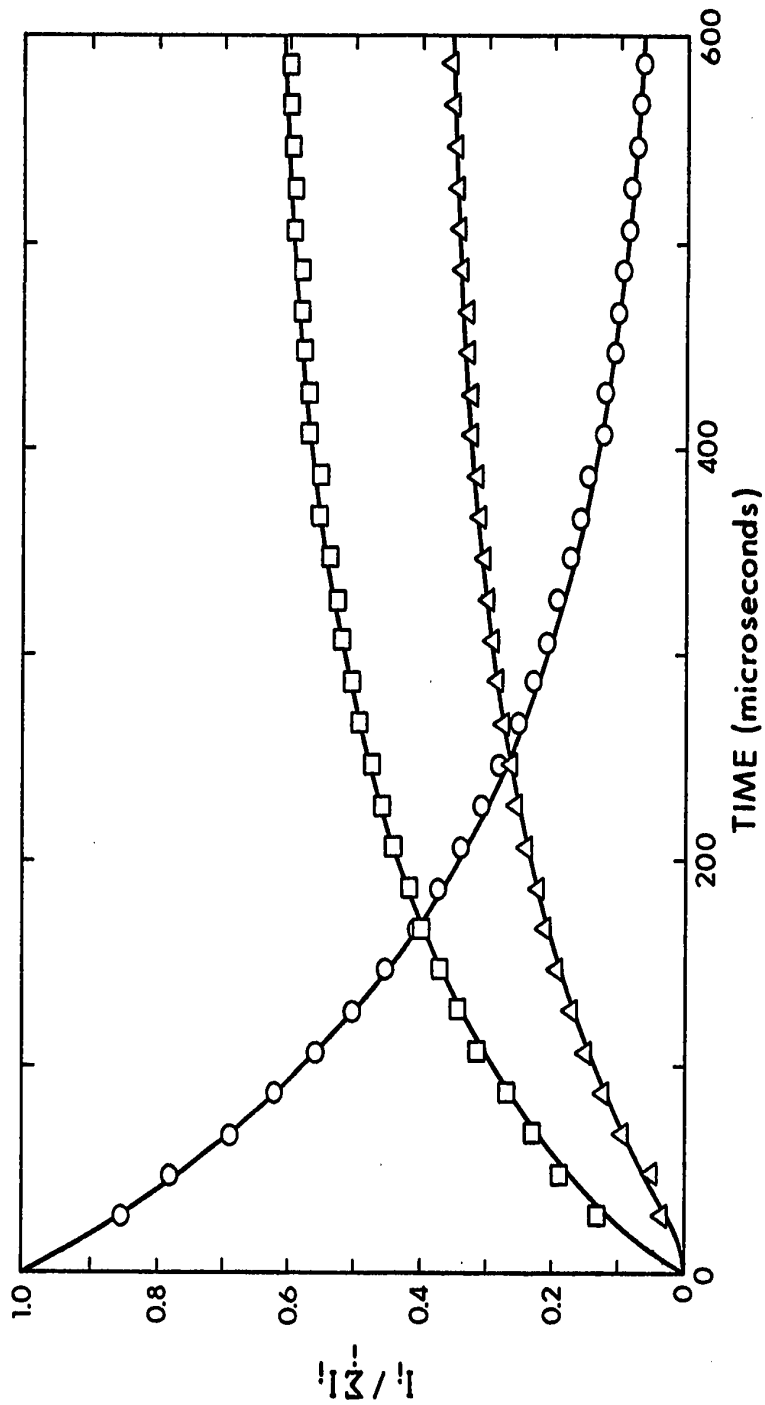


FIGURE 5.1. Time dependence of normalized ion intensities. The curves are the calculated time dependence for the rate parameters summarized in Table 5.2.  $P_{\text{O}_2} = 1.47$  torr  $P_{\text{H}_2\text{O}} = 30.2$  mtorr. O  $\text{NO}_2^-$ , □  $\text{NO}_2^- \cdot \text{H}_2\text{O}$  and Δ  $\text{NO}_2^-(\text{H}_2\text{O})_2$ .

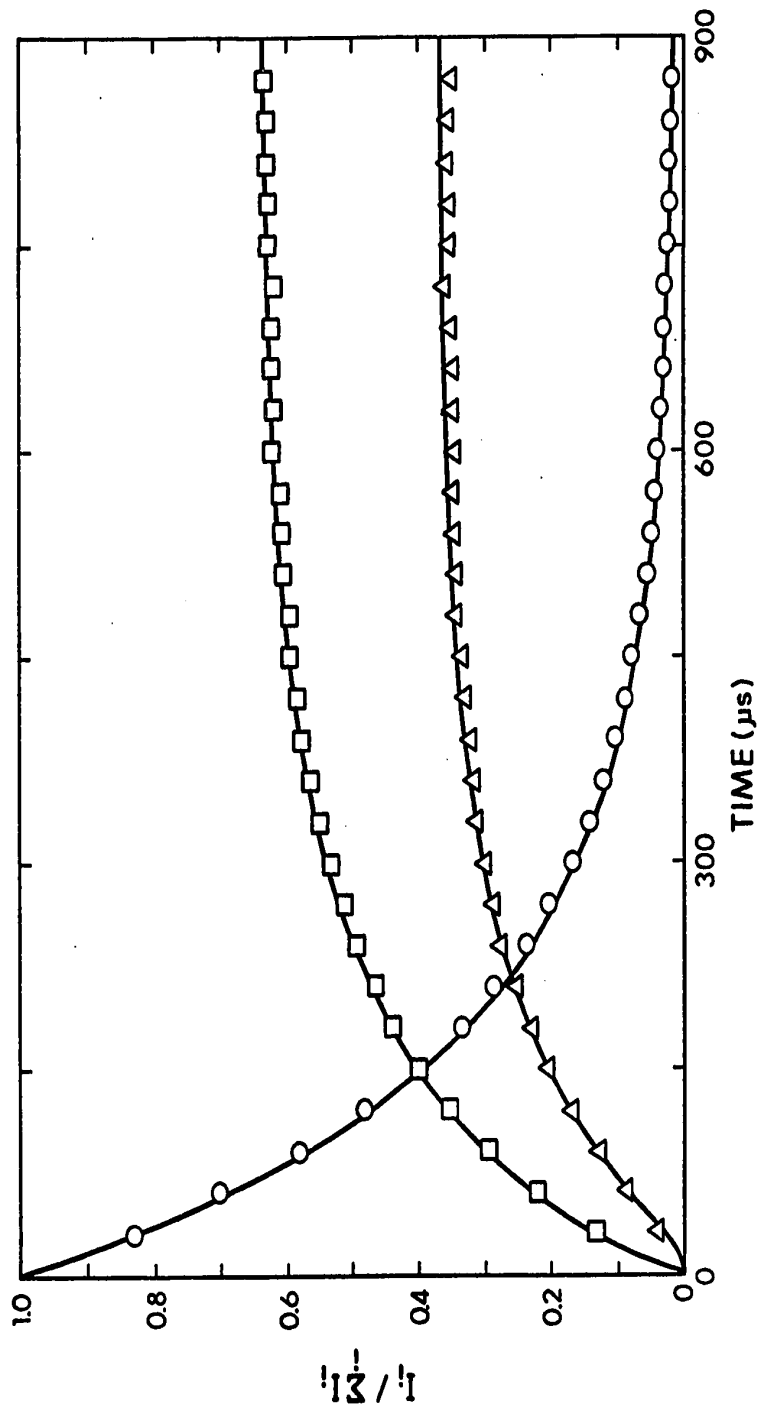


FIGURE 5.2. Time dependence of normalized ion intensities. The curves are the calculated time dependence for the rate parameters summarized in Table 5.2.  $P_{O_2} = 2.14$  torr,  $P_{H_2O} = 27$  mtorr. O  $NO_2^-$ , □  $NO_2^- \cdot H_2O$  and Δ  $NO_2^- (H_2O)_2$ .

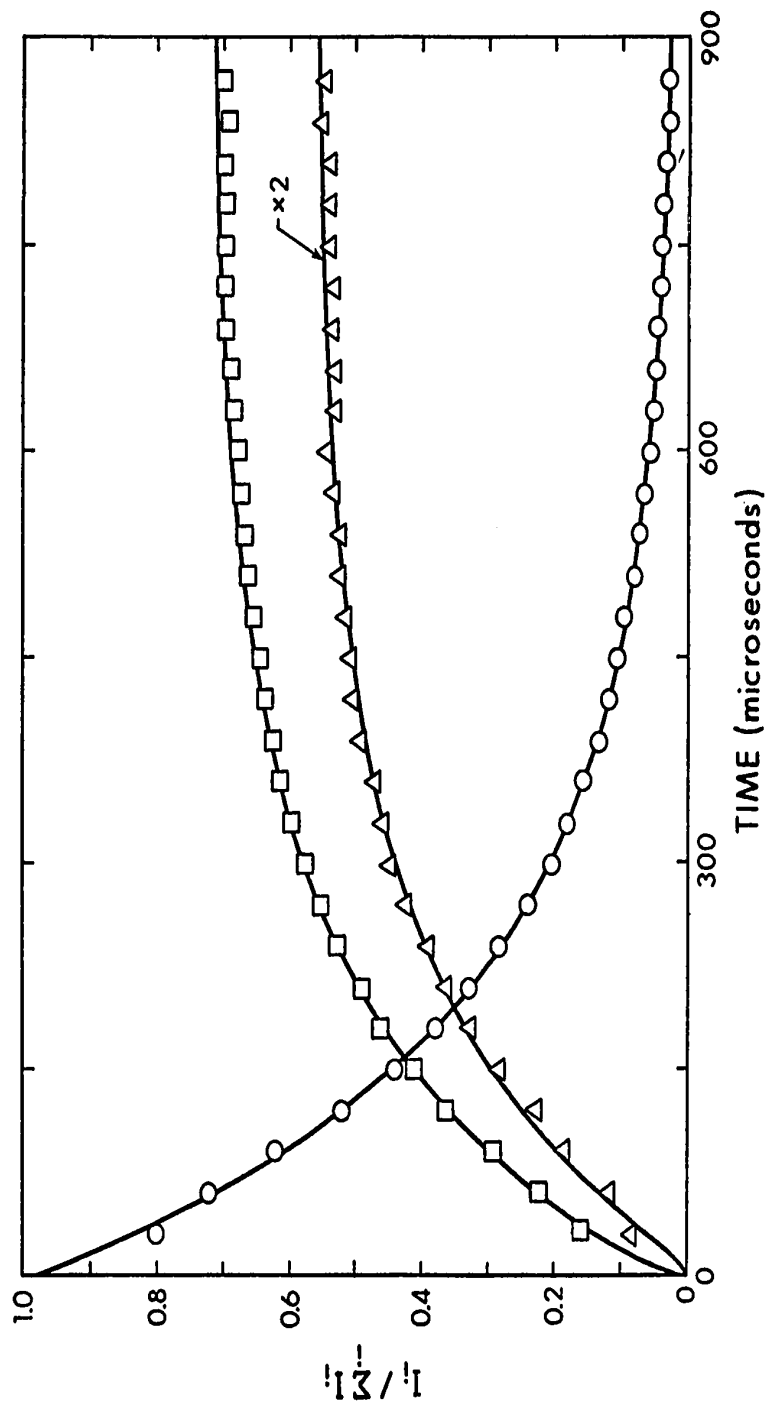


FIGURE 5.3. Time dependence of normalized ion intensities. The curves are the calculated time dependence for the rate parameters summarized in Table 5.2.  $P_{O_2} = 2.85$  torr,  $P_{H_2O} = 18.9$  mtorr.  $\circ$  NO<sub>2</sub><sup>-</sup>,  $\square$  NO<sub>2</sub><sup>-</sup>·H<sub>2</sub>O and  $\Delta$  NO<sub>2</sub><sup>-</sup>(H<sub>2</sub>O)<sub>2</sub>.

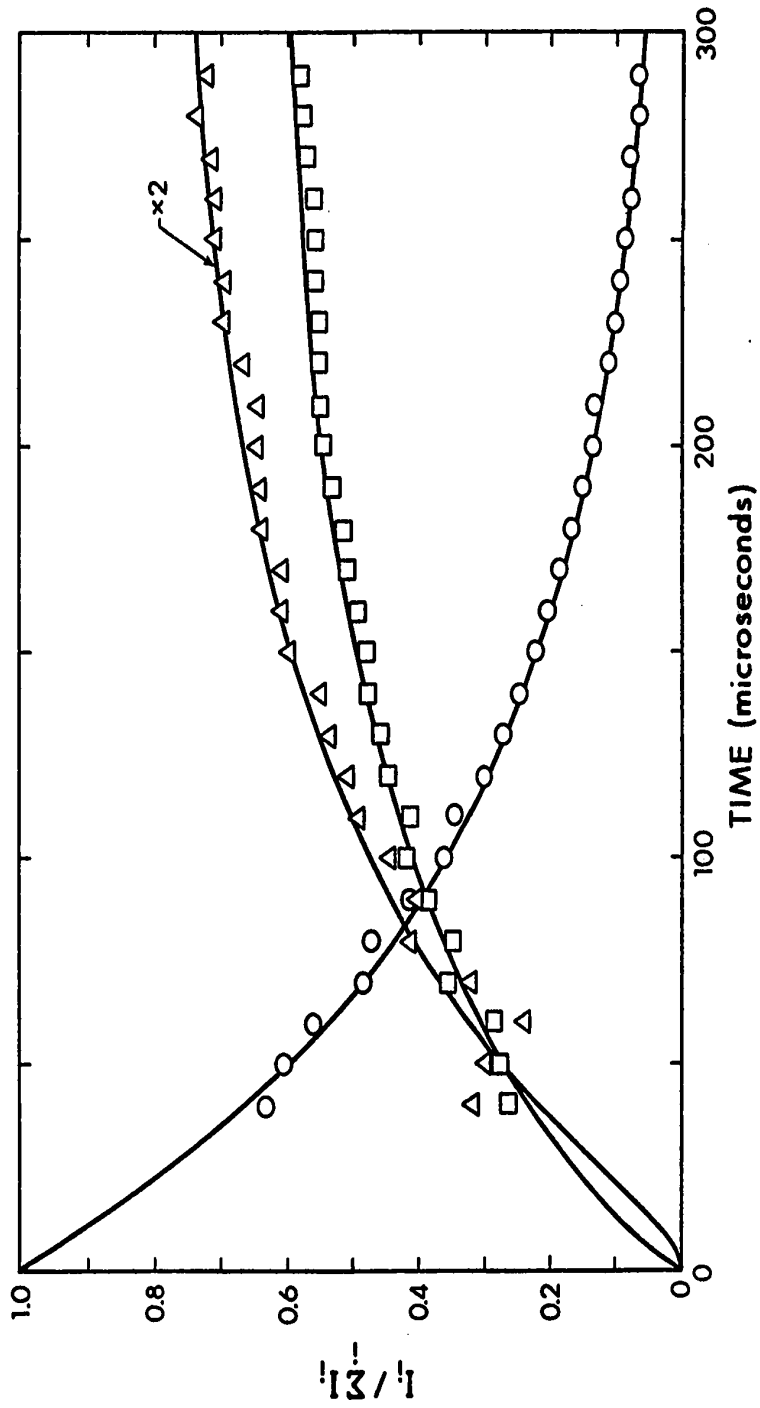


FIGURE 5.4. Time dependence of normalized ion intensities. The curves are the calculated time dependence for the rate parameters summarized in Table 5.2.  $P_{O_2} = 3.61$  torr,  $P_{H_2O} = 32.7$  mtorr. O  $NO_2^-$ , □  $NO_2^-.H_2O$  and Δ  $NO_2^-(H_2O)_2$ .

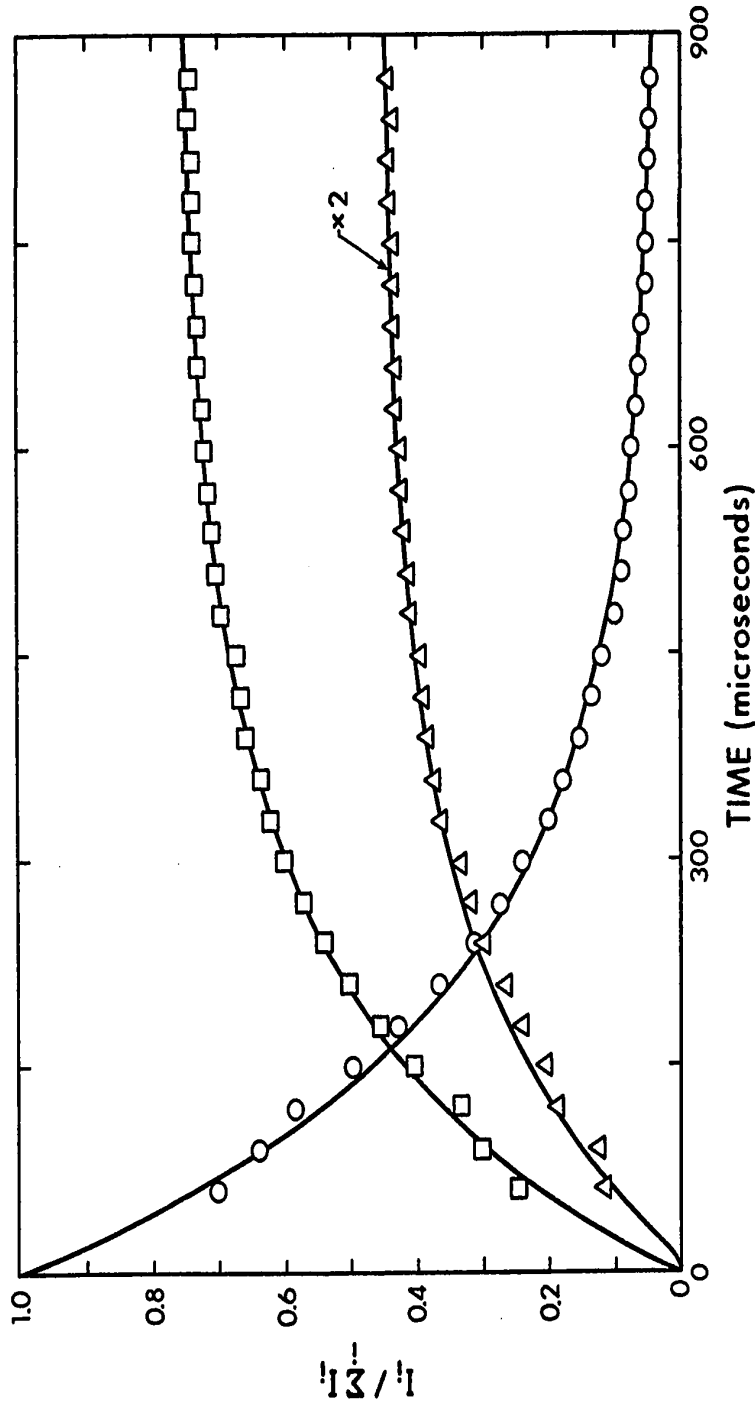


FIGURE 5.5. Time dependence of normalized ion intensities. The curves are the calculated time dependence for the rate parameters summarized in Table 5.2.  $P_{\text{O}_2} = 3.63$  torr,  $P_{\text{H}_2\text{O}} = 13.7$  mtorr.  $\circ$   $\text{NO}_2^-$ ,  $\square$   $\text{NO}_2^-\cdot\text{H}_2\text{O}$  and  $\Delta$   $\text{NO}_2(\text{H}_2\text{O})_2$ .



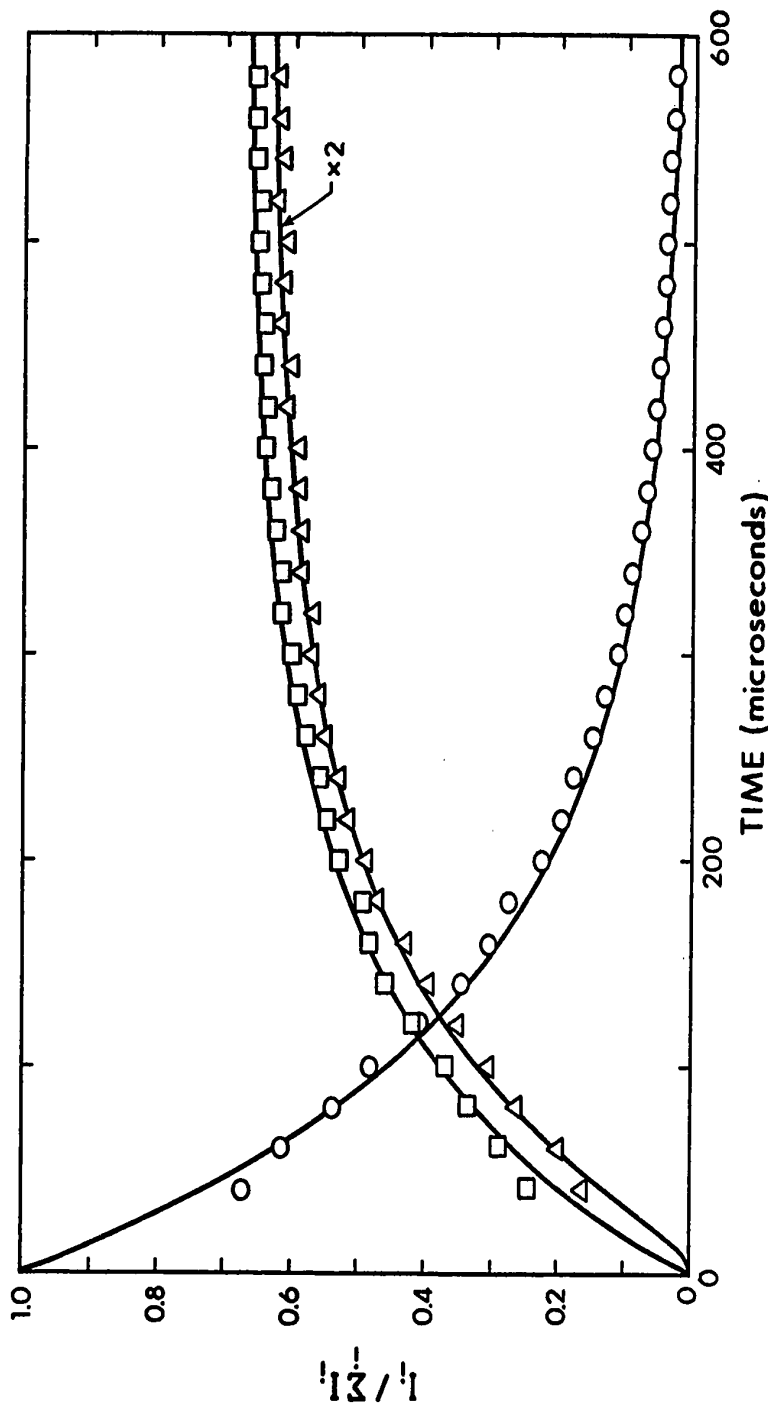


FIGURE 5.6. Time dependence of normalized ion intensities. The curves are the calculated time dependence for the rate parameters summarized in Table 5.2.  $P_{\text{O}_2} = 3.64$  torr,  $P_{\text{H}_2\text{O}} = 23$  mtorr.  $\circ$   $\text{NO}_2^-$ ,  $\square$   $\text{NO}_2^- \cdot \text{H}_2\text{O}$  and  $\Delta$   $\text{NO}_2^- (\text{H}_2\text{O})_2$ .

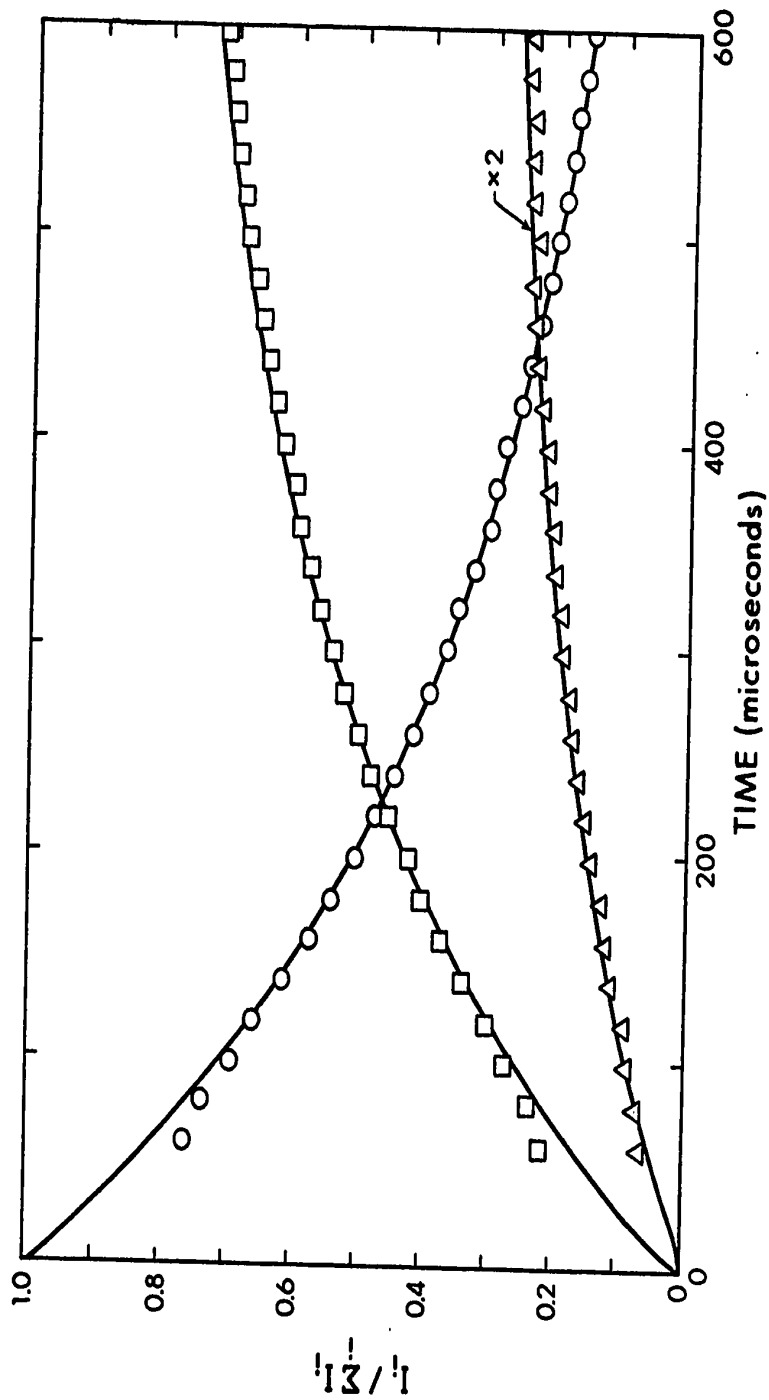


FIGURE 5.7. Time dependence of normalized ion intensities. The curves are the calculated time dependence for the rate parameters summarized in Table 5.2.  $P_{\text{O}_2} = 3.79$   $P_{\text{H}_2\text{O}} = 9.2$  mtorr.  $\circ$   $\text{NO}_2^-$ ,  $\square$   $\text{NO}_2^- \cdot \text{H}_2\text{O}$  and  $\Delta$   $\text{NO}_2^-(\text{H}_2\text{O})_2$ .

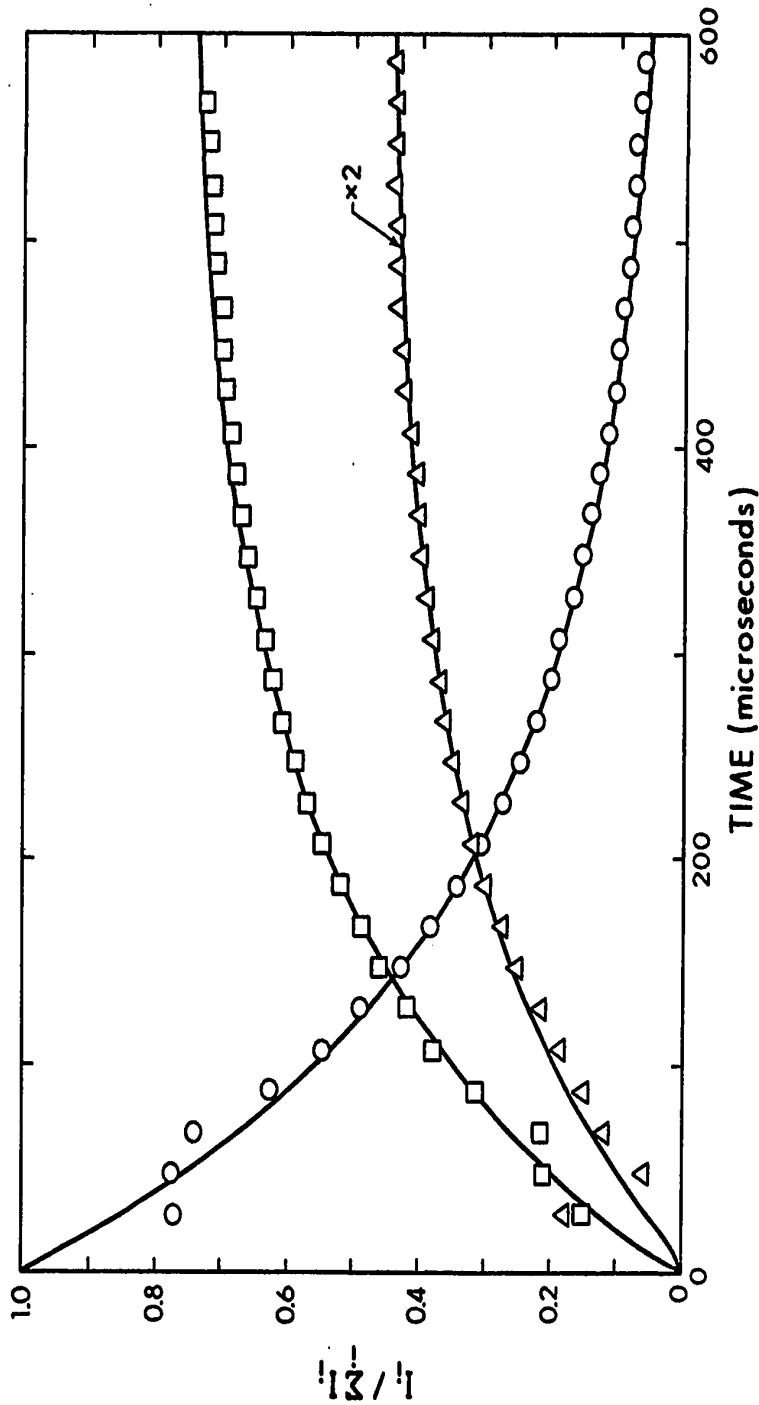


FIGURE 5.8. Time dependence of normalized ion intensities. The curves are the calculated time dependence for the rate parameters summarized in Table 5.2.  $P_{O_2} = 4.73$  torr,  $P_{H_2O} = 14.7$  mtorr.  $\circ$   $NO_2^-$ ,  $\square$   $NO_2^-(H_2O)_2$  and  $\triangle$   $NO_2^-(H_2O)_2$ .

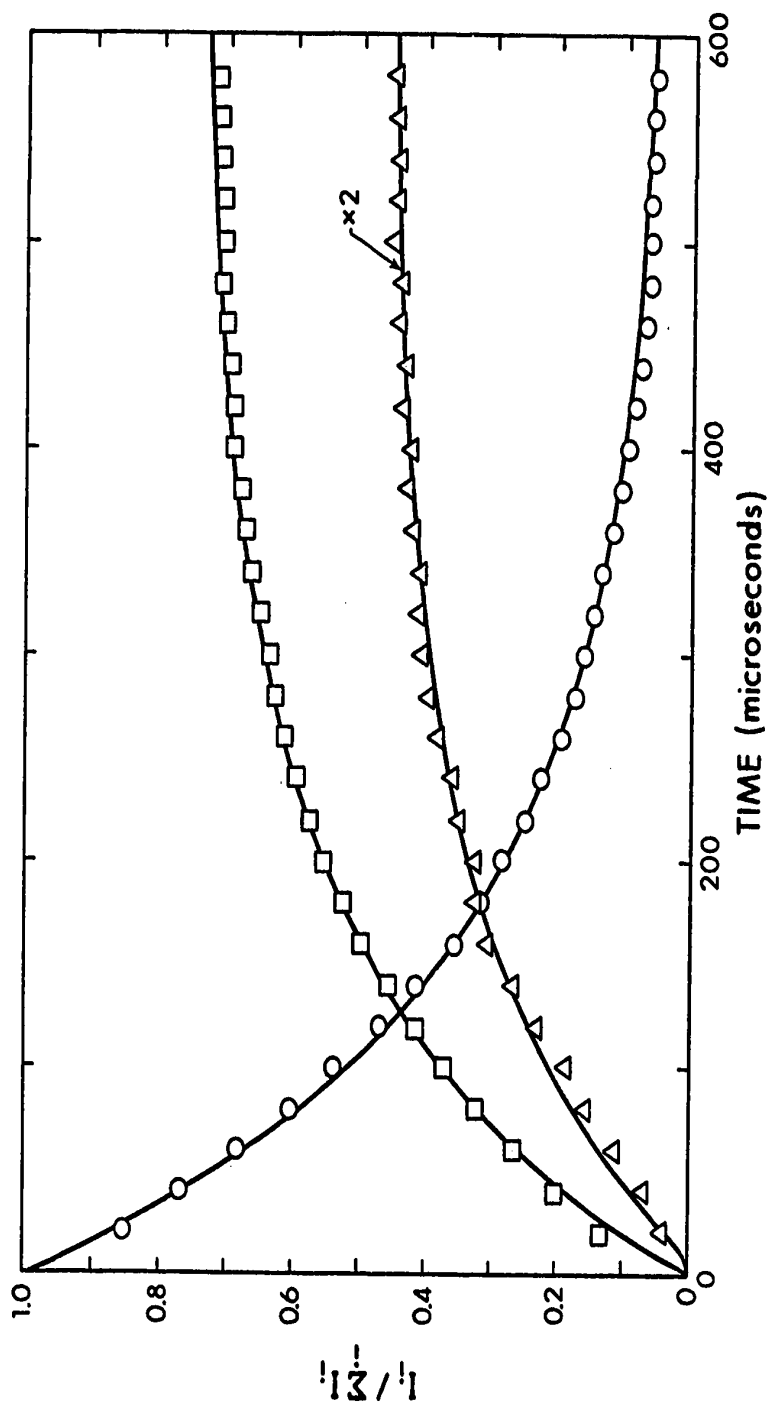


FIGURE 5.9. Time dependence of normalized ion intensities. The curves are the calculated time dependence for the rate parameters summarized in Table 5.2.  $P_{O_2} = 5.40$  torr,  $P_{H_2O} = 14.0$  mtorr.  $\circ$   $NO_2^-$ ,  $\square$   $NO_2^- \cdot H_2O$  and  $\Delta$   $NO_2^-(H_2O)_2$ .

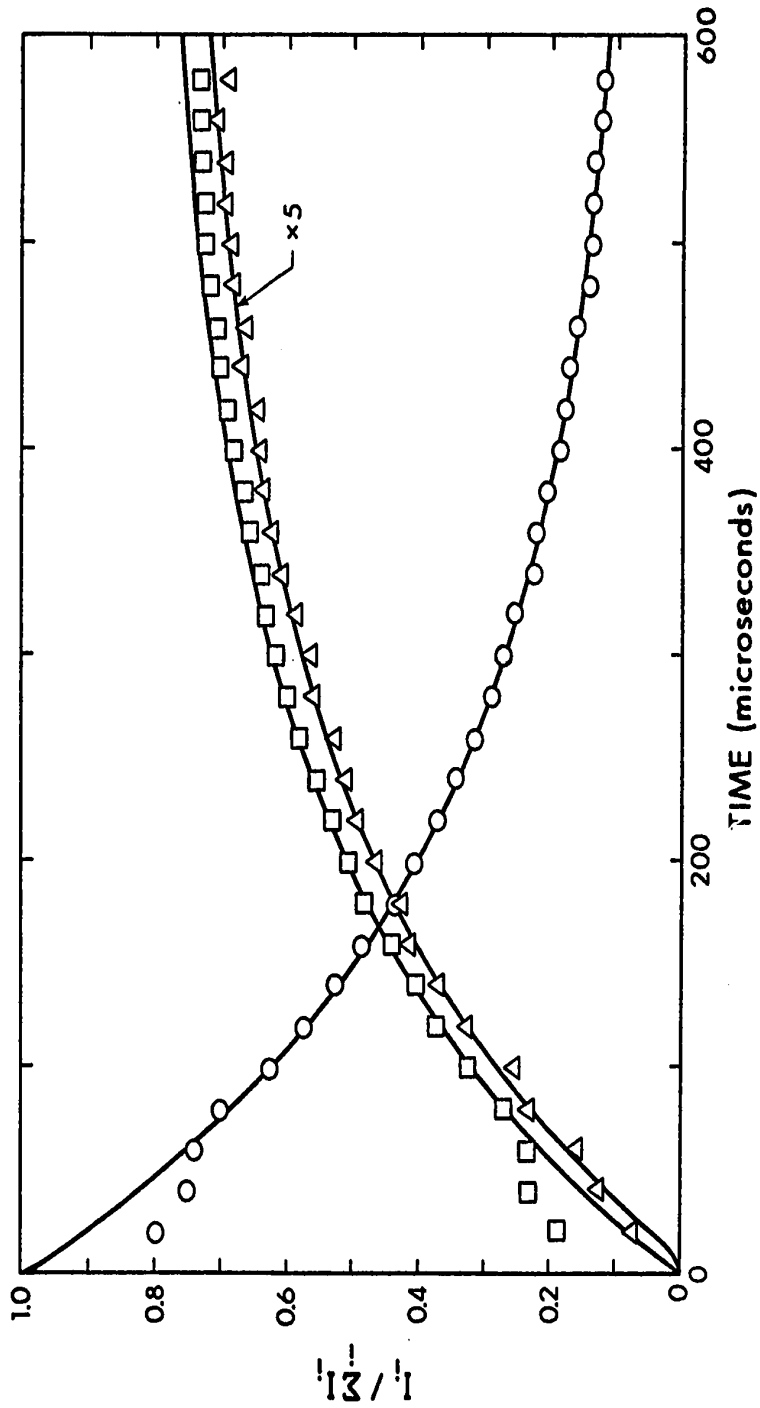


FIGURE 5.10. Time dependence of normalized ion intensities. The curves are the calculated time dependence for the rate parameters summarized in Table 5.2.  $P_{\text{O}_2} = 6.40$  torr,  $P_{\text{H}_2\text{O}} = 8.6$  mtorr. ○  $\text{NO}_2^-$ , □  $\text{NO}_2^-\cdot\text{H}_2\text{O}$  and △  $\text{NO}_2^-(\text{H}_2\text{O})_2$ .

TABLE 5.2

Rate Constants of Reactions Leading to  $\text{NO}_x^-(\text{H}_2\text{O})_n$ <sup>a</sup>

$P_{\text{O}_2}$ <sup>b</sup>	$P_{\text{H}_2\text{O}}$ <sup>c</sup>	$v_1$ <sup>d</sup>	$v_{-1}$ <sup>d</sup>	$v_2$ <sup>d</sup>	$v_{-2}$ <sup>d</sup>	$v_3$ <sup>d</sup>	$v_{-3}$ <sup>d</sup>	Fig. <sup>e</sup>
1.47	30.2	5.16	0.109	2.26	3.91	4.76	0.876	5.1
2.14	27.0	6.14	0.126	2.21	3.89	5.46	1.34	5.2
2.85	11.9	5.47	0.169	2.13	5.44	5.64	1.47	5.3
3.61	32.7	10.7	0.240	5.00	8.16	9.86	1.66	5.4
3.63	13.7	5.15	0.225	2.21	3.89	5.46	1.34	5.5
3.64	22.9	7.75	0.244	3.70	7.84	7.81	1.94	5.6
3.79	9.2	3.42	0.240	1.49	8.16	3.24	1.94	5.7
4.73	14.7	5.98	0.248	3.02	10.2	5.80	2.83	5.8
5.40	14.0	6.53	0.312	2.98	9.66	6.44	2.32	5.9
6.40	8.6	4.92	0.458	2.19	11.7	4.64	2.98	5.10

<sup>a</sup>  $T = 300.5^\circ\text{K}$ <sup>b</sup> Pressure in torr<sup>c</sup> Pressure in millitorr<sup>d</sup> In units of  $10^3 \text{ s}^{-1}$ <sup>e</sup> Figure in which data is displayed.

140.

$$2.303 \log_{10}([A] - [A_{eq}]) = - (v_1 + v_{-1})t + \text{constant} \quad (5.17)$$

where  $[A_{eq}]$  is the equilibrium concentration of A and  $[A]$  is the concentration of A at time  $t$ . Thus a plot of  $\log_{10} (I_{NO_2^-} - I_{NO_2^-}(eq))$  versus time should yield a straight line of slope  $(v_1 + v_{-1})/2.303$ . The relationship

$$\left\{ \frac{I_{NO_2^-} \cdot (H_2O)}{I_{NO_2^-}} \right\}_{\text{equilibrium}} = \frac{v_1}{v_{-1}} \quad (5.18)$$

permits the evaluation of the individual  $v_i$ . The  $v_1$  and  $v_{-1}$  could thus be calculated by two methods. The graphical approach outlined above, examples of which are shown in Figure (5.11) and the computer fit method. The agreement between the two methods is excellent. Table 5.3 shows a comparison of some  $v_1$  calculated by both methods for the data displayed in Figure (5.11).

If the hydration of  $NO_2^-$  is third order then the apparent first order rate coefficient  $v_1$  is given by

$$v_1 = k_1 [H_2O] [M] \quad (5.19)$$

Thus a plot of  $v_1/[H_2O]$  versus  $[M]$  should yield a straight line of slope  $k_1$ . Such plots are shown in Figure (5.12) for  $k_1$ . In Figure (5.13) is shown a similar plot for  $k_2$ . It was found that in argon and helium, the temporal dependence of  $NO_2^-(H_2O)_2$  could not be observed accurately. This

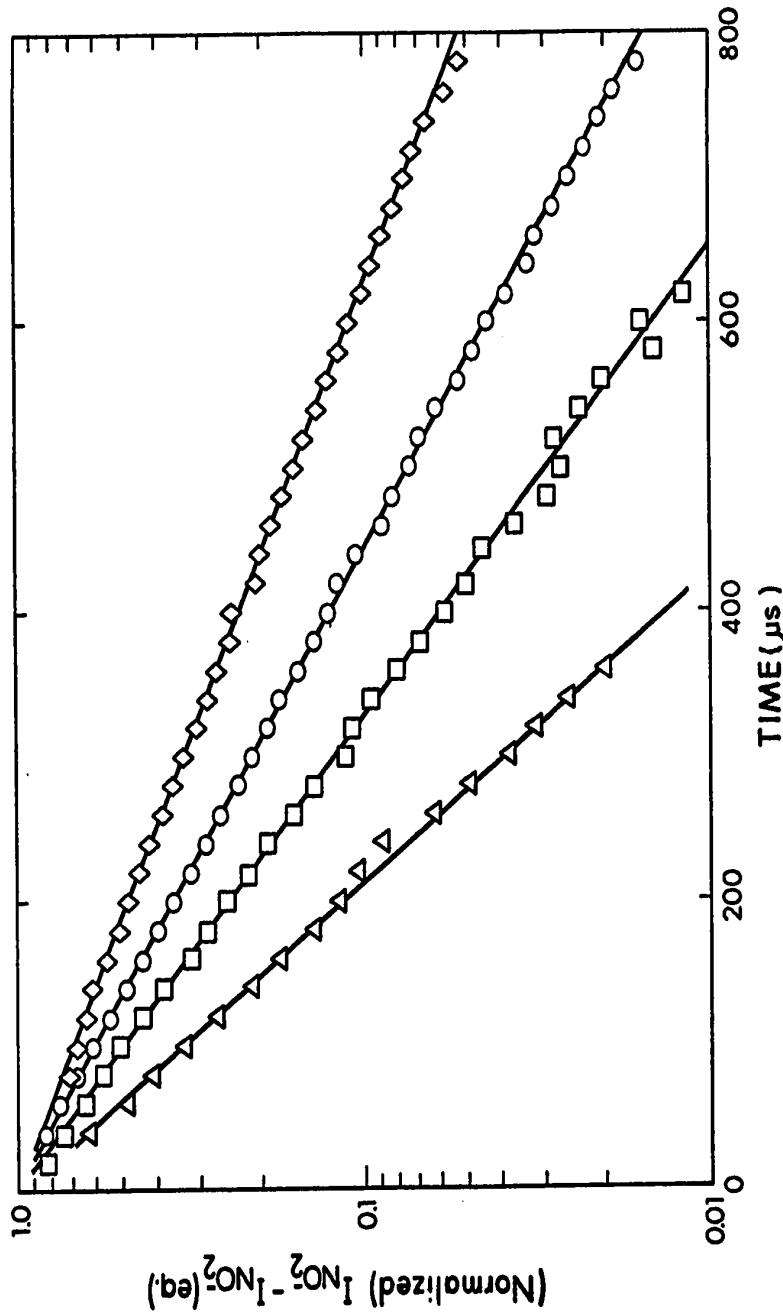


FIGURE 5.11. Logarithmic plots of normalized  $I_{NO_2} - I_{NO_2(eq)}$  versus time. First number after symbol is  $P_{O_2}$  in torr, number in brackets is  $P_{H_2O}$  in mtorr and the third number is  $\nu_1 + \nu_{-1}$  in units of  $10^3 s^{-1}$ .  $\square$  5.4 (14) 6.84,  $\circ$  1.47 (30.2) 5.27,  $\diamond$  3.79 (9.2) 3.66 and  $\Delta$  3.61 (32.7) 10.9.



TABLE 5.3

Comparison of Apparent First Order Rate Coefficients for  
 $\text{NO}_2^- + \text{H}_2\text{O} + \text{O}_2 \longrightarrow \text{NO}_2^- \cdot \text{H}_2\text{O} + \text{O}_2$  Calculated by Graphical<sup>a</sup>  
 and Computer Methods

$P_{\text{O}_2}$ <sup>b</sup>	$P_{\text{H}_2\text{O}}$ <sup>c</sup>	$v_1$ (graphical) <sup>a,d</sup>	$v_1$ (computer) <sup>d</sup>
5.4	14	6.53	6.8
1.47	30.2	5.16	5.6
3.8	9.2	3.42	3.5
3.61	32.7	10.67	10.6

All runs done at  $T = 300.5^\circ\text{K}$ .

<sup>a</sup> See Figure (5.11).

<sup>b</sup> In units of torr

<sup>c</sup> In units of millitorr

<sup>d</sup> In units of  $10^3 \text{ s}^{-1}$

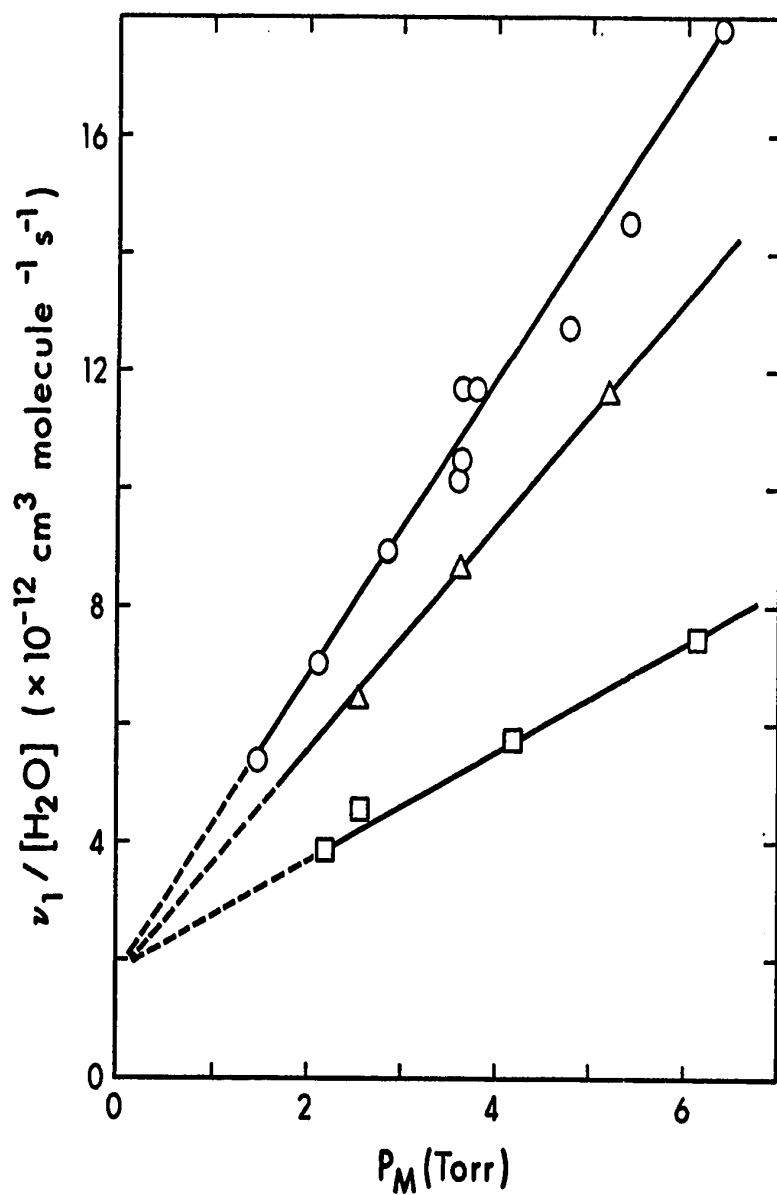


FIGURE 5.12. Dependence of  $v_1/[H_2O]$  on  $P_M$ . Plots show that the reaction  $NO_2^- + H_2O + M \rightarrow NO_2^- \cdot H_2O + M$  is dependent on the concentration of M. O  $M = O_2$ ,  $\Delta M = Ar$ , and  $\square M = He$ . Slopes of lines lead to  $k_1(O_2) = 8.4$ ,  $k_1(Ar) = 6.0$ , and  $k_1(He) = 2.9$  in units of  $10^{-29} \text{ cm}^6 \text{ molecule}^{-2} \text{ s}^{-1}$ .

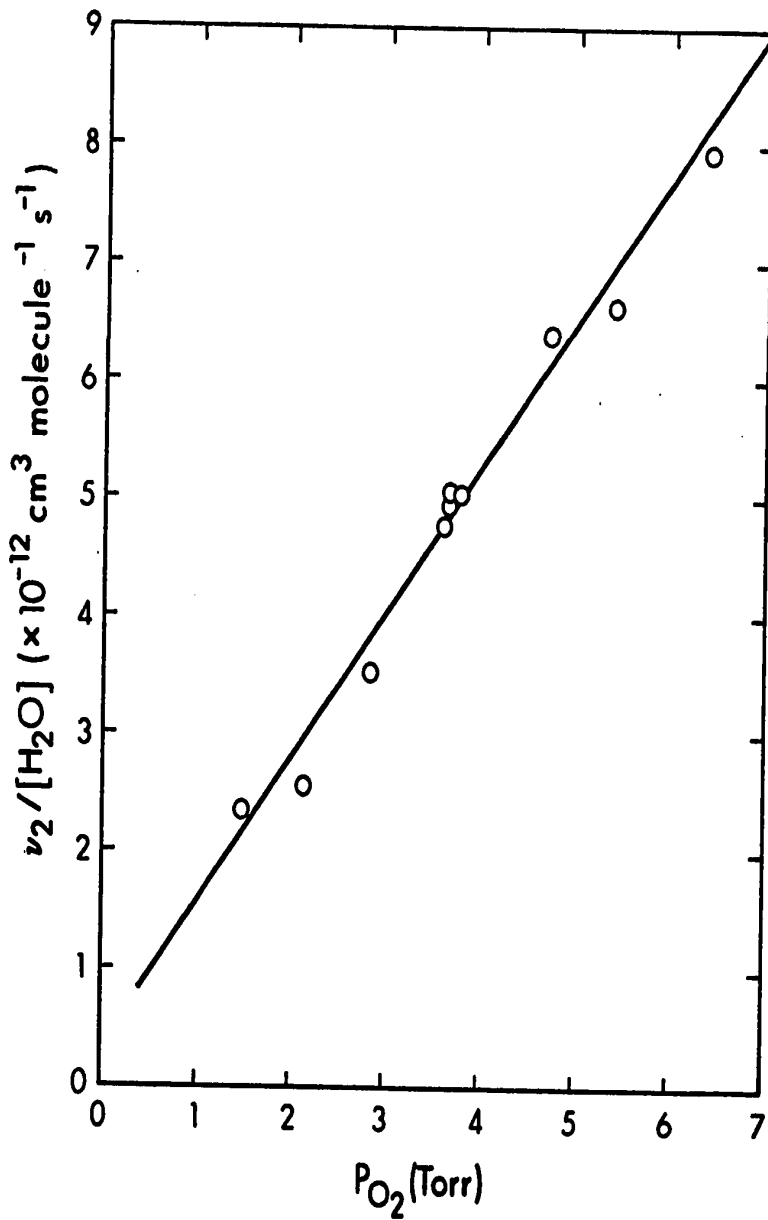


FIGURE 5.13. Dependence of  $v_2/[H_2O]$  on  $P_{O_2}$ . Plot shows that the reaction  $NO_2^-.H_2O + H_2O + O_2 \rightarrow 2NO_2^-(H_2O)_2 + O_2$  is dependent on the concentration of  $O_2$ . Slope of line leads to  $k_2 = 3.8 \times 10^{-29} \text{ cm}^6 \text{ molecule}^{-2} \text{ s}^{-1}$ .

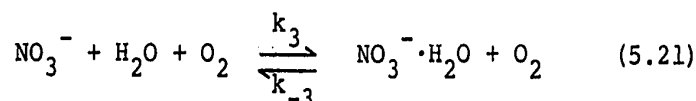
was due to a combination of the fast diffusion of the ions to the walls in the rare gas, and the slowness of these reactions when M = He or Ar. The graphical data obtained in the rare gases are summarized in Table 5.4.

In the experiments where argon and helium were used as carrier gases, the hydration reactions were slower than when oxygen was used as carrier gas. Furthermore diffusion of ions in the rare gases is faster than in oxygen (89,p.481) so the total signal decayed at a faster rate than in oxygen. The combination of these two effects was such that the  $\text{NO}_2^-$  signal became very small before equilibrium was established between  $\text{NO}_2^-$  and  $\text{NO}_2^- \cdot \text{H}_2\text{O}$ . Consequently the values of  $k_{-1}$  for argon and helium recorded in Table 5.5 were calculated using the known value of  $K_{0,1}(\text{NO}_2^-)$  from the study in oxygen and the relationship

$$K_{0,1}(\text{NO}_2^-) = k_1/k_{-1} \quad (5.20)$$

In Figure (5.14) is shown a plot of  $v_{-1}$  versus  $P_{\text{O}_2}$  demonstrating that reaction  $v_{-1}$  is dependent on the first power of the oxygen concentration. A similar plot is shown in Figure (5.15) for  $v_{-2}$ .

The conversion of  $\text{NO}_3^-$  to its monohydrate via the reaction



was observed. The dihydrate  $\text{NO}_3^-(\text{H}_2\text{O})_2$  was not observed

TABLE 5.4

Rate Constants for  $\text{NO}_2^- + \text{H}_2\text{O} + \text{M} \longrightarrow \text{NO}_2^- \cdot \text{H}_2\text{O} + \text{M}^a$

M	$P_M^b$	$P_{\text{H}_2\text{O}}^c$	$v_1^d$	$v_{-1}^d$
He	2.20	35.5	2.91	-
He	2.57	15.1	2.16	0.153
He	4.17	15.5	2.85	0.120
He	6.12	11.7	2.80	0.153
Ar	2.52	32.1	6.70	0.125
Ar	3.65	25.3	7.01	0.216
Ar	5.20	13.5	5.04	0.252

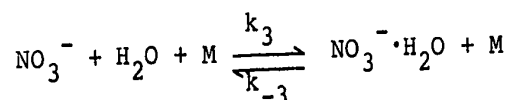
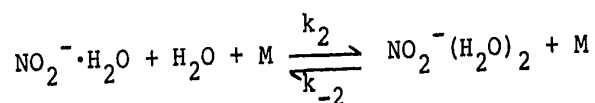
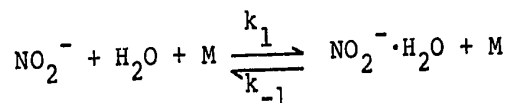
<sup>a</sup> T = 300.5°K

<sup>b</sup> Pressure in torr

<sup>c</sup> Pressure in millitorr

<sup>d</sup> In units of  $10^3 \text{ s}^{-1}$

TABLE 5.5

Summary of Kinetic DataReactionsPresent Results<sup>a</sup>

<u>Rate Constants</u>	<u>M</u>	<u>Rate Constant</u>
$k_1$	$\text{O}_2$	8.4
$k_1$	Ar	6.0
$k_1$	He	2.9
$k_{-1}$	$\text{O}_2$	1.6
$k_{-1}$	Ar	1.2
$k_{-1}$	He	0.6
$k_2$	$\text{O}_2$	$3.8 \times 10^{-29\text{b}}$
$k_{-2}$	$\text{O}_2$	$5.8 \times 10^{-14\text{c}}$
$k_3$	$\text{O}_2$	$7.5 \times 10^{-29\text{b}}$
$k_{-3}$	$\text{O}_2$	$1.4 \times 10^{-14\text{c}}$

Puckett and Lineberger<sup>d</sup> (52)

$k_1$	NO	$13 \pm 3 \times 10^{-29\text{c}}$
-------	----	------------------------------------

<sup>d</sup> T = 293°K<sup>a</sup> T = 300.5°K<sup>b</sup> In units of  $\text{cm}^6 \text{ molecule}^{-2} \text{ s}^{-1}$ <sup>c</sup> In units of  $\text{cm}^3 \text{ molecule}^{-1} \text{ s}^{-1}$

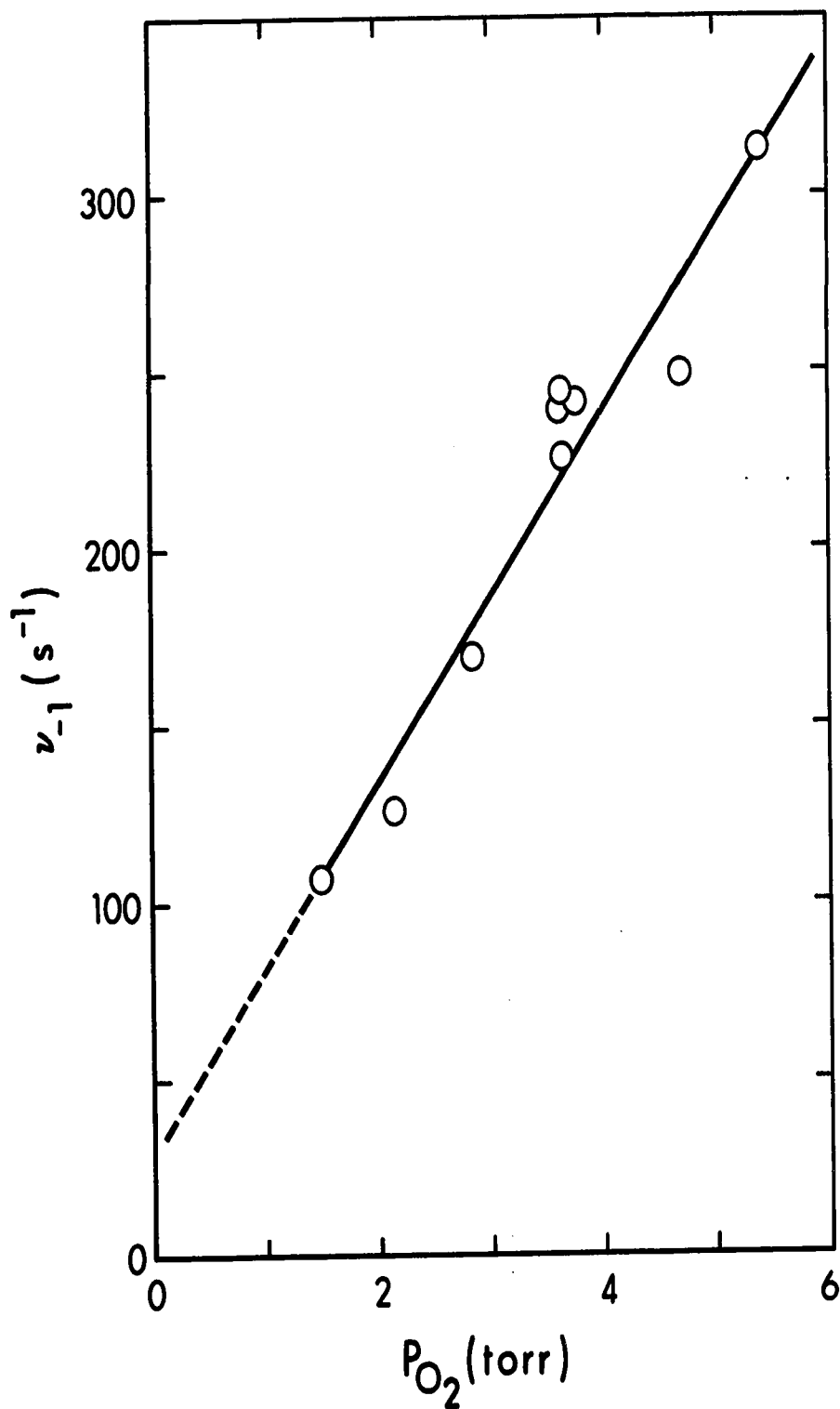


FIGURE 5.14. Dependence of  $v_{-1}$  on  $P_{O_2}$ . Plot shows that the reaction  $NO_2^- \cdot H_2O + O_2 \longrightarrow NO_2^- + H_2O + O_2$  is dependent on the concentration of  $O_2$ . Slope of line leads to  $k_{-1} = 1.6 \times 10^{-15} \text{ cm}^3 \text{ molecule}^{-1} \text{ s}^{-1}$ .

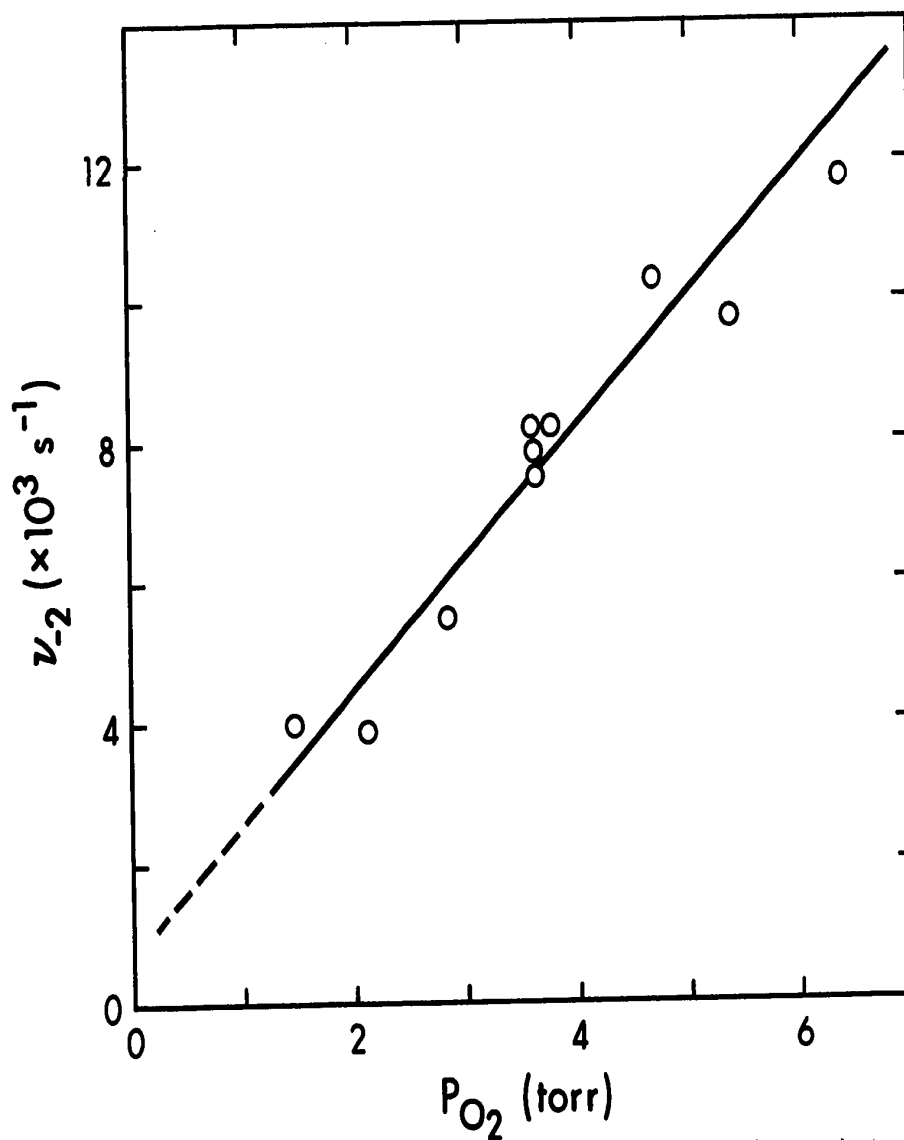


FIGURE 5.15. Dependence of  $v_{-2}$  on  $P_{O_2}$ . Plot shows that the reaction  $\text{NO}_2^-(\text{H}_2\text{O})_2 + \text{O}_2 \longrightarrow \text{NO}_2^{\cdot-} \cdot \text{H}_2\text{O} + \text{H}_2\text{O} + \text{O}_2$  is dependent on the concentration of  $\text{O}_2$ . Slope of line leads to  $k_{-2} = 5.8 \times 10^{-14} \text{ cm}^3 \text{ molecule}^{-1} \text{ s}^{-1}$ .



in significant amounts. It was clearly observed only at high water pressures (~50 mtorr). Consequently the kinetics of formation of  $\text{NO}_3^-(\text{H}_2\text{O})_2$  were not studied. The  $\text{NO}_3^-$  data was analysed graphically in a manner analogous to the  $\text{NO}_2^-$  data. The data is summarized in Table 5.2. Figure (5.16) shows some plots of  $\log_{10}([\text{NO}_3^-] - [\text{NO}_3^-]_{\text{eq}})$  versus time, and finally Figures (5.17) and (5.18) demonstrate that reaction (5.21) depends on the first power of the oxygen concentration. Table 5.5 summarizes the final kinetic results for the hydration of  $\text{NO}_2^-$  and  $\text{NO}_3^-$ .

The equilibrium constants for the hydration of  $\text{NO}_2^-$  and  $\text{NO}_3^-$  are displayed in Table 5.6. The measured equilibrium constants using water at low pressures in a carrier gas compare favourably with those which were obtained using water pressures in the torr range (Chapter 6). The values of  $K_{0,1}(\text{NO}_2^-)$  differ by roughly a factor of two, however, this is not serious since the value of the equilibrium constant in pure water involves an extrapolation of a van't Hoff plot. This extrapolation easily involves an error of a factor of two. The agreement between the K's determined at low and high water pressures is excellent as may be seen from Table 5.6.

The forward rate coefficients  $k_1$ ,  $k_2$  and  $k_3$  (summarized in Table 5.5) are all of similar value. The binding energies of these hydrates are  $-\Delta H_{0,1}(\text{NO}_2^-) = 14.3$ ,  $-\Delta H_{1,2}(\text{NO}_2^-) = 12.9$  and  $-\Delta H_{0,1}(\text{NO}_3^-) = 12.4$ , all in kcal/mole (Chapter 6).

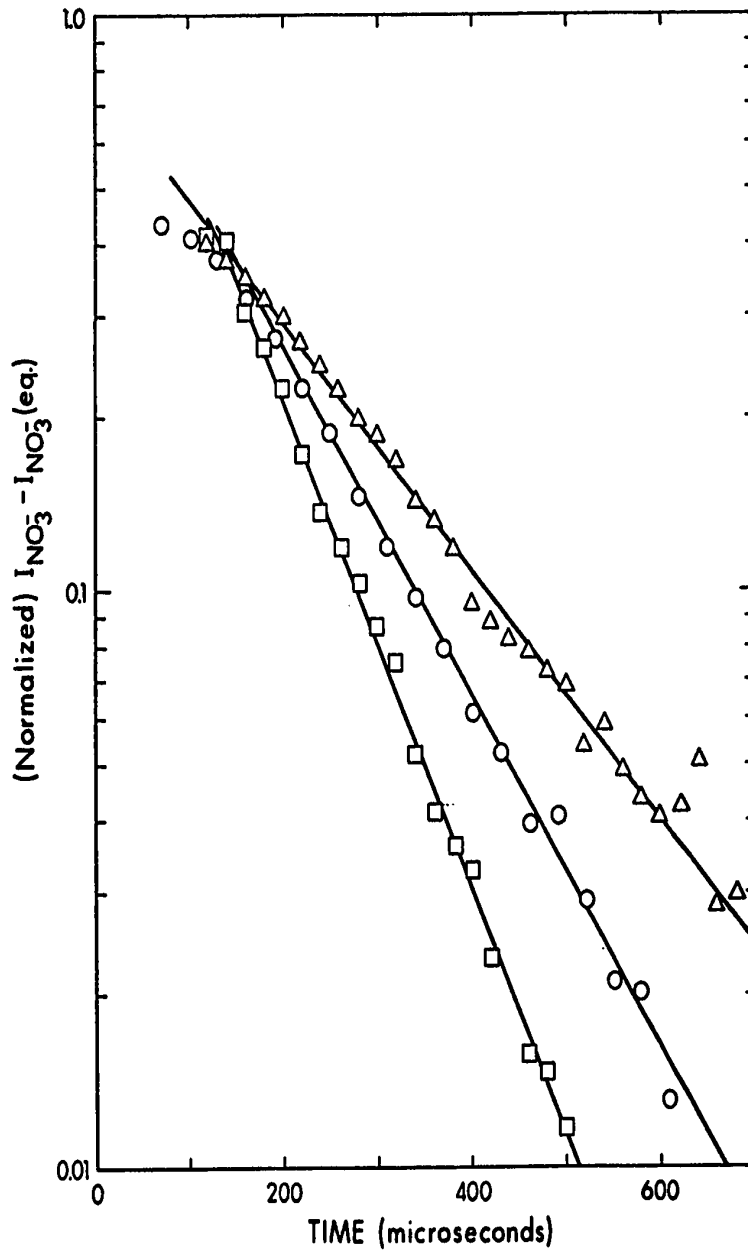


FIGURE 5.16. Logarithmic plots of normalized  $I_{\text{NO}_3} - I_{\text{NO}_3}(\text{eq})$  versus time. First numbers

after symbols is  $P_{\text{O}_2}$  in torr, numbers in brackets is  $P_{\text{H}_2\text{O}}$  in mtorr and the third number is  $\nu_3 + \nu_{-3}$  in units of  $10^3 \text{ s}^{-1}$   $\Delta$  3.79 (9.2) 5.18,  $\square$  3.64 (22.9) 9.75, and  $\circ$  2.14 (27.0) 6.80.

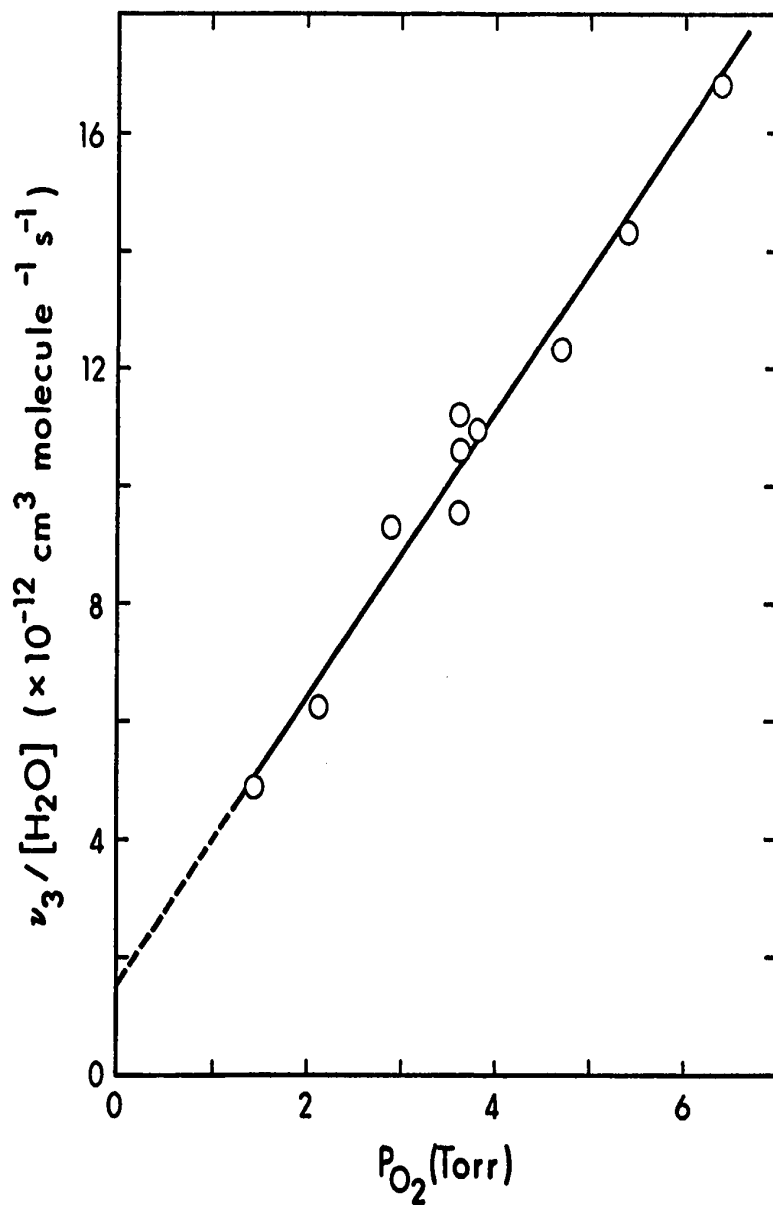


FIGURE 5.17. Dependence of  $v_3/[H_2O]$  on  $P_{O_2}$ . Plot shows that the reaction  $NO_3^- + H_2O + O_2 \rightarrow NO_3^- \cdot H_2O + O_2$  is dependent on the concentration of  $O_2$ . Slope of line leads to  $k_3 = 7.5 \times 10^{-29} \text{ cm}^6 \text{ molecule}^{-2} \text{ s}^{-1}$ .

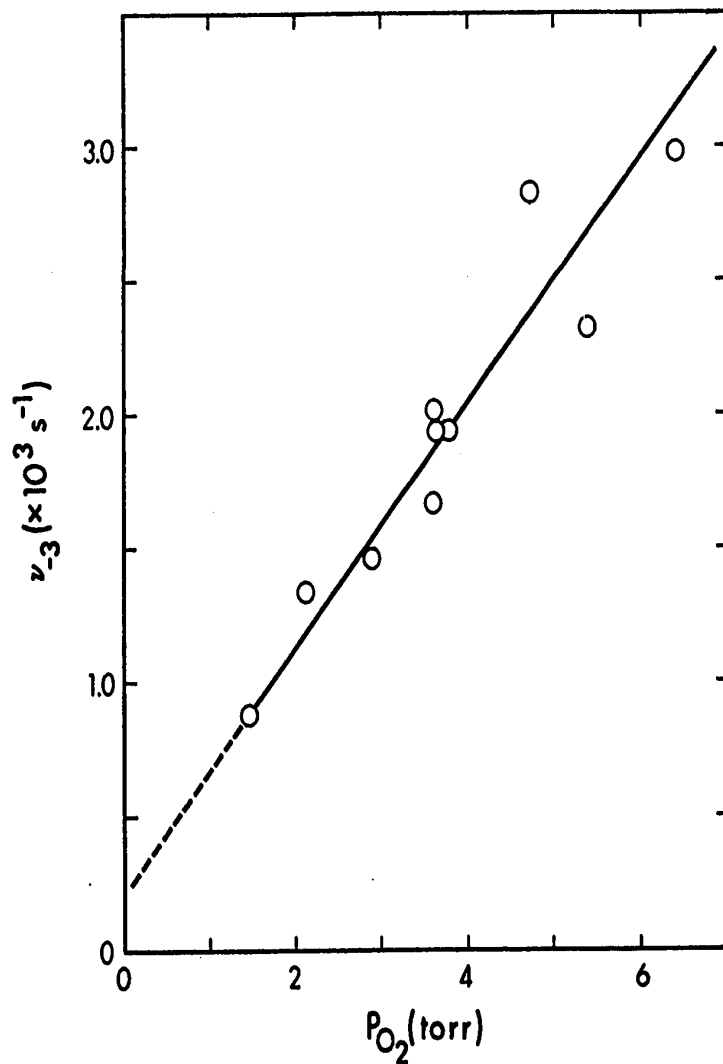


FIGURE 5.18. Dependence of  $v_{-3}$  on  $P_{O_2}$ . Plot shows that the reaction  $\text{NO}_3^- \cdot \text{H}_2\text{O} + \text{O}_2 \longrightarrow \text{NO}_3^- + \text{H}_2\text{O} + \text{O}_2$  is dependent on the concentration of  $\text{O}_2$ . Slope of line leads to  $k_{-3} = 1.4 \times 10^{-14} \text{ cm}^3 \text{ molecule}^{-1} \text{ s}^{-1}$ .

TABLE 5.6

Equilibrium Constants for  $\text{NO}_2^- (\text{H}_2\text{O})_{1,2}$  and  $\text{NO}_3^- \cdot \text{H}_2\text{O}$  <sup>a</sup>

---

	$K_{0,1}(\text{NO}_2^-)^b$	$K_{1,2}(\text{NO}_2^-)^b$	$K_{0,1}(\text{NO}_3^-)^b$
	<hr/>	<hr/>	<hr/>
Low water pressure			
O <sub>2</sub> carrier gas	5.2	0.066	0.53
Pure water as carrier			
gas. Extrapolated	3	0.065	0.49

<sup>a</sup> T = 300.5°K

<sup>b</sup> In units of  $10^{-14} \text{ cm}^3 \text{ molecule}^{-1}$

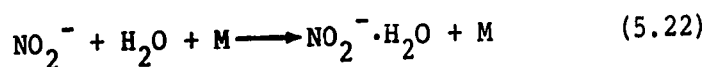
---

The formation of the species  $\text{NO}_2^- \cdot \text{H}_2\text{O}$  is associated with the largest  $-\Delta H_{n-1,n}$  and thus might be expected to display the largest forward rate coefficient. As was shown in Chapter 4, the forward rate of a termolecular reaction should increase the more exothermic the reaction and the greater the number of degrees of freedom of the resulting complex.

It would appear from the similarity of the forward rate constants  $k_1$ ,  $k_2$  and  $k_3$  that the effects of binding energy and degrees of freedom are somewhat self cancelling for these examples.

The rate coefficient for (5.7) is roughly a factor of two greater with  $M = \text{Ar}$  than with  $M = \text{He}$  and is a factor of three greater with  $M = \text{O}_2$ . This is to be expected considering the greater polarizability of argon and oxygen compared to helium. The lower efficiencies of argon and helium observed in the present determination are consistent with previous measurements in similar systems (115).

Puckett and Lineberger (52) have obtained a value of  $13 \pm 3 \times 10^{-29} \text{ cm}^6 \text{ molecule}^{-2} \text{ s}^{-1}$  for the reaction



at 293°K with  $M = \text{NO}$ . The present experiments yield a value of  $8.4 \times 10^{-29} \text{ cm}^6 \text{ molecule}^{-2} \text{ s}^{-1}$  at 300.5°K with  $M = \text{O}_2$ . There is no a priori reason to believe that  $\text{NO}$  should be a more efficient third body than  $\text{O}_2$ . However,

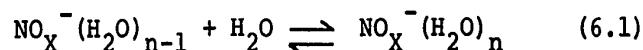
the difference between the present value and that of Puckett and Lineberger is probably within combined experimental error.

## VI The Thermodynamics of the Hydration of $\text{NO}_2^-$ and $\text{NO}_3^-$

### 6.1 Introduction

As was mentioned previously, the ions  $\text{NO}_3^-(\text{H}_2\text{O})_n$  are believed to be the dominant negative ion in the earth's ionosphere below  $\sim 90$  km (69,70). The determination of the thermodynamic data for the addition of successive molecules of water to  $\text{NO}_3^-$  will assist in the calculation of the equilibrium populations of the  $\text{NO}_3^-(\text{H}_2\text{O})_n$  in the D region.

The ions  $\text{NO}_2^-$  and  $\text{NO}_3^-$  are not only of interest in terms of the ion chemistry of the earth's ionosphere, but they are commonly occurring ions in aqueous solution. The addition of water to  $\text{NO}_2^-$  and  $\text{NO}_3^-$  via



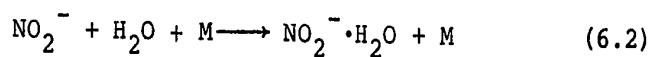
represents the first steps in the transformation of  $\text{NO}_X^-(\text{g})$  to  $\text{NO}_X^-(\text{aq})$ . The determination of the enthalpy for the successive additions of water molecules to the ions provides information regarding the nature of the species in aqueous solution. Kebarle et al (74-76,101) have conducted extensive studies on the formation of hydrated ions in the gas phase. The hydration of the halide ions,  $\text{O}_2^-$ , the alkali metal positive ions and the solvation of the halide ions by acetonitrile have been studied. It was believed that a study of the hydration of  $\text{NO}_2^-$  and  $\text{NO}_3^-$  would complement and extend the previous work.



## 6.2 Experimental

The equilibrium constants were measured by observing the relative intensities of the  $\text{NO}_x^-(\text{H}_2\text{O})_n$  species escaping from the ion source. The measurements were performed using water as the carrier gas at a pressure of several torr containing small amounts of ethyl nitrate. The mechanism of ion generation has been discussed in Chapter 5. To ensure that the measured ratios of the ions reflected the equilibrium ratios, the measurements were performed at some two to four different water pressures in the range 2.0 to 4.1 torr of water at each ion source temperature. It was noted that the equilibrium constant was independent of water pressure over a range of a factor of two. By using the pulsing circuitry the temporal profiles of the species of interest could be recorded. It was observed that in all cases the ratios of the  $\text{NO}_x^-(\text{H}_2\text{O})_n$  ions were constant with time - except for the first 50  $\mu\text{s}$  or so immediately after the electron pulse. The invariance of the ratio of the hydrated species with time is necessary if the ions are in thermodynamic equilibrium. An example of the observed temporal behaviour is shown in Figure (6.1).

In the preceding Chapter it was shown that the rate constant for



was  $8.5 \times 10^{-29} \text{ cm}^6 \text{ molecule}^{-2} \text{ s}^{-1}$  with  $\text{M} = \text{O}_2$ . Assuming

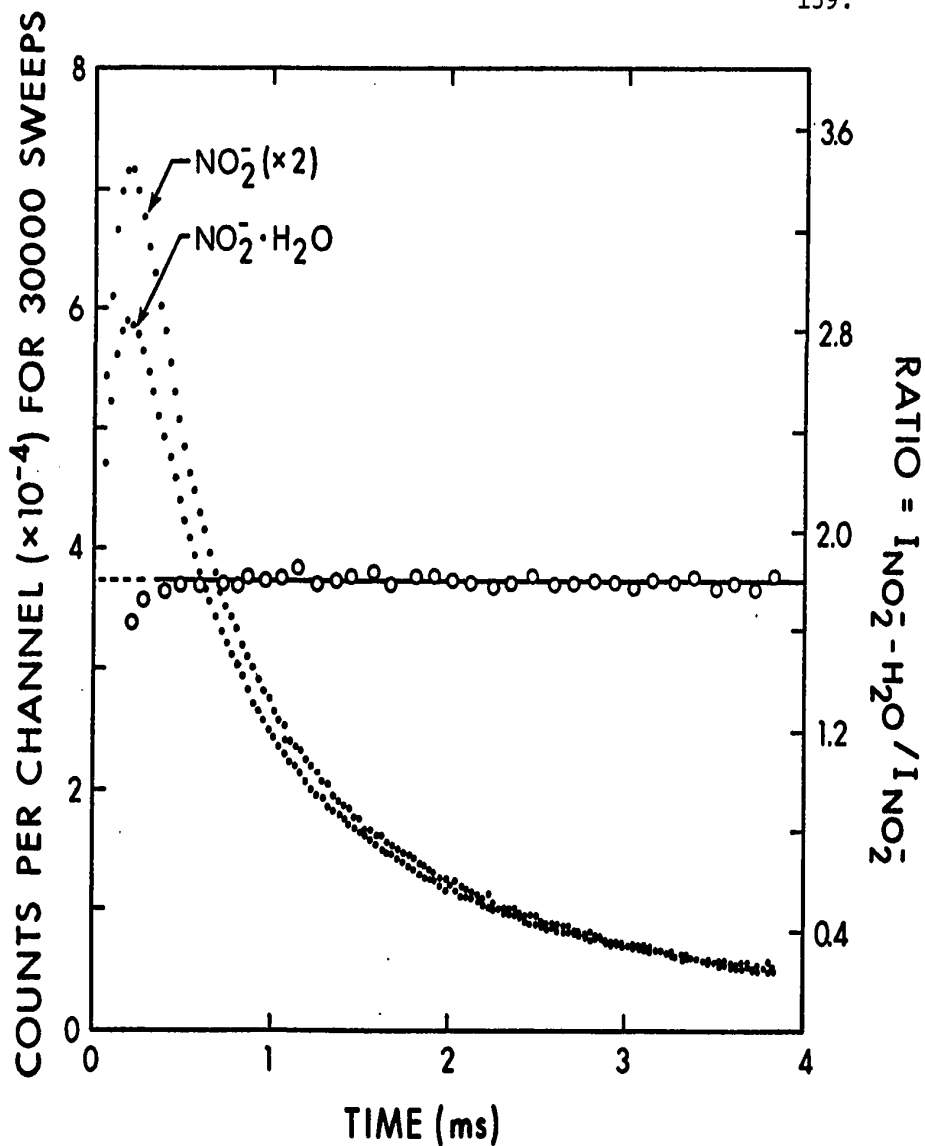


FIGURE 6.1. Time dependence of  $\text{NO}_2^-$  and  $\text{NO}_2^-\cdot\text{H}_2\text{O}$  escaping from the ion source after a short ( $\sim 10 \mu\text{s}$ ) electron pulse. Ion source pressure 4.1 torr of  $\text{H}_2\text{O}$  containing small ( $\sim 10$  mtorr) amounts of  $\text{C}_2\text{H}_5\text{ONO}_2$ .  $T = 164^\circ\text{C}$ . Ion intensity ratio required to be constant if equilibrium is achieved in the reaction  $\text{NO}_2^- + \text{H}_2\text{O} \rightleftharpoons \text{NO}_2^-\cdot\text{H}_2\text{O}$ .

that the forward rate constant for reaction (6.2) with  $M = H_2O$  is of the same magnitude i.e.  $\sim 10^{-28} \text{ cm}^6 \text{ molecule}^{-2} \text{ s}^{-1}$ , then for water pressures in the torr range and a temperature of  $\sim 100^\circ\text{C}$  it may be calculated that the half-life of the forward reaction is less than  $1 \mu\text{s}$ . This may be compared with the time interval over which the ions may be observed which is several milliseconds. Equilibrium is therefore expected to be achieved quickly in this system as was observed. Figure (6.2) shows the van't Hoff plots for the addition of three molecules of water to  $\text{NO}_2^-$  and one to  $\text{NO}_3^-$ . The calculated thermodynamic parameters are listed in Table 6.1.

### 6.3 Results and Discussion

#### A Calculation of Total Single Ion Heats of Hydration

The total single ion heats of hydration  $\Delta H_h(A^-)$  which are listed in Table 6.2 correspond to the enthalpy change for the process



The  $\Delta H_h(A^-)$  may be calculated using the expressions

$$\Delta H_h(A^-) = \Delta H_f(A^-,aq)_{\text{abs}} - \Delta H_f(A^-,g) \quad (6.4)$$

$$\Delta H_f(A^-,aq)_{\text{abs}} = \Delta H(A^-,aq)_{\text{conv}} - \Delta H_f(H^+,aq)_{\text{abs}} \quad (6.5)$$

$$\Delta H_f(A^-,g) = \Delta H_f(A,g) - EA(A) \quad (6.6)$$

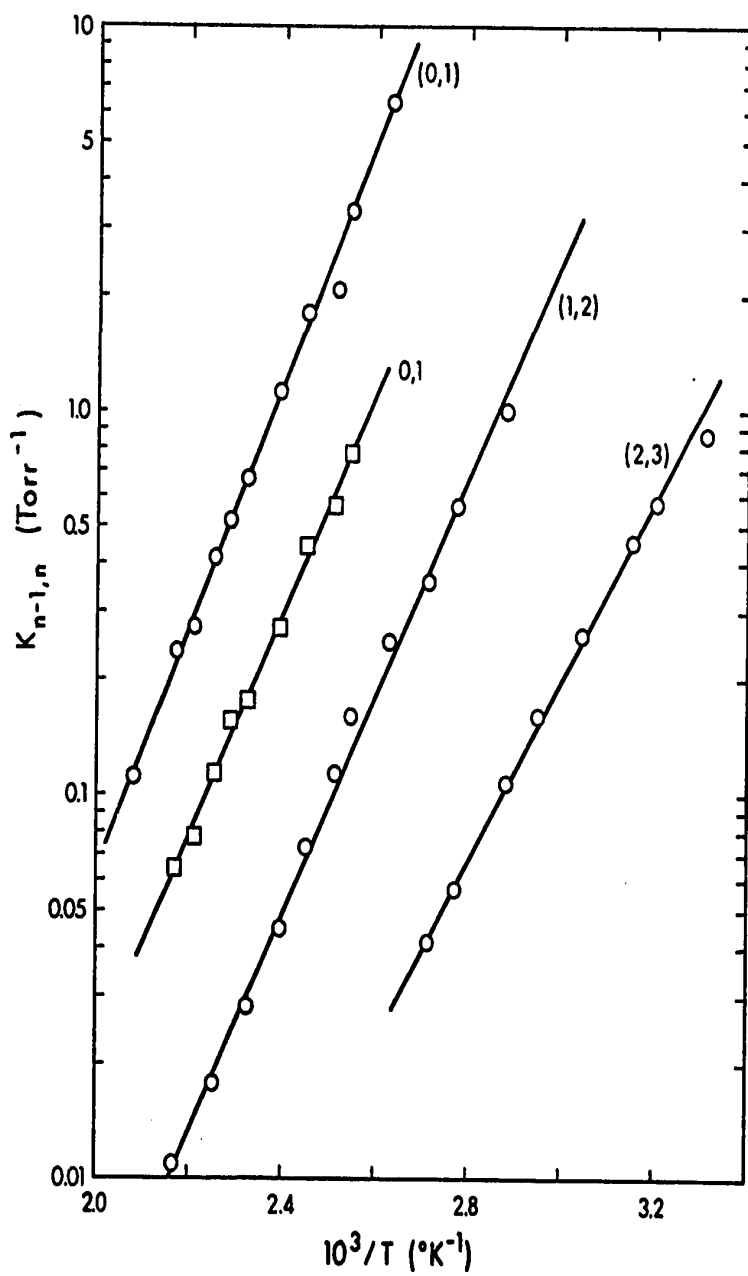


FIGURE 6.2. van't Hoff plots of equilibrium constants

$K_{n-1,n}$  for reactions  $A^-(\text{H}_2\text{O})_{n-1} + \text{H}_2\text{O} \rightleftharpoons A^-(\text{H}_2\text{O})_n$ .

O  $A = \text{NO}_2^-$ , and  $\square A = \text{NO}_3^-$ .

TABLE 6.1

Thermodynamic Values for the Hydration of  $\text{NO}_2^-$  and  $\text{NO}_3^-$

<u>Ion</u>	<u>n-1,n</u>	<u><math>-\Delta H_{n-1,n}^a</math></u>	<u><math>-\Delta S_{n-1,n}^{b,c}</math></u>	<u><math>-\Delta G_{n-1,n}^{a,c}</math></u>
$\text{NO}_2^-$	0,1	$14.3 \pm 0.3^d$	$21.0 \pm 0.7$	$8.1 \pm 0.5$
$\text{NO}_2^-$	1,2	$12.9 \pm 0.3$	$23.7 \pm 0.7$	$5.8 \pm 0.5$
$\text{NO}_2^-$	2,3	$10.4 \pm 0.3$	$21.2 \pm 0.7$	$4.0 \pm 0.5$
$\text{NO}_3^-$	0,1	$12.4 \pm 0.4$	$19.1 \pm 1.0$	$6.7 \pm 0.7$

<sup>a</sup> In kcal/mole

<sup>b</sup> In entropy units

<sup>c</sup> Standard state 1 atm and 300°K

<sup>d</sup> Quoted errors are one standard deviation

TABLE 6.2Total and Partial Enthalpies of Hydration of Some SingleNegative Ions<sup>a</sup>

$A^-$	$-\Delta H_h$	$-\Delta H_{0,1}$	$-\Delta H_{1,2}$	$-\Delta H_{2,3}$	Ref.
$OH^-$	116.3 <sup>b</sup>	24.0	17.9	15.1	101
$F^-$	113.3 <sup>c</sup>	23	16.6	13.7	75
$Cl^-$	81.3 <sup>c</sup>	13.1	12.7	11.7	75
$Br^-$	77.9 <sup>c</sup>	12.6	12.3	11.5	75
$I^-$	64.1 <sup>c</sup>	10.2	9.8	9.4	75
$CN^-$	78.1 <sup>b</sup>	13.8	-	-	116
$NO_2^-$	73 <sup>b</sup>	14.3	12.9	10.4	Present work
$NO_3^-$	68 <sup>b</sup>	12.4	-	-	Present work

<sup>a</sup> All values in kcal/mole,  $T = 300^\circ K$

<sup>b</sup> See Table 6.3

<sup>c</sup> Ref. (115)

where  $\Delta H_f(A^-,aq)_{abs}$  is the absolute heat of formation of the species  $A^-(aq)$  while  $\Delta H_f(A^-,aq)_{conv}$  is the "conventional" heat of formation relative to  $\Delta H_f(H^+,aq)_{conv} = 0$ . The value  $\Delta H_f(H^+,aq)_{abs} = 95.6$  kcal/mole (115) was used in these calculations. This is based on  $\Delta H_f(H^+,g) = 365.6$  kcal/mole and  $\Delta H_h(H^+) = -270$  kcal/mole (115). The parameters used in the calculation are summarized in Table 6.3.

The  $-\Delta H_{0,1}$  values for the hydration of several ions are compared to the  $-\Delta H_h$  of these ions in Figure (6.3). The halide ions appear to lie on a smooth curve and there appears to be a trend toward increasing  $-\Delta H_h$  as  $-\Delta H_{0,1}$  increases. The halide ions might well be expected to vary smoothly since as one moves from one ion to another the dimensions of the ions change systematically. The ion  $OH^-$  also follows the trend of the halide ions perhaps reflecting the difference in size between O and H. The electron cloud of the hydrogen atom being so much smaller than that of the oxygen atom that the species  $OH^-$  is nearly spherical. The other more structured ions deviate somewhat from the trend of the halide ions which perhaps reflects their non-spherical nature.

#### B. Determination of $EA(NO_2)$ and $EA(NO_3)$

The heterolytic bond dissociation energy of  $HB$ ,  $D(H^+ - B^-)$  is the enthalpy of the process

TABLE 6.3  
Heats of Hydration<sup>a</sup>

$A^-$	$\Delta H_f(A^-, aq)_{conv}$	$\Delta H_f(A, g)$	EA (A)	$-\Delta H_h(A^-)$
$OH^-$	-55 <sup>b</sup>	9.31 <sup>b</sup>	42.5 <sup>c</sup>	116.3 <sup>d</sup>
$CN^-$	36 <sup>b</sup>	106.5 <sup>e</sup>	88 <sup>e</sup>	78.1 <sup>d</sup>
$NO_2^-$	-25 <sup>b</sup>	7.9 <sup>b</sup>	~55 <sup>f</sup>	73 <sup>d</sup>
$NO_3^-$	-45.6 <sup>b</sup>	16.6 <sup>g</sup>	~90 <sup>f</sup>	68 <sup>d</sup>

<sup>a</sup> All values in kcal/mole, 300°K

<sup>b</sup> Ref. (117)

<sup>c</sup> Ref. (118)

<sup>d</sup> Mode of calculation described in section 6.3A

<sup>e</sup> Ref. (119)

<sup>f</sup> See Table 6.4

<sup>g</sup> Ref. (114).



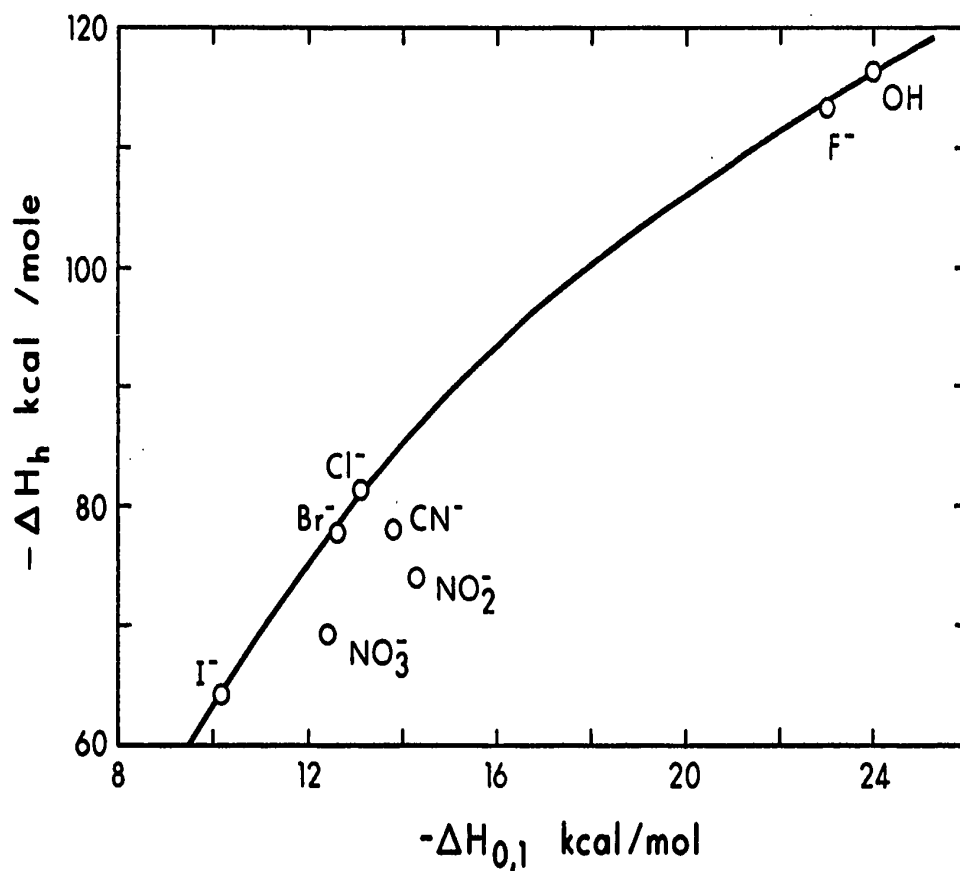
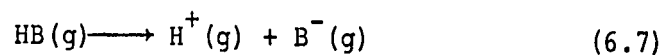


FIGURE 6.3. Plot of heat of hydration for negative ions  $A^-$  versus  $-\Delta H_{0,1}$  where  $\Delta H_{0,1}$  corresponds to the enthalpy change in the reaction  $A^- + H_2O \rightarrow A^- \cdot H_2O$ .



which is given by

$$D(\text{H}^+ - \text{B}^-) = D(\text{H} - \text{B}) + I_p(\text{H}) - \text{EA}(\text{B}) \quad (6.8)$$

where  $\text{EA}(\text{B})$  is the electron affinity of B,  $I_p(\text{H})$  is the ionization potential of the hydrogen atom, and  $D(\text{H} - \text{B})$  is the bond dissociation energy of the neutral HB. The bigger  $D(\text{H}^+ - \text{B}^-)$ , the stronger is the basicity of the Bronsted gas phase base  $\text{B}^-$ . The enthalpy change  $-\Delta H_{0,1}$  for the addition of water to various bases  $\text{B}^-$  may be visualized as an almost complete donation of the proton by  $\text{H}^+ - \text{B}^-$  to  $\text{OH}^-$ . Thus  $-\Delta H_{0,1}$  should also be an expression of the gas phase basicity of  $\text{B}^-$ . A plot of  $-\Delta H_{0,1}$  versus  $D(\text{H}^+ - \text{B}^-)$  is shown in Figure (6.4) for various bases.

As may be seen there is a trend in the data. The line shown is drawn to pass through the halide ion points. Since the  $\Delta H_{0,1}$  for  $\text{NO}_2^-$  and  $\text{NO}_3^-$  have been determined, these points have been placed on the line. From this plot  $D(\text{H}^+ - \text{B}^-)$  may be estimated for  $\text{HNO}_2$  and  $\text{HNO}_3$  and from equation (6.8) values for the electron affinities of  $\text{NO}_2$  and  $\text{NO}_3$  may be estimated. The present values along with other reported measurements are presented in Table 6.4. The present estimate of  $\text{EA}(\text{NO}_3)$  and  $\text{EA}(\text{NO}_2)$  are seen to be in fortuitously good agreement with more precise

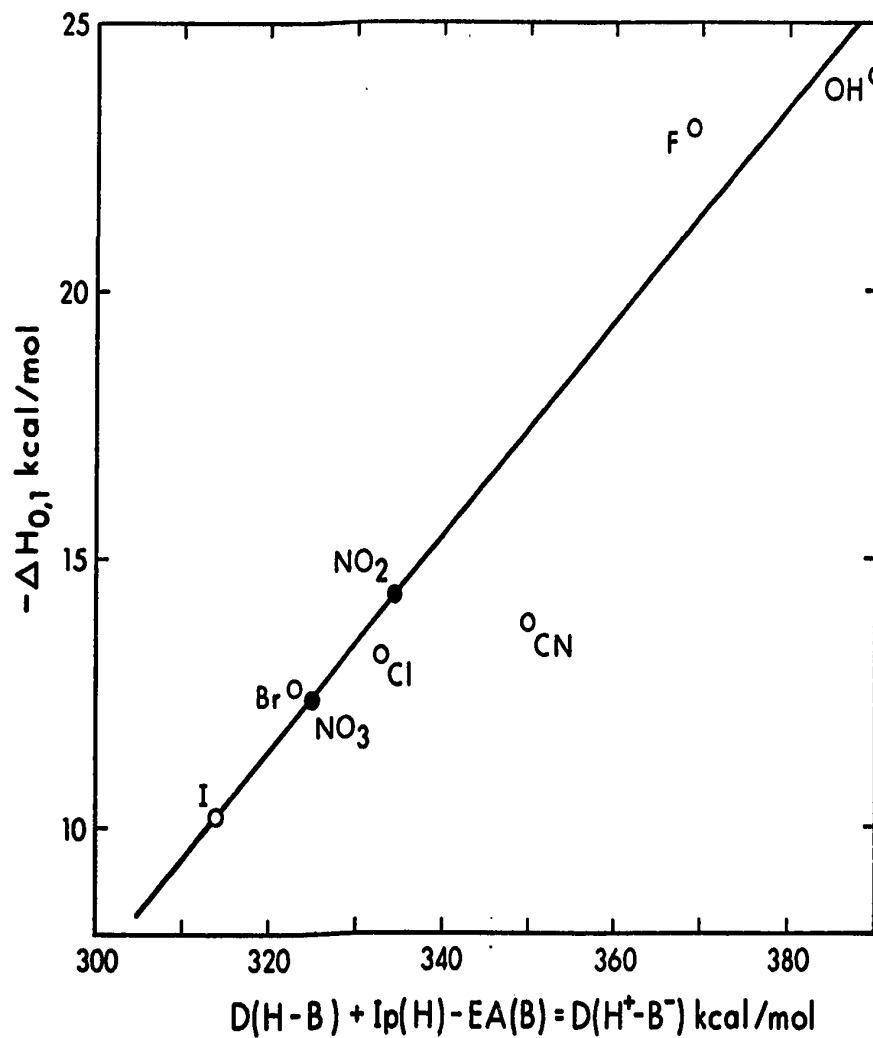


**FIGURE 6.4.** Plot of  $\Delta H_{0,1}$  for the reaction  $\text{A}^- + \text{H}_2\text{O} \longrightarrow \text{A}^-\cdot\text{H}_2\text{O}$  versus the heterolytic bond dissociation energy  $D(\text{H}^+\cdot\text{B}^-)$  corresponding to the process  $\text{HB} \longrightarrow \text{H}^+ + \text{B}^-$ .

TABLE 6.4Electron Affinities of NO<sub>2</sub> and NO<sub>3</sub><sup>a</sup>

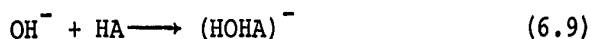
<u>EA(NO<sub>2</sub>)</u>	<u>Ref.</u>
2.4 ± 0.3	Present work
2.38 ± 0.06	Ferguson et al (120)
2.30 ± 0.15	Tiernan et al (121)
2.5 ± 0.1	Baede (122)
>2.04	Berkowitz et al (123)
>3.612 = EA(Cl)	Curran (124), Nalley et al (125)
<3.612 = EA(Cl)	Ferguson et al (126)
3.10 ± 0.05	Warneck (127)
<2.3	Vogt (128)
<u>EA(NO<sub>3</sub>)</u>	<u>Ref.</u>
3.9 ± 0.3 <sup>b</sup>	Present work
>2.48	Berkowitz et al (123)
>3.09	Ferguson et al (129)
3.9	Yalsimirskii (130)
3.9 ± 0.2	Ferguson et al (47)

<sup>a</sup> All values in electron volts.

<sup>b</sup> Estimated error.

estimates of these quantities which appeared in the literature after the present results were obtained (1970).

Consider the reaction



compared to the reaction



Let us assume that the resulting cluster ions  $(\text{HOHA})^-$  in reactions (6.9) and (6.10) are identical. Reaction (6.9) corresponds to HA virtually completely donating its proton to  $\text{OH}^-$  so that the electron may be crudely visualized as associated with A and the proton with the OH. The present experiment measures the enthalpy for reaction (6.10), thus knowing the  $\Delta H_f(\text{A}^-)$  and  $\Delta H_f(\text{H}_2\text{O})$  the  $\Delta H_f(\text{HOHA}^-)$  may be calculated. From the  $\Delta H_f(\text{OH}^-)$  and  $\Delta H_f(\text{HA})$  the exothermicity of reaction (6.9) may be calculated. This exothermicity varies from 86 kcal/mole for HA = HI to 24 kcal/mole for HA = HOH. Since the proton of HA is largely donated to  $\text{OH}^-$  in (6.9), the  $-\Delta H$ 's (6.9) should be a reflection of the gas phase strength of the the acid HA. Thus a correlation might be expected between the  $-\Delta H$ 's of (6.9) and  $D(\text{H}^+ - \text{A}^-)$ . This is shown in Figure (6.5) and as may be seen, there is an excellent correlation

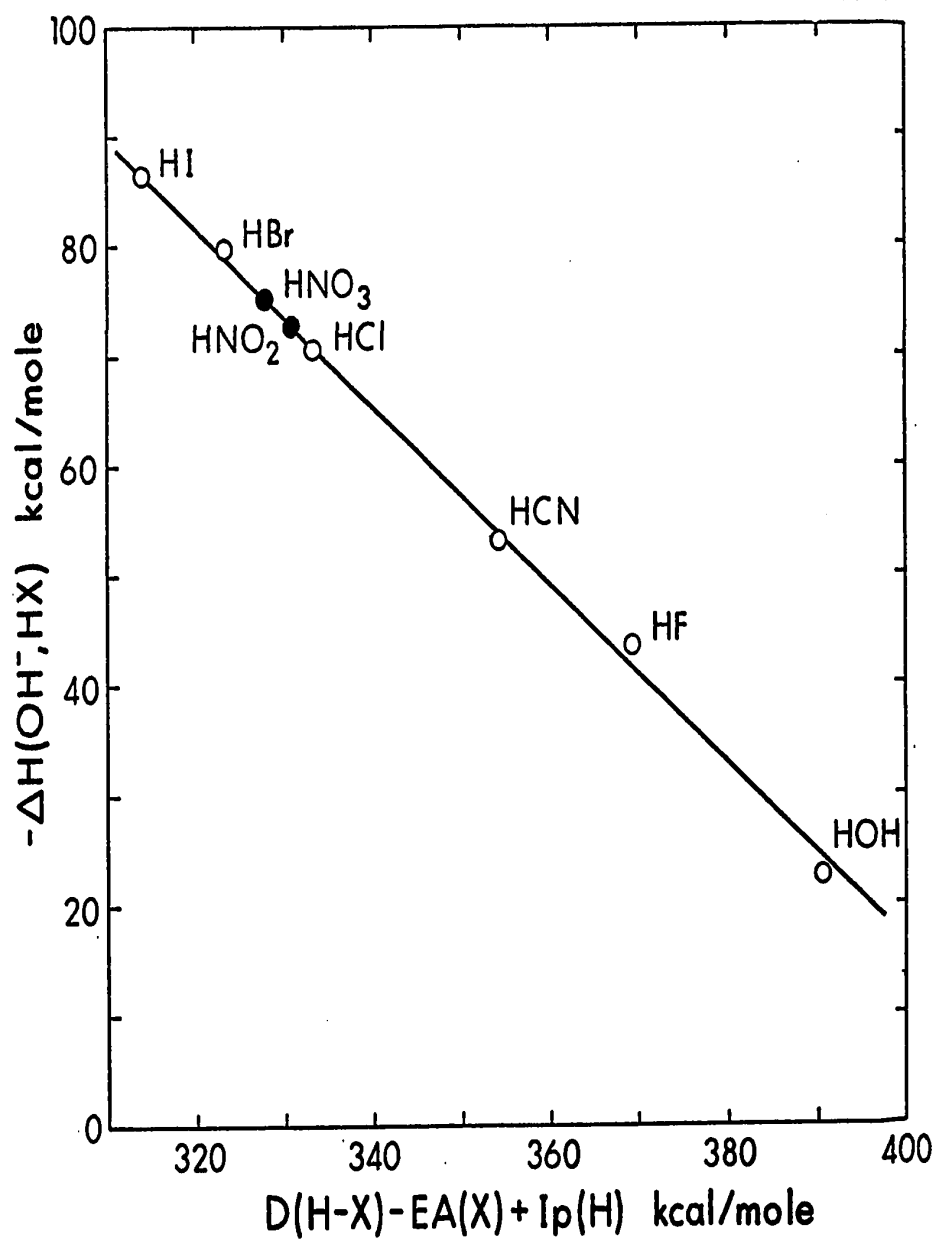
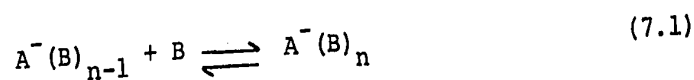


FIGURE 6.5. Plot of  $\Delta H(\text{OH}^-, \text{HX})$  for the reaction  $\text{OH}^- + \text{HX} \rightarrow \text{OH}^-\cdot\text{HX}$  versus the heterolytic bond dissociation energy  $D(\text{H}^+-\text{X}^-) = D(\text{H-X}) - \text{EA}(\text{X}) + I_p(\text{H})$ .

VII Solvation of  $O_2^-$  and  $Cl^-$  with  $H_2O$ ,  $CH_3OH$  and  $CH_3CN$

7.1 Introduction

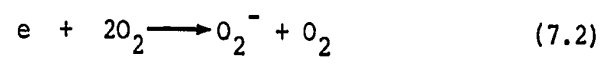
In this laboratory extensive studies have been conducted on reactions of the type



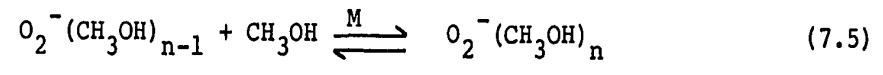
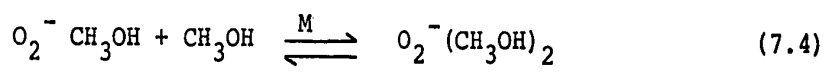
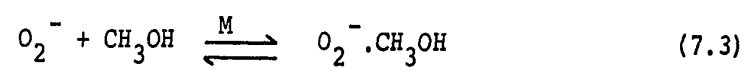
Arshadi and Kebarle (101) have studied the ( $O_2^- - H_2O$ ) system and Yamdagni and Kebarle (116) have studied the clustering of  $Cl^-$  with  $H_2O$ ,  $CH_3OH$  and  $CH_3CN$  and  $O_2^-$  with  $CH_3CN$ . To complement and extend these investigations a study was undertaken of the ( $O_2^- - CH_3OH$ ) system, the results of which are the subject of this Chapter.

7.2 Experimental Results

The apparatus and method of measurement were essentially the same as that described in the study of the kinetics of hydration of  $O_2^-$  (Chapter 4) and in the thermodynamics of the hydration of  $NO_x^-$  (Chapter 6). Pure oxygen gas was flowed through the ion source at a pressure of 4.0 torr. To the flowing stream of oxygen was added methanol vapour in the pressure range 0.5 to 2.0 torr. The methanol was added through a capillary which had been calibrated by "weight loss" measurements similar to those which were described in Chapter 4. The ion  $O_2^-$  was presumably generated as before by the third body attachment reaction



The methanol then clustered about the  $O_2^-$  forming  $O_2^-(CH_3OH)_n$  via the reactions



The  $O_2^-(CH_3OH)_n$  ions were observed to remain a constant fraction of the total ionization with time after the initial electron pulse. The equilibrium constants for the reaction (7.5) were found to be independent of the partial pressure of methanol. Plots of the  $K_{n-1,n}$  for the methanol system versus  $P_{CH_3OH}$  are shown in Figures (7.1-7.3) for various ion source temperatures. As can be seen the  $K_{n-1,n}$  are independent of the partial pressure of methanol within experimental error. In Figure (7.4) are displayed the van't Hoff plots for reaction (7.5). The thermodynamic parameters obtained from these plots are summarized in Table 7.1 along with some other data obtained in this laboratory for purposes of comparison.

7.3 Discussion of Results

For a visual comparison, the variation of  $-\Delta H_{n-1,n}$



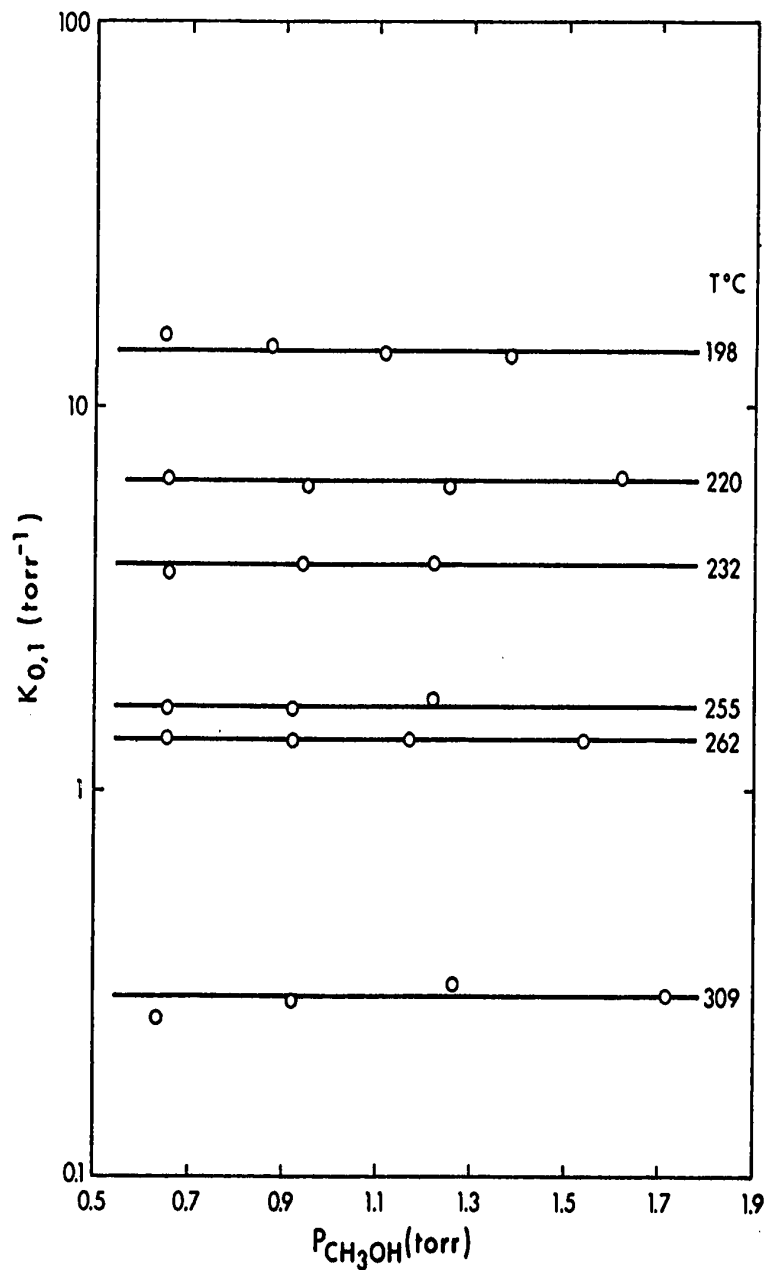


FIGURE 7.1. Plot of the equilibrium constant  $K_{0,1}$  for the reaction  $O_2^- + CH_3OH \rightleftharpoons O_2^- \cdot CH_3OH$  as a function of the partial pressure of methanol at various experimental temperatures. Total pressure is 4.0 torr ( $O_2$ ). As may be seen the equilibrium constants are independent of the partial pressure of methanol.

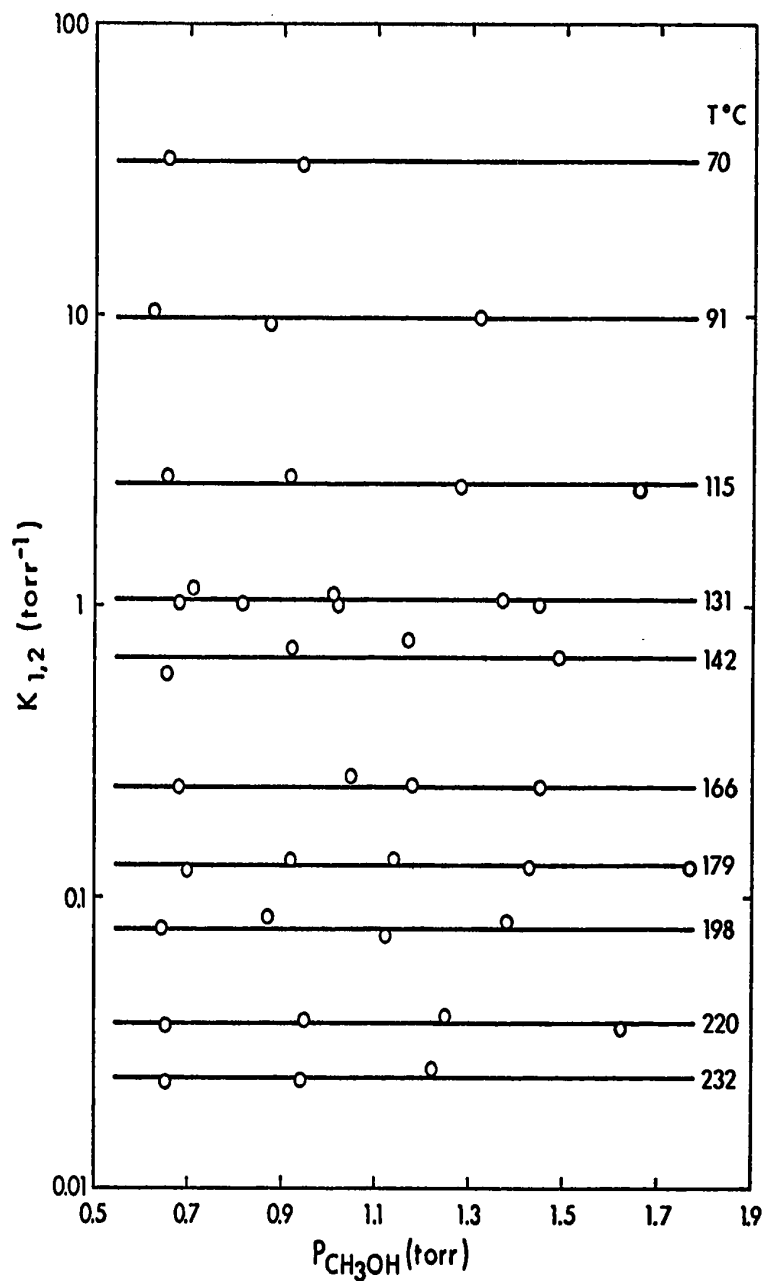


FIGURE 7.2. Plot of the equilibrium constant  $K_{1,2}$  for the reaction  $O_2^{\cdot-} \cdot CH_3OH + CH_3OH \rightleftharpoons O_2^{\cdot-} (CH_3OH)_2$  as a function of the partial pressure of methanol at various experimental temperatures. Total pressure is 4.0 torr ( $O_2$ ). As may be seen the equilibrium constants are independent of the partial pressure of methanol.

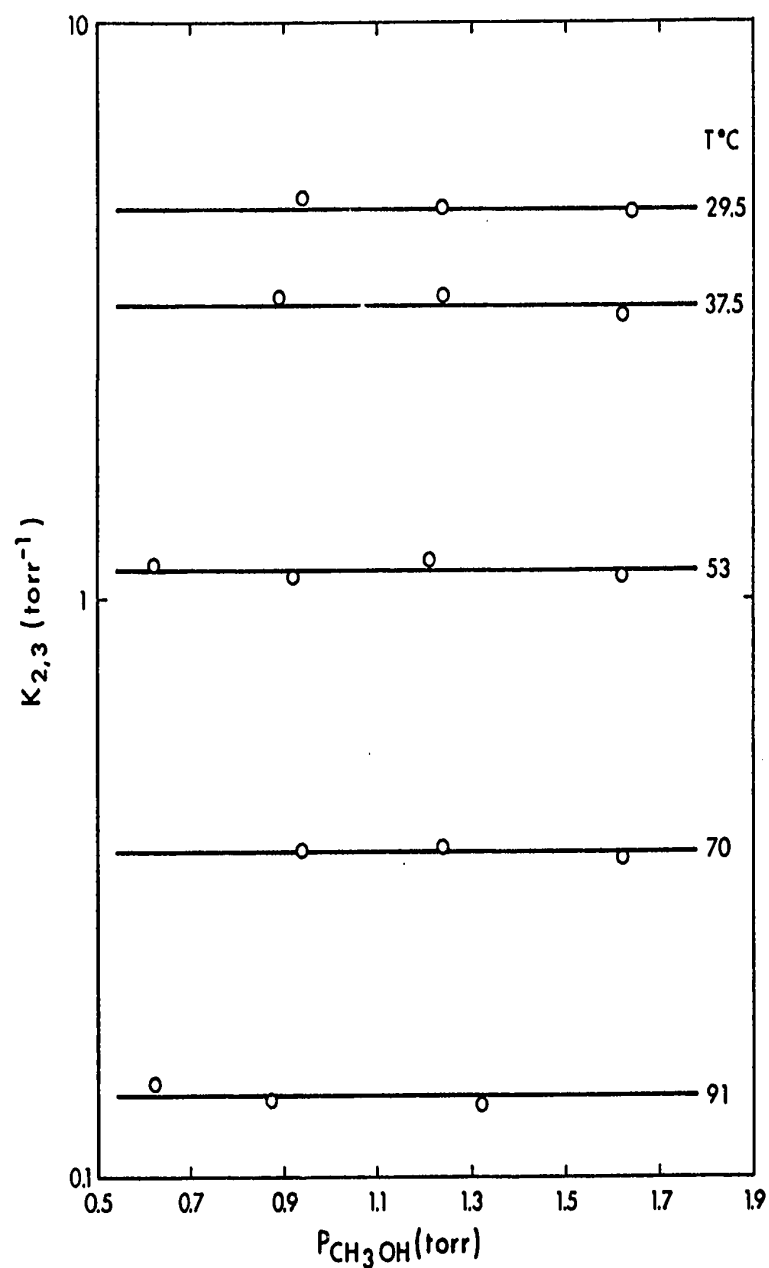


FIGURE 7.3. Plot of the equilibrium constant  $K_{2,3}$  for the reaction  $O_2^-(CH_3OH)_2 + CH_3OH \rightleftharpoons O_2^-(CH_3OH)_3$  as a function of the partial pressure of methanol at various experimental temperatures. Total pressure is 4.0 torr ( $O_2$ ). As may be seen the equilibrium constants are independent of the partial pressure of methanol.

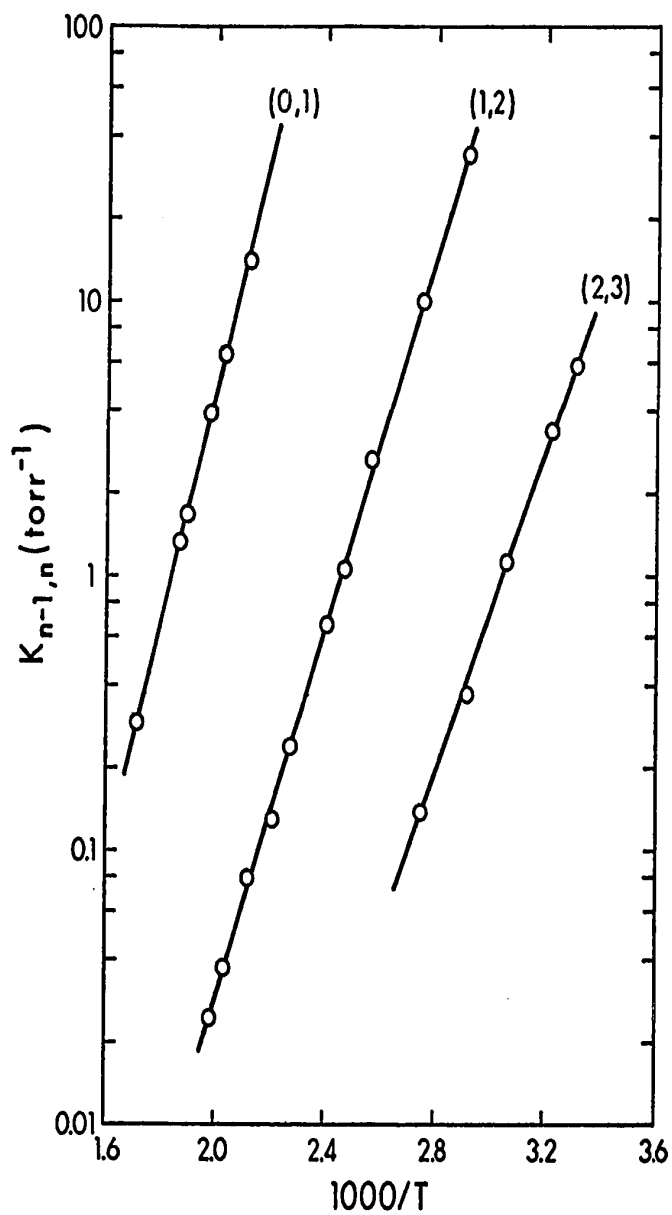


FIGURE 7.4. van't Hoff plot of the data of Figures (7.1-7.3) for the reaction  $\text{O}_2^-(\text{CH}_3\text{OH})_{n-1} + \text{CH}_3\text{OH} \rightleftharpoons \text{O}_2^-(\text{CH}_3\text{OH})_n$ . The thermodynamic data determined from these plots is summarized in Table 7.1.

TABLE 7.1

Thermodynamic Data for the Reaction  $A^{\cdot-}.B_{n-1} + B \rightleftharpoons A^{\cdot-}.B_n$

A	B		n-1,n				
			(0,1)	(1,2)	(2,3)	(3,4)	(4,5)
F <sup>-</sup>	H <sub>2</sub> O <sup>d</sup>	-ΔH <sup>a</sup>	23.3	16.6	13.7	13.5	13.2
		-ΔS <sup>b,c</sup>	17.4	18.7	20.4	36.9	30.7
		-ΔG <sup>a,c</sup>	18.1	11.0	7.6	5.5	7.1
O <sub>2</sub> <sup>-</sup>	H <sub>2</sub> O <sup>e</sup>	-ΔH	18.4	17.2	15.4		
		-ΔS	20.1	25.1	28.2		
		-ΔG	12.5	9.7	7.0		
O <sub>2</sub> <sup>-</sup>	CH <sub>3</sub> OH	-ΔH	19.1	15.5	13.5		
		-ΔS	21.9	24.8	27.9		
		-ΔG	12.5	8.1	5.2		
O <sub>2</sub> <sup>-</sup>	CH <sub>3</sub> CN <sup>f</sup>	-ΔH	16.4	14.2	11.9	9.5	
		-ΔS	17.4	22.0	24.7	22.4	
		-ΔG	11.2	7.7	4.5	2.8	
Cl <sup>-</sup>	H <sub>2</sub> O <sup>d</sup>	-ΔH	13.1	12.7	11.7	11.1	
		-ΔS	16.5	20.8	23.2	25.8	
		-ΔG	8.2	6.5	4.5	3.4	
Cl <sup>-</sup>	CH <sub>3</sub> OH <sup>f</sup>	-ΔH	14.2	13.0	12.3	11.2	10.5
		-ΔS	14.8	19.4	23.6	26.4	25.5
		-ΔG	9.8	7.2	5.2	3.3	2.9

(continued.....)

Table 7.1 (continued)

	-ΔH	13.4	12.2	10.6	6.2
Cl <sup>-</sup> CH <sub>3</sub> CN <sup>g</sup>	-ΔS	14.3	18.9	20.1	10.8
	-ΔG	9.2	6.6	4.6	3.0

<sup>a</sup> In kcal/mole

<sup>b</sup> In entropy units

<sup>c</sup> Standard state 1 atm, T = 300°K

<sup>d</sup> Ref. (75)

<sup>e</sup> Ref. (101)

<sup>f</sup> Ref. (116)

<sup>g</sup> Ref. (74)

with  $n$  for the ions  $F^-$ ,  $O_2^-$  and  $Cl^-$  are shown in Figure (7.5). We may start the discussion with the behaviour of  $Cl^-$  which is a typical "medium size" spherical negative ion. The strongest (largest  $-\Delta H_{n-1,n}$ ) interaction is observed with  $CH_3OH$  followed by  $CH_3CN$  and  $HOH$ . Methanol and water are both protic solvents while  $CH_3CN$  is aprotic. The dependence of the  $-\Delta H_{0,1}$  interactions of  $Cl^-$  on the nature of the protic solvents  $RH$  has been examined by Yamdagni and Kebarle (134) who discussed hydrogen bonding to negative ions. It was concluded that the  $-\Delta H_{0,1}$  which corresponds to the dissociation energy of the hydrogen bond  $D(Cl^- - HR)$ , increases with the proton donating power i.e., the gas phase acidity of  $HR$ . The higher  $-\Delta H_{0,1}$  for methanol relative to water was ascribed to a higher gas phase acidity of methanol which was in agreement with gas phase acidity measurements by Brauman and Blair (131). The present results extend the comparison to higher  $n$ . In Figure (7.5) one observes that methanol remains a better "solvent" also for higher  $n$  but that the difference between methanol and water decreases with increasing  $n$ . Extrapolation of these  $-\Delta H_{n-1,n}$  values indicates a possible cross over i.e. a larger  $-\Delta H$  for water at the  $\Delta H_{4,5}$  step. Earlier gas phase solvation work (75) has indicated that the trends in the  $-\Delta H_{n-1,n}$  values observed even for only the first four or five steps reflect differences in the total single ion enthalpies and free energies of solvation. This seems

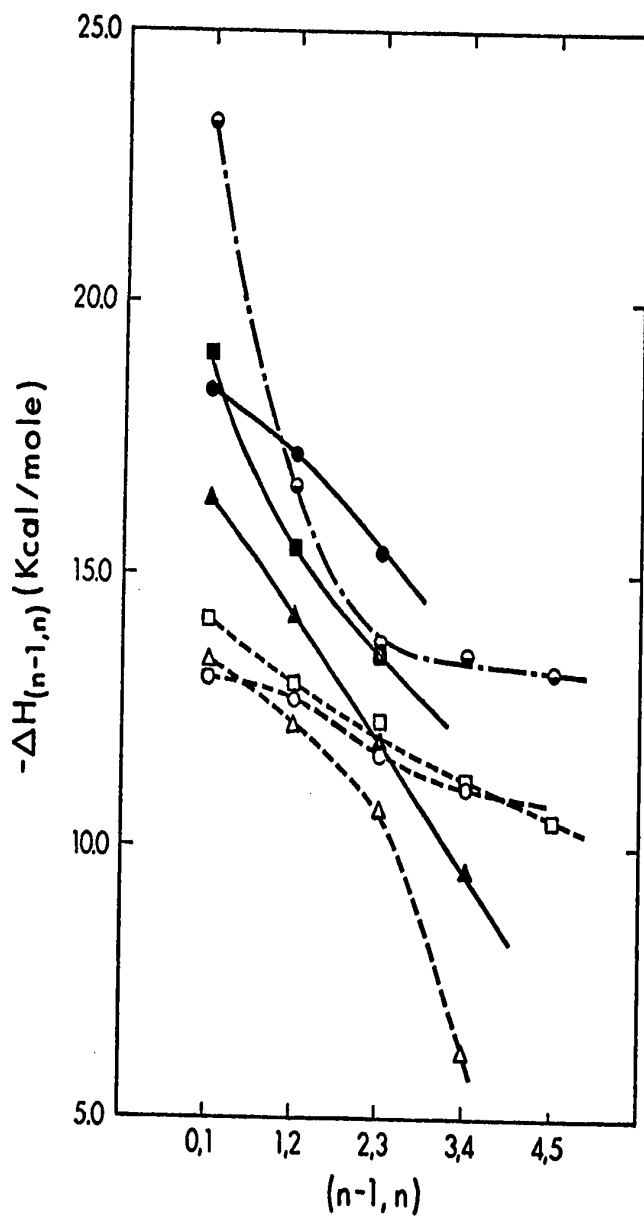


FIGURE 7.5. Plot of  $-\Delta H_{n-1,n}$  versus  $n-1,n$  for the reactions  $\text{A}^-\text{B}_{n-1} + \text{B} \rightleftharpoons \text{A}^-\text{B}_n$ .  $\bullet$   $\text{O}_2^-(\text{H}_2\text{O})_n$ ,  $\blacksquare$   $\text{O}_2^-(\text{CH}_3\text{OH})_n$ ,  $\blacktriangle$   $\text{O}_2^-(\text{CH}_3\text{CN})_n$ ,  $\circ$   $\text{Cl}^-(\text{H}_2\text{O})_n$ ,  $\square$   $\text{Cl}^-(\text{CH}_3\text{OH})_n$ ,  $\triangle$   $\text{Cl}^-(\text{CH}_3\text{CN})_n$ , and  $\circ$   $\text{F}^-(\text{H}_2\text{O})_n$ .



to be the case also for the  $\text{Cl}^-$  solvation by water and methanol. Since the measured differences between the  $-\Delta H_{n-1,n}$  for methanol and water are small and followed by a possible cross over, the present results indicate only a small difference between the total enthalpies of solvation of  $\text{Cl}^-$  by water and methanol. Choux and Benoit (132) have estimated a small positive enthalpy for transfer of  $\text{Cl}^-$  from  $\text{H}_2\text{O}$  to  $\text{CH}_3\text{OH}$ :  $\Delta H_{\text{transfer}} = +1.9$  kcal/mole. If this estimate is correct then the indicated cross over in Figure (7.5) is probably real. The free energy differences (Table 7.1) show a trend similar to that of the  $-\Delta H$  differences, however the relative decrease of the  $-\Delta G_{n-1,n}$  for methanol is more rapid, such that a reversal with water becoming more favoured is observed already for the (3,4) step. This suggests that the free energy of  $\text{Cl}^-$  transfer from HOH to  $\text{CH}_3\text{OH}$  should be small and positive - a result which is in agreement with the conclusions of Parker et al (133).

A comparison between the  $-\Delta H_{n-1,n}$  and  $-\Delta G_{n-1,n}$  values for  $\text{Cl}^-$  and the other halide ions and the protic and aprotic solvents HOH and  $\text{CH}_3\text{CN}$  was reported earlier (74). The most significant finding was that acetonitrile at close range (low n) gives stronger interactions than water but that the interactions become very much less favorable at high n. Furthermore it was found (74) that the small ions ( $\text{F}^-$ ) showed stronger interactions with water while the

interaction with acetonitrile became relatively more favorable as the size of the ion increased. This result was found to be in agreement with transfer enthalpies and free energies for the liquid solvents (HOH  $\longrightarrow$  aprotic solvent) which had been determined (132,133) to be positive for small ions ( $F^-$ ) becoming progressively smaller and turning negative for large ions ( $I^-$ ).

The solvation of  $O_2^-$  (Figure (7.5) and Table 7.1) fits similar general trends. The  $-\Delta H_{n-1,n}$  values of Figure (7.5) show that  $O_2^-$  falls between  $F^-$  and  $Cl^-$  and may thus be considered as an ion which has a "radius" falling between those of  $F^-$  and  $Cl^-$ . Correspondingly the difference between the values for HOH and  $CH_3CN$  observed for  $O_2^-$  is larger than that observed for the larger  $Cl^-$  ion. It is also found that the solvation by methanol becomes unfavorable at much smaller  $n-1,n$  values since a cross over occurs already after (0,1). From the example we are led to expect that ion transfer from the liquid solvent water to methanol should show transfer enthalpies which decrease as the size of the ion is increased. This is borne out by the determinations of Choux and Benoit (132).

Of course the  $O_2^-$  ion is not symmetrical. The simple MO description puts the three outer electrons in the doubly degenerate nonbonding  $2p\pi_g$  orbital. This means that in the unperturbed  $O_2^-$  the negative charge should be spread out to the two ends of the ion. One would expect that the

presence of a molecule like HOH and CH<sub>3</sub>OH with a partially positively charged hydrogen atom will induce a partial shift of electronic charge to the one side of the O<sub>2</sub><sup>-</sup> ion with the polar molecule attaching itself effectively to that side. The behaviour of O<sub>2</sub><sup>-</sup> as an ion "smaller" than Cl<sup>-</sup> is thus not unexpected. The addition of a second and further molecules might then engage both oxygen atoms. Unfortunately the data in Figure (7.5) do not seem to show a consistent behaviour. Thus the hydrates show a small fall off between  $-\Delta H_{0,1}$  and  $-\Delta H_{1,2}$  (compared to that of F<sup>-</sup>) however, the methanol results give a fairly large fall off for the same step.

From the general position of the O<sub>2</sub><sup>-</sup> in Figure (7.5) one can predict that its total enthalpy of hydration will be close but lower than that for F<sup>-</sup>. Since  $\Delta H_h(F^-) = -113$  kcal/mole and  $\Delta H_h(Cl^-) = -81.3$  kcal/mole (115) one might expect a  $\Delta H_h(O_2^-) \approx -100$  kcal/mole. The transfer enthalpy from water to methanol should be small and positive while that to acetonitrile also positive but considerably larger.

## VIII The Competitive Solvation of $\text{NH}_4^+$ by $\text{H}_2\text{O}$ and $\text{NH}_3$

### 8.1 Introduction

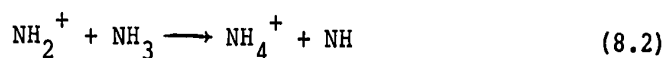
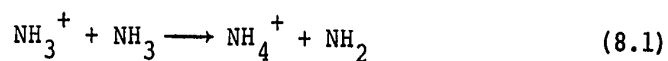
The positive ion-molecule reactions occurring in pure ammonia were one of the first systems investigated in this laboratory by high pressure mass spectrometry (71-73). Hogg and Kebarle investigating the relative concentrations of the mixed composition clusters  $\text{H}^+(\text{NH}_3)_n(\text{H}_2\text{O})_w$  present in various mixtures of water and ammonia observed that the composition of the clusters showed the following trends. One molecule of ammonia seemed to be retained under all circumstances. In clusters containing less than five molecules in addition to the proton, five ammonia molecules were found to be retained with a probability greater than statistical. These results were interpreted to mean that the clusters had the  $\text{NH}_4^+$  ion as a central species and that there was an inner shell corresponding to four molecules hydrogen bonded to the  $\text{NH}_4^+$ . The ammonia molecule retained under all circumstances corresponded to the  $\text{NH}_4^+$  while the other four ammonia molecules corresponded to the ammonia preferentially taken up in the inner shell.

The early investigation of water ammonia mixed clusters was done at a single temperature and at a time when the investigative techniques had not been well developed. Therefore it was considered of importance to reinvestigate this system and its temperature dependence.

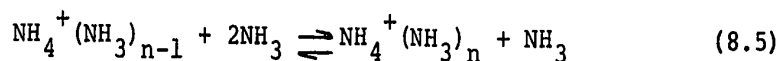
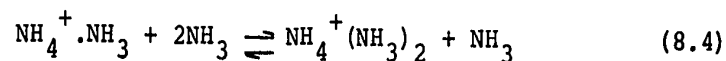
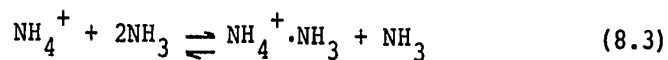
## 8.2 Experimental Results

### A. Pure Ammonia

In dry ammonia the main positive ions formed on electron bombardment are  $\text{NH}_3^+$  and  $\text{NH}_2^+$ . Both of these ions react rapidly with ammonia to yield the  $\text{NH}_4^+$  ion.



These reactions are fast, proceeding at rates of  $5 \times 10^{-10}$  and  $8.4 \times 10^{-10} \text{ cm}^3 \text{ molecule}^{-1} \text{ s}^{-1}$  respectively (136). The  $\text{NH}_4^+$  then forms  $\text{NH}_4^+(\text{NH}_3)_n$  by the following reactions:



The only significant positive ions formed in dry ammonia were found to be  $\text{NH}_4^+(\text{NH}_3)_n$ .

The time dependence of the  $\text{NH}_4^+(\text{NH}_3)_n$  ions was observed in all measurements, and it was found that the ratios of the ion signals remained constant with time after the initial electron pulse except for the first 100  $\mu\text{s}$  or so. To ensure that the ions were in equilibrium several determinations of the equilibrium constant were made at

various ammonia pressures at a given temperature. Some results are shown in Figure (8.1) for several experimental temperatures. As can be seen from Figure (8.1) the measured equilibrium constants are independent of ammonia pressure within the scatter of the data. Van't Hoff plots of the data are shown in Figure (8.2) and the thermodynamic parameters are summarized and compared with previous results from this laboratory in Table 8.1.

#### B. The Ammonia-Water System

To study the solvation of  $\text{NH}_4^+$  by water it is convenient to generate  $\text{NH}_4^+$  in such a way that only the  $\text{NH}_4^+(\text{H}_2\text{O})_n$  ions will be formed. It was found that by adding a small amount of ammonia (~1 mtorr) to a flowing stream of several torr of water the species  $\text{NH}_4^+(\text{H}_2\text{O})_n$  were formed in abundance. By maintaining a low partial pressure of ammonia the undesired ions  $\text{NH}_4^+(\text{NH}_3)_n$  and  $\text{NH}_4^+(\text{NH}_3)_n(\text{H}_2\text{O})_w$  were not formed in significant amounts.

The study of  $\text{NH}_4^+(\text{H}_2\text{O})_n$  clusters is practical only in mixtures which contain traces of ammonia in water vapour. Higher concentrations of ammonia lead to the mixed clusters  $\text{NH}_4^+(\text{NH}_3)_n(\text{H}_2\text{O})_w$ . On the other hand no  $\text{H}_3\text{O}^+$  is present even when only traces of ammonia are used since the proton affinity of ammonia ( $\text{PA}(\text{NH}_3) = 207$  kcal/mole (137)) is so much greater than that of water ( $\text{PA}(\text{H}_2\text{O}) = 165$  kcal/mole (137)) that  $\text{NH}_4^+$  is the exclusive ion at equil-

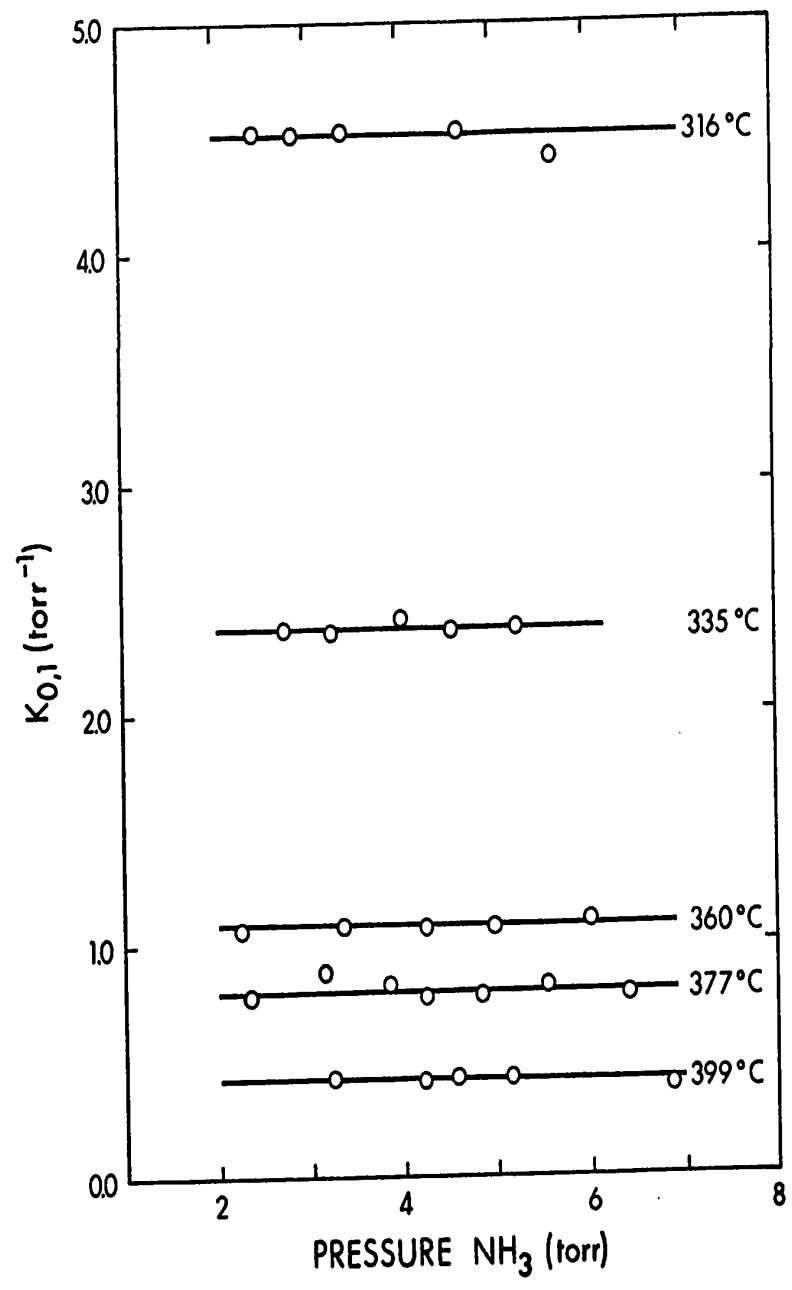


FIGURE 8.1. Equilibrium constant  $K_{0,1}$  for the reaction  $\text{NH}_4^+ + \text{NH}_3 \rightleftharpoons \text{NH}_4^+ \cdot \text{NH}_3$  at several temperatures plotted versus ammonia pressure.

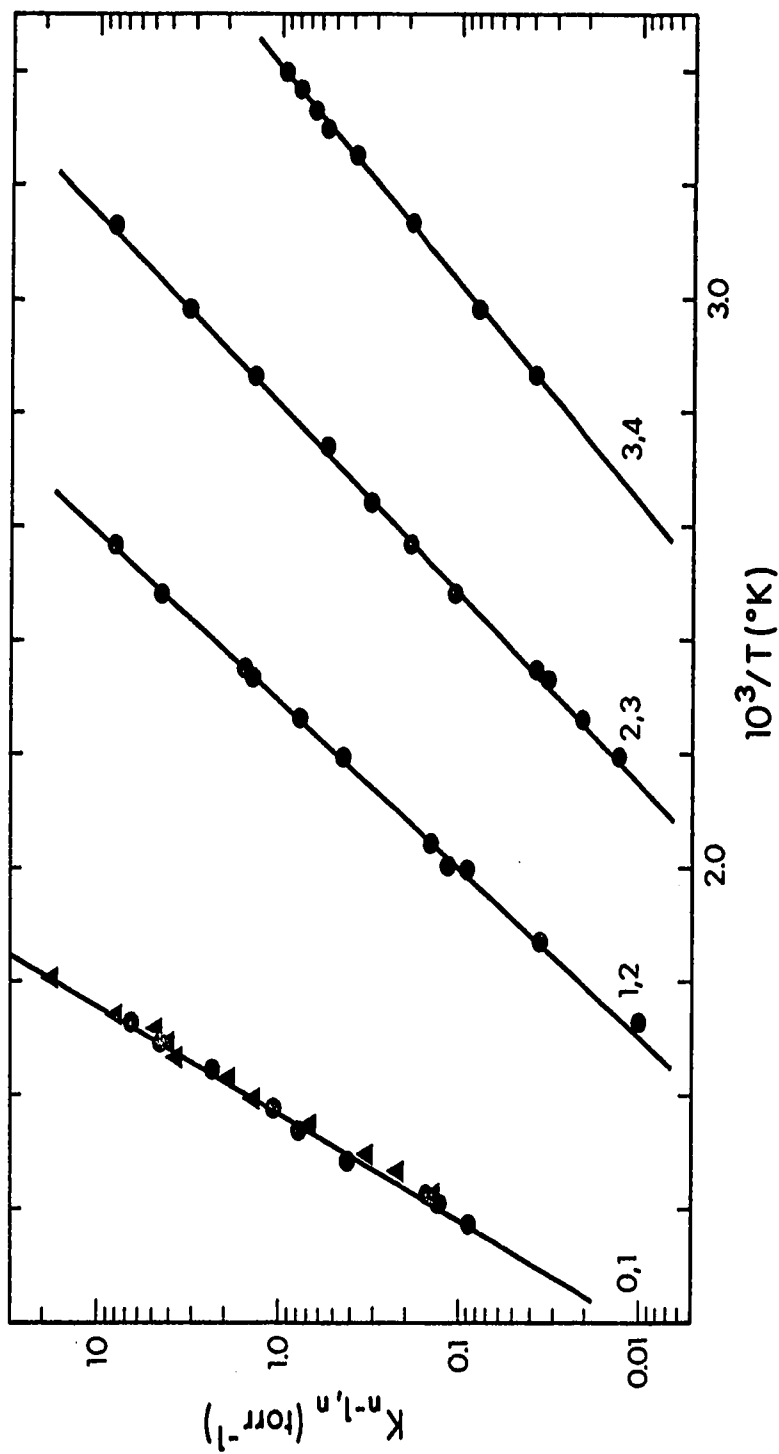
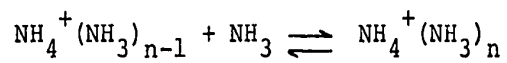


FIGURE 8.2. van't Hoff plots of equilibrium constants  $K_{n-1,n}$  for the  $\text{NH}_4^+ (\text{NH}_3)_{n-1} + \text{NH}_3 \rightleftharpoons \text{NH}_4 \cdot (\text{NH}_3)_n$  equilibria. O Present results,  $\blacktriangle$  Yamdagni Ref. (116).



TABLE 8.1

Thermodynamic Values for the Reactions



	n-1,n	Present work	S.K.S. <sup>a</sup>	S.K.S. & P.K. <sup>b</sup>	Hogg <i>et al</i> <sup>c</sup>
$-\Delta H_{n-1,n}^d$	0,1	24.8 ± 0.4 <sup>e</sup>	27	27	-
	1,2	17.5 ± 0.2	17	17	-
	2,3	13.8 ± 0.2	14.0	16.5	17.8
	3,4	12.5 ± 0.4	13.1	14.5	15.9
	4,5	-	7.5	7.5	-
$-\Delta S_{n-1,n}^{f,g}$	0,1	25.9 ± 0.7	32	32	-
	1,2	22.9 ± 0.5	27	26.8	-
	2,3	25.7 ± 0.4	27	34	38
	3,4	29.4 ± 1.2	32	36	40
	4,5	-	25	25	-
$-\Delta G_{n-1,n}^{d,g}$	0,1	17.1 ± 0.5	17.5	17.5	-
	1,2	8.9 ± 0.3	9.0	9.0	-
	2,3	6.1 ± 0.2	6.1	6.4	6.4
	3,4	3.7 ± 0.5	3.6	3.8	3.8
	4,5	-	0.2	0.2	0.5

<sup>a</sup> Ref. (135)<sup>b</sup> Ref. (71)<sup>c</sup> Ref. (73)<sup>d</sup> In kcal/mole<sup>e</sup> Quoted errors are one standard deviation.<sup>f</sup> In e.u.<sup>g</sup> Standard state 1 atm. T = 300°K

ilibrium. The  $\text{NH}_4^+$  ion will then form  $\text{NH}_4^+(\text{H}_2\text{O})_n$  in a manner analogous to that described in the previous section for  $\text{NH}_4^+(\text{NH}_3)_n$ . As before the  $\text{NH}_4^+(\text{H}_2\text{O})_n$  ion ratios were stationary with time and the equilibrium constants were found to be independent of the water pressure. Examples are shown in Figure (8.3) for several experimental temperatures. The equilibrium constants in the  $\text{NH}_4^+(\text{H}_2\text{O})_n$  system were independent of the partial pressure of ammonia. A van't Hoff plot of the data is shown in Figure (8.4) and the thermodynamic data are summarized in Table 8.2.

C. Competitive Solvation of  $\text{NH}_4^+$  by Water and Ammonia

The mixed cluster ions  $\text{NH}_4^+(\text{H}_2\text{O})_w(\text{NH}_3)_n$  were formed in water containing a small (few percent) amount of ammonia. Since water was the carrier gas, its pressure could be determined directly with the manometer. The partial pressure of ammonia was determined by observing the equilibrium in reaction (8.5). The equilibrium constant for the individual steps in reaction (8.5) at various temperatures may be obtained by an interpolation of the van't Hoff plots shown in Figure (8.2). Thus knowledge of the equilibrium constant, the temperature and the ratio of the clustered "pure" ammonia species permitted the evaluation of the partial pressure of ammonia.

In this mixed solvent system the number of different positive ions that may be observed at a given temperature

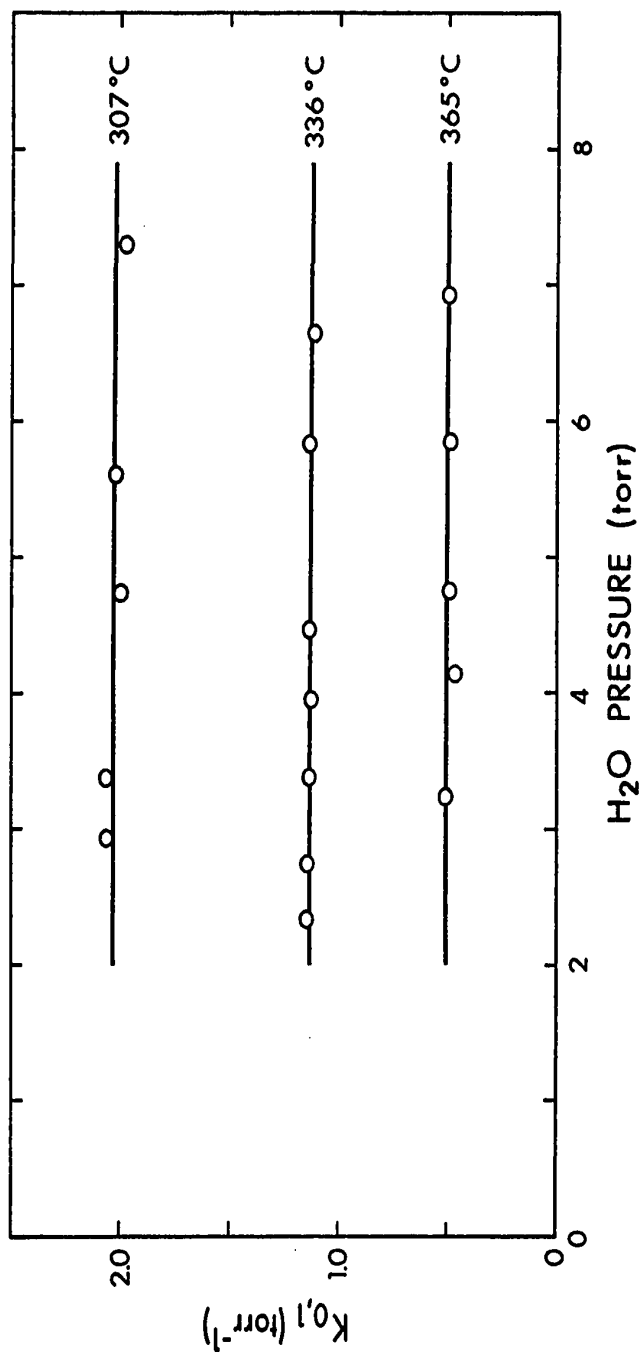


FIGURE 8.3. Equilibrium constant  $K_{0,1}$  for the reaction  $\text{NH}_4^+ + \text{H}_2\text{O} \rightleftharpoons \text{NH}_4^+ \cdot \text{H}_2\text{O}$  at several temperatures plotted versus water pressure.

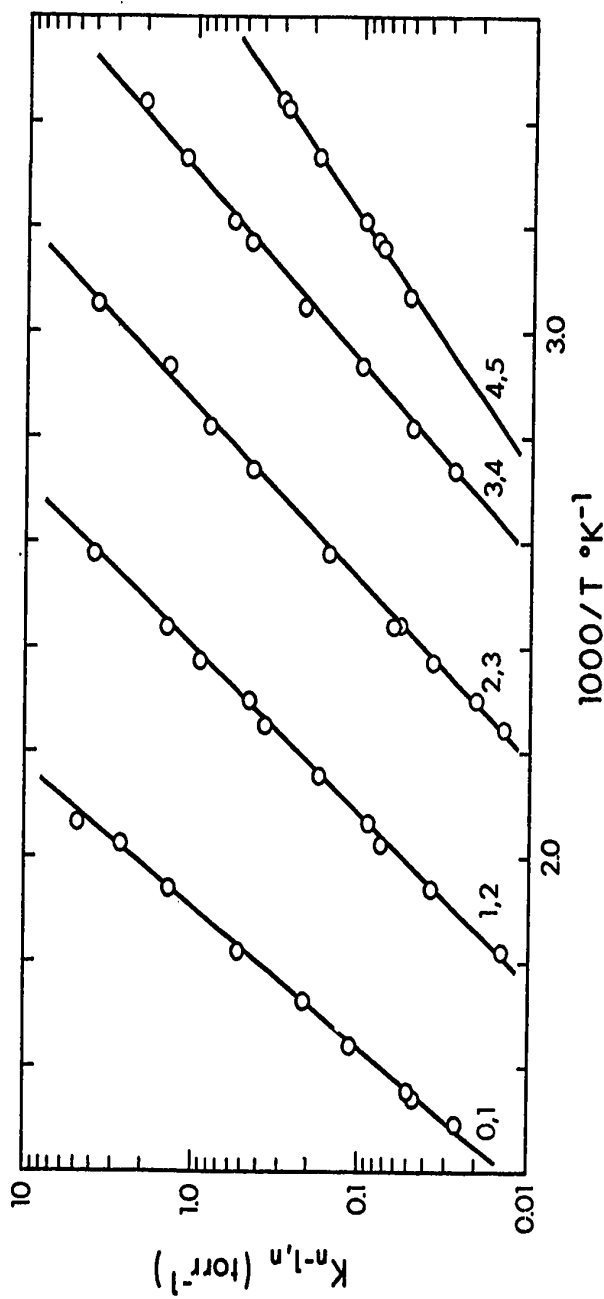
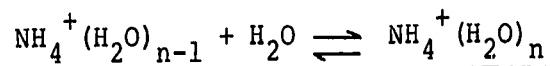


FIGURE 8.4. van't Hoff plots of equilibrium constants  $K_{n-1,n}$  for the  $\text{NH}_4^+(\text{H}_2\text{O})_{n-1} + \text{H}_2\text{O} \rightleftharpoons \text{NH}_4^+(\text{H}_2\text{O})_n$  equilibrium.

TABLE 8.2

Thermodynamic Values for the Reactions



$n-1,n$	$-\Delta H_{n-1,n}^a$	$-\Delta S_{n-1,n}^{b,c}$	$-\Delta G_{n-1,n}^{a,c}$
0,1	$17.3 \pm 0.4^d$	$19.7 \pm 0.7$	$11.4 \pm 0.4$
1,2	$14.7 \pm 0.2$	$21.9 \pm 0.3$	$8.2 \pm 0.2$
2,3	$13.4 \pm 0.2$	$25.1 \pm 0.6$	$5.9 \pm 0.3$
3,4	$12.2 \pm 0.3$	$27.3 \pm 0.8$	$4.1 \pm 0.4$
4,5	$9.7 \pm 0.3$	$22.4 \pm 0.8$	$3.0 \pm 0.4$

<sup>a</sup> Kcal/mole.<sup>b</sup> Entropy units.<sup>c</sup> Standard state 1 atm, 300°K.<sup>d</sup> Quoted errors are one standard deviation.

may be as large as 12. These ions may differ considerably in relative intensities and thus a long time is required to accumulate a signal in the multiscaler. It was found in practice that as much as two hours was required to record all signals. However, during this time period the all over intensity of the signal would drift substantially and the results were unsatisfactory. To overcome the problems centering about the long time required to perform the measurements, the integrated ion intensities were recorded in a gated single channel scaler. A pulse generator was introduced between the master pulse generator which closed the gate for an initial time interval such that the scaler would only count those ions which arrived at the detector at times greater than 100  $\mu$ s after the electron beam pulse. This was done because in the time interval when the electron beam is on and for a short period thereafter the ion intensities are not representative of the equilibrium populations. Spot checks were made with the multichannel scaler to ensure that the ratios of various ions were constant with time. No significant difference was found between the equilibrium constants evaluated by both methods. Several measurements were made at different water and ammonia pressures at each experimental temperature and the equilibrium constants were averaged at each temperature for a best value.

Figure (8.5) displays the van't Hoff plots for the

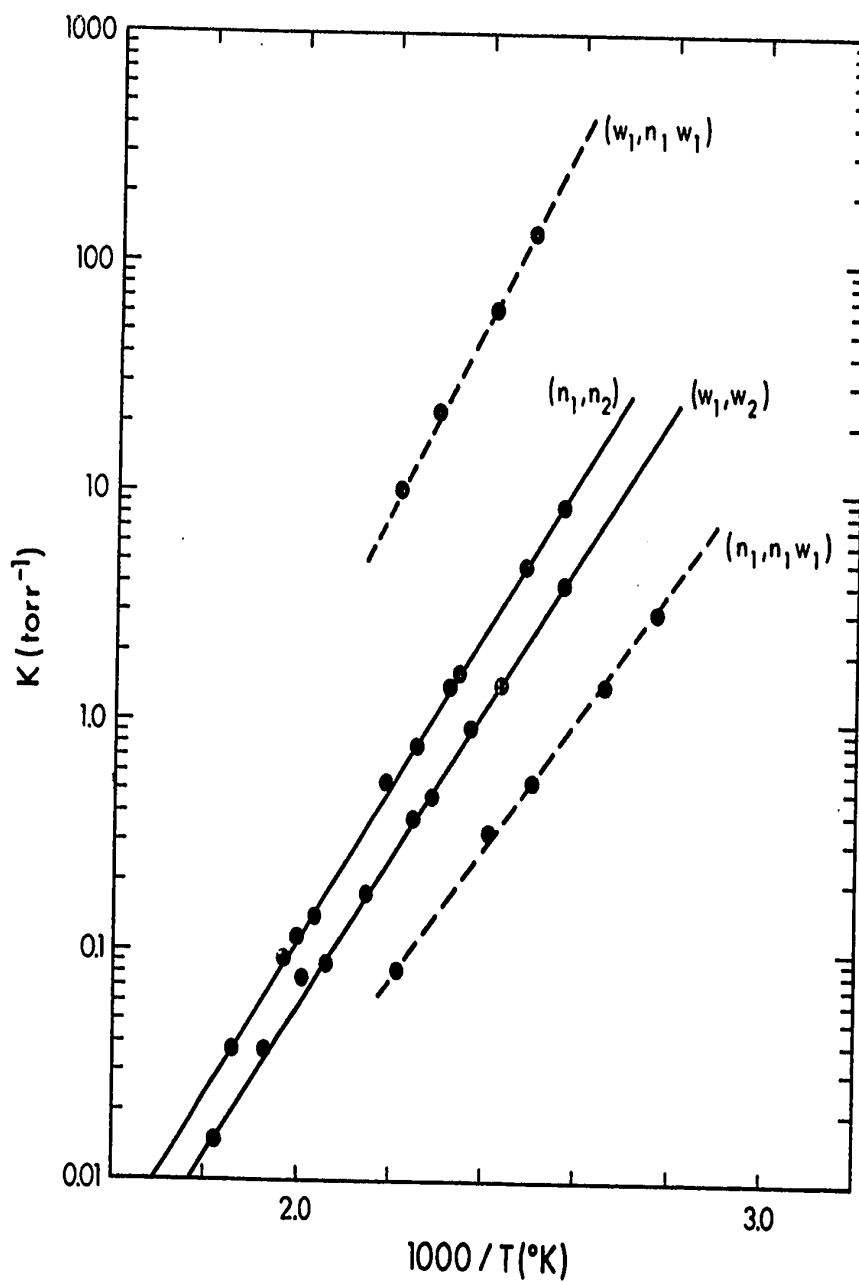
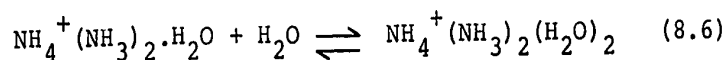


FIGURE 8.5. van't Hoff plots of equilibrium constants for the formation of  $\text{NH}_4^+(\text{NH}_3)_n(\text{H}_2\text{O})_w$  where  $n + w = 2$ . For explanation of notation see text.

cases when the  $\text{NH}_4^+$  ion has two ligands attached. Figure (8.6) and Figure (8.7) display similar plots when the  $\text{NH}_4^+$  ion has three and four ligands respectively. The reaction corresponding to each van't Hoff plot is indicated with the following notation. For example  $(n_2w_1, n_2w_2)$  corresponds to the reaction



The enthalpy changes for the interconversion of the various ions as calculated from the van't Hoff plots are summarized in Table 8.3.

### 8.3 Discussion of Results

#### A. The $\text{NH}_4^+(\text{NH}_3)_n$ and $\text{NH}_4^+(\text{H}_2\text{O})_n$ Systems

The present results for the  $\text{NH}_4^+(\text{NH}_3)_n$  system are presented in Table 8.1. The present results compare favourably with those of Searles (135). However, there is some disagreement with the earlier published results from this laboratory (71-73).

As may be seen from Table 8.1 there is a sharp drop in  $-\Delta H_{n-1,n}$  from (3,4) to (4,5). The enthalpy for the addition of the fourth molecule of ammonia to  $\text{NH}_4^+$  ( $-\Delta H_{3,4}$ ) is only 1.3 kcal/mole less than  $-\Delta H_{2,3}$  while  $-\Delta H_{4,5}$  is some 5 kcal/mole less than  $-\Delta H_{3,4}$ . Also there is a sharp drop from  $-\Delta S_{3,4}$  to  $-\Delta S_{4,5}$  indicating that the fifth



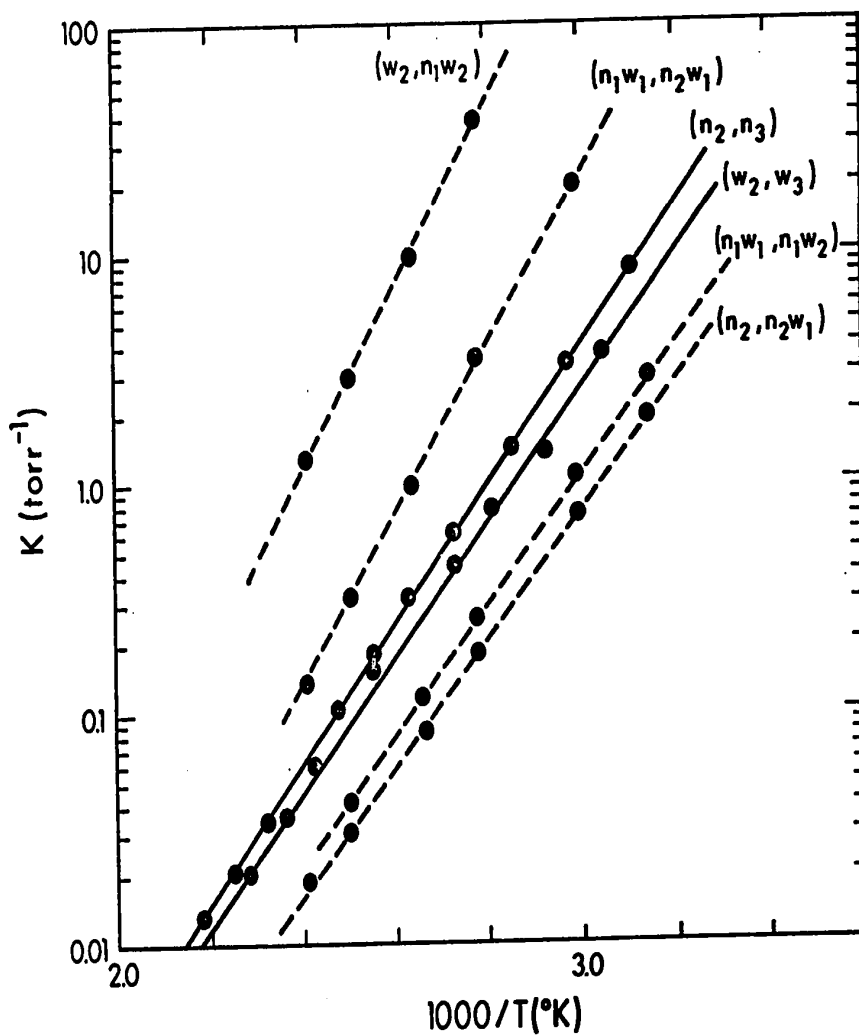


FIGURE 8.6. van't Hoff plots of equilibrium constants for the formation of  $\text{NH}_4^+(\text{NH}_3)_n(\text{H}_2\text{O})_w$  where  $n + w = 3$ . For explanation of notation see text.

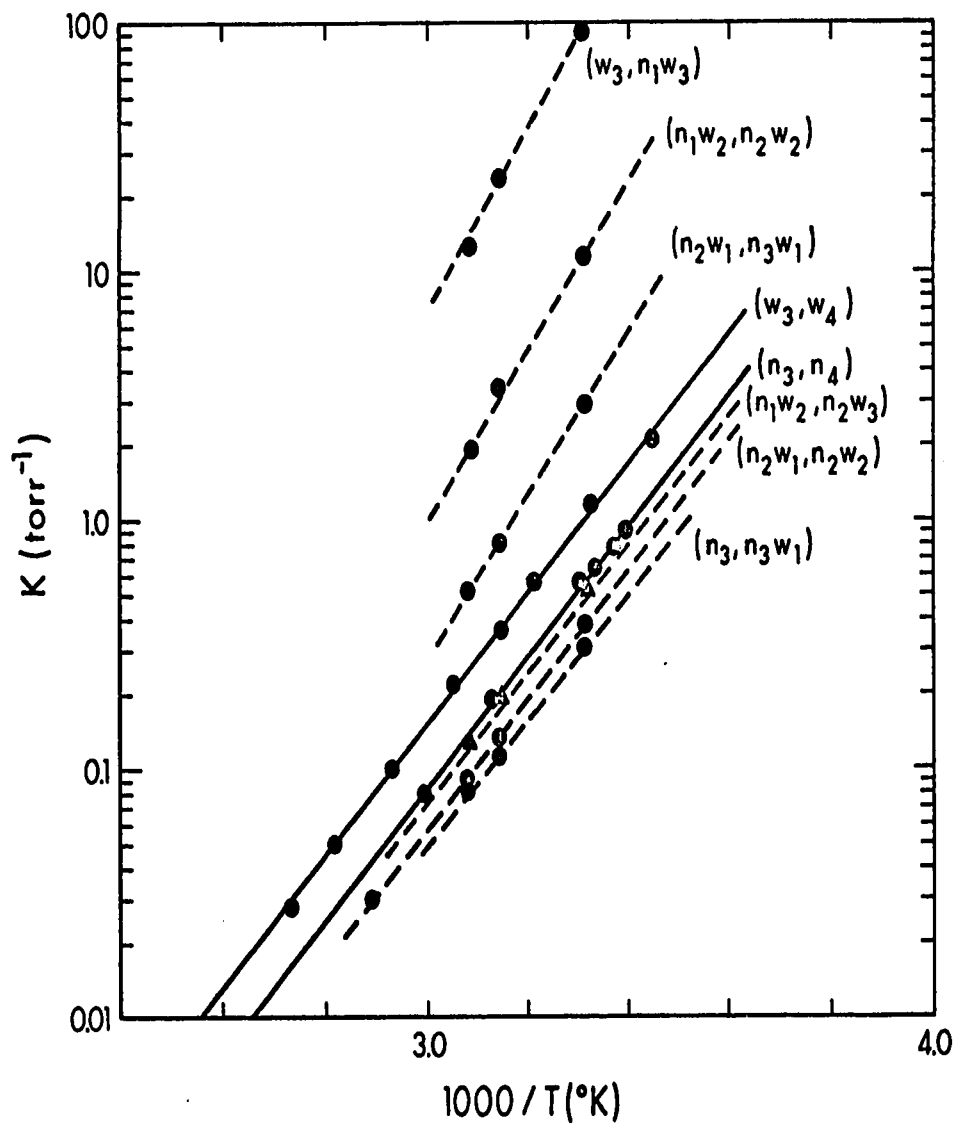


FIGURE 8.7. van't Hoff plots of equilibrium constants for the formation of  $\text{NH}_4^+(\text{NH}_3)_n(\text{H}_2\text{O})_w$  where  $n + w = 4$ . For explanation of notation see text.

TABLE 8.3

Thermodynamic Parameters for the Addition of Successive

Reaction <sup>a</sup>	Ligands to NH <sub>4</sub> <sup>+</sup>		
	$-\Delta H^b$	$-\Delta S^{c,d}$	$-\Delta G^{b,d}$
0,n <sub>1</sub>	24.8 ± 0.4 <sup>e</sup>	25.9 ± 0.7	17.1 ± 0.5
0,w <sub>1</sub>	17.3 ± 0.4	19.7 ± 0.7	11.4 ± 0.4
n <sub>1</sub> ,n <sub>2</sub>	17.5 ± 0.2	22.9 ± 0.5	8.9 ± 0.3
n <sub>1</sub> ,n <sub>1</sub> w <sub>1</sub>	12.9 ± 0.3	20.3 ± 0.7	6.9 ± 0.4
w <sub>1</sub> ,n <sub>1</sub> w <sub>1</sub>	18.4 ± 0.5	23.0 ± 1.2	11.6 ± 0.6
w <sub>1</sub> ,w <sub>2</sub>	14.7 ± 0.2	21.9 ± 0.3	8.2 ± 0.2
n <sub>2</sub> ,n <sub>3</sub>	13.8 ± 0.2	25.7 ± 0.4	6.1 ± 0.2
n <sub>2</sub> ,n <sub>2</sub> w <sub>1</sub>	12.4 ± 0.2	24.6 ± 0.6	5.0 ± 0.3
n <sub>1</sub> w <sub>1</sub> ,n <sub>2</sub> w <sub>1</sub>	17.1 ± 0.3	31.8 ± 0.7	7.6 ± 0.3
n <sub>1</sub> w <sub>1</sub> ,n <sub>1</sub> w <sub>2</sub>	12.7 ± 0.3	25.0 ± 0.9	5.3 ± 0.4
w <sub>2</sub> ,n <sub>1</sub> w <sub>2</sub>	18.2 ± 0.4	30.3 ± 1.0	9.2 ± 0.5
w <sub>2</sub> ,w <sub>3</sub>	13.4 ± 0.2	25.1 ± 0.6	5.9 ± 0.3
n <sub>3</sub> ,n <sub>4</sub>	12.5 ± 0.4	29.4 ± 1.2	3.7 ± 0.5
n <sub>3</sub> ,n <sub>3</sub> w <sub>1</sub>	11.7 ± 0.3	27.9 ± 1.1	3.4 ± 0.5
n <sub>2</sub> w <sub>1</sub> ,n <sub>3</sub> w <sub>1</sub>	15.0 ± 0.4	34.3 ± 1.0	4.7 ± 0.5
n <sub>2</sub> w <sub>1</sub> ,n <sub>2</sub> w <sub>2</sub>	11.7 ± 0.3	27.8 ± 0.9	3.5 ± 0.4
n <sub>1</sub> w <sub>2</sub> ,n <sub>2</sub> w <sub>2</sub>	15.7 ± 0.6	33.9 ± 1.9	5.6 ± 0.8
n <sub>1</sub> w <sub>2</sub> ,n <sub>1</sub> w <sub>3</sub>	12.2 ± 0.3	28.5 ± 0.9	3.7 ± 0.4
w <sub>3</sub> ,n <sub>1</sub> w <sub>3</sub>	17.3 ± 1.0	35.1 ± 3.3	6.9 ± 1.4
w <sub>3</sub> ,w <sub>4</sub>	12.2 ± 0.3	27.3 ± 0.8	4.1 ± 0.4

(continued.....)

TABLE 8.3 (continued)

$n_4, n_5$	7.5	25	$0.2^f$
$w_4, w_5$	$9.7 \pm 0.3$	$22.4 \pm 0.8$	$3.0 \pm 0.4$

a For explanation of notation see text

b In kcal/mole

c In entropy units

d Standard state 1 atm,  $T = 300^\circ\text{K}$

e Quoted errors are one standard deviation

f Ref. (71).

ammonia molecule is not as tightly bound as was the fourth. This was previously interpreted as evidence for the formation of an "inner shell" of ligands (71). This behaviour must be due to the tetrahedral shape of the  $\text{NH}_4^+$  ion and the pyramidal shape of the ammonia molecule which in the  $\text{NH}_4^+(\text{NH}_3)_4$  species permits the formation of a compact but uncrowded structure.

As may be seen from Table 8.1 there is a large drop in  $-\Delta H_{n-1,n}$  between (0,1) and (1,2). A possible explanation of this phenomena is that the reaction (0,1) leads to a symmetrical species of the form  $\text{H}_3\text{N}\dots\text{H}\dots\text{NH}_3^+$  where the proton is shared between the two ammonia molecules. Theoretical calculations (138-140) have shown that the corresponding ion  $\text{H}_2\text{O}\dots\text{H}\dots\text{OH}_2^+$  in the proton hydrate system has a structure in which the proton is equidistant between the two oxygen atoms (see Chapter 9). Thus such a symmetrical structure for  $(\text{NH}_3)_2\text{H}^+$  does not appear unreasonable. The addition of the third molecule of ammonia to form  $\text{NH}_4^+(\text{NH}_3)_2$  may lead to a reorganization of the cluster in which the special symmetry of the  $\text{H}_2\text{N}\dots\text{H}\dots\text{NH}_3^+$  is absent. This is consistent with the decrease of  $-\Delta H_{1,2}$  relative to  $-\Delta H_{0,1}$ .

Table 8.2 summarizes the data for the formation of  $\text{NH}_4^+(\text{H}_2\text{O})_n$ . Comparing the  $-\Delta H_{0,1}$  for the addition of ammonia (Table 8.1) and water to  $\text{NH}_4^+$  one finds that the

$-\Delta H_{0,1}$  for the addition of ammonia (24.8 kcal/mole) is considerably greater than that for the addition of water (17.3 kcal/mole). This may be interpreted to mean that ammonia is a stronger gas phase base than water. The trends in  $-\Delta H_{n-1,n}$  for the  $\text{NH}_4^+(\text{H}_2\text{O})_n$  system are similar to those for the  $\text{NH}_4^+(\text{NH}_3)_n$  system although these trends are less pronounced. The addition of the fifth molecule of water involves a smaller enthalpy change relative to the addition of the fourth molecule than was the case in the  $\text{NH}_4^+(\text{NH}_3)_n$  system. Also the difference between  $-\Delta H_{0,1}$  and  $-\Delta H_{1,2}$  is smaller. In the  $\text{NH}_4^+(\text{H}_2\text{O})_n$  system the  $-\Delta S_{n-1,n}$  increase regularly from (0,1) to (3,4) and then there is a drop from  $-\Delta S_{3,4}$  to  $-\Delta S_{4,5}$  which may be interpreted as the formation of an "inner solvation shell" of four water molecules about the  $\text{NH}_4^+$ .

If the  $-\Delta H_{n-1,n}$  or  $-\Delta G_{n-1,n}$  for the addition of water and ammonia to  $\text{NH}_4^+$  are compared it can be seen that these parameters are larger for the addition of ammonia than the addition of water. This is particularly pronounced for the addition of the first few ligands ( $n = 1,2$ ). However, for  $n = 3,4$  the measured thermodynamic parameters appear to be equal for the two systems. Thus the attachment of ammonia to  $\text{NH}_4^+$  is preferred over water for the first two steps but after this the preference is minimal.

B. The Mixed Clusters  $\text{NH}_4^+(\text{H}_2\text{O})_w(\text{NH}_3)_n$

The enthalpy values for the addition of ligands to the mixed clustered species are displayed in Table 8.3 and Figure (8.8). The values for the "pure" clusters  $\text{NH}_4^+(\text{NH}_3)_n$  and  $\text{NH}_4^+(\text{H}_2\text{O})_n$  are taken from Tables 8.1 and 8.2. The remaining values were calculated from Figures (8.5 - 8.7) and are less precise than the values for the "pure" systems since the van't Hoff's plots in some cases cover a rather narrow temperature range.

Some interesting correlations are immediately evident from an examination of Table 8.3. The addition of an ammonia molecule to any one of the mixed clusters is in all cases favoured over the addition of a water molecule. For example the  $-\Delta H$  for the addition of ammonia to  $\text{NH}_4^+ \cdot \text{H}_2\text{O}$  is 18.4 kcal/mole, while  $-\Delta H$  for the addition of water is only 14.7 kcal/mole. Similar trends in  $-\Delta H$  may be seen from an examination of Figure (8.8) for the higher clusters, although as the number of ligands about the  $\text{NH}_4^+$  increases the effect is less pronounced.

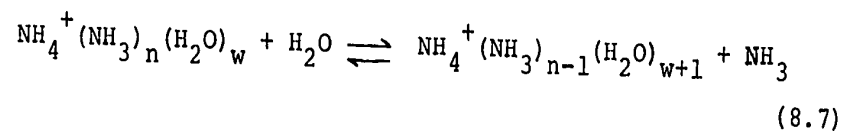
The addition of ammonia to a cluster is most favoured when the cluster has no ammonia ligands and the favourability decreases as the number of ammonia molecules in a cluster of given size increases. The preference for ammonia is not only reflected in the larger  $-\Delta H$ 's for the addition of ammonia to the clusters compared to water (see Figure (8.8) but is also reflected in the free energy changes.





For the addition of the first ligand to  $\text{NH}_4^+$ , the  $-\Delta G$  for the addition of ammonia is 17.1 versus 11.4 kcal/mole for the addition of water. Ammonia is preferentially attached when the  $\text{NH}_4^+$  has one ligand. The  $-\Delta G$  for the addition of ammonia to  $\text{NH}_4^+ \cdot \text{H}_2\text{O}$  is 11.6 kcal/mole while for the addition of water  $-\Delta G$  is only 8.2 kcal/mole. The trends are similar although less pronounced as the number of ligands about the central  $\text{NH}_4^+$  increases. For the addition of the third ligand, ammonia uptake is most favoured for  $\text{NH}_4^+ (\text{H}_2\text{O})_2$  where  $-\Delta G = 9.2$  kcal/mole, is less favoured for  $\text{NH}_4^+ \cdot \text{H}_2\text{O} \cdot \text{NH}_3$  when  $-\Delta G = 7.6$  kcal/mole, and is even less for  $\text{NH}_4^+ (\text{NH}_3)_2$  where  $-\Delta G = 6.1$  kcal/mole. For the three ligand clusters,  $-\Delta G$  for addition of ammonia decreases in the order 6.9, 5.6, 4.7, 3.7 kcal/mole as the number of ammonia molecules in the starting cluster increases from 0 to 3. These results strongly suggest that ammonia is the preferred solvent for  $\text{NH}_4^+$  compared to water. This is probably due to the higher proton affinity of ammonia compared to water. That is ammonia is a stronger gas phase base than water.

Hogg and Kebarle (72) were able to interpret their results for the formation of  $\text{NH}_4^+ (\text{NH}_3)_n (\text{H}_2\text{O})_w$  in terms of a shell structure when the number of ligands about the  $\text{NH}_4^+$  is 4 by assuming that the free energy change for reactions such as

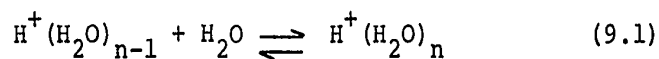


was positive and the same for all values of  $n$  and  $w$ . In the light of the present data this is not true. The approximation is quite bad for the small clusters but becomes progressively better as the number of ligands on the  $\text{NH}_4^+$  increases.

## IX The Proton Hydrates

### 9.1 Introduction

The attachment of water molecules to the proton to form  $H^+(H_2O)_n$  may be regarded as the first steps leading to the hydration of the proton. Thus the reactions



are of a fundamental nature. Kebarle and Godbole (141) while studying the ions formed by the alpha particle radiation of laboratory air some ten years ago made the accidental observation of  $H^+(H_2O)_n$ . These ions were formed by ion-molecule reactions involving traces of water. A systematic study was undertaken of the thermodynamics of formation of  $H^+(H_2O)_n$  (82).

This study, the first of its type done in this laboratory, involved sampling ions from the ion source continuously while ionization was induced by alpha particles or high energy protons. It was assumed that the measured ion ratios reflected the equilibrium populations. The equilibrium constant is then given by

$$K_{n-1,n} = \frac{I_{H^+(H_2O)_n}}{I_{H^+(H_2O)_{n-1}} \cdot P_{H_2O}} \quad (9.2)$$

and the thermodynamic parameters were obtained from the variation of  $K_{n-1,n}$  with temperature using van't Hoff's

relationship.

Recently Field and coworkers (37,40,41,43) (hereafter referred to as Field) have undertaken a study of reaction (9.1) using the chemical ionization technique. This approach is essentially the same as the present except that there is a repeller electrode in the ion source which reduces the ion residence time in the ion source to 10-30  $\mu$ s (40).

The results of Field are in vast disagreement with the previous results from this laboratory for the lower equilibria, i.e. for (1,2) and (2,3). However, agreement is quite good for the higher clustering reactions (3,4) etc. The value of  $K_{1,2}$  (at 300°K) obtained by Field (40) is from ten to thirteen orders of magnitude different from the previously reported value from this laboratory. The results of Field are in such vast disagreement with those of this laboratory that the entire basis of the experimental method is open to question. The proton hydrates equilibrium was one of the earliest systems investigated in this laboratory and considerable improvement in experimental technique has been made since then. Consequently it was decided to repeat the measurements.

There are several things which suggest that Field's data is in error. First, the measured equilibrium "constants" reported by Field vary with all variable parameters of his instrument. Field (40) reports that the equilibrium

"constant" varies with the total pressure of gas in the ion source, the nature of the carrier gas, the partial pressure of water, the value of the repeller voltage, the accelerating voltage of the mass spectrometer and the potentials of the electrodes in the ion acceleration system. These variations are between a factor of two and a thousand. After noting this Field concludes that he does "..... not understand the reason for the discrepancy [between his data and that previously reported]!"

The second and probably more important source of errors in Field's experiments is that the residence time of an ion in his ion source is so short ( $\sim 20 \mu\text{s}$ ) and the partial pressure of water so low in many measurements ( $< 1 \text{ mtorr}$ ) that the reactions proceed only to a very slight extent. That is the kinetics and reaction times are such that equilibrium will not be even remotely approached except under the most favourable of conditions.

## 9.2 Experimental Method

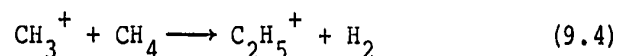
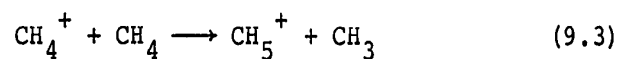
In this experiment an attempt was made to approach the conditions used in the experiments of Field. The previous work from this laboratory had been performed either using pure water or small amounts of water in argon. Field conducted his experiments of the lower equilibria either in methane, propane or isobutane containing traces of water. Most of the experiments in the present study were

conducted with methane as the major gas, but some experiments were performed with ethane or propane as the major gas.

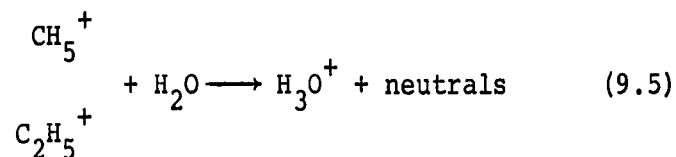
The partial pressure of water in the flowing gas was determined using a calibrated capillary for the addition of water. This capillary consisted of roughly 1 m of 0.010" i.d. stainless steel tubing. This type of capillary has a number of advantages over the short glass capillaries used in the previous work described in this thesis. The glass capillaries, because of their short length, have a very small diameter and consequently easily plug with foreign material. The larger diameter of the metal capillary overcomes this difficulty. It is possible to calibrate the metal capillary using the "weight loss" method described in Chapter 4. The calibration of this capillary has been found to remain constant for long (1 year) periods of time.

### 9.3 Ion Production and Data Analysis

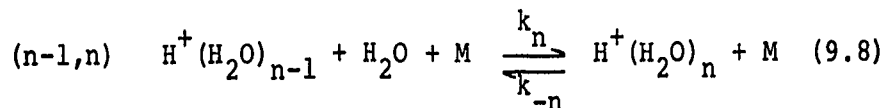
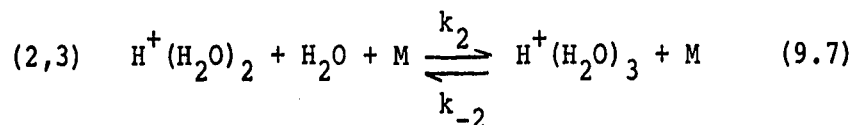
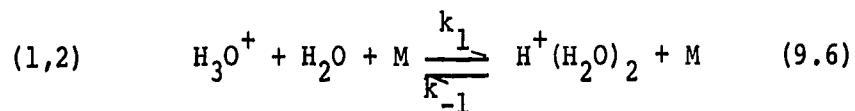
The principal ions formed by electron impact in methane are  $\text{CH}_4^+$  and  $\text{CH}_3^+$  (35). These ions react rapidly ( $\sim 10^{-9} \text{ cm}^3 \text{ molecule}^{-1} \text{ s}^{-1}$ ) with methane to yield  $\text{CH}_5^+$  and  $\text{C}_2\text{H}_5^+$  (35,83).



The resulting product ions  $\text{CH}_5^+$  and  $\text{C}_2\text{H}_5^+$  react rapidly with water yielding  $\text{H}_3\text{O}^+$ .



The resulting  $\text{H}_3\text{O}^+$  then forms the higher proton hydrates by the reaction sequence



Extensive studies from this laboratory (61,67) and from measurements with stationary afterglows (142), flowing afterglows (48) and drift tubes (143) suggest that reactions such as (9.8) are third order in the forward direction and second order in the reverse direction for total gas pressures in the torr range.

The temporal profiles of the ionic species were recorded in a manner analogous to that previously described (Chapters 2 and 4). The kinetic analysis and equilibrium constant determinations were done in the usual manner (see Chapters 2, 4, 5 and 6).

## 9.4 Experimental Results

### A. Kinetic Measurements

The kinetic measurements were done at methane pressures from 2.5 to 6.0 torr and water pressures in the range 3 to 100 mtorr. In Figure (9.1) is displayed the time dependence of the proton hydrates in a typical determination. As may be seen from Figure (9.1) the reaction sequence is  $\text{H}_3\text{O}^+ \rightarrow \text{H}^+(\text{H}_2\text{O})_2 \rightleftharpoons \text{H}^+(\text{H}_2\text{O})_3$ . The normalized data for Figure (9.1) is shown in Figure (9.2). The solid lines through the experimental points are the analogue computer calculated intensities based on the above reaction mechanism and the rate parameter summarizes in Table 9.1. In Figures (9.3-9.13) are displayed the normalized ion intensities along with the calculated time dependencies for the data of Table 9.1.

The rate of conversion of  $\text{H}_3\text{O}^+$  to  $\text{H}^+(\text{H}_2\text{O})_2$  could also be determined from plots of the  $\log I_{\text{H}_3\text{O}^+}$  vs time. Some typical examples determined at 125°C for various water pressures are shown in Figure (9.14). In Figures (9.15-9.17) are shown several plots of  $v_1/[\text{CH}_4]$  vs  $[\text{H}_2\text{O}]$  at various experimental temperatures demonstrating that the reactions depend on the first power of the water concentration. Table 9.2 summarizes the final kinetic parameters for the proton hydration reactions. As may be seen from Table 9.2 the rate constant is sharply dependent on the temperature. The rate of the reaction



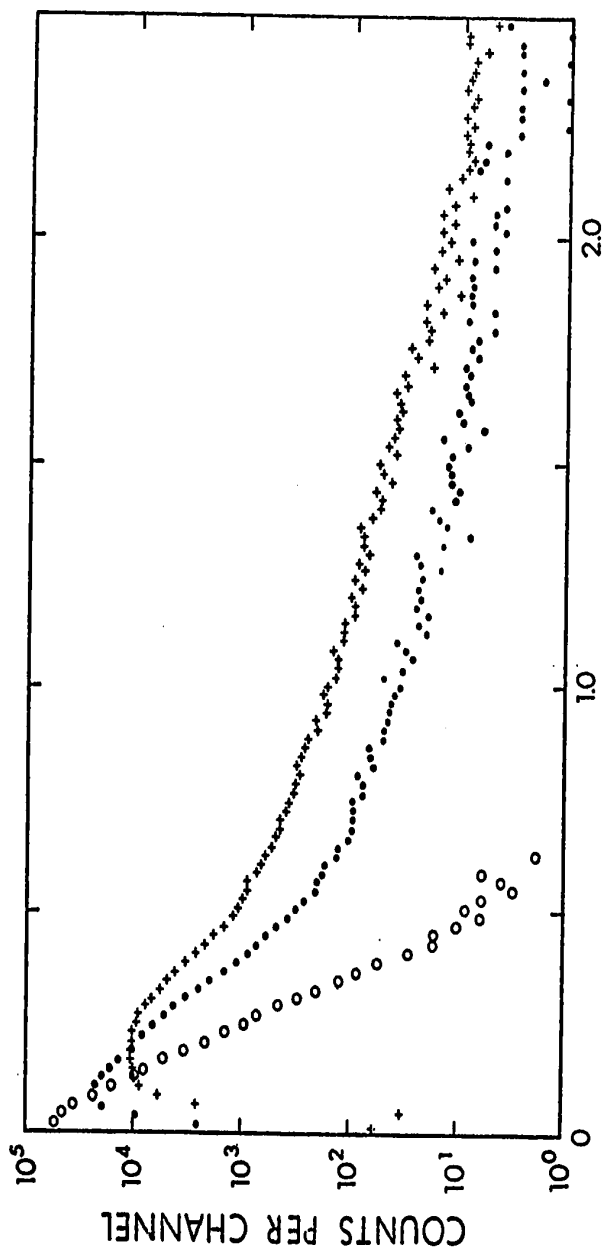


FIGURE 9.1. Time dependence of ion counts as observed with the multiscaler:  
 $P_{\text{CH}_4} = 3.55 \text{ torr}$ ;  $P_{\text{H}_2\text{O}} = 3.22 \text{ mtorr}$ ,  $125^\circ\text{C}$ .  $\text{O}$   $\text{H}_3\text{O}^+$ ,  $\text{O}$   $\text{H}^+(\text{H}_2\text{O})_2$ , +  $\text{H}^+(\text{H}_2\text{O})_3$ .  
 The reaction sequence  $\text{H}_3\text{O}^+ \rightleftharpoons \text{H}^+(\text{H}_2\text{O})_2 \rightleftharpoons \text{H}^+(\text{H}_2\text{O})_3$  is easily observed. The  
 equilibrium appears as a constant difference in the log of the ion counts.

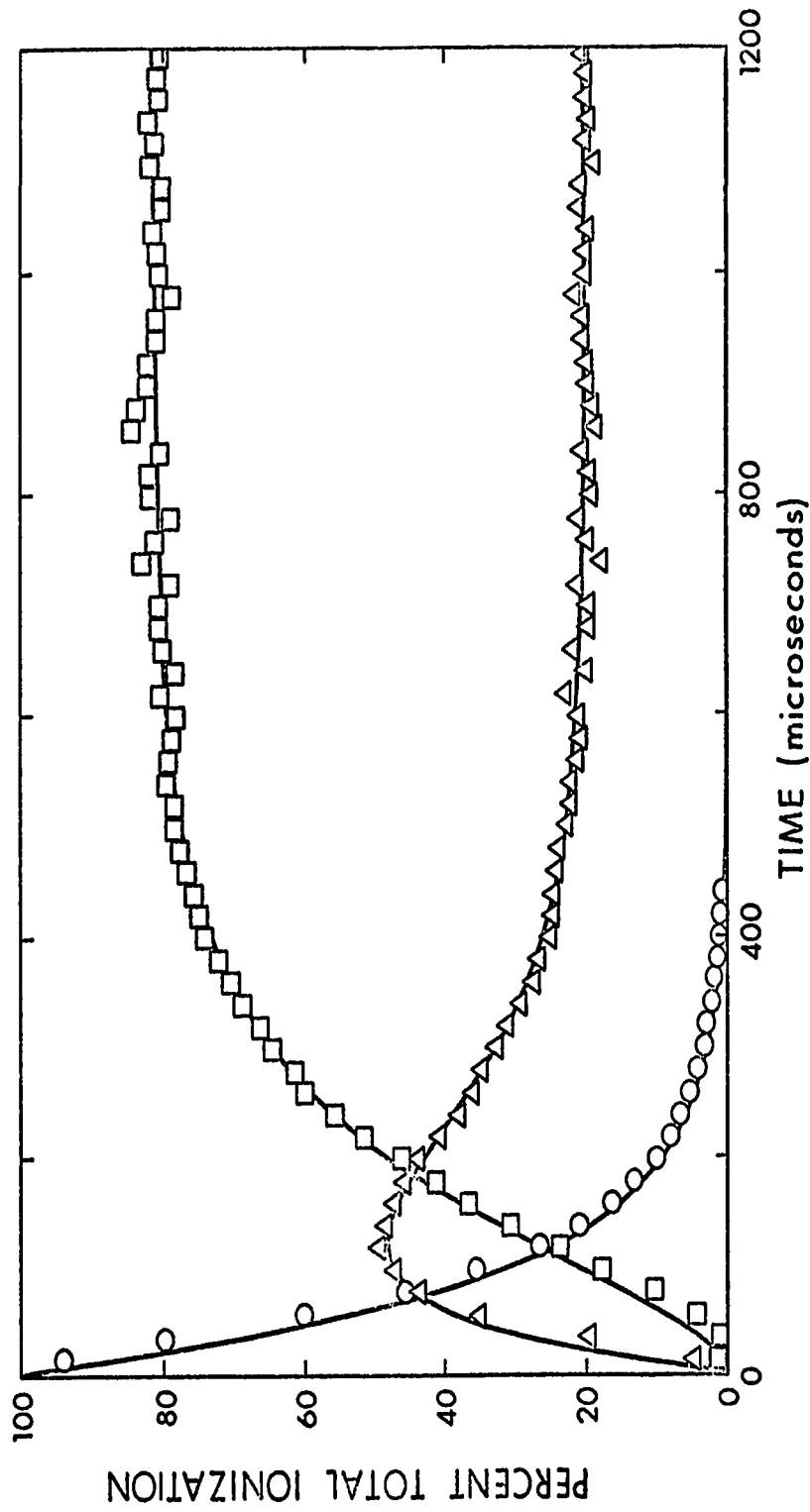


FIGURE 9.2.2. Results of Figure (9.1) but presented as percent total ionization.  $\circ$   $\text{H}_3\text{O}^+$ ,  $\Delta$   $\text{H}^+(\text{H}_2\text{O})_2$ , and  $\square$   $\text{H}^+(\text{H}_2\text{O})_3$ . Solid lines connecting experimental points are calculated concentrations for the rate parameters summarized in Table 9.1

TABLE 9.1

Rate Constants of Reactions Leading to  $H^+(H_2O)_n$ 

Temp (°K)	$P_{CH_4}^a$	$P_{H_2O}^b$	$v_1^c$	$v_{-1}^c$	$v_2^c$	$v_{-2}^c$	$v_3^c$	$v_{-3}^c$	Fig. <sup>d</sup>
672	6.0	27	7.64	2.08					9.20
672	6.0	72	16.9	2.13					
672	4.0	108	15.6	1.36					
672	6.0	48	11.9	2.10					
496	4.0	25	18.8		9.67	46.7			9.3
496	4.0	29.6	23.2		11.0	46.7			9.4
496	4.0	15.5	13.1		6.03	46.7			9.5
496	4.0	7.7	7.1		3.14	46.7			9.6
398	4.0	7.5	27.8		13.4	1.60	5.85	179	9.7
398	4.0	13	42.4		28.0	1.98	12.5	192	9.8
398	4.0	19	63.2		42.2	1.98	17.5	192	9.9
398	4.0	33	107		72.5	2.20	31.0	175	9.10
398	3.55	3.22	12.2		7.22	1.64			9.2
398	5.5	2.50	11.8		6.47	1.89			9.11
398	2.54	4.58	13.3		7.41	0.96			9.12
398	3.94	2.58	12.2		7.17	1.89			9.13

<sup>a</sup> In units of torr

<sup>b</sup> In units of mtorr

<sup>c</sup> In units of  $10^3 s^{-1}$

<sup>d</sup> Figure in which data is displayed

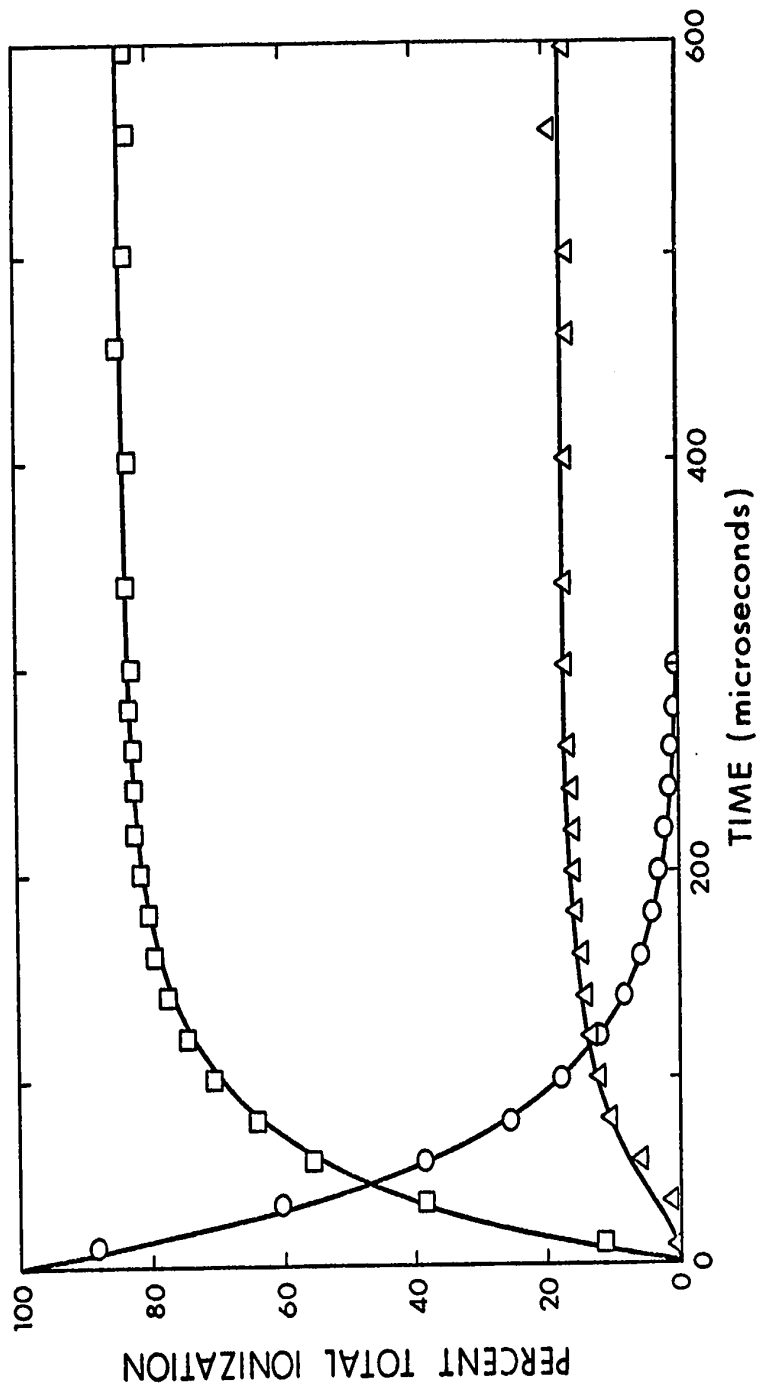


FIGURE 9.3. Time dependence of normalized ion intensities. The curves are the calculated time dependence for the rate parameters summarized in Table 9.1.  $P_{\text{CH}_4} = 4.0$  torr,  $P_{\text{H}_2\text{O}} = 25$  mtorr,  $T = 223^\circ\text{C}$ .  $\circ$   $\text{H}_3\text{O}^+$ ,  $\square$   $\text{H}^+(\text{H}_2\text{O})_2$ , and  $\triangle$   $\text{H}^+(\text{H}_2\text{O})_3$ .

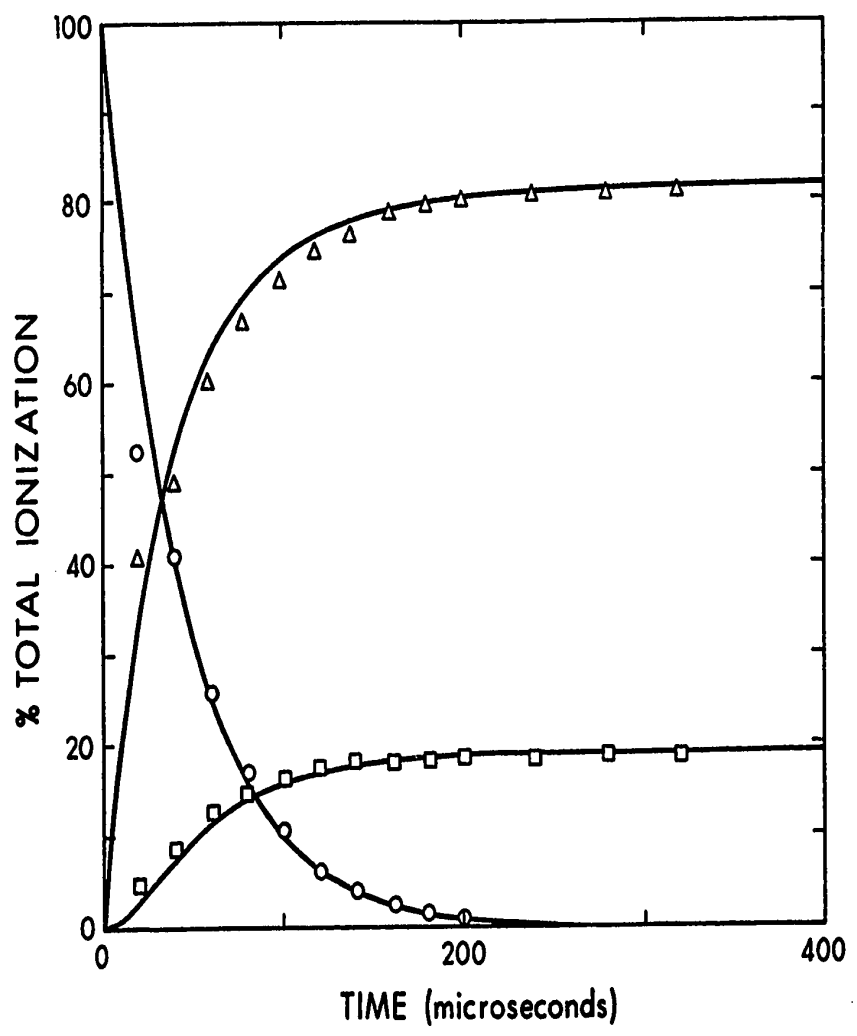


FIGURE 9.4. Time dependence of normalized ion intensities. The curves are the calculated time dependence for the rate parameters summarized in Table 9.1.  $P_{CH_4} = 4.0$  torr,  $P_{H_2O} = 29.6$  mtorr,  $T = 223^\circ C$ .  $\circ$   $H_3O^+$ ,  $\square$   $H^+(H_2O)_2$  and  $\Delta$   $H^+(H_2O)_3$ .

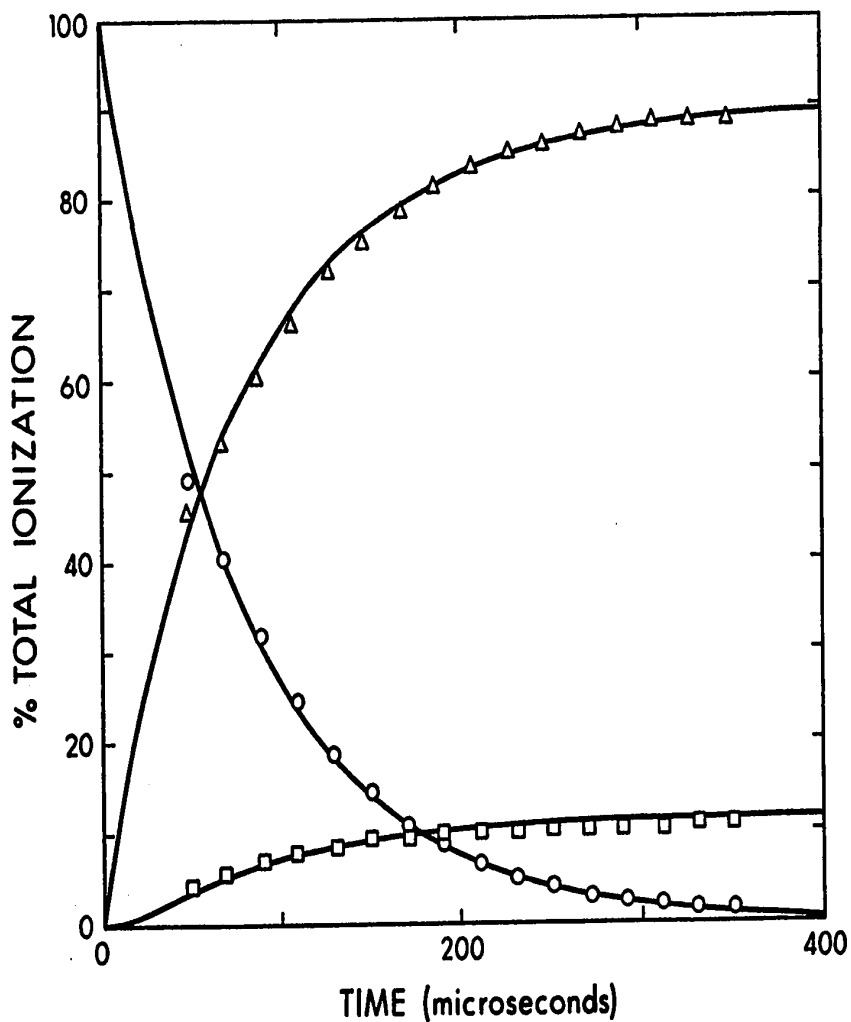


FIGURE 9.5. Time dependence of normalized ion intensities. The curves are the calculated time dependence for the rate parameters summarized in Table 9.1.  $P_{\text{CH}_4} = 4.0$  torr,  $P_{\text{CH}_4} = 15.5$  mtorr.  $\circ$   $\text{H}_3\text{O}^+$ ,  $\square$   $\text{H}^+(\text{H}_2\text{O})_2$  and  $\Delta$   $\text{H}^+(\text{H}_2\text{O})_3$ .  $T = 223^\circ\text{C}$ .

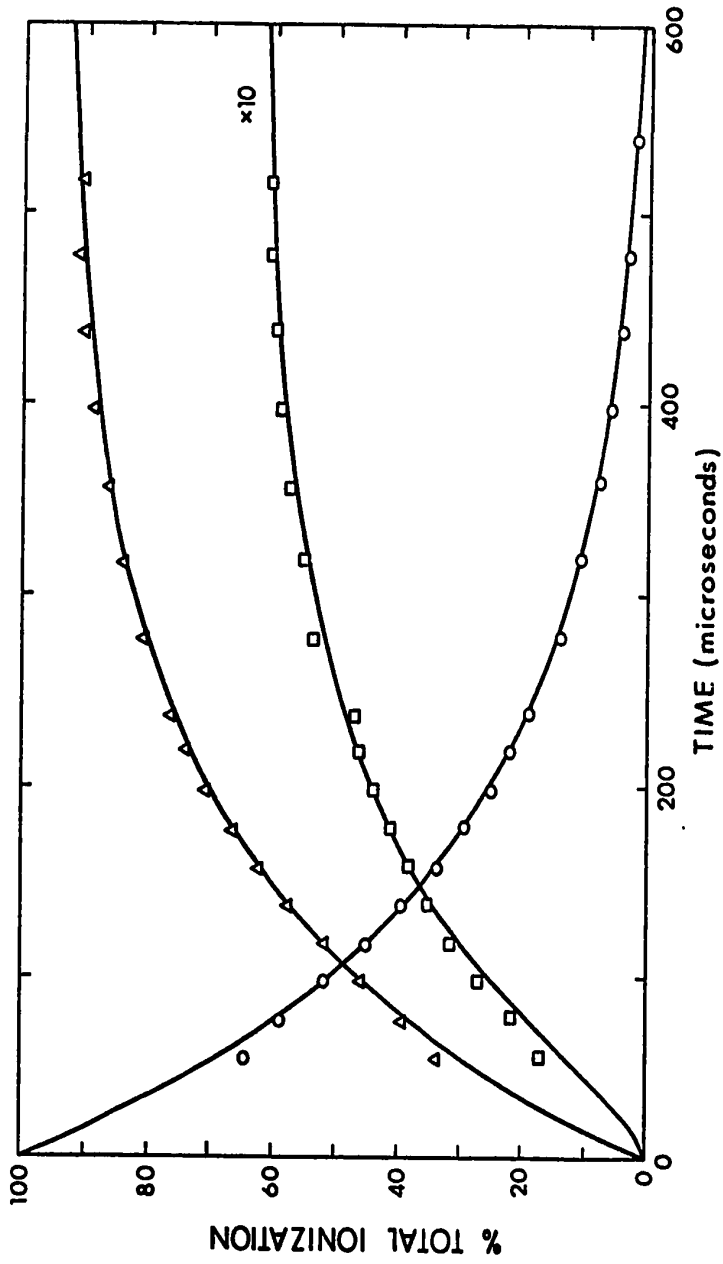


FIGURE 9.6. Time dependence of normalized ion intensities. The curves are the calculated time dependence for the rate parameters summarized in Table 9.1.  $P_{CH_4} = 4.0$  torr,  $P_{H_2O} = 7.7$  mtorr.  $\circ$   $H_3O^+$ ,  $\square$   $H^+(H_2O)_2$  and  $\triangle$   $H^+(H_2O)_3$ .  $T = 223^\circ C$ .

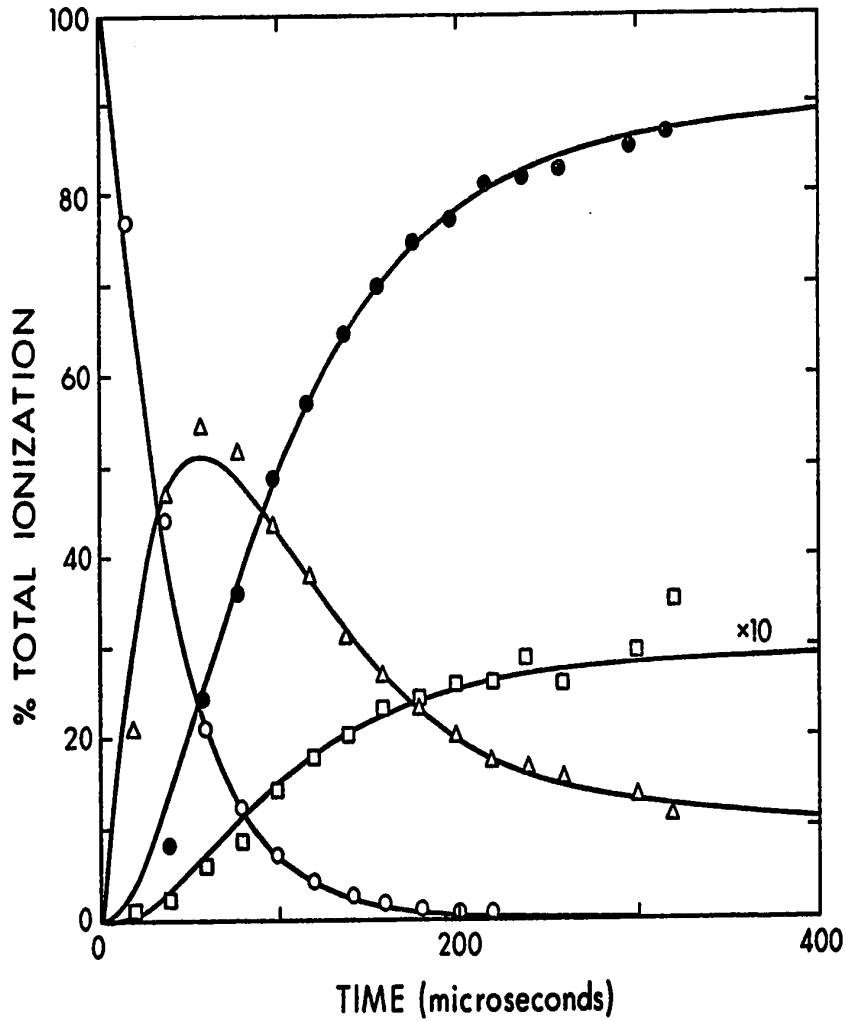


FIGURE 9.7 Time dependence of normalized ion intensities. The curves are the calculated time dependence for the rate parameters summarized in Table 9.1.  $P_{\text{CH}_4} = 4.0$  torr,  $P_{\text{H}_2\text{O}} = 7.5$  mtorr,  $T = 125^\circ\text{C}$ .  $\circ$   $\text{H}_3\text{O}^+$ ,  $\Delta$   $\text{H}^+(\text{H}_2\text{O})_2$ ,  $\bullet$   $\text{H}^+(\text{H}_2\text{O})_3$ ,  $\square$   $\text{H}^+(\text{H}_2\text{O})_4$ .



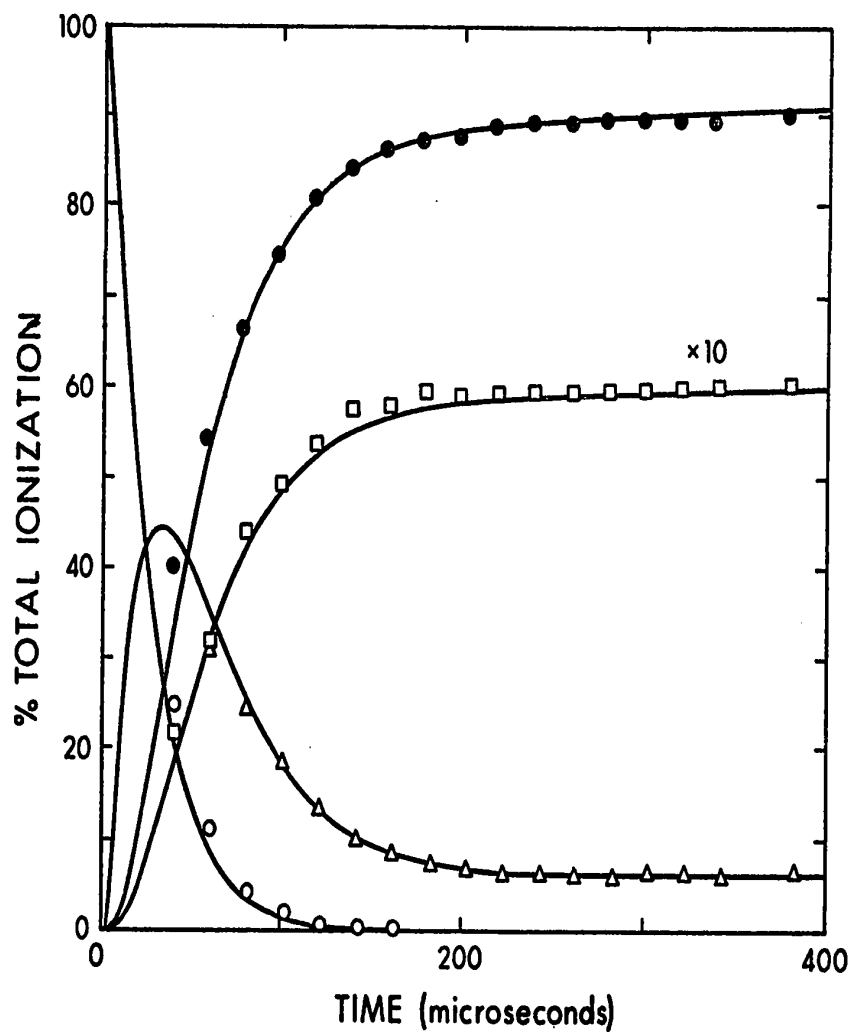


FIGURE 9.8. Time dependence of normalized ion intensities. The curves are the calculated time dependence for the rate parameters summarized in Table 9.1.  $P_{\text{CH}_4} = 4.0$  torr,  $P_{\text{H}_2\text{O}} = 13$  mtorr.  $T = 125^\circ\text{C}$ .  $\circ$   $\text{H}_3\text{O}^+$ ,  $\Delta$   $\text{H}^+(\text{H}_2\text{O})_2$ ,  $\bullet$   $\text{H}^+(\text{H}_2\text{O})_3$ ,  $\square$   $\text{H}^+(\text{H}_2\text{O})_4$ .

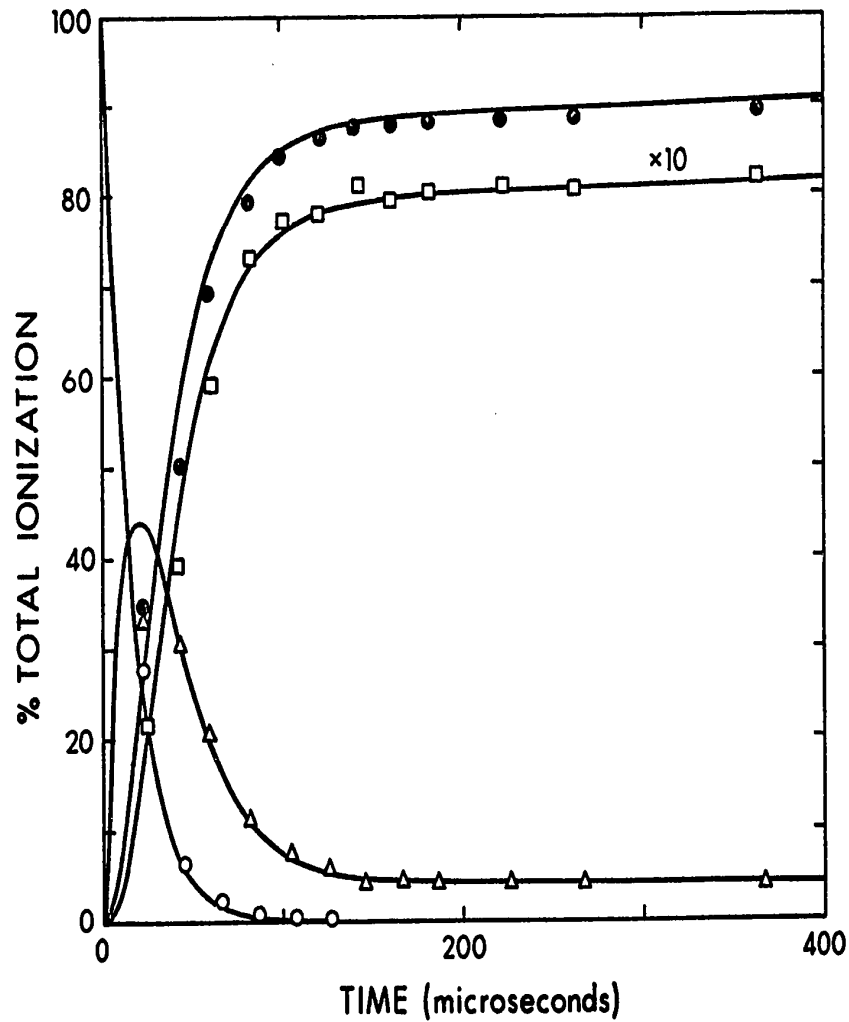
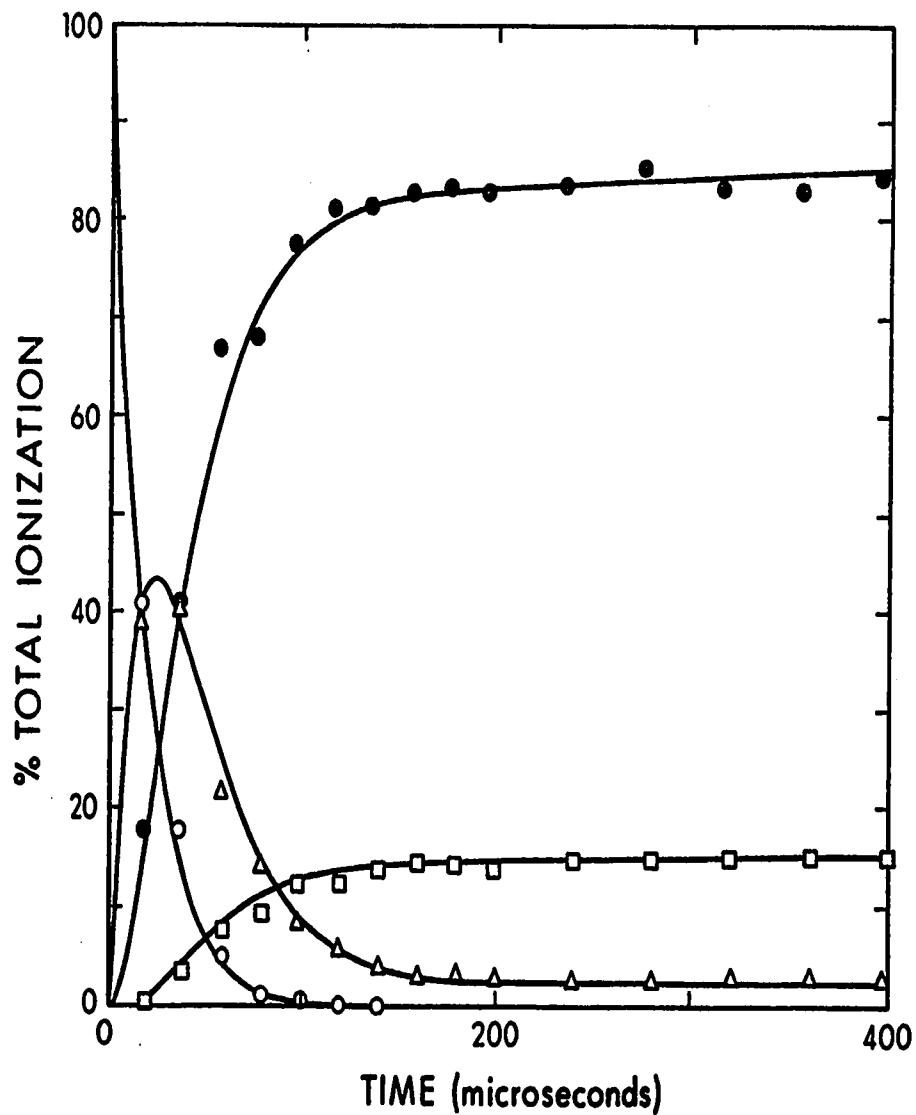


FIGURE 9.9. Time dependence of normalized ion intensities. The curves are the calculated time dependence for the rate parameters summarized in Table 9.1.  $P_{\text{CH}_4} = 4.0$  torr,  $P_{\text{H}_2\text{O}} = 19$  mtorr.  $T = 125^\circ\text{C}$ .  $\circ$   $\text{H}_3\text{O}^+$ ,  $\Delta$   $\text{H}^+(\text{H}_2\text{O})_2$ ,  $\bullet$   $\text{H}^+(\text{H}_2\text{O})_3$ ,  $\square$   $\text{H}^+(\text{H}_2\text{O})_4$ .



**FIGURE 9.10.** Time dependence of normalized ion intensities. The curves are the calculated time dependence for the rate parameters summarized in Table 9.1.  $P_{\text{CH}_4} = 4.0$  torr,  $P_{\text{H}_2\text{O}} = 33$  mtorr,  $T = 125^\circ\text{C}$ .  $\circ$   $\text{H}_3\text{O}^+$ ,  $\Delta$   $\text{H}^+(\text{H}_2\text{O})_2$ ,  $\bullet$   $\text{H}^+(\text{H}_2\text{O})_3$  and  $\square$   $\text{H}^+(\text{H}_2\text{O})_4$

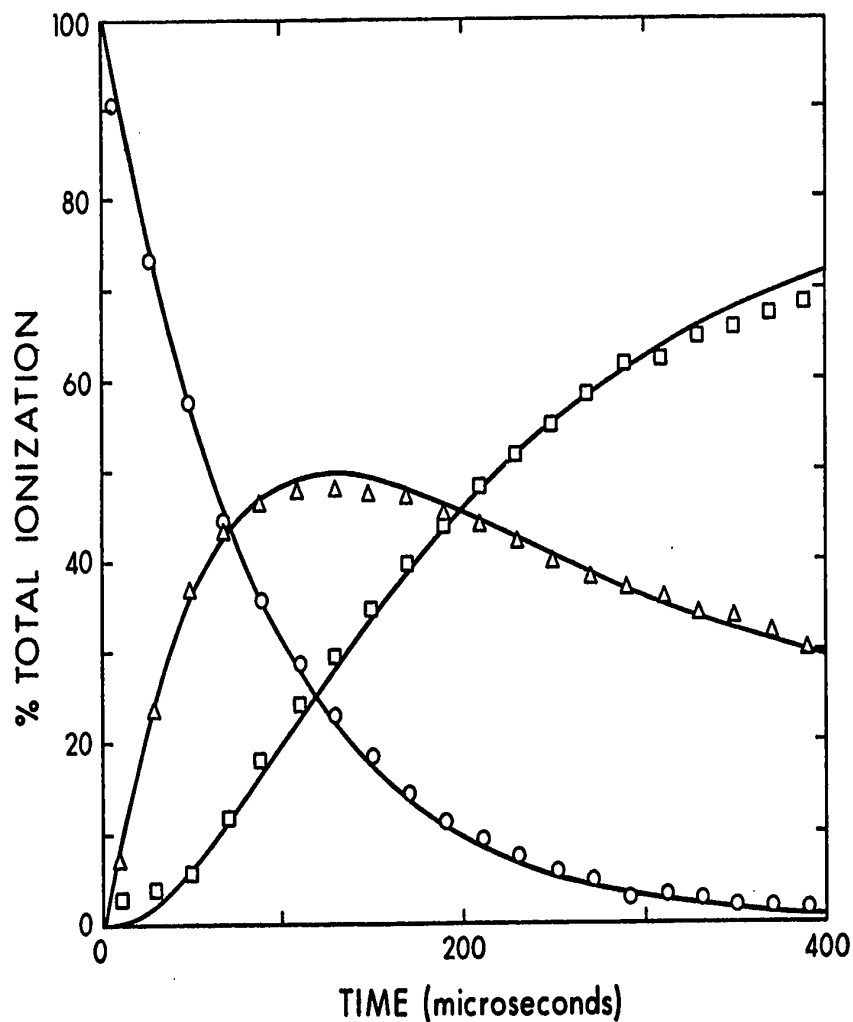


FIGURE 9.11. Time dependence of normalized ion intensities. The curves are the calculated time dependence for the rate parameters summarized in Table 9.1.  $P_{\text{CH}_4} = 5.5$  torr,  $P_{\text{H}_2\text{O}} = 2.5$  mtorr.  $T = 125^\circ\text{C}$ .  $\circ$   $\text{H}_3\text{O}^+$ ,  $\Delta$   $\text{H}^+(\text{H}_2\text{O})_2$ , and  $\square$   $\text{H}^+(\text{H}_2\text{O})_3$ .

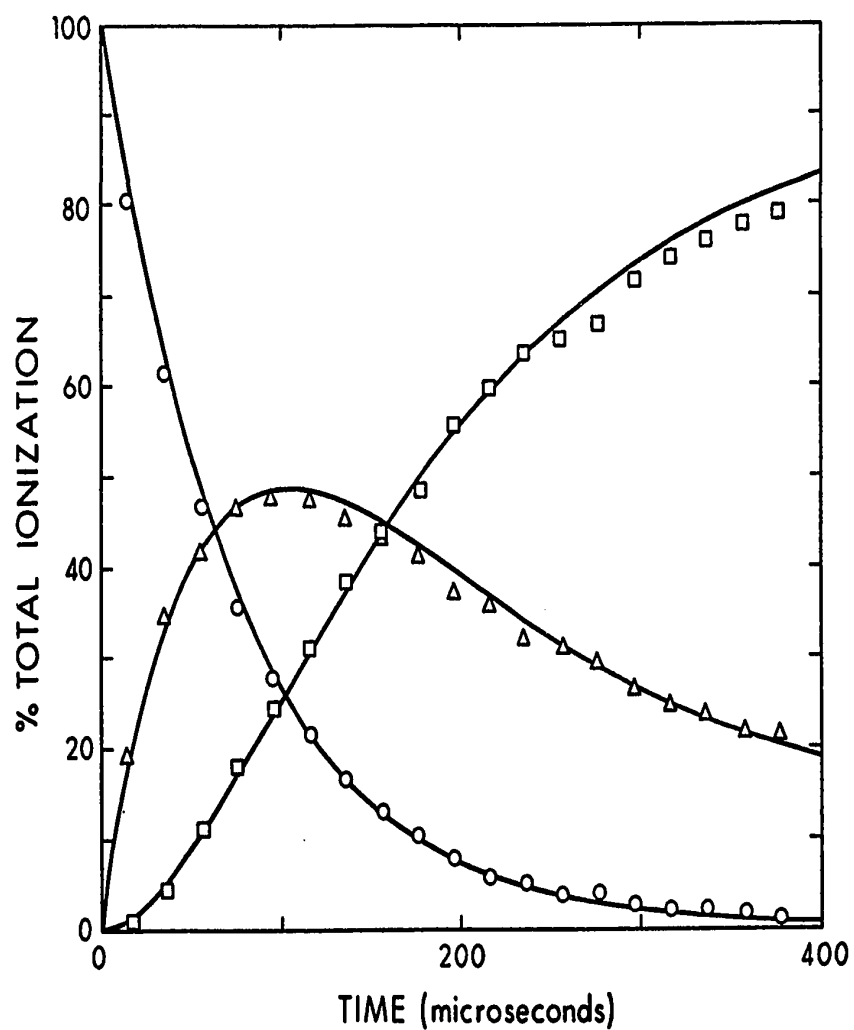


FIGURE 9.12. Time dependence of normalized ion intensities. The curves are the calculated time dependence for the rate parameters summarized in Table 9.1.  $P_{\text{CH}_4} = 2.54$  torr,  $P_{\text{H}_2\text{O}} = 4.58$  mtorr.  $T = 125^\circ\text{C}$ .  $\circ$   $\text{H}_3\text{O}^+$ ,  $\Delta$   $\text{H}^+(\text{H}_2\text{O})_2$ , and  $\square$   $\text{H}^+(\text{H}_2\text{O})_3$ .

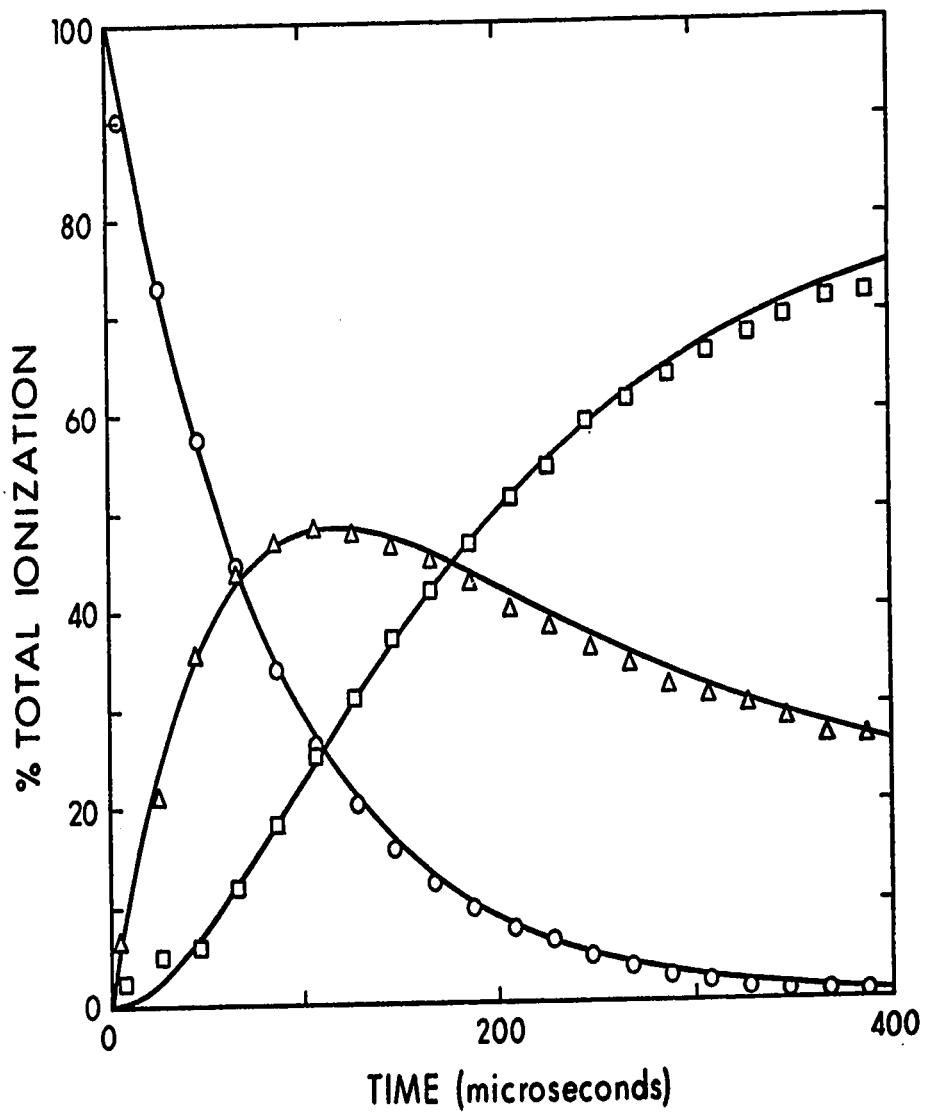
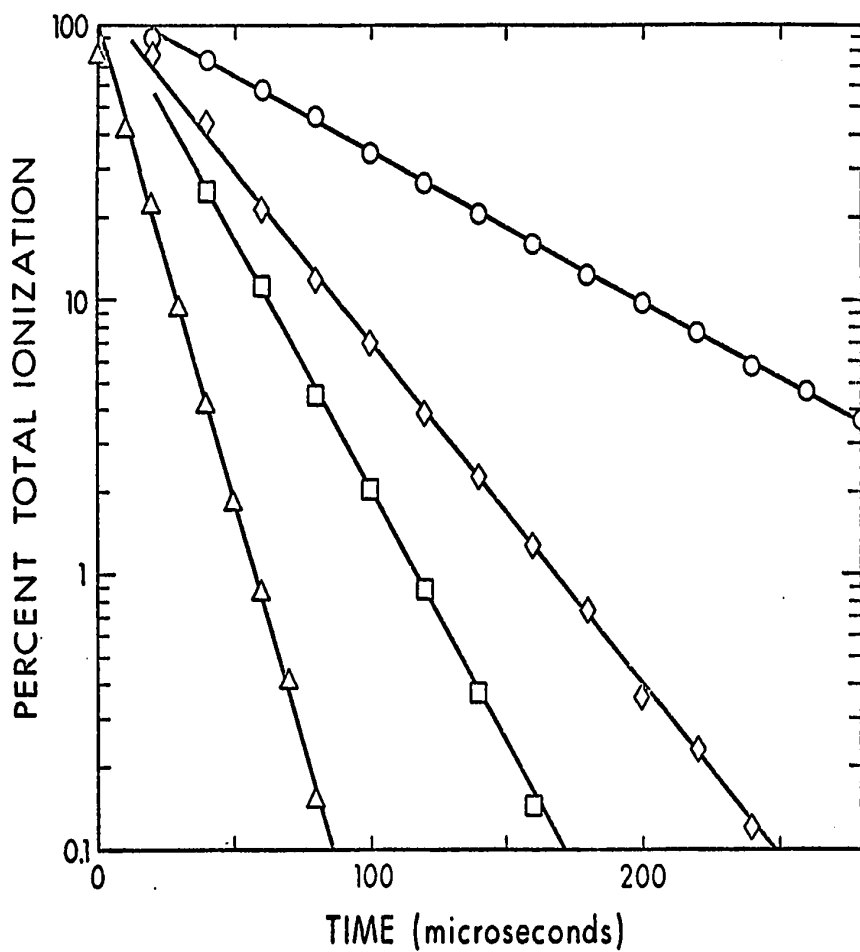


FIGURE 9.13. Time dependence of normalized ion intensities. The curves are the calculated time dependence for the rate parameters summarized in Table 9.1.

$P_{\text{CH}_4} = 3.94$  torr,  $P_{\text{H}_2\text{O}} = 2.58$  mtorr.  $T = 125^\circ\text{C}$ .  
 ○  $\text{H}_3\text{O}^+$ , △  $\text{H}^+(\text{H}_2\text{O})_2$ , and □  $\text{H}^+(\text{H}_2\text{O})_3$ .



**FIGURE 9.14.** Logarithmic plots of normalized  $\text{H}_3\text{O}^+$  intensity with time. Slope leads to  $\nu_1$ . First number after symbol is  $P_{\text{H}_2\text{O}}$  in mtorr, and the second number is  $\nu_1$  in units of  $10^3 \text{ s}^{-1}$ .  $\Delta$  23.5, 78.5;  $\square$  13, 43.1;  $\diamond$  7, 28.1;  $\circ$  3.21, 12.2.  $P_{\text{CH}_4} = 4.0 \text{ torr}$ ,  $T = 125^\circ\text{C}$ .

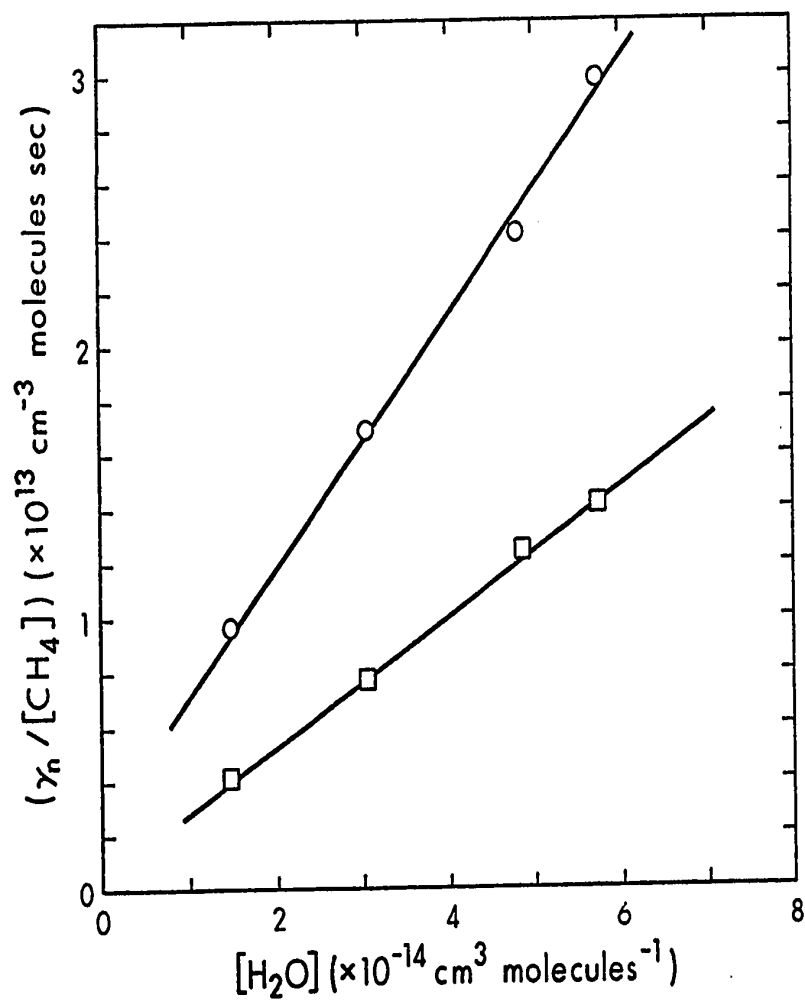


FIGURE 9.15. Dependence of apparent first order rate constant  $v_1 = k_1[\text{H}_2\text{O}][\text{CH}_4]$  on water concentration.  $\circ$   $v_1/[\text{CH}_4]$ ,  $\square$   $v_2/[\text{CH}_4]$ .  $T = 223^\circ\text{C}$ .



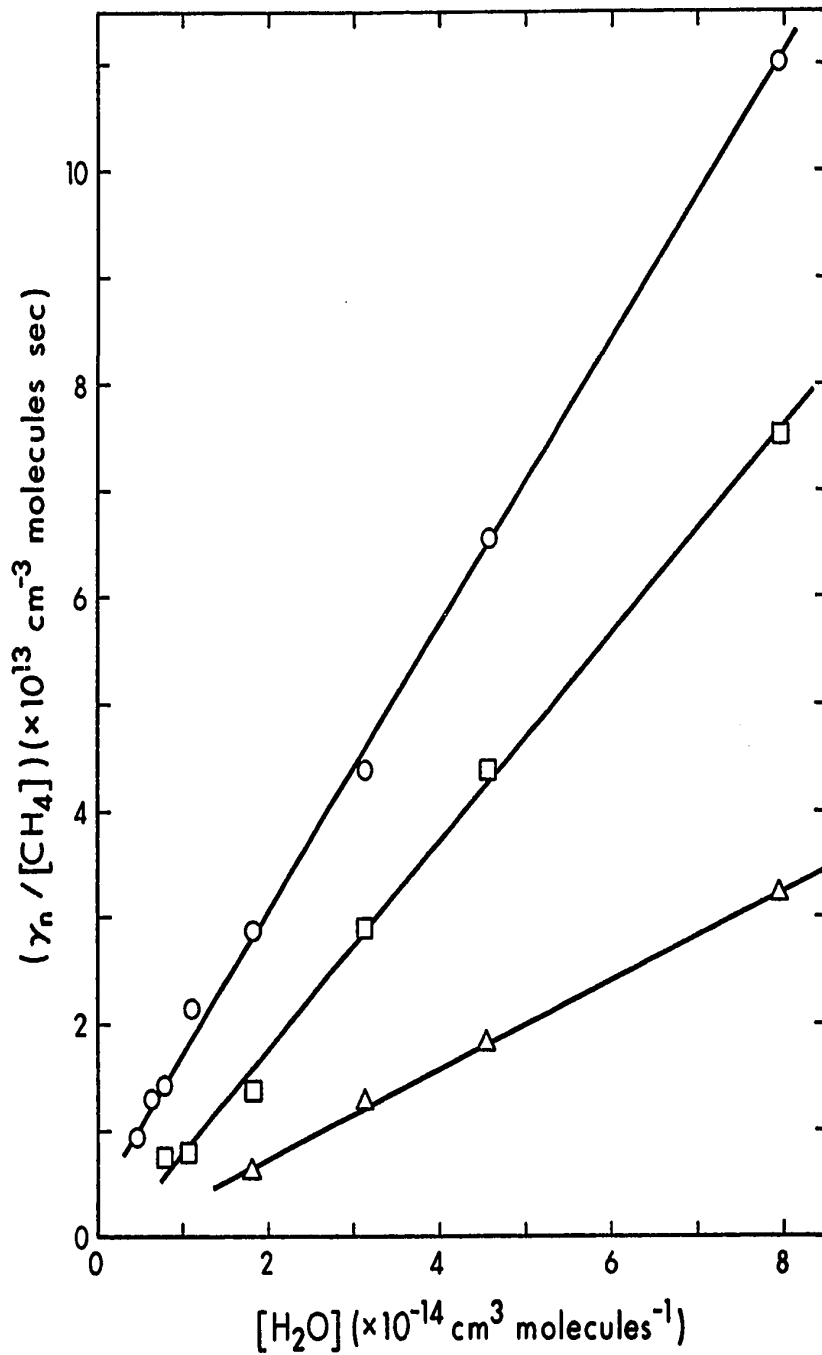


FIGURE 9.16. Dependence of the  $v_i/[CH_4]$  on  $[H_2O]$ .

○  $v_1$ , □  $v_2$ , △  $v_3$ ,  $T = 125^\circ\text{C}$ . Slopes of lines lead to  $k_1 = 1.34 \times 10^{-27}$ ,  $k_2 = 9.8 \times 10^{-27}$  and  $k_3 = 4.2 \times 10^{-28}$  all in  $\text{cm}^6 \text{molecule}^{-2} \text{s}^{-1}$ .

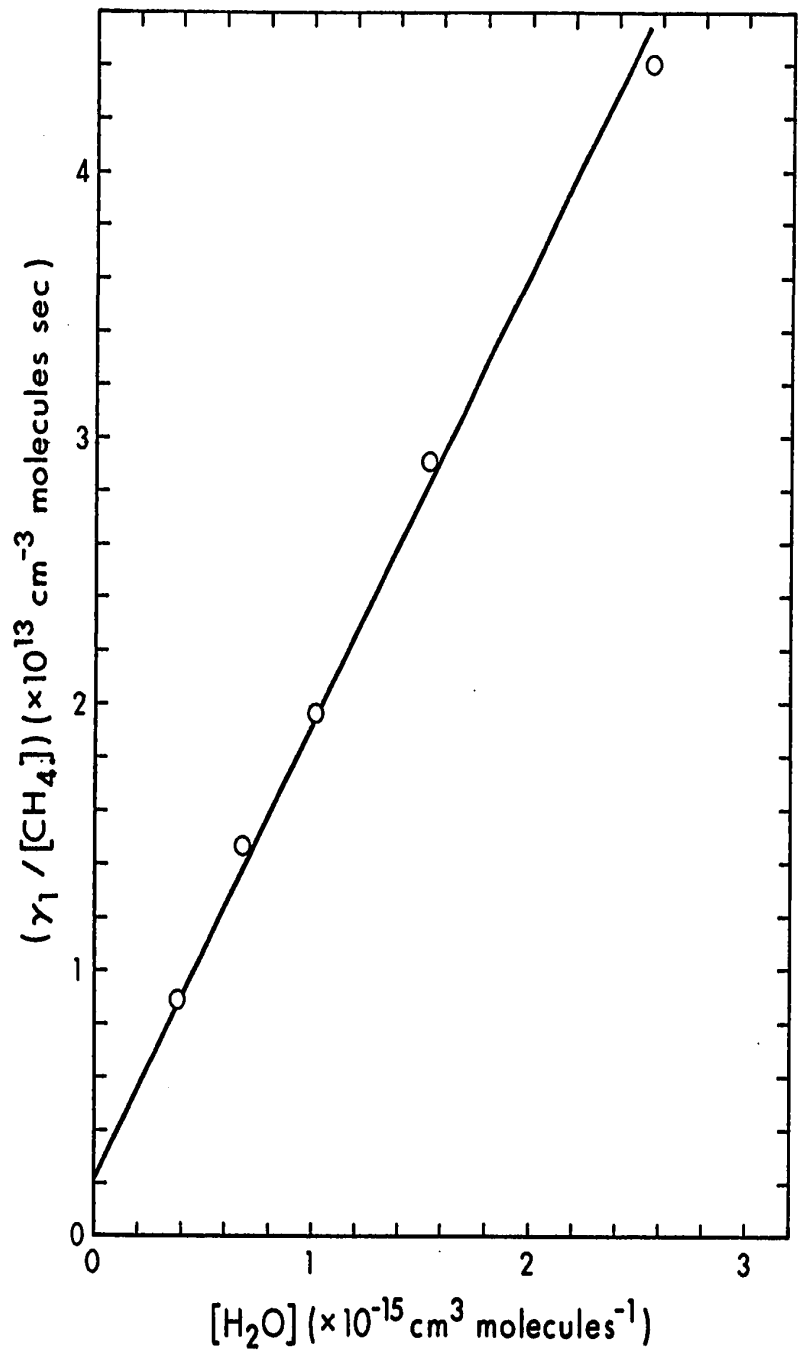
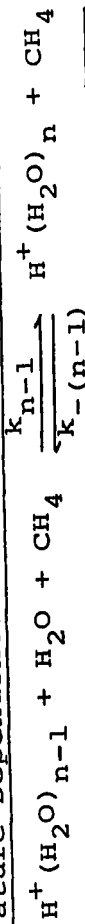


FIGURE 9.17. Dependence of  $v_1/[CH_4]$  on  $[H_2O]$ .  $T = 399^\circ C$ . Slope of line leads to  $k_1 = 1.71 \times 10^{-28} \text{ cm}^6 \text{ molecule}^{-2} \text{ s}^{-1}$ .

TABLE 9.2

Temperature Dependence of the Proton Hydration Reactions



Temp (°K)	$k_1^a$	$k_2^a$	$k_3^a$	$k_{-1}^d$	$k_{-2}^d$	$k_{-3}^d$	$k_{1,2}^e$	$k_{2,3}^e$	$k_{3,4}^e$
296	1.4(-26) <sup>b,c</sup>			5.4(-25) <sup>b</sup>			8.0(14) <sup>b</sup>		
398	1.34(-27)	0.98(-27)	0.42(-27)	3.2(-20) <sup>b</sup>	1.9(-14)	2.13(-12)	1.02(9) <sup>b</sup>	1240	4.75
496	4.64(-28)	2.2(-28)		1.97(-17) <sup>b</sup>	5.4(-13)		4.5(5) <sup>b</sup>	7.9	
672	1.71(-28)			2.78(-14)			112		
805	7.15(-29)			3.9(-13)			2.2		

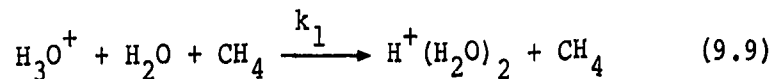
a In units of cm<sup>6</sup> molecule<sup>-2</sup>s<sup>-1</sup>

b Extrapolated value

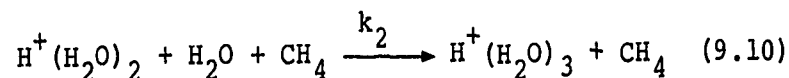
c Read as 1.4 x 10<sup>-26</sup>

d In units of cm<sup>3</sup> molecule<sup>-1</sup>s<sup>-1</sup>

e Standard State 1 torr.



which is  $\sim 1.4 \times 10^{-26} \text{ cm}^6 \text{ molecule}^{-2} \text{ s}^{-1}$  at room temperature decreases to  $\sim 7 \times 10^{-29} \text{ cm}^6 \text{ molecule}^{-2} \text{ s}^{-1}$  at  $800^\circ\text{K}$ . This is a decrease in the rate by a factor of 200. This temperature dependence of  $k_1$  is displayed in Figure (9.18) where a plot of  $\log k_1$  vs  $1/T$  is shown. This plot leads to an "activation energy" of  $-4.9 \text{ kcal/mole}$ . The temperature dependence of this termolecular reaction and several other reactions is discussed in detail in Chapter 10. As may be seen from Table 9.2 the rate of reaction



also decreases with increasing temperature.

From Figure (9.18) a value of  $\sim 1.4 \times 10^{-26} \text{ cm}^6 \text{ molecule}^{-2} \text{ s}^{-1}$  for reaction (9.9) at  $300^\circ\text{K}$  may be estimated as was mentioned previously. However, from Figure (10.19) in which the temperature dependence of (9.9) is expressed in a somewhat different form from Figure (9.18) a value of  $\sim 5 \times 10^{-27} \text{ cm}^6 \text{ molecule}^{-2} \text{ s}^{-1}$  may be estimated. The values of  $k_1$  at  $300^\circ\text{K}$  reported here must be regarded therefore as rather inaccurate.

Other workers have studied the kinetics of the proton hydration reactions. Schiff et al (48) report values of  $k_1 \sim 5 \times 10^{-27} \text{ cm}^6 \text{ molecule}^{-2} \text{ s}^{-1}$ ,  $k_2 \sim 2 \times 10^{-27}$

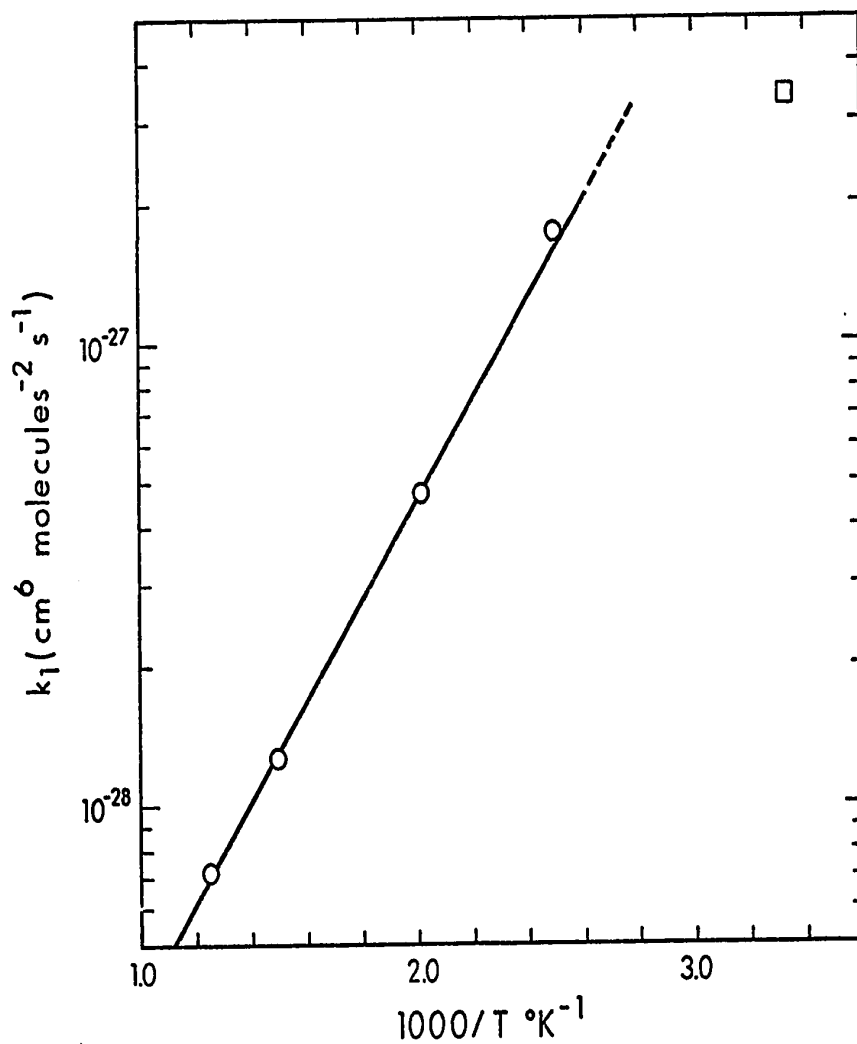
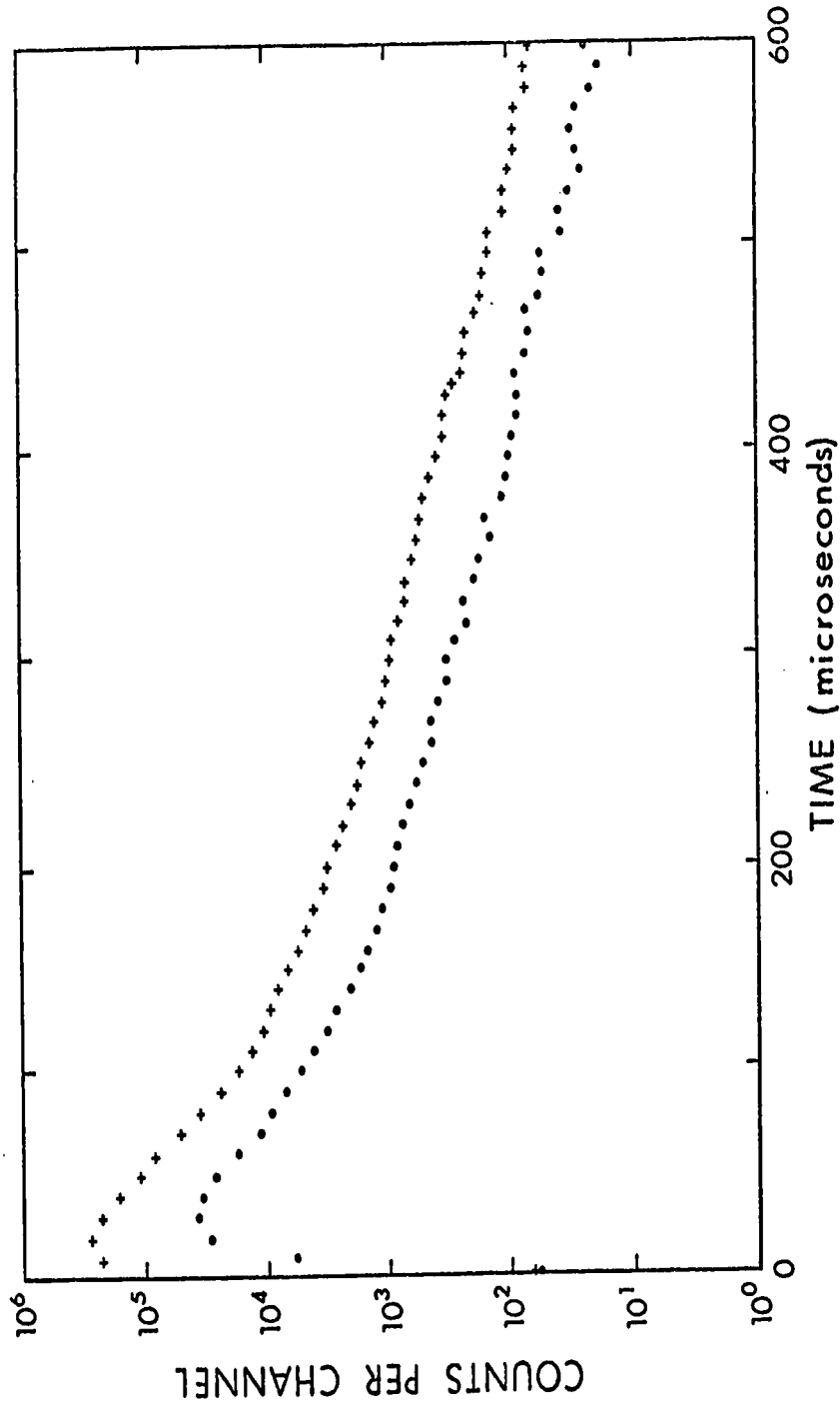


FIGURE 9.18. Temperature dependence of third order rate constant  $k_1$  for the reaction  $\text{H}_3\text{O}^+ + \text{H}_2\text{O} + \text{M} \rightarrow \text{H}^+(\text{H}_2\text{O})_2 + \text{M}$ . Arrhenius-type plot leads to negative "activation energy" of 4.9 kcal/mole.  $\circ$   $\text{M} = \text{CH}_4$ ,  $\square$   $\text{M} = \text{N}_2$  Ref. (61).

$\text{cm}^6 \text{ molecule}^{-2} \text{ s}^{-1}$  and  $k_3 \sim 1 \times 10^{-29} \text{ cm}^3 \text{ molecule}^{-2} \text{ s}^{-1}$   
 with  $M = \text{H}_2$  at  $300^\circ\text{K}$ . Kebarle et al (61) report values  
 of  $k_1, k_2$  and  $k_3$  of  $\sim 3 \times 10^{-27} \text{ cm}^6 \text{ molecule}^{-2} \text{ s}^{-1}$  with  
 $M = \text{O}_2, \text{N}_2$  at  $317^\circ\text{K}$ . Young and Falconer (143) determined  
 $k_1 = 1.7 \times 10^{-27} \text{ cm}^6 \text{ molecule}^{-2} \text{ s}^{-1}$ ,  $k_2 = 1.0 \times 10^{-27} \text{ cm}^6$   
 $\text{molecule}^{-2} \text{ s}^{-1}$  and  $k_3 \sim 2 \times 10^{-29} \text{ cm}^6 \text{ molecule}^{-2} \text{ s}^{-1}$  with  
 $M = \text{O}_2$  at  $310^\circ\text{K}$ . Puckett and Teague (142) have measured  
 $k_4 = 3.5 \pm 0.8 \times 10^{-27} \text{ cm}^6 \text{ molecule}^{-2} \text{ s}^{-1}$  at  $296^\circ\text{K}$  with  
 $M = \text{NO}$ . Thus the present extrapolated values at room  
 temperature appear reasonable. The somewhat higher value  
 of  $k_1$  determined in the present experiments with  $M = \text{CH}_4$   
 is reasonable in that a higher stabilization efficiency  
 is expected for  $\text{CH}_4$  over the diatomic gases.

#### B. Equilibria Measurements

The determination of the equilibrium constants for  
 the hydration was done as previously described in Chapter  
 6. In Figure (9.19) is shown the time dependence of the  
 ions  $\text{H}_3\text{O}^+$  and  $\text{H}^+(\text{H}_2\text{O})_2$  at  $518^\circ\text{C}$  in 4.0 torr of methane  
 containing 99.7 mtorr of water. As may be seen the log  
 plots of the ion intensities are parallel over most of the  
 observed range indicating that the ion ratios are station-  
 ary with time and that equilibrium has been achieved  
 between the ions. Figure (9.20) shows a plot of the  
 normalized ion intensities as a function of time at  $518^\circ\text{C}$ .  
 As may be seen from this Figure some 400  $\mu\text{s}$  are required



**FIGURE 9.19.** Time dependence of ion counts with rapid achievement of  $\text{H}_3\text{O}^+$  +  $\text{H}_2\text{O} \rightleftharpoons \text{H}^+(\text{H}_2\text{O})_2$  equilibrium.  $P_{\text{CH}_4} = 4.0$  torr,  $P_{\text{H}_2\text{O}} = 99.7$  mtorr.  $T = 518^\circ\text{C}$ . +  $\text{H}_3\text{O}^+$ , and  $\bullet$   $\text{H}^+(\text{H}_2\text{O})_2$ .

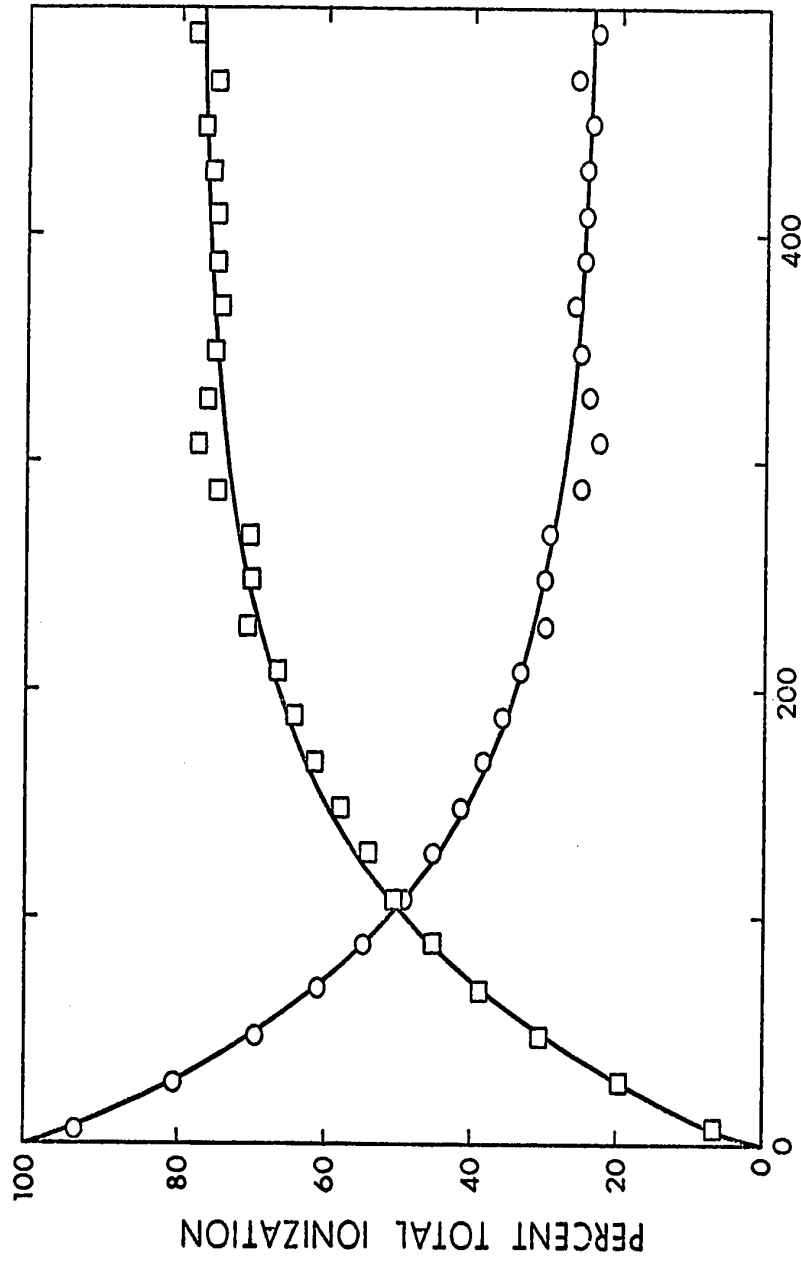


FIGURE 9.20. Time dependence of normalized ion intensities. The curves are

the calculated time dependence for the rate parameters summarized in Table 9.1.  $P_{\text{CH}_4} = 6.0$  torr,  $P_{\text{H}_2\text{O}} = 27$  mtorr,  $T = 399^\circ\text{C}$ .  $\circ$   $\text{H}_3\text{O}^+$  and  $\square$   $\text{H}_2\text{O}^+$ . Note that more than  $400 \mu\text{s}$  is required for the achievement of equilibrium.



for the achievement of equilibrium under these conditions ( $P_{\text{CH}_4} = 6.0$  torr,  $P_{\text{H}_2\text{O}} = 27$  mtorr).

The equilibrium constants were found to be independent of the water pressure over a wide range. In Figure (9.21) is shown a plot of  $K_{1,2}$  as a function of water pressure for several experimental temperatures. The equilibrium constants were found to be independent of the pressure of methane. Several experiments were conducted with ethane and propane as the carrier gases. This was done since Field (40,41,43) reports a rather drastic variation in the equilibrium constant on altering the major gas. In ethane so many ions were observed that it was difficult to determine values of the  $K_{n-1,n}$ . It is believed that the ions other than  $\text{H}^+(\text{H}_2\text{O})_n$  were caused by small amounts of impurities in the ethane. Unsaturated hydrocarbons have ionization potentials which are generally lower than that of ethane and thus charge transfer to these impurities is expected.

Several determinations were made using propane as the carrier gas. In this case the impurities were not as severe a problem. The principal ion series in this case was  $\text{C}_3\text{H}_7^+(\text{H}_2\text{O})_n$ . The propyl hydrates were also reported by Field (41). The proton hydrates formed the second most important series of ions, but many other apparently pure hydrocarbon ions were also present

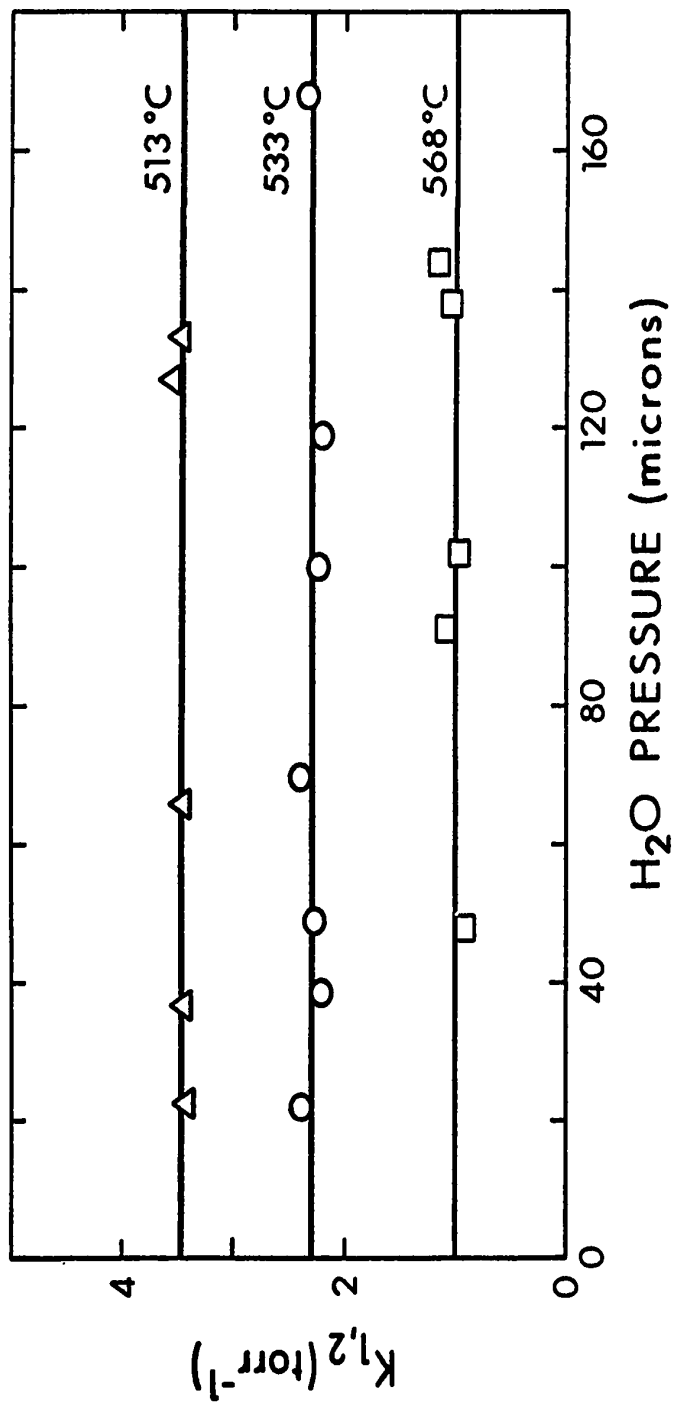


FIGURE 9.21. Equilibrium constant  $K_{0,1}$  for the reaction  $\text{H}_3\text{O}^+ + \text{H}_2\text{O} \rightleftharpoons \text{H}^+(\text{H}_2\text{O})_2$  at several temperatures versus water pressure.

(e.g.  $m/e = 86$  corresponding to  $C_6H_{14}^+$ ). The proton hydrate intensities at long reaction times led to equilibrium constants which were equal, within experimental error, to those observed with methane. The propane system was not subjected to detailed study since being rather complex it was not convenient to use.

In Figure (9.22) is shown a van't Hoff plot of the present values of the equilibrium constants along with the previously reported measurements from this laboratory (82). The thermodynamic data from the van't Hoff plots is summarized in Table 9.3 along with the results of Field.

As may be seen from Table 9.3 the results for the (3,4) equilibrium are the same within experimental error for all investigations. The difference between the present results and those of Field for the lower equilibria is huge and will be discussed in section 9.5. The difference between the present results for the lower equilibria and those of Searles (82,135) is rather large and is beyond experimental error. The present work yields values of  $31.6 \pm 0.4$  and  $19.5 \pm 0.3$  kcal/mole for  $-\Delta H_{1,2}$  and  $-\Delta H_{2,3}$  respectively. Searles (135) reports values of 36 and 22.3 kcal/mole. However, analysis of the data of Searles (135, Table 5.1) by the present author yields values of  $35.0 \pm 1.5$  and  $20.2 \pm 0.7$  kcal/mole for the respective enthalpy changes. Furthermore,

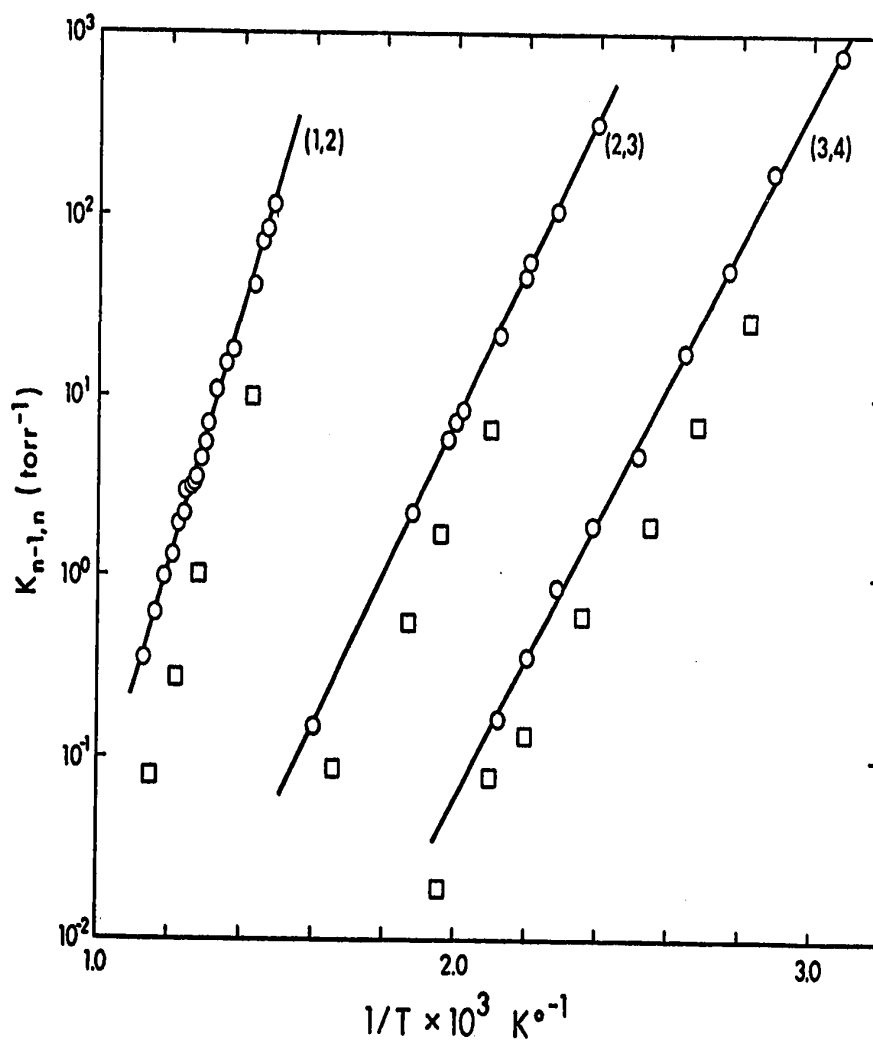
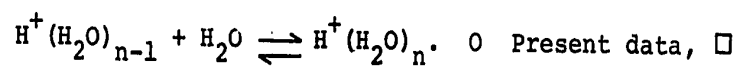


FIGURE 9.22. van't Hoff plots for the reaction



Searles (135).

TABLE 9.3

Thermochemical Data for  $\text{H}^+(\text{H}_2\text{O})_{n-1} + \text{H}_2\text{O} \rightleftharpoons \text{H}^+(\text{H}_2\text{O})_n$

n-1,n	Present work	<u>Equilibria</u>		
		Kebarle et al (82)	Beggs and Field CH <sub>4</sub> (40)	C <sub>3</sub> H <sub>8</sub> (41)
		<u><math>-\Delta H_{n-1,n}^a</math></u>		
1,2	31.6 ± 0.4 <sup>b</sup>	36	7	16.3
2,3	19.5 ± 0.3	22.3	13	14.3
3,4	17.5 ± 0.4	17	16.8	17.6
		<u><math>-\Delta S_{n-1,n}^{c,d}</math></u>		
1,2	24.3 ± 0.5	33.3	-1	17.2
2,3	21.9 ± 0.6	29	14	16.9
3,4	27.3 ± 1.0	28.3	28	30.0
		<u><math>-\Delta G_{n-1,n}^{a,d}</math></u>		
1,2	24.3 ± 0.4	25	7.7	11.2
2,3	13.0 ± 0.4	13.6	9.3	9.7
3,4	9.3 ± 0.5	8.5	8.4	8.6

<sup>a</sup> In kcal/mole

<sup>b</sup> Quoted errors are one standard deviation

<sup>c</sup> In entropy units

<sup>d</sup> Standard state 1 atm, T = 300°K.

it appears that the temperature measurements of Searles (135, Table 5.1) are rather questionable. Searles employed an averaging technique to obtain a value of the ion source temperature. If this averaging technique is not employed, the data of Searles are equivalent within experimental error to the present results. Thus the difference between the present data in Figure (9.22) and that previously reported from this laboratory is not regarded as serious.

#### C. Temperature Dependence of Diffusion

In Figures (9.1) and (9.19) are shown the temporal behaviour of the ions for two quite different ion source temperatures (125°C and 518°C respectively) at roughly the same total pressure. As may be seen the decay of the total ionization is much faster at the higher temperature. As was mentioned in Chapter 3 the accelerated rate of diffusion at the high temperatures casts some doubt on the measurements of the  $N_2^+ + N_2 \rightleftharpoons N_4^+$  equilibrium. The increase in the rate of diffusion with temperature is to be expected since the Chapman-Enskog (89,p.435) theory of ionic diffusion predicts that the diffusion coefficient  $D$  varies with temperature as

$$D \propto T^2 \quad (9.11)$$

for a constant gas pressure and assuming that the potential

between the colliding particles may be expressed as

$$V(r) \propto r^{-4}.$$

D. Temperature Measurement

At high experimental temperatures ( $\sim 450^\circ\text{C}$ ), temperature measurement becomes difficult due to drifting of the ion source temperature during the course of a measurement. Also since heat loss by radiation is substantial, difficulties may arise from heat loss from the region of the sampling orifice. This problem has been discussed previously (section 2.5). The temperature of the ion source assembly was monitored at three points; the usual thermocouple ( $T_1$ ) imbedded deep in the ion source block; a thermocouple ( $T_2$ ) mounted in the copper plate ([14] in Figure (2.1)) and finally a thermocouple ( $T_3$ ) in the large disk (see section 2.5) mounted at the bottom of the electrostatic screen ([11] in Figure (2.1)). Both the copper plate [14] and the disk [11] possessed independent electric heaters.

In Figure (9.23) is shown the effect on the equilibrium constant  $K_{1,2}$  of varying  $T_2$  and  $T_3$ . With the heaters in the copper plate turned off it was found that the plate was over  $100^\circ\text{C}$  cooler than the ion source at these temperatures. The disk however was several hundred degrees cooler. As may be seen from Figure (9.23) the effect of varying  $T_2$  and  $T_3$  on  $K_{1,2}$  is nil. The dashed

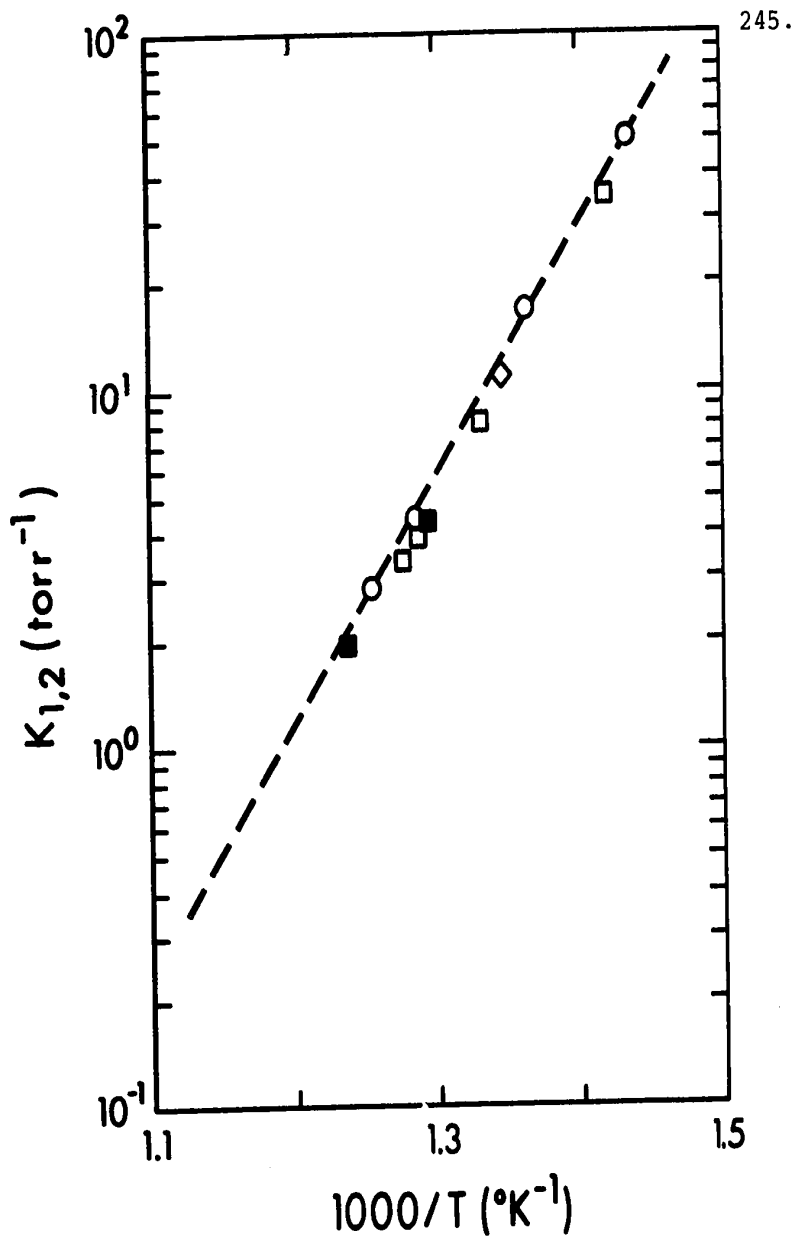


**FIGURE 9.23.** Effect on the equilibrium constant  $K_{1,2}$  of varying the temperature of portions of the ion source.  $\circ$   $T_1 > T_2 \gg T_3$ ,  $\diamond$   $T_1 > T_2 > T_3$ ,  $\square$   $T_1 \approx T_2 > T_3$ , and  $\blacksquare$   $T_1 \approx T_2 \approx T_3$ . See text for more detailed explanation. Plot shows that radiative heat lost from the ion exit slit does not significantly alter the temperature of the slit. (----) Data of Figure (9.22).



line in the Figure corresponds to the van't Hoff plot of Figure (9.22). In Figure (9.23) the symbol  $>$  implies that the temperatures differ by a small ( $30^\circ$ ) amount while  $>>$  implies a several hundred degree difference and  $\approx$  implies near equality.

Unfortunately only two measurements were performed for high values of  $T_3$ . The radiation from the disk at the high temperatures ( $\sim 550^\circ\text{C}$ ) destroyed a portion of the ion acceleration system and the experiment was abandoned at this point. Nevertheless the results indicate that radiative heat loss from the sampling orifice does not introduce any substantial experimental error, even at very high temperatures. It is concluded that the ion source thermocouple reflects the gas temperature.

#### E. Effect of Repeller

In Figure (9.24) is shown a plot of the observed temporal profile of the ion signal as a function of repeller voltage. The repeller was mounted some 5 mm from the ion exit slit and the electron beam entered the ion source roughly halfway between the two. As may be seen the application of a repeller voltage has a drastic effect on the temporal behaviour of the ions. At high repeller voltages, the ions are "pushed" out of the ion source in a few tens of microseconds. At intermediate values of the repeller voltage the effect is less

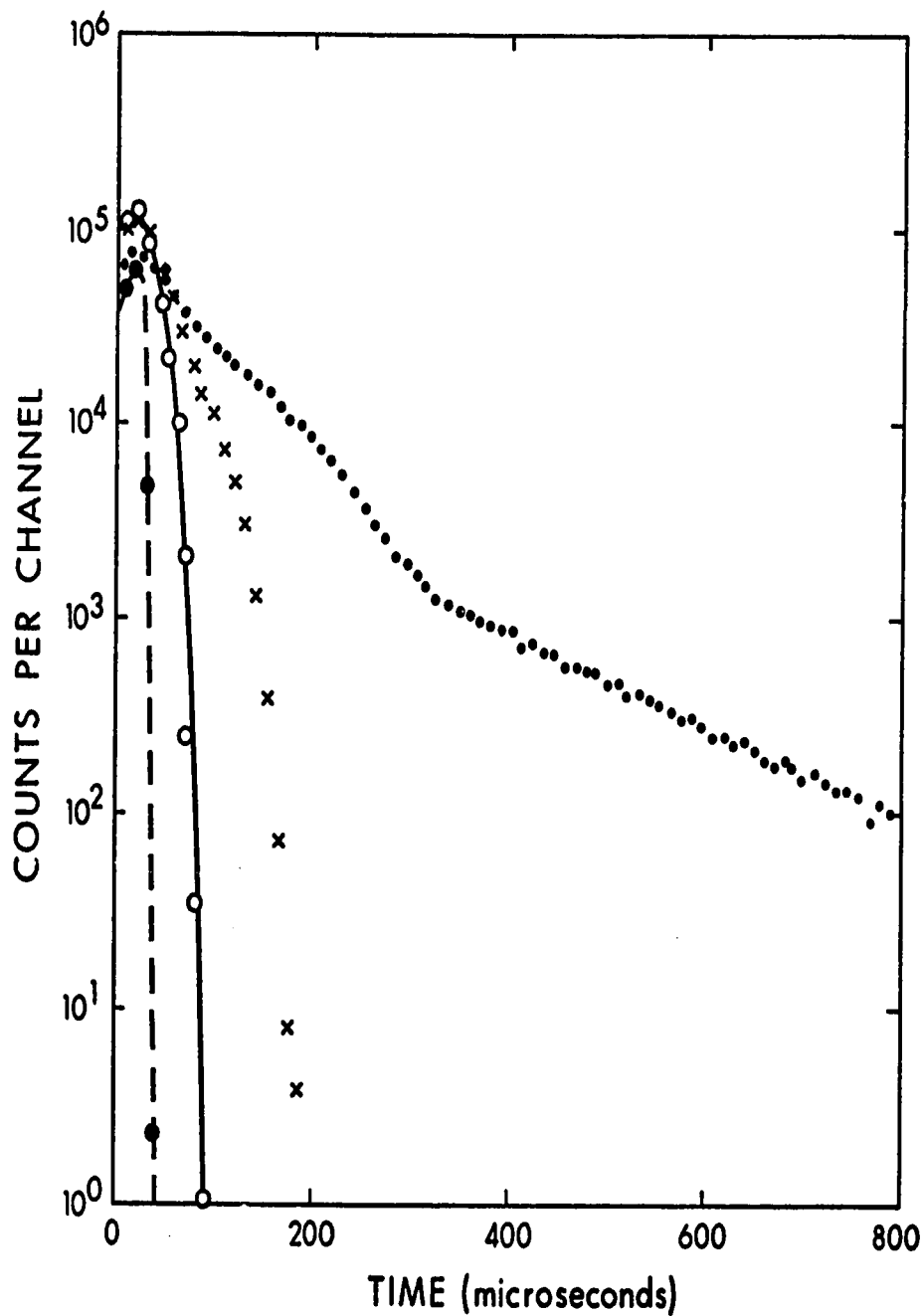


**FIGURE 9.24.** Effect of repeller voltage on the temporal behaviour of the ion signal. Points represent sum of all ions ( $\text{H}^+(\text{H}_2\text{O})_n$ ).  $P_{\text{CH}_4} = 3.94$  torr,  $P_{\text{H}_2\text{O}} = 2.6$  mtorr,  $T = 126^\circ\text{C}$ . Number following symbol is repeller voltage in volts. ● 0, X 2, ○ 4, and ● 8. At high repeller voltage the ion residence time in the ion source is reduced to a few tens of microseconds.

pronounced. Field has calculated that at typical repeller voltages in the chemical ionization technique that the ions are in the ion source for some 10-30  $\mu$ s. The electric field from the repeller under the chemical ionization conditions of Field is comparable to the high values of the repeller voltage in the present experiments. Thus the present measurements support Field's arguments that the ions spend some 10-30  $\mu$ s in the ion source under chemical ionization conditions.

In Figures (9.25) and (9.26) is shown the effect of the repeller voltage on the integrated ion signal. If equilibrium is achieved quickly between the ions then the integrated signal should reflect the equilibrium ionic populations. At comparatively high water concentration (27 mtorr) the value of the equilibrium constant calculated from the integrated ion intensities (Figure (9.25)) at zero repeller field is  $K_{2,3} = 1240 \text{ torr}^{-1}$  which is close to the value of  $1210 \text{ torr}^{-1}$  calculated from the time dependence plots at zero repeller field. In Figure (9.26) the water pressure is low (2.85 mtorr) and the value of  $K_{2,3} = 365 \text{ torr}^{-1}$  at zero repeller voltage is roughly a factor of four different from that measured by observing the temporal behaviour of the ions at zero repeller field. As may be seen from Figures (9.25) and (9.26) the relative intensities of the ions vary with repeller voltage as does the apparent equilibrium constant.

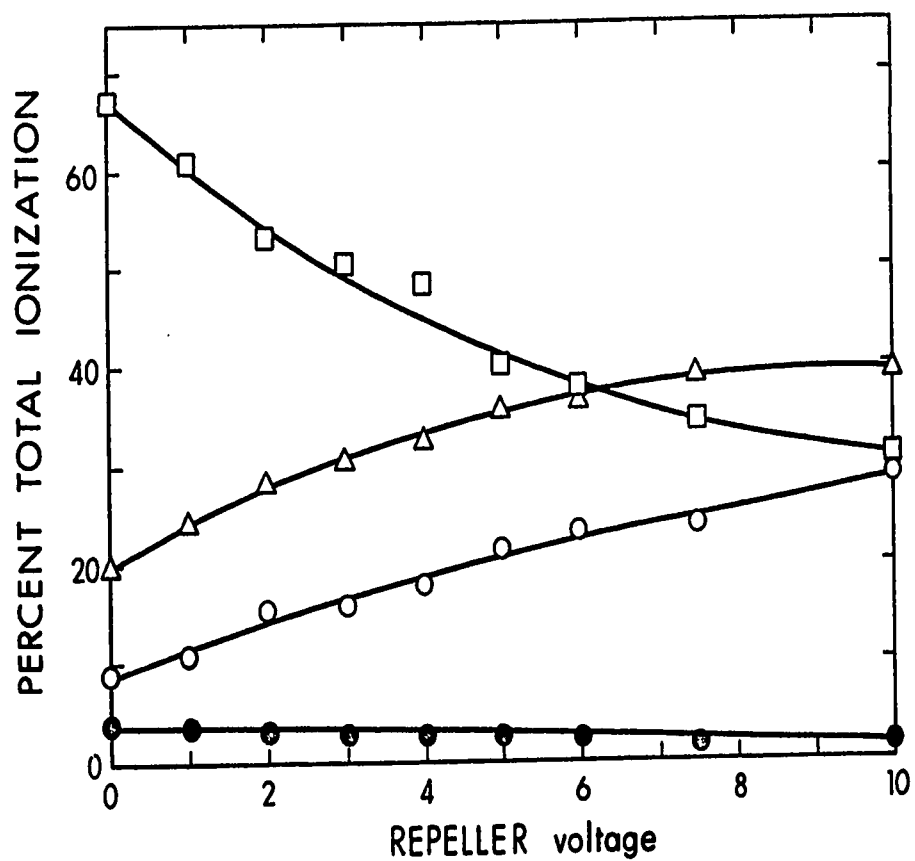


FIGURE 9.25. Relative concentrations of proton hydrates as a function of repeller voltage.

$P_{\text{CH}_4} = 4.0$  torr,  $P_{\text{H}_2\text{O}} = 27$  mtorr,  $T = 125^\circ\text{C}$ .

$\circ$   $\text{H}_3\text{O}^+$ ,  $\Delta$   $\text{H}^+(\text{H}_2\text{O})_2$ ,  $\square$   $\text{H}^+(\text{H}_2\text{O})_3$ , and  $\bullet$   $\text{H}^+(\text{H}_2\text{O})_4$ .

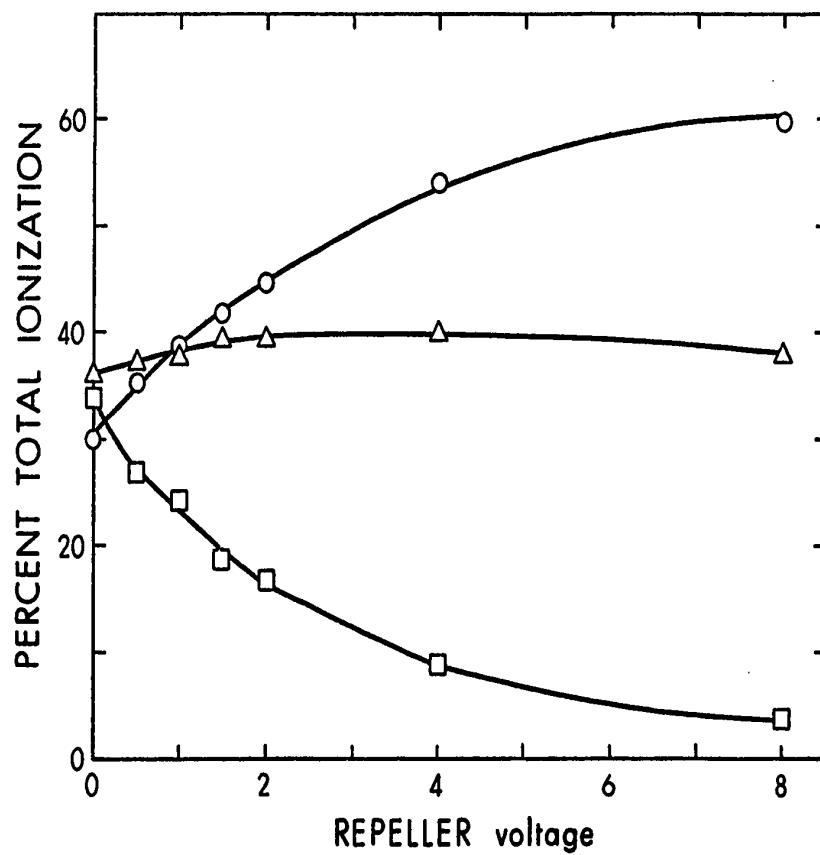


FIGURE 9.26. Relative concentration of proton hydrates as a function of repeller voltage.  $P_{\text{CH}_4} = 4.0$  torr,  $P_{\text{H}_2\text{O}} = 2.85$  mtorr,  $T = 125^\circ\text{C}$ .  $\circ \text{H}_3\text{O}^+$ ,  $\Delta \text{H}^+(\text{H}_2\text{O})_2$ , and  $\square \text{H}^+(\text{H}_2\text{O})_3$ .

From Figure (9.26) one may calculate a value of  $K_{1,2} \sim 10^3 \text{ torr}^{-1}$ . Interestingly the ratio of  $\text{H}_3\text{O}^+$  to  $\text{H}^+(\text{H}_2\text{O})_2$  is roughly independent of the repeller voltage under these conditions. In Figure (9.27) is shown the temporal behaviour of the ions under similar conditions. In this plot the  $\text{H}_3\text{O}^+$  signal decays exponentially to the noise level. From this figure one may calculate that  $K_{1,2} > 10^5 \text{ torr}^{-1}$ . From Table 9.2 the extrapolated value of  $K_{1,2}$  at this temperature (125°C) is  $1 \times 10^9 \text{ torr}^{-1}$ . This is a factor of  $10^6$  different from that calculated from the total ion intensities and demonstrates that considerable care must be exercised in determining the equilibrium constant when the concentration of the substrate is low.

#### 9.5 Discussion of Results

The present results are contrasted graphically with those of Field in Figure (9.28). As was mentioned previously the agreement is fair for the (3,4) equilibria. In general differences of up to a factor of two in the equilibrium constant may be expected. Such differences arise from errors in measuring the water pressure, temperature, errors due to the method of sampling, and mass discrimination effects in the mass spectrometer. The difference between the present results and those of Field for the (2,3) equilibrium is large and the difference for

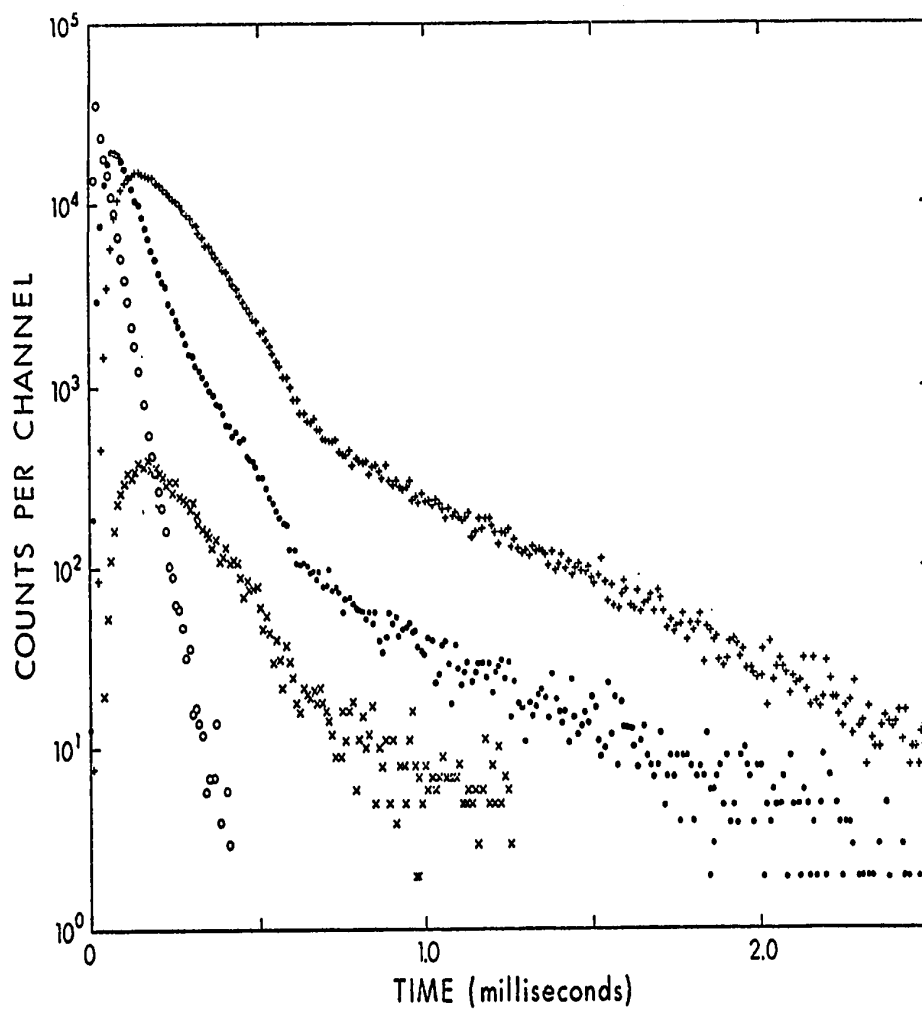


FIGURE 9.27. Time dependence of ion counts observed with multiscaler.  $\circ$   $\text{H}_3\text{O}^+$ ,  $\bullet$   $\text{H}^+(\text{H}_2\text{O})_2$ ,  $\times$   $\text{H}^+(\text{H}_2\text{O})_3$  and  $+$   $\text{H}^+(\text{H}_2\text{O})_4$ .  $P_{\text{CH}_4} = 4.1$  torr,  $P_{\text{H}_2\text{O}} = 10.2$  mtorr,  $T = 125^\circ\text{C}$ . Equilibrium between the ions appears as a constant difference in the log of the ion counts. Note complete disappearance of  $\text{H}_3\text{O}^+$  in contrast with the behavior of the other ions.

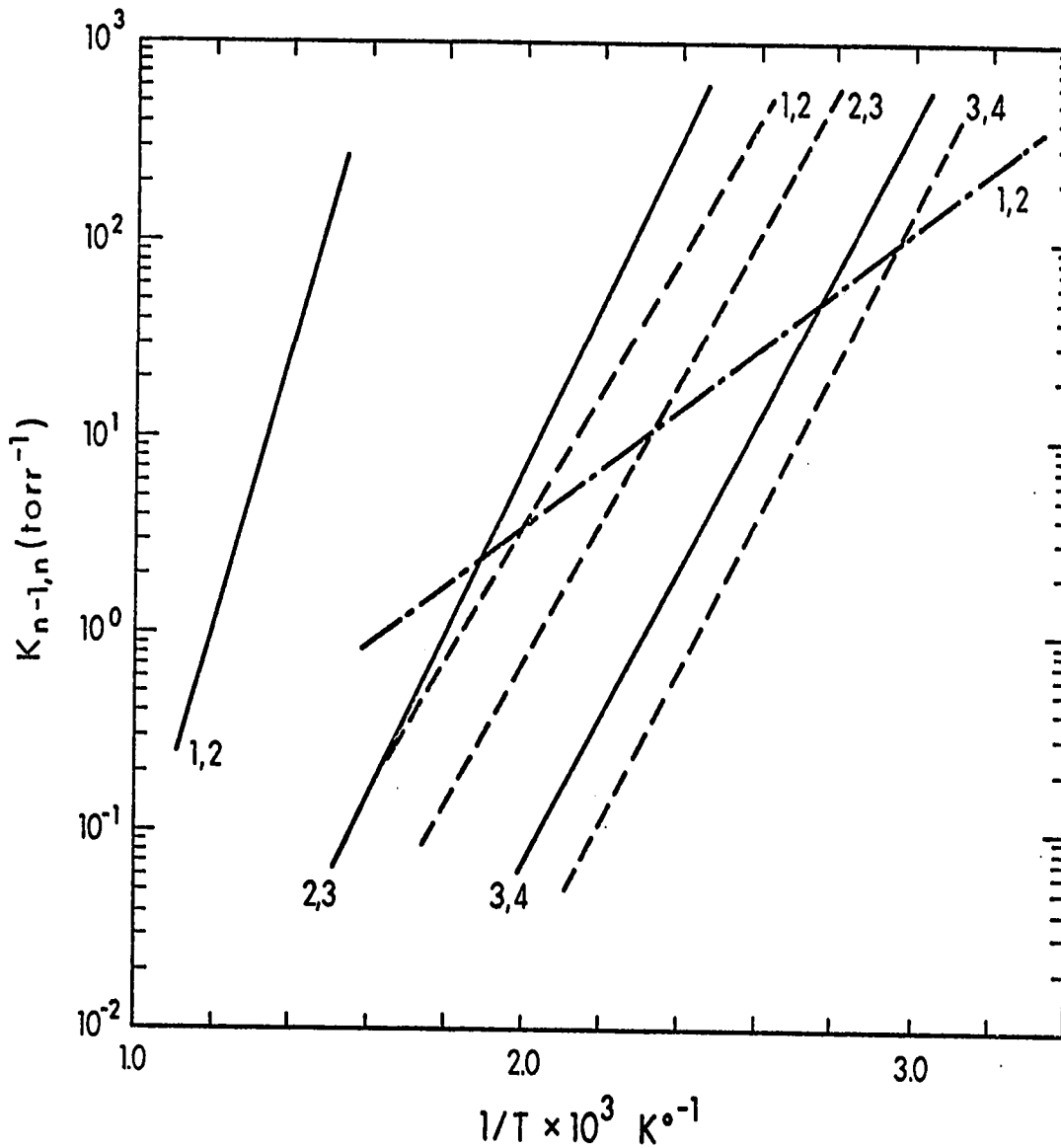


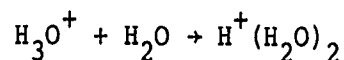
FIGURE 9.28. Comparison of van't Hoff plots from present work with those obtained by Field. (—) present work, (---) Field (41) propane as major gas, (-.-) Field (40) methane as major gas. Note large discrepancy between 1,2 plot from present results and the two completely different plots of Field.



the (1,2) equilibrium is huge.

Field has applied the chemical ionization technique to the measurement of the (1,2) equilibrium using three different major gases. With propane and isobutane (41,43) Field's results are identical but with methane he reports a vast difference. This is shown in Figure (9.28) as the two completely different van't Hoff plots reported by Field. These plots are to be contrasted with the present results. As may be seen from Figure (9.28) and Table 9.3 the results of Field are not self consistent.

Using methane as the carrier gas, Field reports a positive entropy change for the reaction



This means that the species  $\text{H}^+(\text{H}_2\text{O})_2$  is less ordered than the two species  $\text{H}_3\text{O}^+$  and  $\text{H}_2\text{O}$ . This is absurd if one assumes a reasonable geometry (bond lengths in the order of angstroms) and vibrational frequencies for  $\text{H}^+(\text{H}_2\text{O})_2$ . The thermodynamic parameters reported by Field using propane as the major gas are less unreasonable however.

The temperature range used by Field for the (1,2) equilibria centres at about 125°C. The time dependent concentration changes displayed in Figure (9.1) show the  $\text{H}_3\text{O}^+$  being completely converted to  $\text{H}^+(\text{H}_2\text{O})_2$  and higher hydrates for a water pressure of 3.2 mtorr at 125°C. Similar results are shown in Figure (9.27). The  $\text{H}_3\text{O}^+$  -

$\text{H}^+(\text{H}_2\text{O})_2$  equilibrium is clearly observed only at much higher temperatures i.e. above 250°C (Figure (9.19)). Unfortunately the highest temperature explored by Field was only 255°C. Examining the van't Hoff plot given by Field (Figure (3) ref. (41)) one finds that all the  $K_{1,2}$  equilibrium constants for temperatures below 160°C, which corresponds to over half of the temperature range covered were obtained with a constant water pressure of 0.7 mtorr. Using  $k_1 = 1.3 \times 10^{-27}$  (Table 9.2, 125°C) which is in the right range for clustering reactions of this type (48,61,142,143) one calculates a half life for conversion of  $\text{H}_3\text{O}^+$  to  $\text{H}^+(\text{H}_2\text{O})_2$  of about 1000  $\mu\text{s}$  (1 torr of methane, 0.7 mtorr of  $\text{H}_2\text{O}$ ). The ion residence time in Field's source according to his own estimate (40) is only 10-30  $\mu\text{s}$ , strongly suggesting that his measurements were obtained prior to the establishment of equilibrium. It is therefore difficult to rationalize the linearity of his van't Hoff plot and the resultant  $-\Delta H_{1,2}$  value of 16.3 kcal/mole (41,43).

As was mentioned previously, there is essentially complete agreement between the present results and those reported by Field for the (3,4) and higher equilibria. Initially this appears rather surprising considering the vast disagreement for the lower (1,2) and (2,3) equilibria. A careful examination of the data of Field will show that Field's measurements are not conducted under the same

conditions in both experiments. For the studies of the higher equilibria, Field uses comparatively high (10-100 mtorr) water concentrations while somewhat lower concentrations ( $\lesssim 1$  mtorr) were used for the lower equilibria. Furthermore, and of the greatest importance to the understanding the reason for the error in Field's experiments, is that the temperature range used by Field is such that the equilibrium between the proton hydrates will be observable for the high clusters and not for the lower ones. The temperature range used by Field centres about 125°C. At this temperature, for water pressures in the tens of mtorr, the ratios of the 2,3 and 4 clusters will be comparable - that is they will be within a factor of say  $10^2$  at equilibrium. However, the ratio of the  $\text{H}_3\text{O}^+$  to  $\text{H}^+(\text{H}_2\text{O})_2$  will be very small - as small as  $10^{-9}$ . Thus the  $\text{H}_3\text{O}^+$  will be beyond the limits of detection at equilibrium. Field lowers the water pressure such that he observes  $\text{H}_3\text{O}^+$ , largely because it has not had the opportunity to react further to give  $\text{H}^+(\text{H}_2\text{O})_2$ . The assumption is then made by Field that equilibrium is close, that is the  $\text{H}_3\text{O}^+$  and  $\text{H}^+(\text{H}_2\text{O})_2$  are of comparable intensities at equilibrium under these conditions. If this were true the equilibrium constants reported by Field would not be too seriously in error.

The above argument is of a cyclic nature. That is if the present data are correct then the error in Field's

data is obvious. However, Field (43) argues that if his data is correct then it is self supporting. The present data however is reproducible and has been found to be independent of all experimental variables. On the other hand Field's data varies with all reported experimental parameters. Thus the present data is considered more reliable than the results of Field.

Friedman et al (144) have measured the dissociation energies of the proton hydrates. Their experimental method consists of determining the minimum kinetic energy required to dissociate a proton hydrate cluster on impact with a helium atom. The results of Friedman et al (144) are in excellent agreement with the previous results of Kebarle et al (82) and therefore support the present measurements.

Recently three ab initio calculations have been performed to determine the binding energies and geometrical configurations of the proton hydrates. For the  $\text{H}_3\text{O}^+$  -  $\text{H}_2\text{O}$  bond energy Kraemer and Diercksen (138) obtained 32.3 kcal/mole, Kollman and Allen (139) 36.9 kcal/mole and Newton and Ehrenson (140) 33.5 kcal/mole. These calculations thus support the present value of 31.6 kcal/mole.

A conclusion which is common to all of these calculations on the ion  $\text{H}_5\text{O}_2^+$  is that of geometry. Here the energetically favoured structure is one in which the

proton is equidistant between the two oxygen atoms ( $r_{\text{O-O}} = 2.39 \text{ \AA}$  (64)). The hydrogen atoms on the oxygen atoms point away from the central proton and the planes formed by the H-O-H's are oriented at right angles to each other. The potential energy of the system for asymmetrical motion of the proton along the O-O axis is found to be almost constant over a range of some  $0.3 \text{ \AA}$  (47). In fact Kraemer and Dierksen (45) find a double minimum corresponding to asymmetrical structures of the form  $\text{H}_2\text{OH}^+ \dots \text{OH}_2$ . However, the barrier between the two minima is so small as to be almost negligible (45). This type of potential minimum for the central proton in the  $\text{H}_5\text{O}_2^+$  ion suggests relatively easy formation and breaking of bonds in aqueous solution, and thus offers an explanation of the positive charge mobility in aqueous solution. The theoretical calculations are supported by a neutron diffraction study (145) of crystals containing the  $\text{H}_5\text{O}_2^+$  moiety. In this study it was shown that the proton lies equidistant between the two oxygen atoms.

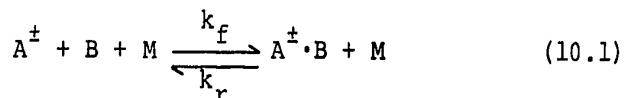
Newton and Ehrenson (140) have also performed theoretical calculations on the binding energies and structures of the higher proton hydrates. The binding energies calculated by them are in good agreement with the previous results from this laboratory (82) and with those of Freidman et al (144). Newton and Ehrenson

report that as the number of water molecules in the ion increases that it becomes unclear as to whether a "centrosymmetrical" structure about the proton or a "chain" form is energetically favoured. The "chain" form is apparently slightly favoured. However, the authors (140) considered the difference marginal.

X The Temperature Dependence of Selected Termolecular Reactions

10.1 Introduction

The study of termolecular reactions such as



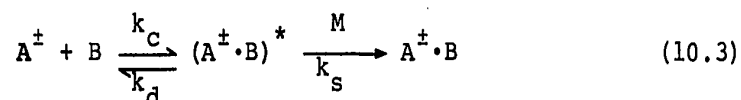
is of interest from the stand point of reaction kinetic theory. Also some specific termolecular reactions are believed to be of importance in the ion chemistry of the D region of the earth's ionosphere. Most studies of termolecular reactions have been undertaken at room temperature (300°K), although a few determinations have been made at other temperatures (5,61,83,105,146,147). In the D region of the earth's ionosphere, the gas temperature is from 180°K to 270°K (148). In order to perform model calculations pertaining to ionospheric conditions it is necessary to know the rate constants of the ionic reactions of interest at these temperatures. In model calculations reaction rates are usually taken to be the same as at 300°K (149,150) or are assumed to have only a small temperature dependence. This is necessary since extensive temperature studies of termolecular rate constants are not available.

Several theoretical treatments have been undertaken of reaction (10.1) where  $A^{\pm}$ , B and M are atomic species

(106,147,151-154). These considerations predict that the temperature dependence of the forward rate coefficient of (10.1) may be approximately expressed in the form

$$k_f \propto T^{-n} \quad (10.2)$$

where  $n$  is roughly unity for the atomic reactions. The theoretical treatments, as was mentioned in Chapter 4, assume that the termolecular reaction may be visualized as composed of three competing processes



Thus  $k_f = \frac{k_c k_s}{k_d}$  in the steady state approximation. The difficulties in the theories centre about the evaluation of  $k_d$  since this evaluation requires knowledge of how the energy of the reaction is distributed in the excited species  $(A^\pm \cdot B)^*$ . In general the energy levels of the ionic intermediate  $(A^\pm \cdot B)^*$  are unknown and must be approximated.

Recently Good (106) has derived a simple expression for reaction (10.1) where the reactants are not necessarily atomic by means of the energy transfer mechanism mentioned above. He was able to show that the temperature dependence was of the form

$$k_f = C \left[ \frac{D + rRT}{rRT} \right]^{s-2} \quad (10.4)$$

where  $C$  is an empirical constant,  $D$  is the bond dissociation energy of  $A^\pm \cdot B$ ,  $T$  is the temperature,  $R$  is the gas constant,

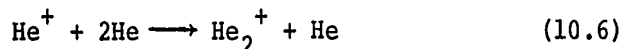


$r$  is the number of square terms contributing to the internal energy of the molecule and  $s$  is the number of vibrational degrees of freedom in the molecule  $A^{\pm} \cdot B$ . For the case when  $D \gg RT$  equation (10.4) reduces to

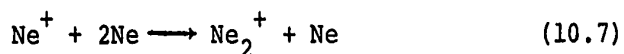
$$k_f \propto T^{-(s-2)} \quad (10.5)$$

Thus as the number of degrees of freedom of the ion  $A^{\pm} \cdot B$  increases the temperature dependence of  $k_f$  is predicted to increase. However, for the atomic reactions equation (10.5) predicts a positive temperature coefficient for  $k_f$ . This is the opposite of what is observed experimentally (146, 147).

Niles and Robertson (147) have studied the reaction



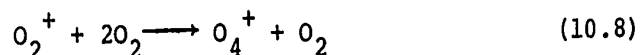
over the temperature range  $77^\circ - 449^\circ\text{K}$ . They reported that the  $k_f \propto T^{-1}$ . However, some details of their technique have been criticized by Gerber et al (155). Hackman (146) has studied the rate of the reaction



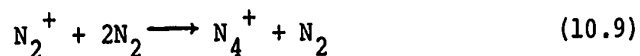
in the temperature range  $195^\circ - 523^\circ\text{K}$ . It was reported that  $k_f \propto T^{-1}$  in this temperature range in accord with the previous theories (147,154). However, Hackman's value (146) at  $300^\circ\text{K}$  is considerably lower than those obtained by other investigators (151). Ferguson et al (5,105) using the flowing afterglow technique have measured the forward

rate coefficients for several termolecular reactions. Unfortunately these measurements were only performed at two or in some cases three temperatures. Consequently the form of the temperature dependence was not uniquely defined by these experiments. The work of Ferguson et al (5,105) did demonstrate that the termolecular reactions had a negative temperature dependence - that is the rate coefficient increased with decreasing temperature.

Good, Durden and Kebarle (61) have studied the reactions



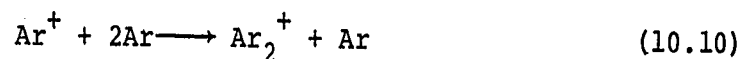
and



over a rather narrow ( $\sim 300\text{-}350^\circ\text{K}$ ) temperature range. The authors expressed the temperature dependence of  $k_f$  in the form of an Arrhenius-type equation. They found that reactions (10.8) and (10.9) possessed "activation energies" which were negative and in the order of a few kcal/mole. The shallow temperature dependence of the reaction coupled with the narrow temperature range and the experimental scatter of the data precluded the determination of a more detailed expression for the temperature dependence.

The present apparatus is capable of the study of ion-molecule reactions over a wide  $90\text{-}850^\circ\text{K}$  temperature range and is thus well suited for the study of the tempera-

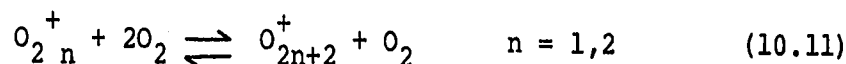
ture dependence of termolecular reactions. It was thought that a comparison of the temperature dependence of  $k_f$  for reaction (10.8) and for the reaction



would provide an interesting test of the theory of Good (106). Also the previous studies of the temperature dependence of the termolecular rate coefficients in Ne (146) and He (147) appear to be somewhat questionable (151).

## 10.2 Experiments in Oxygen

To study the kinetics of the clustering reactions



it is necessary to lower the temperature of the ion source to a point where the formation of the species  $\text{O}_{2n+2}^+$  is favoured. Consequently the low temperature version of the ion source was used. Nitrogen gas from a cylinder was passed through a coil immersed in refrigerant and then through a length of tubing to the ion source inlet system. Liquid nitrogen was used as the refrigerant when temperatures less than  $\sim -50^\circ\text{C}$  were required and dry ice acetone for higher temperatures. By varying the length of the tube to the ion source and/or the flow rate of nitrogen different ion source temperatures could be achieved. At the lowest accessible temperatures ( $\sim 90^\circ\text{K}$ ) it was found

that several hours were required for the ion source to reach a stable temperature.

The oxygen used in the experiments had a stated purity of 99.998%. In order to eliminate the undesirable presence of trace amounts of water the gas was not admitted to the ion source via the gas handling system. The oxygen flow to the ion source was regulated by an all metal needle valve which reduced the pressure to the desired level (torr range). The gas then passed through a coil immersed in liquid nitrogen and then directly to the ion source. The system bleeding gas to the ion source was made as short as possible (~50 cm) and was constructed of glass and metal only. The pressure was monitored after the gas left the ion source. The gas was then exhausted through a capillary by a mechanical pump. In most experiments the gas was flowed (~25 cm<sup>3</sup> atm min<sup>-1</sup>) through the ion source. Several determinations were made under "static" conditions. That is the gas was not flowed but introduced into the ion source at the rate at which it leaked through the ion source slits. This was done to see if the gas achieved thermal equilibrium with the ion source at low temperatures. No difference was observed between the "static" and "flow" experiments. This was taken as evidence that thermal equilibrium was achieved. After baking out the apparatus overnight, the only ions observed in oxygen were O<sub>2n</sub><sup>+</sup>. No (<0.1%) impurity species were noted.

The data recording and manipulations were the same as has been discussed in Chapter 4 on the negative ion-molecule reactions in moist oxygen.

### 10.3 Experiments in Argon

Argon, because of its high ionization potential, will charge exchange to almost any simple molecule. Exceptions being He, Ne and  $N_2$ . Consequently the argon must be of very high purity to avoid complicating side reactions. Argon of 99.9995% purity was used in the present studies and because of the cost of gas of this purity all determinations were conducted under "static" conditions of gas flow. When using argon of this purity no species other than  $Ar_n^+$  ( $n = 1, 2, 3$ ) were noted except for a small signal at  $m/e = 20$ . This signal disappeared very rapidly with time, and it was concluded that the species was  $Ar^{2+}$ .

Approximately 25 measurements were performed in argon all of which must be regarded as failures since the data was not reproducible. The reason for this is not understood. Even at very low temperatures when reaction (10.10) must proceed to completion the  $Ar^+$  signal did not decay but remained a constant fraction (10% - 50%) of the  $Ar_2^+$  signal with time. Initially this may be regarded as an equilibrium condition in the reaction. However, such is not the case. Increasing the argon pressure results in an increase in the  $Ar^+$  signal relative to  $Ar_2^+$  - the

opposite of what should be observed if thermodynamic equilibrium is being achieved. At low temperatures the  $\text{Ar}_3^+$  ion was observed to become the dominant ion (~90%) at long reaction times, but still the  $\text{Ar}^+$  signal did not decay. No evidence was found to suggest that  $\text{Ar}^+$  was produced outside the ion source. It is difficult to conceive of any mechanism which would produce  $\text{Ar}^+$  outside the ion source in such a way that its temporal behaviour would exactly reflect that of the  $\text{Ar}_2^+$ .

Other experimentalists (45,146,147) have studied reactions of this type and did not report this type of phenomena. Thus it is concluded that this phenomena is characteristic of the present apparatus. It is believed that the observation reflects a surface effect of the ion exit slit. This phenomena was not observed in any other system studied. A few experiments were conducted in neon and a similar effect was observed.

It is believed that the effect was due to the ion exit slit somehow perturbing the sample. Consequently efforts were made to "clean" the slit. Prolonged and repeated baking at elevated temperatures had no effect. The ion exit slit of the ion source is manufactured from razor blades which, as they are obtained commercially, have a plastic coating on the edges. This coating was removed by softening in solvent and gentle scraping. It was thought that perhaps the coating was not completely removed

by this technique and thus razor blades were obtained which did not possess this coating.

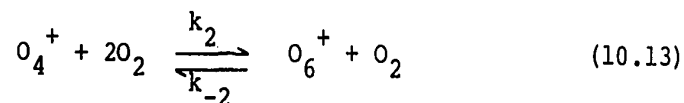
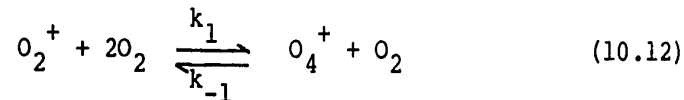
In one experiment, and only one experiment, the  $\text{Ar}^+$  signal was observed to decay to zero. This experiment could not be reproduced. In this case a new slit, manufactured from the uncoated blades was used. The instrument was evacuated overnight and the following day the temperature of the ion source lowered to  $\sim 100^\circ\text{K}$ , argon was admitted to the ion source and the electronics of the instrument turned on. The electron gun was not turned on until the system had stabilized. The electron gun was turned on and the signal observed immediately thereafter. The  $\text{Ar}^+$  signal decayed beautifully. When an attempt was made to repeat the observation a few minutes later the  $\text{Ar}^+$  did not decay. Perhaps this reflected a rapid buildup of material on the slit.

Molybdenum is a material which is often used in the manufacture of orifices through which charged particles are to be sampled (47). Apparently it possesses very good surface characteristics. The edge of a thin sheet of molybdenum was polished to achieve a razor sharpness after which the material was assembled into a slit. It was found that even in this case the  $m/e = 40$  signal did not decay. Experiments were done in which the slit was covered with carbon black. No effect was observed. At this point the experiment was abandoned.

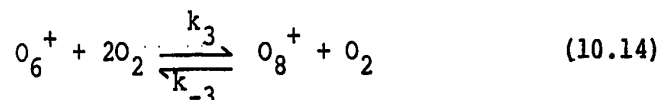
No satisfactory explanation of the observations are apparent, although certain theories may be excluded. The signal at  $m/e = 40$  is presumably  $\text{Ar}^+$  and not an impurity species. The complete absence of charged species other than argon ions, the high purity of the argon used and the similar observations in neon suggest that the explanation does not lie with impurities. In all the other experiments conducted in this work, the gases in the ion source always contained some non-monoatomic species. Such molecules may form free radicals upon electron bombardment and thus may act as a "cleansing" agent on the slit. In the pure rare gases this is not possible. The behaviour of metal surfaces towards charged particles is not well understood (47), but it would appear that the only explanation for the experimental observations lies in some type of surface phenomena.

### 10.3 Results and Discussion

In pure oxygen some 28 measurements of the rate coefficients at 22 different temperatures between  $93^\circ$  and  $292^\circ\text{K}$  were performed. The reactions observed were







The normalized ion intensities are displayed in Figures (10.1-10.13) along with the calculated ion intensities based on the rate coefficients given in Table 10.1. Examples of the exponential decay of the normalized  $\text{O}_2^+$  signal are displayed in Figures (10.14-10.16). Figure (10.17) shows a plot of the apparent first order rate coefficient for reactions (10.12) and (10.13) vs  $P_{\text{O}_2}^2$  at 143°K. As can be seen from Figure (10.17) reactions (10.12) and (10.13) are dependent on the second power of the oxygen concentration and are therefore third order.

Only one determination was made of reaction (10.14) and that at 93°K. Assuming the reaction to be third order a value of  $k_3 = 2.45 \times 10^{-29} \text{ cm}^6 \text{ molecule}^{-2} \text{ s}^{-1}$  was determined. This may be compared to values of  $k_2 = 4.14 \times 10^{-29} \text{ cm}^6 \text{ molecule}^{-2} \text{ s}^{-1}$  and  $k_1 = 10.7 \times 10^{-29} \text{ cm}^6 \text{ molecule}^{-2} \text{ s}^{-1}$  determined at the same temperature. The value of  $k_3$  appears to be reasonable in that  $k_1 > k_2 > k_3$ . This also follows the trend of the  $-\Delta H$ 's of the reaction:  $-\Delta H_{2,4} = 10.8$ ,  $-\Delta H_{4,6} = 6.87$ , and  $-\Delta H_{6,8} = 2.54 \text{ kcal/mole}$  (156). At higher temperatures  $k_{-3}$  becomes sufficiently large that the equilibrium position of reaction (10.14) is displaced forward in favour of the  $\text{O}_6^+$  ion and thus reaction (10.14) could not be observed. At 93°K a small signal due to  $\text{O}_{10}^+$  could be observed. However, its low intensity precluded any

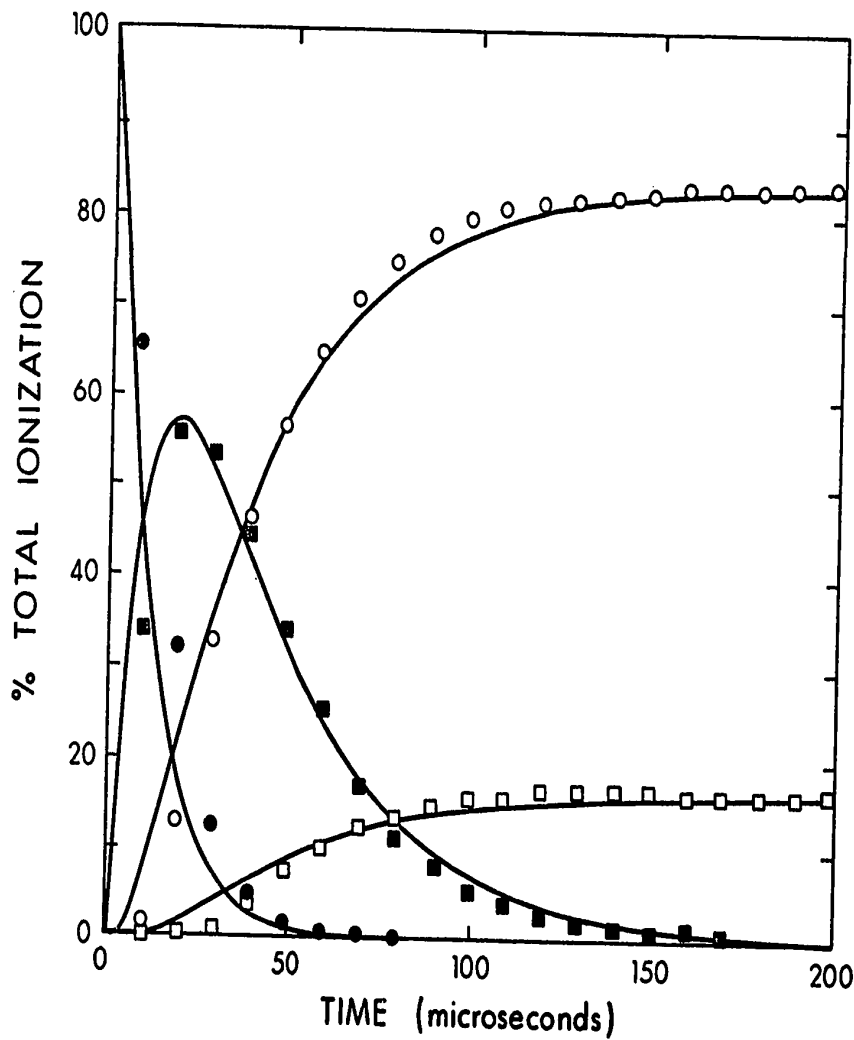


FIGURE 10.1. Time dependence of normalized ion intensities. The curves are the calculated time dependence for the rate parameters summarized in Table 10.1.  $P_{O_2} = 0.28$  torr,  $T = 93^\circ\text{K}$ ,  $\bullet$   $O_2^+$ ,  $\blacksquare$   $O_4^+$ ,  $\circ$   $O_6^+$ , and  $\square$   $O_8^+$ .

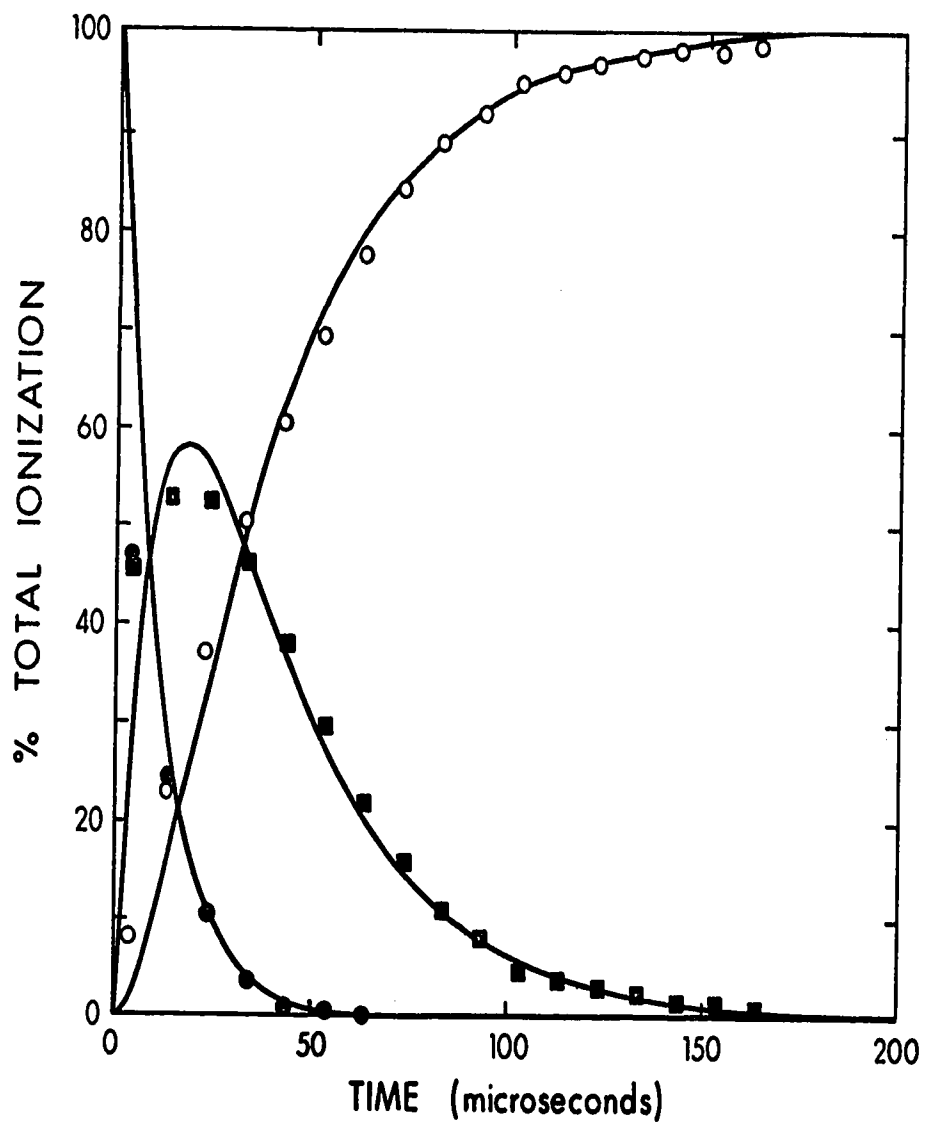


FIGURE 10.2. Time dependence of normalized ion intensities. The curves are the calculated time dependence for the rate parameters summarized in Table 10.1.  $P_{O_2} = 0.43$  torr,  $T = 106^\circ\text{K}$ ,  $\bullet$   $O_2^+$ ,  $\blacksquare$   $O_4^+$ , and  $\circ$   $O_6^+$ .

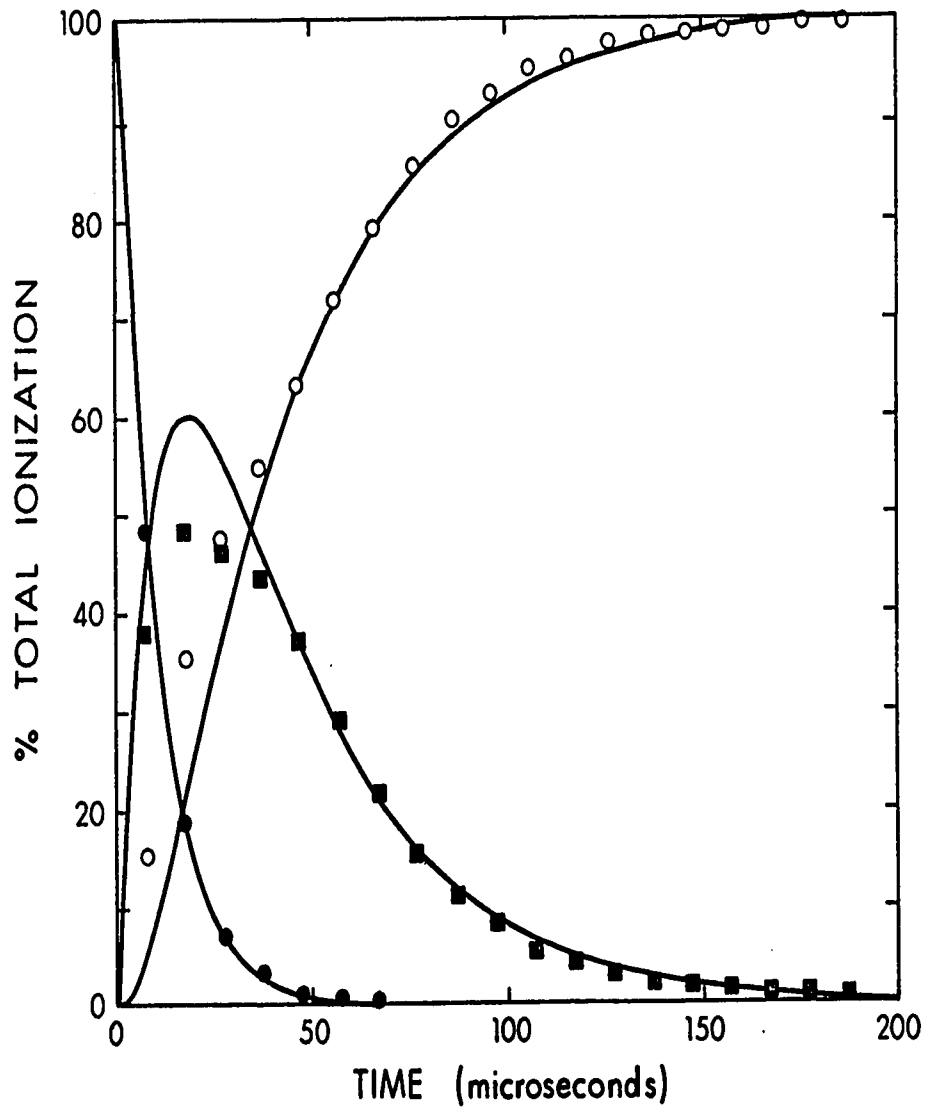


FIGURE 10.3. Time dependence of normalized ion intensities. The curves are the calculated time dependence for the rate parameters summarized in Table 10.1  $P_{O_2} = 0.435$  torr,  $T = 108^\circ\text{K}$ ,  $\bullet$   $O_2^+$ ,  $\blacksquare$   $O_4^+$ , and  $\circ$   $O_6^+$ .

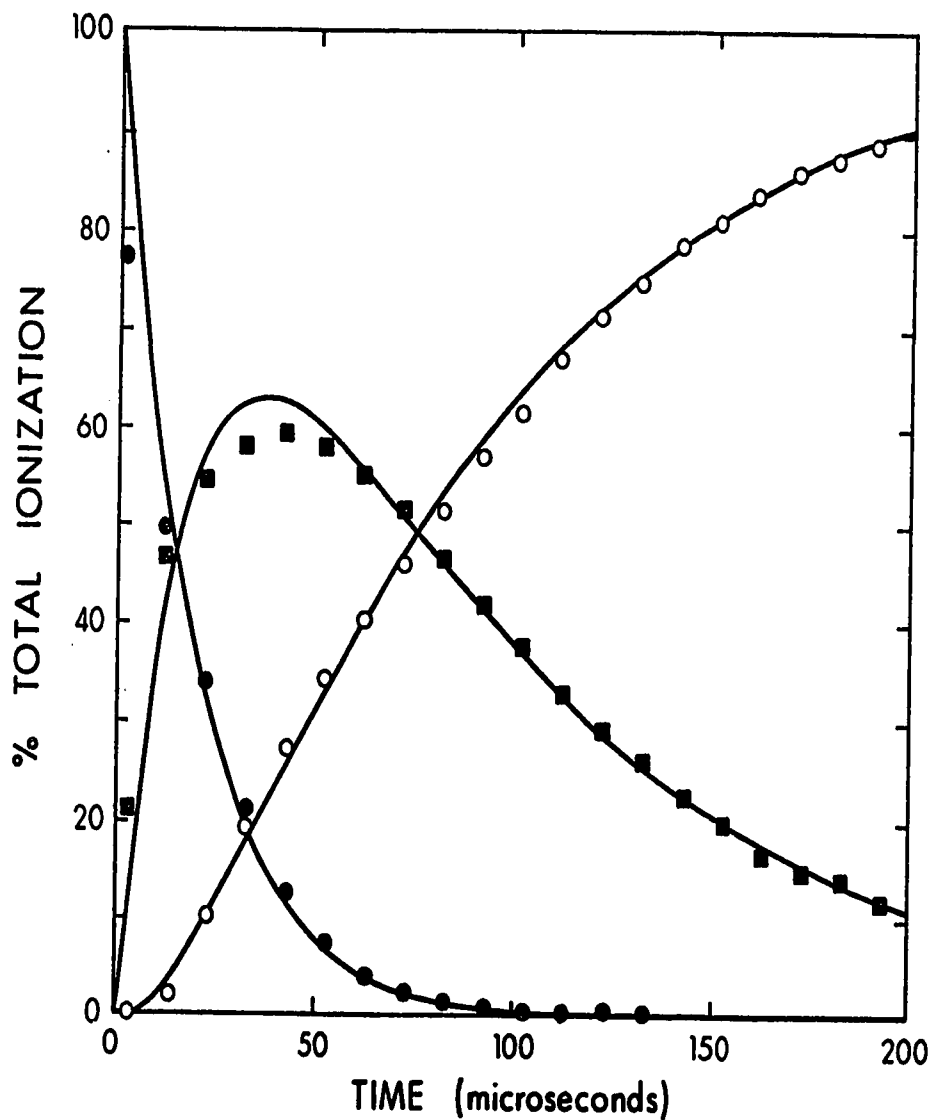


FIGURE 10.4. Time dependence of normalized ion intensities. The curves are the calculated time dependence for the rate parameters summarized in Table 10.1.  $P_{O_2} = 0.44$  torr,  $T = 126^\circ\text{K}$ ,  $\bullet$   $O_2^+$ ,  $\blacksquare$   $O_4^+$ , and  $\circ$   $O_6^+$ .

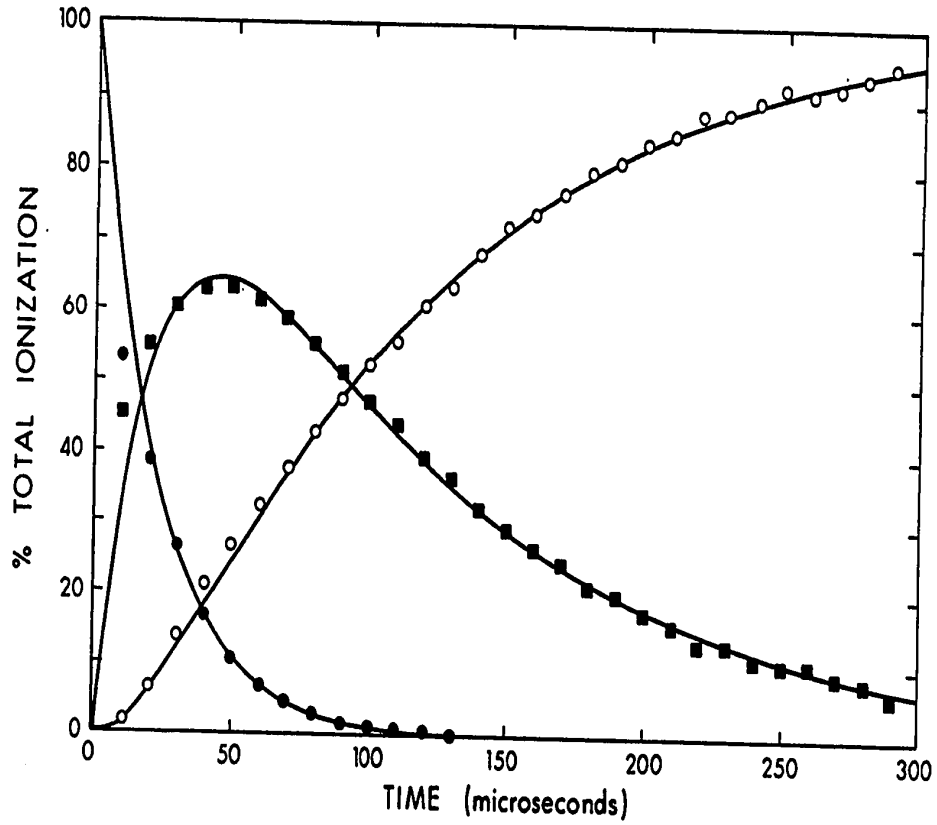


FIGURE 10.5. Time dependence of normalized ion intensities. The curves are the calculated time dependence for the rate parameters summarized in Table 10.1  $P_{O_2} = 0.43$  torr,  $T = 130^\circ\text{K}$ , ●  $O_2^+$ , ■  $O_4^+$ , and ○  $O_6^+$ .

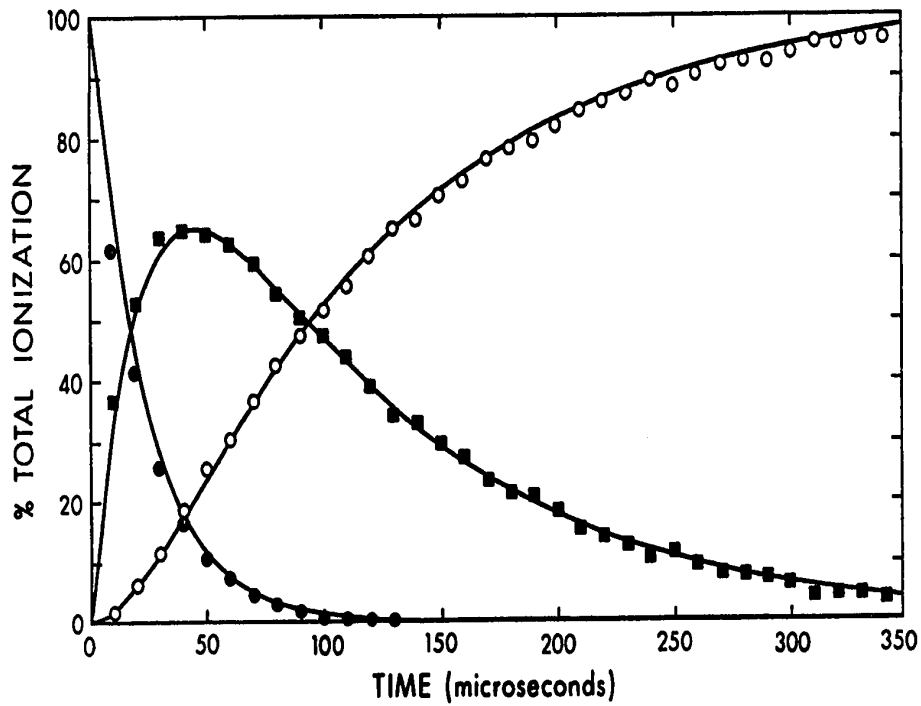


FIGURE 10.6. Time dependence of normalized ion intensities. The curves are the calculated time dependence for the rate parameters summarized in Table 10.1  $P_{O_2} = 0.44$  torr,  $T = 129^\circ$ ,  $\bullet$   $O_2^+$ ,  $\blacksquare$   $O_4^+$ , and  $\circ$   $O_6^+$ .

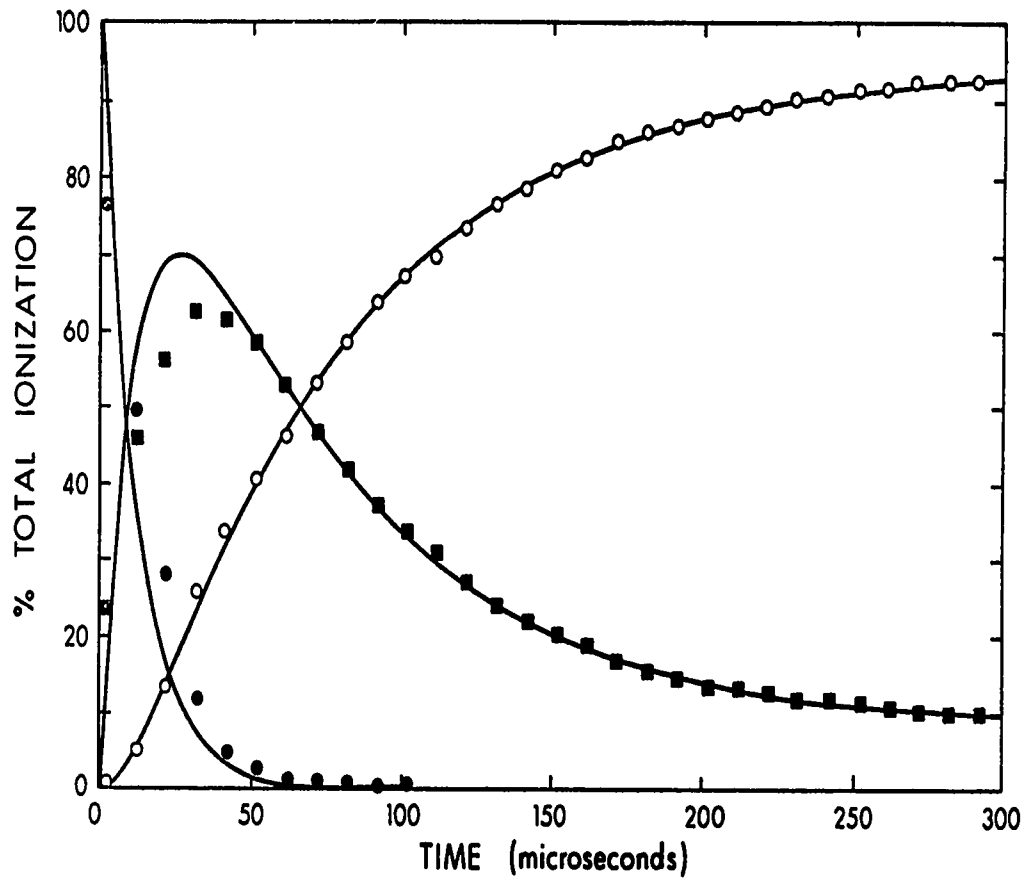


FIGURE 10.7. Time dependence of normalized ion intensities. The curves are the calculated time dependence for the rate parameters summarized in Table 10.1  $P_{O_2} = 0.765$  torr,  $T = 143^\circ\text{K}$ ,  $\bullet$   $O_2^+$ ,  $\blacksquare$   $O_4^+$ , and  $\circ$   $O_6^+$ .



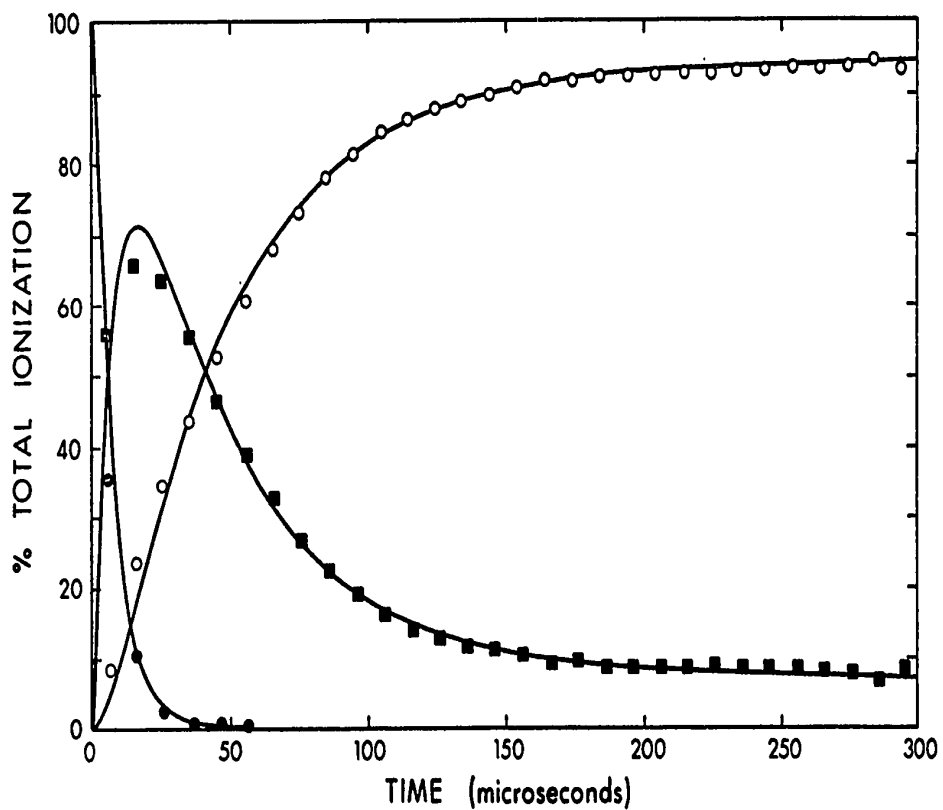


FIGURE 10.8. Time dependence of normalized ion intensities. The curves are the calculated time dependence for the rate parameters summarized in Table 10.1  $P_{O_2} = 1.02$  torr,  $T = 143^\circ\text{K}$ ,  $\bullet$   $O_2^+$ ,  $\blacksquare$   $O_4^+$ , and  $\circ$   $O_6^+$ .

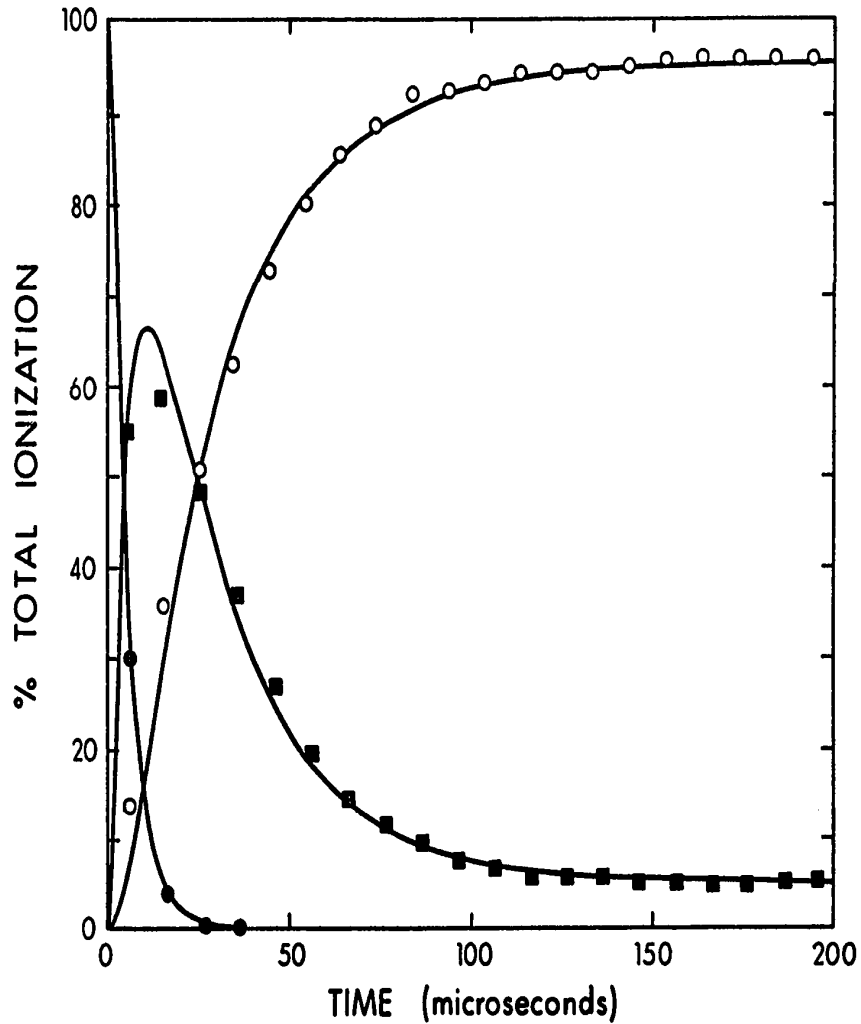


FIGURE 10.9. Time dependence of normalized ion intensities. The curves are the calculated time dependence for the rate parameters summarized in Table 10.1.  $P_{O_2} = 1.21$  torr,  $T = 143^\circ\text{K}$ , ●  $O_2^+$ , ■  $O_4^+$ , and ○  $O_6^+$ .

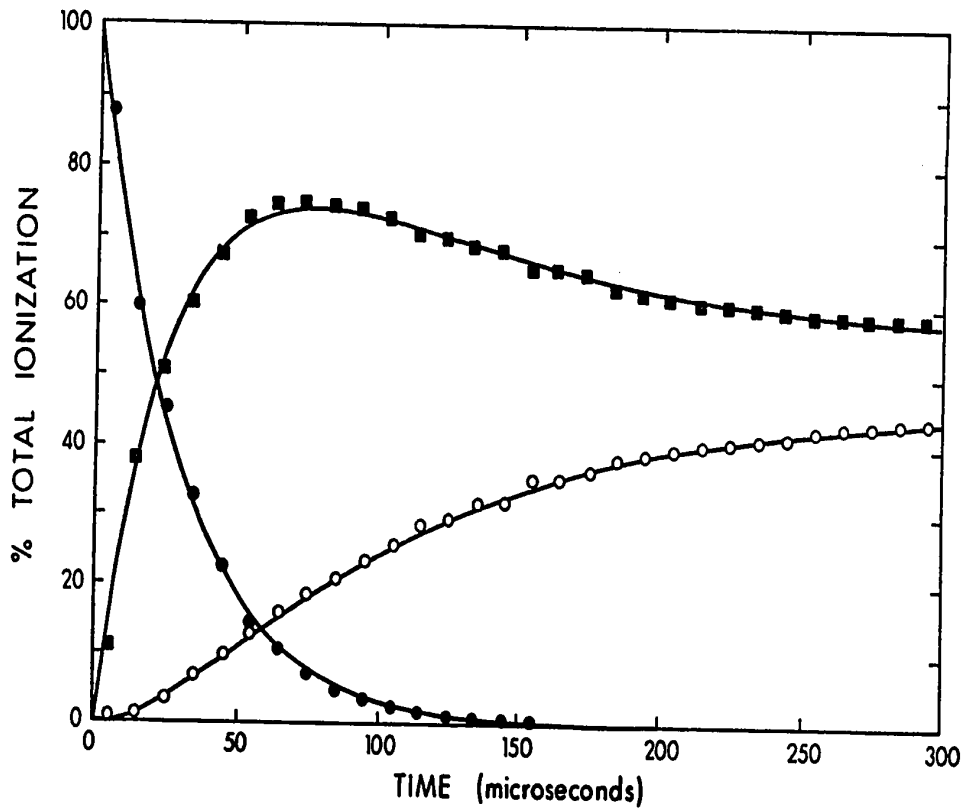


FIGURE 10.10. Time dependence of normalized ion intensities. The curves are the calculated time dependence for the rate parameters summarized in Table 10.1.  $P_{O_2} = 0.68$  torr,  $T = 154^\circ K$ ,  $\bullet$   $O_2^+$ ,  $\blacksquare$   $O_4^+$ , and  $\circ$   $O_6^+$ .

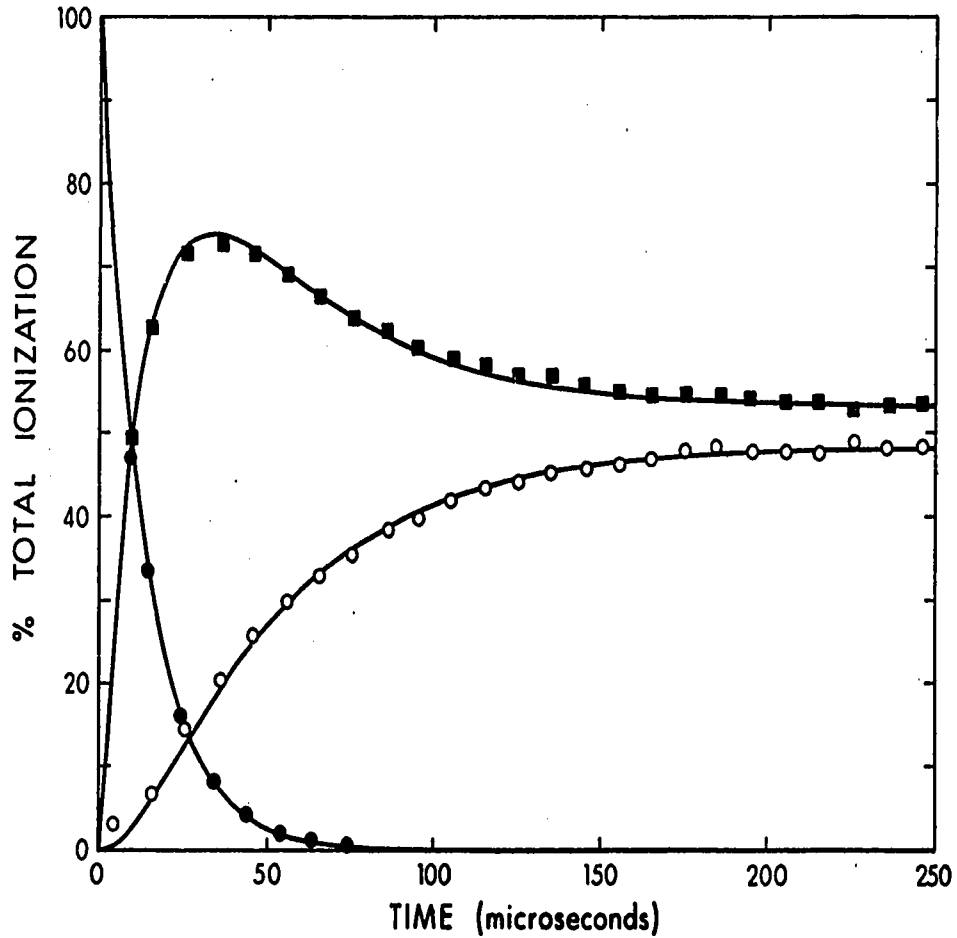


FIGURE 10.11. Time dependence of normalized ion intensities. The curves are the calculated time dependence for the rate parameters summarized in Table 10.1.  $P_{O_2} = 1.01$  torr,  $T = 157^\circ\text{K}$ ,  $\bullet$   $O_2^+$ ,  $\blacksquare$   $O_4^+$ , and  $\circ$   $O_6^+$ .

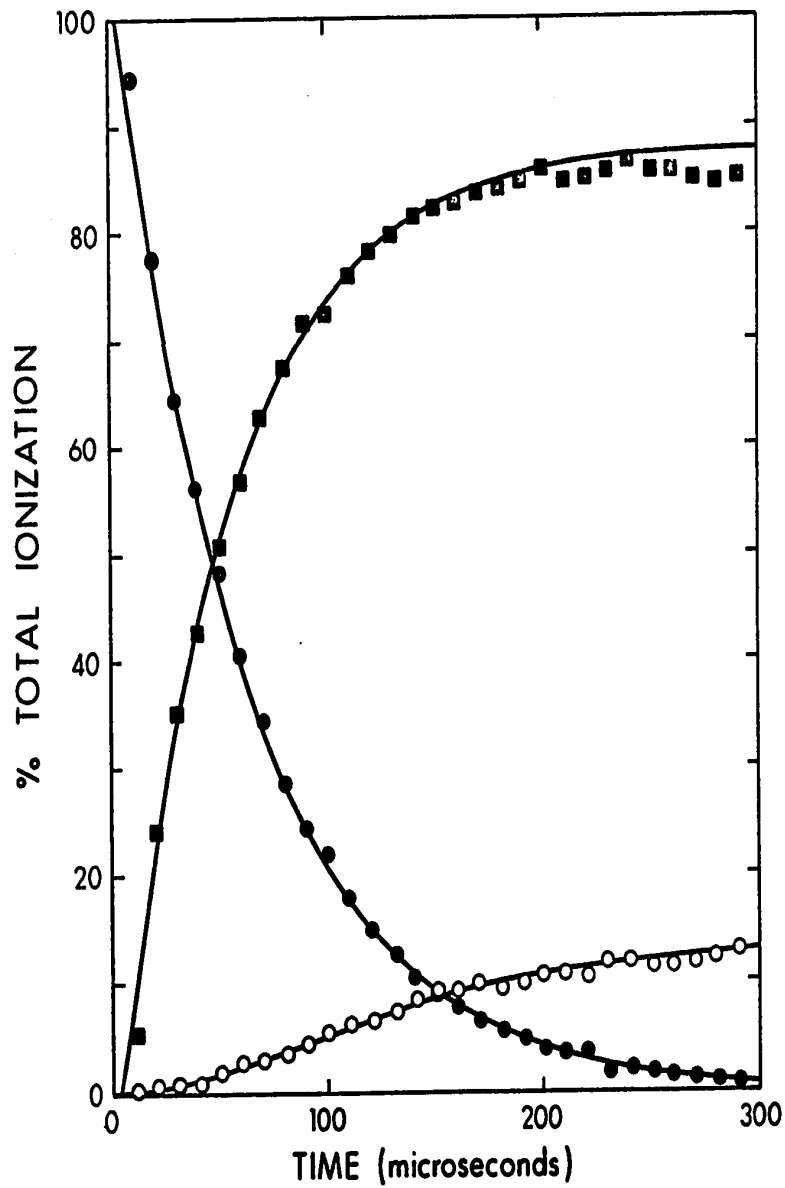


FIGURE 10.12. Time dependence of normalized ion intensities. The curves are the calculated time dependence for the rate parameters summarized in Table 10.1.  $P_{O_2} = 0.46$  torr,  $T = 164^\circ\text{K}$ ,  $\bullet$   $O_2^+$ ,  $\blacksquare$   $O_4^+$ , and  $\circ$   $O_6^+$ .

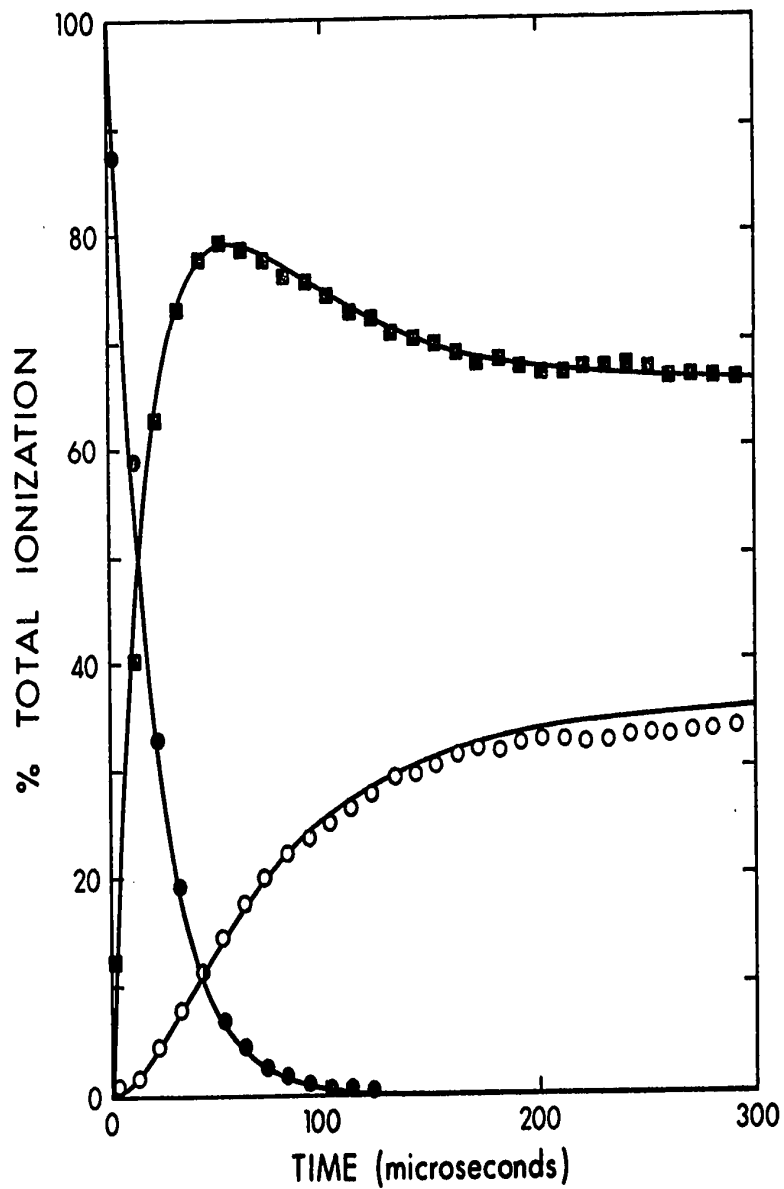


FIGURE 10.13. Time dependence of normalized ion intensities. The curves are the calculated time dependence for the rate parameters summarized in Table 10.1  $P_{O_2} = 0.838$  torr,  $T = 164^\circ K$ , ●  $O_2^+$ , ■  $O_4^+$ , and ○  $O_6^+$ .

TABLE 10.1

Calculated Values of Rate Coefficients for Positive Ion-

Molecule Reactions in Pure Oxygen

T(°K)	P <sub>O<sub>2</sub></sub> (torr)	v <sub>1</sub> <sup>a</sup>	v <sub>2</sub> <sup>a</sup>	v <sub>-2</sub> <sup>a</sup>	k <sub>1</sub> <sup>b</sup>	k <sub>2</sub> <sup>b</sup>	Fig. <sup>c</sup>
93 <sup>d</sup>	0.28	9.08	3.37		107	41.4	10.1
106	0.43	9.58	2.96		62	19.3	10.2
108	0.435	9.78	2.80		63	18.5	10.3
126	0.44	5.05	1.26		42.2	11.1	10.4
130	0.43	4.47	1.00		43.5	9.77	10.5
129	0.44	4.42	1.00		40.8	9.20	10.6
143	0.245	0.728			27		
143	0.765	8.54	1.34	0.118	32	5.02	10.7
143	1.02	14.6	2.24	0.167	30.8	4.72	10.8
143	1.21	19.4	3.78	0.22	29	5.66	10.9
154	0.35	1.13			23.4		
154	0.68	3.83	0.52	0.643	21.1	2.86	10.10
157	1.01	7.77	1.13	1.24	22	2.91	10.11
164	0.46	1.66	0.180	1.13	22.7	2.45	10.12
164	0.838	5.34	0.517	2.06	22	2.12	10.13
176	0.54	1.02			11.6		
176	1.09	3.97			10.9		
198	1.55	6.5			11.8		
200	2.64	12.4			7.6		
211	2.20	7.3			7.5		
212	1.60	4.18			7.7		(continued...)

T(°K)	P <sub>O<sub>2</sub></sub> (torr)	v <sub>1</sub> <sup>a</sup>	v <sub>2</sub> <sup>a</sup>	v <sub>-2</sub> <sup>a</sup>	k <sub>1</sub> <sup>b</sup>	k <sub>2</sub> <sup>b</sup>	Fig. <sup>c</sup>
217	1.78				8.4		
238	2.26	5.07			6.03		
247	3.42	9.00			4.9		
248	2.35	4.60			5.1		
254	1.88	2.54			4.6		
256	1.23	0.704			3.7		
292	2.42	4.06			2.88		

a In units of  $10^4 \text{ sec}^{-1}$

b In units of  $10^{-30} \text{ cm}^6 \text{ molecule}^{-2} \text{ sec}^{-1}$

c Figure in which data is displayed

d At 93°K  $v_3 = 2.0 \times 10^4 \text{ s}^{-1}$ ,  $v_{-3} = 10.5 \times 10^4 \text{ s}^{-1}$  and  
 $k_3 = 2.45 \times 10^{-29} \text{ cm}^6 \text{ molecule}^{-2} \text{ s}^{-1}$



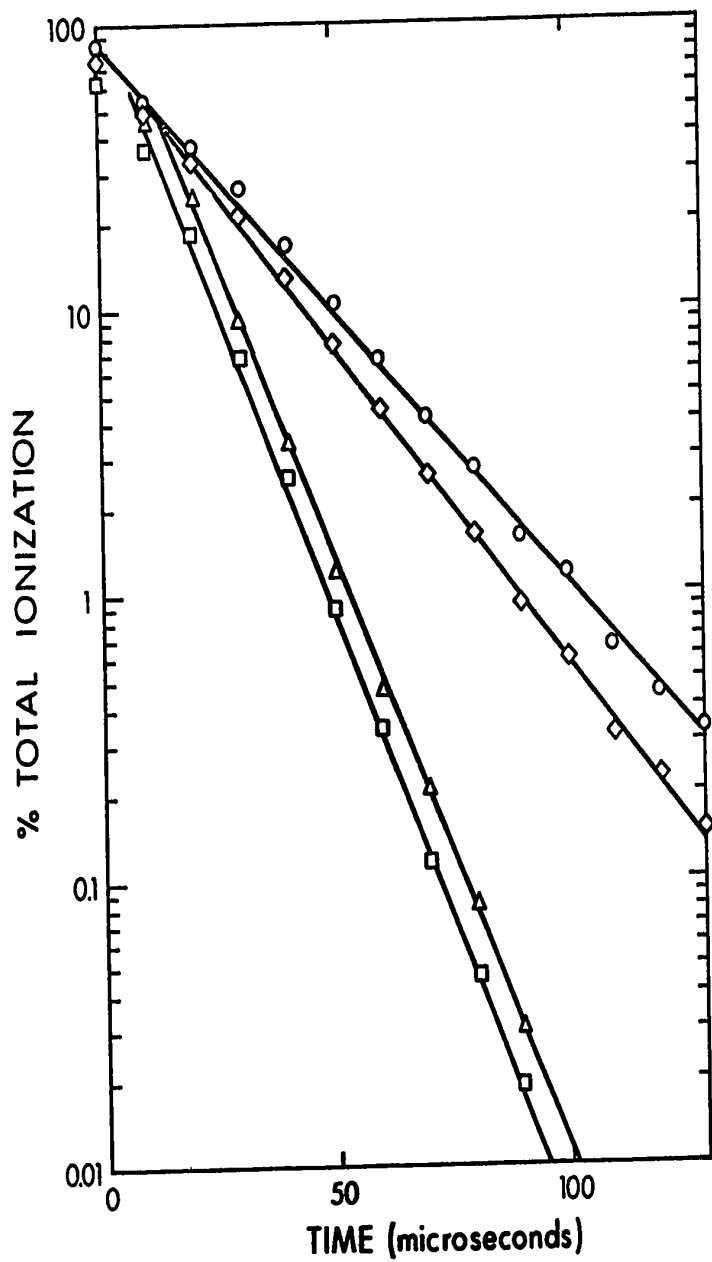


FIGURE 10.14. Plot of the normalized  $O_2^+$  intensity versus time. Slopes of lines give  $\nu_1$  under different conditions. The first number give is the  $O_2$  pressure in torr, the number in brackets is  $\nu_1$  in units of  $10^4 s^{-1}$  and the third number is temperature in  $^{\circ}K$ .  $\circ$  0.43 (4.47) 130,  $\square$  0.435 (9.78) 108,  $\diamond$  0.44 (5.05) 126, and  $\Delta$  0.43 (9.58) 106.

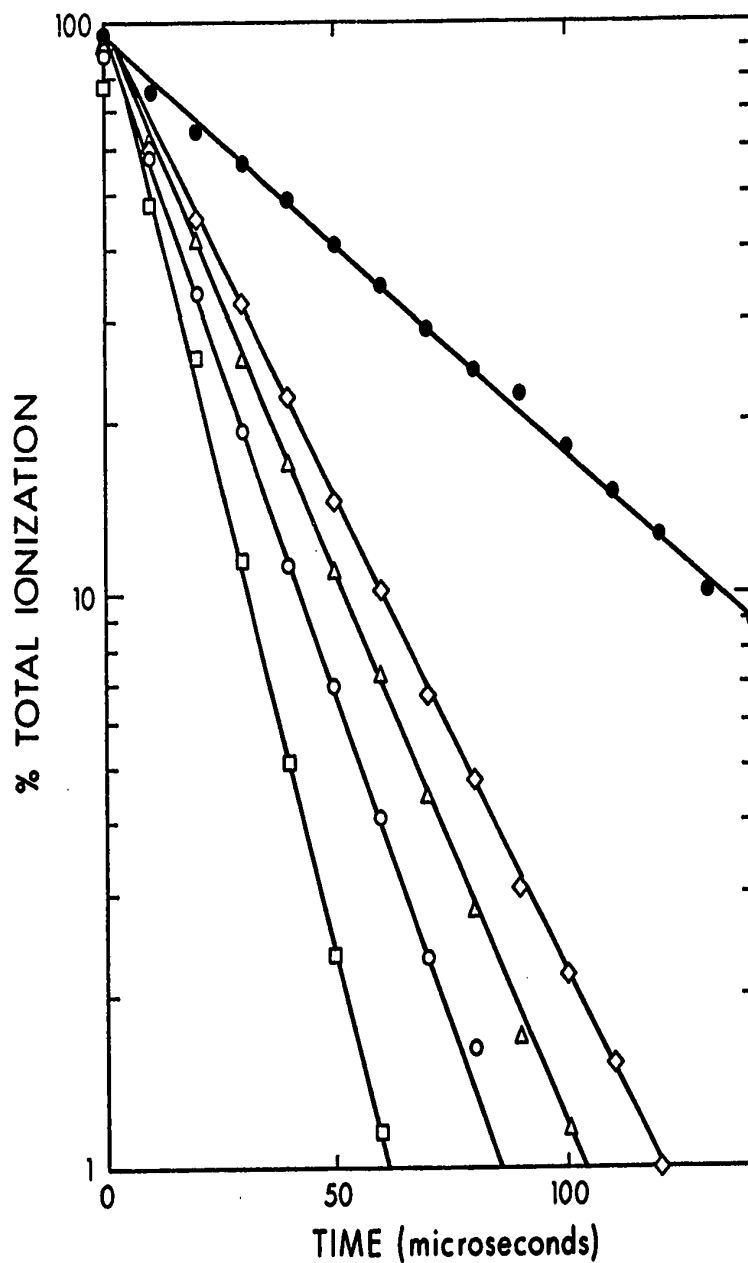


FIGURE 10.15. Plot of the normalized  $O_2^+$  intensity versus time. Slope of lines give  $\nu_1$  under different condition. The first number given is the  $O_2$  pressure in torr, the number in brackets is  $\nu_1$  in units of  $10^4 s^{-1}$ , and the third number is temperature in  $^\circ K$ .  $\circ$  0.038 (5.34) 164,  $\square$  1.01 (7.77) 157,  $\diamond$  0.68 (3.83) 154,  $\triangle$  0.44 (4.42) 129 and  $\bullet$  0.46 (1.66) 164.

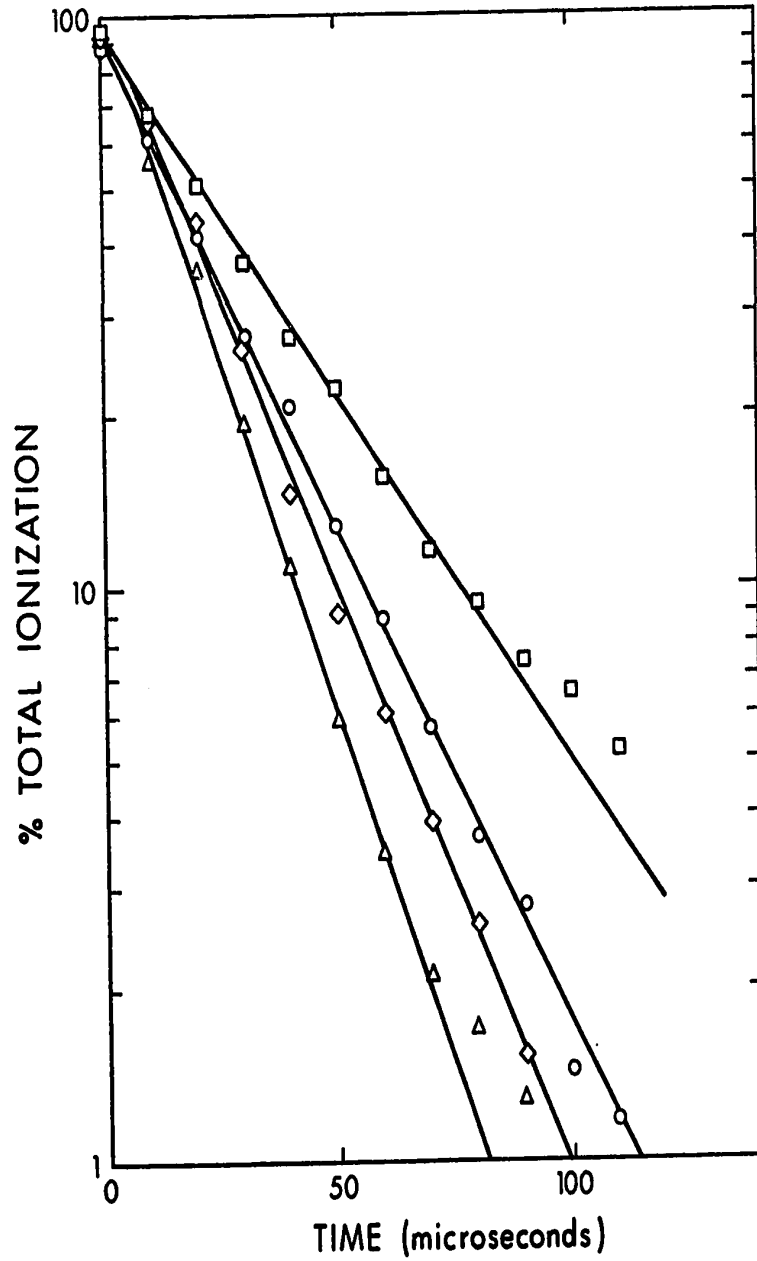


FIGURE 10.16. Plots of the normalized  $O_2^+$  intensity versus time. Slopes of lines give  $\nu_1$  under different conditions. The first number given is the  $O_2$  pressure in torr, the number in brackets is  $\nu_1$  in units of  $10^4 s^{-1}$  and the third number is the temperature in  $^{\circ}K$ .  $\square$  0 1.09 (3.97) 177,  $\circ$  1.88 (2.54) 254,  $\diamond$  2.35 (4.6) 248, and  $\triangle$  2.26 (5.07) 238.

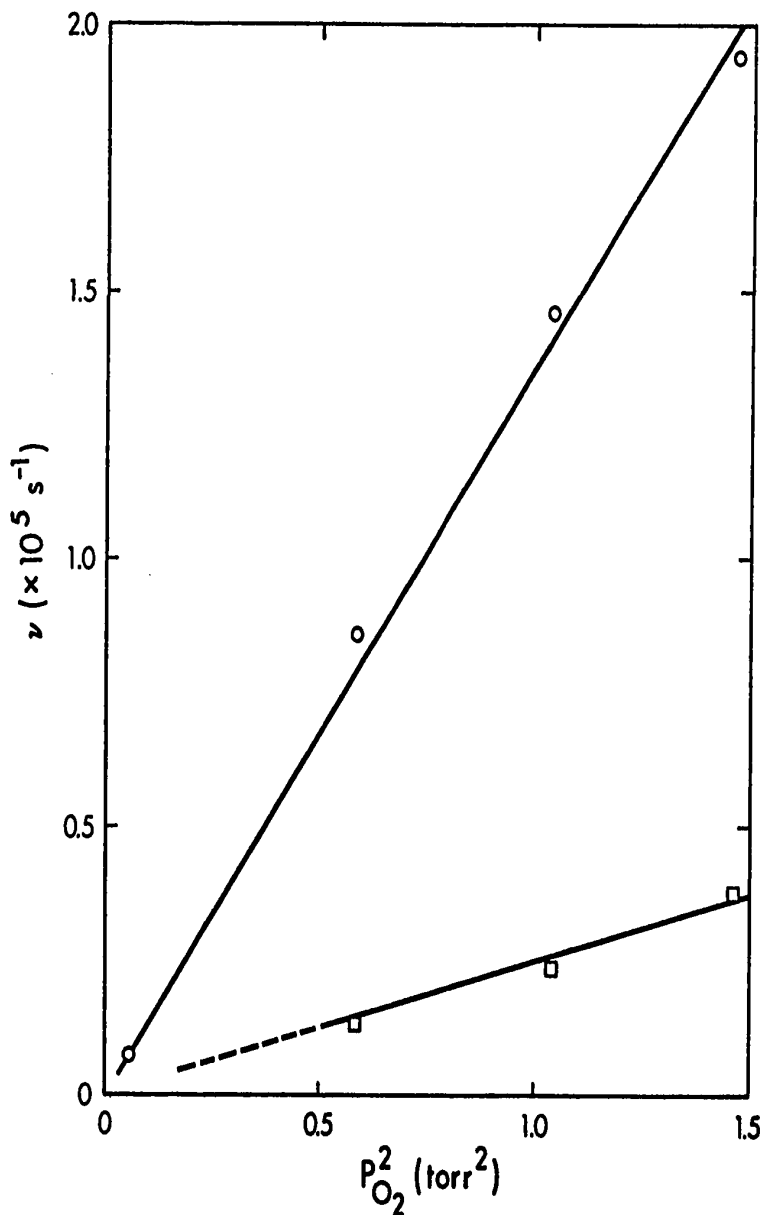
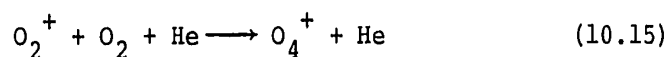
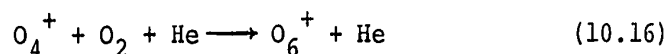


FIGURE 10.17. Plot of  $\nu$  versus the square of the oxygen pressure for the reactions  $O_2^+ + 2O_2 \xrightarrow{k_1} O_4^+ + O_2$  (O), and  $O_4^+ + 2O_2 \xrightarrow{k_2} O_6^+ + O_2$  (□). The plots show that the reactions are dependent on the second power of the oxygen concentration. Slopes of the lines led to  $k_1 = 2.98 \times 10^{-29} \text{ cm}^6 \text{ molecule}^{-2} \text{ s}^{-1}$  and  $k_2 = 5.41 \times 10^{-30} \text{ cm}^6 \text{ molecule}^{-2} \text{ s}^{-1}$ .  $T = 143^\circ\text{K}$ .

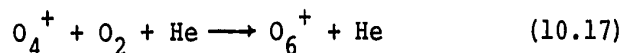
kinetic study. Ferguson et al (5,105) have studied the reactions



and



using the flowing afterglow technique. For reaction (10.15) they (5) reported a value of  $2.4 \times 10^{-30} \text{ cm}^6 \text{ molecule}^{-2} \text{ s}^{-1}$  at 200°K, and  $3.1 \times 10^{-29} \text{ cm}^6 \text{ molecule}^{-2} \text{ s}^{-1}$  at 82°K (105). The corresponding values at these temperatures determined in the present study are  $9.9 \times 10^{-29}$  and  $\sim 1.6 \times 10^{-28} \text{ cm}^6 \text{ molecule}^{-2} \text{ s}^{-1}$  respectively. Thus the present values of  $k_f$  with oxygen as third body are roughly a factor of 4 larger than those reported by Ferguson et al with helium as third body. The lower efficiency for helium is to be expected (Chapter 5). It is interesting to note that the data of Ferguson et al although obtained only at two temperatures parallels the present data. Ferguson et al (5) also report a value of  $\sim 5 \times 10^{-30} \text{ cm}^6 \text{ molecule}^{-2} \text{ s}^{-1}$  for the reaction



at 80°K. The present data with oxygen as third body extrapolates to a value of  $\sim 7 \times 10^{-29} \text{ cm}^6 \text{ molecule}^{-2} \text{ s}^{-1}$  at 80°K.

The equilibrium constants for reactions (10.12) and (10.13) may be written as

$$K_{2,4} = \left[ \frac{I_{O_4}^+}{I_{O_2}^+ \cdot P_{O_2}} \right]_{eq} \quad (10.18)$$

and

$$K_{4,6} = \left[ \frac{I_{O_6}^+}{I_{O_4}^+ \cdot P_{O_2}} \right]_{eq} \quad (10.19)$$

respectively. Figure (10.18) displays the van't Hoff plots of these equilibrium constants as determined by Durden et al (83) ( $K_{2,4}$ ) and Conway and Janik (156), ( $K_{2,4}$  and  $K_{4,6}$ ) along with the present data.

At low temperatures the clustering reactions become fast. In order to observe the kinetics of the reactions it is necessary to conduct the experiments at low pressures (<0.5 torr). At such low pressures the ions diffuse rapidly to the walls of the ion source and in many cases the ion signal is at such a low level by the time equilibrium is apparently achieved that the ratio of the ions could not be determined with precision. The measured values of the equilibrium constants therefore are not of high accuracy. The agreement between the present values of the equilibrium constants and those previously reported is within experimental error.

As mentioned previously Good (106) has derived an

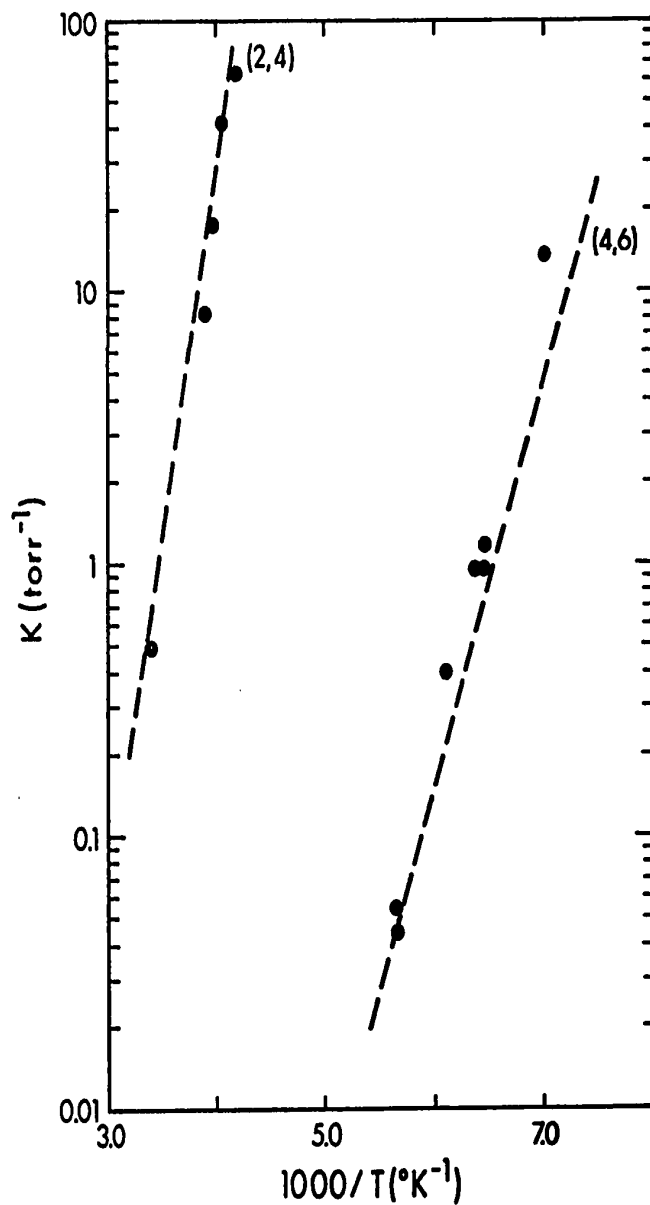
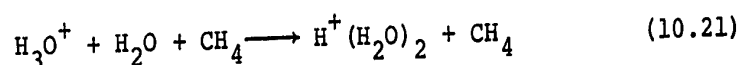


FIGURE 10.18. van't Hoff plot for the reactions  
 $O_{2n}^+ + O_2 \rightleftharpoons O_{2n+2}^+$ . The solid points are the present  
 data, and the dashed lines are the data of Durden (55)  
 and Conway and Janik (156).

expression for  $k_f$  of the form

$$k_f \propto T^{-(s-2)} \quad (10.20)$$

According, plots of  $\log k$  vs  $\log T$  for reactions (10.12) and (10.13) and the reaction



are presented in Figure (10.19). The data for reaction (10.21) is taken from Chapter 9. As can be seen equation (10.16) adequately expresses the form of the temperature dependence. Shown also in Figure (10.19) are the data previously obtained in this laboratory for reaction (10.12) by Durden et al (83). It is gratifying to note that the present data for reaction (10.12) extrapolates smoothly into Durden's data. The values of the exponent in equation (10.16) calculated from Figure (10.19) are given in Table 10.2.

In Good's (106) expression (10.20)  $s$  is the number of oscillators in the clustered species over which the energy of the excited species may be distributed. Thus for reaction (10.12),  $n$  is calculated to be 4 which compares favourably with the experimental value of 3.2. However, for reaction (10.13) and (10.21),  $n$  is calculated to be 10 and 13 respectively. This is to be compared to the experimental values of 5.1 and 4.0. It has been found



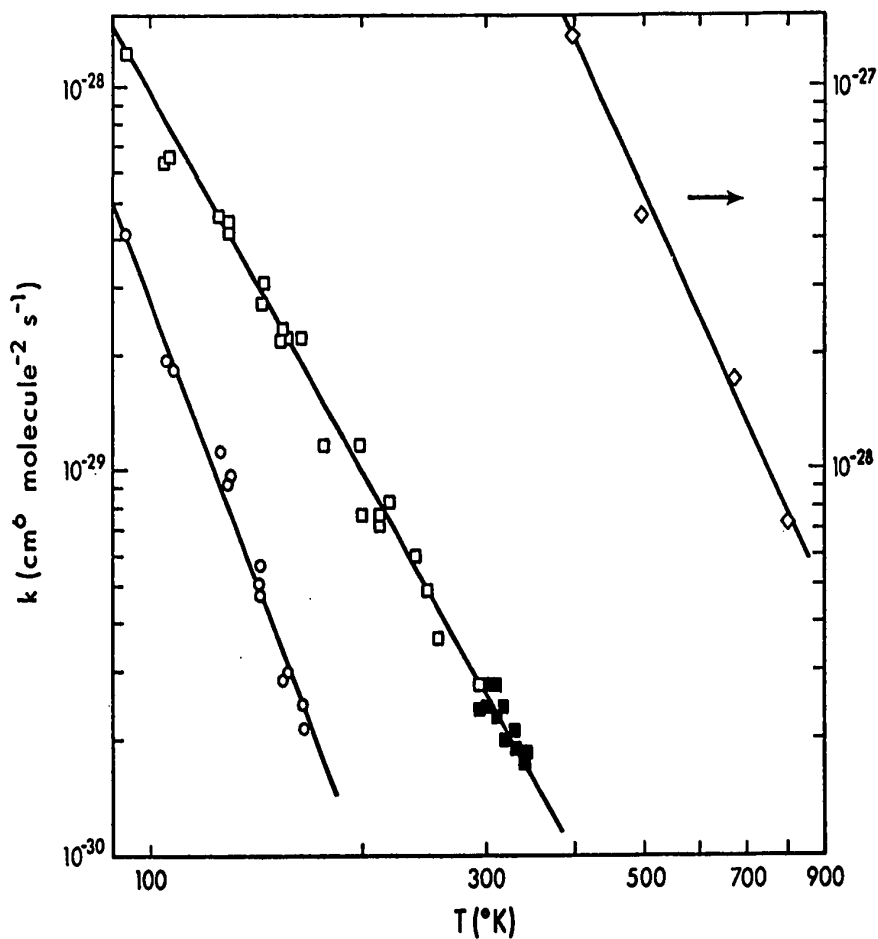


FIGURE 10.19. plot of the log of the third order rate constant versus the log of temperature. After each reaction is given the appropriate symbol and the value of  $n$  in the expression  $k \propto T^{-n}$ .  $\text{O}_2^+ + 2\text{O}_2 \rightarrow \text{O}_4^+ + \text{O}_2$  ( $\square$ ),  $3.2 \pm 0.1$ ;  $\text{O}_4^+ + 2\text{O}_2 \rightarrow \text{O}_6^+ + \text{O}_2$  ( $\circ$ ),  $5.1 \pm 0.2$ ;  $\text{H}_3\text{O}^+ + \text{H}_2\text{O} + \text{CH}_4 \rightarrow \text{H}^+(\text{H}_2\text{O})_2 + \text{CH}_4$  ( $\diamond$ ),  $4.0 \pm 0.2$ . The  $\blacksquare$  are the data of Durden (55).

TABLE 10.2

The Temperature Dependence of  $k_f$  for Selected Ion-Molecule Reactions

Reaction	Temperature Range (°K)	$n^a$	$-\Delta H$ (kcal/mole)
$O_2^+ + 2O_2 \longrightarrow O_4^+ + O_2$	90 - 350	$3.2 \pm 0.1^b$	$10.8^c$
$O_4^+ + 2O_2 \longrightarrow O_6^+ + O_2$	90 - 160	$5.1 \pm 0.2$	$6.87^c$
$H_3O^+ + H_2O + CH_4 \longrightarrow H^+(H_2O)_2 + CH_4$	400 - 800	$4.0 \pm 0.2$	$31.6^d$

a  $n$  is the value of the exponent in the expression  $k_f \propto T^{-n}$ .

b Quoted errors are one standard deviation.

c Ref. (156).

d Table 9.3.

296.

that the value of  $s$  in the RRK expression is usually substantially less than the number of normal modes in the molecule. Typically  $s$  is about half the number of normal modes (157). Taking this into consideration the correlation between the calculated and experimentally observed values of  $n$  is reasonable.

R E F E R E N C E S

1. E. W. McDaniel, V. Cermak, A. Dalgarno, E. E. Ferguson and L. Friedman, Ion Molecule Reactions, John Wiley and Sons, New York (1970).
2. G. Giomousis and D. P. Stevenson, *J. Chem. Phys.*, 29, 294 (1958).
3. E. E. Ferguson, D. K. Bohme, F. C. Fehsenfeld and D. B. Dunkin, *J. Chem. Phys.*, 50, 5039 (1969).
4. J. L. Pack and A. V. Phelps, *J. Chem. Phys.*, 44, 1870 (1966).
5. N. G. Adams, D. K. Bohme, D. B. Dunkin, F. C. Fehsenfeld and E. E. Ferguson, *J. Chem. Phys.*, 52, 3133 (1970).
6. J. J. Thompson, *Phil. Mag.*, 24, 209 (1912).
7. A. J. Dempster, *Phil. Mag.*, 31, 438 (1916).
8. H. D. Smyth, *Phys. Rev.*, 25, 452 (1925).
9. T. P. Hogness and E. G. Lunn, *Phys. Rev.*, 26, 44 (1925).
10. V. L. Tal'rose and A. K. Lyubimova, *Doklady Akad. Nauk. SSSR*, 86, 909 (1952), per *Chem. Abstracts*, 47, 2590 (1953).
11. D. P. Stevenson and D. O. Schissler, *J. Chem. Phys.*, 23, 1353 (1955).
12. D. O. Schissler and D. P. Stevenson, *J. Chem. Phys.*, 24, 926 (1956).
13. von H. Gutbier, *Z. Naturforsch.*, A12, 499 (1957).

14. V. L. Tal'rose and E. L. Frankevich, Russian J. Phys. Chem., 34, 1275 (1960).
15. V. L. Tal'rose, Pure Appl. Chem., 5, 455 (1962).
16. T. W. Shannon, F. Meyer and A. G. Harrison, Can. J. Chem., 43, 159 (1965).
17. K. R. Ryan and J. H. Futrell, J. Chem. Phys., 42, 824 (1965) and 43, 3009 (1965).
18. V. L. Tal'rose and G. V. Karachevtsev, "Ion Molecule Reactions" in Advances in Mass Spectrometry, W. L. Mead, ed., Vol. 3, Institute of Petroleum, London (1966).
19. A. A. Herod and A. G. Harrison, Int. J. Mass Spectrom. Ion Phys., 4, 415 (1970).
20. N. A. McAskill and A. G. Harrison, Int. J. Mass Spectrom. Ion Phys., 5, 193 (1970).
21. A. G. Harrison, Int. J. Mass Spectrom. Ion Phys., 6, 297 (1971).
22. L. Anders, J. Beauchamp, R. Dunbar, and J. Baldeschwieler, J. Chem. Phys., 45, 1062 (1966).
23. J. L. Beauchamp, J. Chem. Phys., 46, 1231 (1967).
24. J. L. Beauchamp and J. T. Armstrong, Rev. Sci. Instr., 40, 123 (1969).
25. J. I. Brauman and L. K. Blair, J. Amer. Chem. Soc., 90, 5636, 9561 (1968) and 91, 2126 (1969).
26. J. M. S. Henis, J. Amer. Chem. Soc., 90, 844 (1968), and J. Chem. Phys., 52, 282 (1970).

27. J. H. Yang and D. C. Conway, *J. Chem. Phys.*, 40, 1729 (1964).
28. D. C. Conway and J. H. Yang, *J. Chem. Phys.*, 43, 2900 (1965).
29. G. S. Janik and D. C. Conway, *J. Phys. Chem.*, 71, 823 (1967).
30. D. C. Conway and L. E. Nesbitt, *J. Chem. Phys.*, 48, 509 (1968).
31. S. L. Chong and J. L. Franklin, *J. Chem. Phys.*, 54, 1487 (1971).
32. S. M. Schildcrout and J. L. Franklin, *J. Chem. Phys.*, 51, 4055 (1969).
33. S. M. Schildcrout, J. G. Collins and J. L. Franklin, *J. Chem. Phys.*, 52, 5767 (1970).
34. W. E. W. Ruska and J. L. Franklin, *Int. J. Mass Spectrom. Ion Phys.*, 3, 221 (1969).
35. M. S. B. Munson and F. H. Field, *J. Amer. Chem. Soc.*, 88, 2621 (1966).
36. F. H. Field, *Accounts Chem. Res.*, 1, 42 (1968).
37. F. H. Field, *J. Amer. Chem. Soc.*, 91, 2827 (1969).
38. F. H. Field, P. Hamlet and W. F. Libby, *J. Amer. Chem. Soc.*, 91, 2839 (1969).
39. F. H. Field, *J. Amer. Chem. Soc.*, 91, 6334 (1969).
40. D. P. Beggs and F. H. Field, *J. Amer. Chem. Soc.*, 93, 1567 (1971).
41. D. P. Beggs and F. H. Field, *J. Amer. Chem. Soc.*, 93,

- 1576 (1971).
42. F. H. Field and D. P. Beggs, *J. Amer. Chem. Soc.*, 93, 1585 (1971).
43. S. L. Bennett and F. H. Field, *J. Amer. Chem. Soc.*, 94, 5186 (1972).
44. S. L. Bennett and F. H. Field, *J. Amer. Chem. Soc.*, 94, 6305 (1972).
45. E. E. Ferguson, F. C. Fehsenfeld and A. L. Schmeltekopf *Advan. Atomic and Mol. Phys.*, 5, 1 (1969).
46. E. E. Ferguson, *Accounts Chem. Res.*, 3, 402 (1970).
47. E. E. Ferguson, D. B. Dunkin and F. C. Fehsenfeld, *J. Chem. Phys.*, 57, 1459 (1972).
48. J. A. Burt, J. L. Dunn, M. J. McEwan, M. M. Sutton, A. E. Roche and H. I. Schiff, *J. Chem. Phys.*, 52, 6062 (1970).
49. A. E. Roche, M. S. Sutton, D. K. Bohme and H. I. Schiff, *J. Chem. Phys.*, 55, 5480 (1971).
50. W. L. Fite, J. A. Rutherford, W. R. Snow and V. A. J. van Lint, *Disc. Faraday Soc.*, 33, 264 (1962).
51. J. Sayers and D. Smith, *Disc. Faraday Soc.*, 37, 167 (1964).
52. L. J. Puckett and W. C. Lineberger, *Phys. Rev. A*, 1, 1635 (1970).
53. R. M. Snuggs, D. J. Volz, I. R. Gatland, J. H. Schummers, D. W. Martin and E. W. McDaniel, *Phys. Rev. A*, 3, 487 (1971).

54. E. W. McDaniel, Drift Tube Studies of the Transport Properties and Reactions of Slow Ions in Gases, a chapter in Case Studies in Atomic Collision Physics I, edited by E. W. McDaniel and M. R. C. McDowell, North-Holland Publishing Co., Amsterdam (1969).
55. D. A. Durden, Ph.D. Thesis, University of Alberta (1968).
56. M. R. Arshadi, Ph.D. Thesis, University of Alberta (1969).
57. R. S. Narcisi and A. D. Bailey, *J. Geophys. Res.*, 70, 3687 (1965).
58. F. C. Fehsenfeld, A. L. Schmeltekopf and E. E. Ferguson, *J. Chem. Phys.*, 46, 2802 (1967).
59. F. C. Fehsenfeld and E. E. Ferguson, *J. Geophys. Res.*, 74, 2217 (1969).
60. D. K. Bohme, *Can. J. Chem.*, 47, 1899 (1969).
61. A. Good, D. A. Durden and P. Kebarle, *J. Chem. Phys.*, 52, 222 (1970).
62. F. C. Fehsenfeld, M. Mosesman and E. E. Ferguson, *J. Chem. Phys.*, 55, 2115 (1971).
63. C. E. Young and W. E. Falconer, *J. Chem. Phys.*, 57, 918 (1972).
64. W. C. Lineberger and L. J. Puckett, *Phys. Rev.* 187, 286 (1969).
65. C. J. Howard, H. W. Rundle and F. Kaufman, *Bull. Amer. Phys. Soc.*, 16, 213 (1971).



66. F. C. Fehsenfeld and E. E. Ferguson, Bull. Am. Phys. Soc., 16, 213 (1971).
67. M. A. French, L. P. Hills and P. Kebarle, Can. J. Chem., (in press 1973).
68. G. C. Reid, COSPAR Symposium on D and E Region in Chemistry, Urbana, Illinois (1971).
69. R. S. Narcisi, A. D. Bailey, L. Della Lucca, C. Sherman and D. M. Thomas, J. Atmospheric Terrest. Phys., 33, 1147 (1971).
70. R. Arnold, J. Kissel, D. Krankowsky, H. Wieder and J. Zahringer, J. Atmospheric Terrest. Phys., 33, 1169 (1971).
71. S. K. Searles and P. Kebarle, J. Phys. Chem., 72, 742 (1968).
72. A. M. Hogg and P. Kebarle, J. Chem. Phys., 43, 449 (1965).
73. A. M. Hogg, R. M. Haynes and P. Kebarle, J. Amer. Chem. Soc., 88, 28 (1966).
74. R. Yamdagni and P. Kebarle, J. Amer. Chem. Soc., 94, 2940 (1972).
75. M. Arshadi, R. Yamdagni and P. Kebarle, J. Phys. Chem., 74, 1475 (1970).
76. I. Džidić and P. Kebarle, J. Phys. Chem., 74, 1466 (1970).
77. E. Wicke, M. Eigen and Th. Ackermann, Z. Physic. Chem. (NF) 1, 340 (1954).

78. E. Glueckauf, *Trans. Farad. Soc.*, 51, 1235 (1966).
79. D. G. Tuck and R. M. Diamond, *J. Phys. Chem.*, 65, 193 (1961).
80. K. N. Bascombe and R. P. Bell, *Disc. Farad. Soc.*, 24, 158 (1957).
81. R. Grahn, *Arkiv fur Fysik*, 21, 13 (1962).
82. P. Kebarle, S. K. Searles, A. Zolla, J. Scarborough and M. Arshadi, *J. Amer. Chem. Soc.*, 89, 6393 (1967).
83. D. A. Durden, P. Kebarle and A. Good, *J. Chem. Phys.*, 50, 805 (1969).
84. S. Dushman, Scientific Foundation of Vacuum Technique John Wiley & Sons, New York (1949) p.84.
85. W. G. Walker, B. D. Klettke and P. W. Graves, *Rev. Sci. Instr.*, 41, 724 (1970).
86. C. N. Burrows, A. J. Lieber and V. T. Zaviantseff, *Rev. Sci. Instr.*, 38, 1477 (1967).
87. W. E. Potter and K. Mauersberger, *Rev. Sci. Instr.*, 43, 1327 (1972).
88. J. M. Goodings, J. M. Jones and D. A. Parker, *Int. J. Mass Spectrom. Ion Phys.*, 9, 417 (1972).
89. E. W. McDaniel, Collision Phenomena in Ionized Gases, John Wiley & Sons, New York (1964).
90. J. G. Collins, Ph.D. Thesis, University of Alberta (1966).
91. A. von Engel, Ionization in Gases by Electrons in Electric Fields, a chapter in *Handbuch der Physik XXI*, Springer-Verlag (Berlin) (1956).

92. S. C. Lind, Radiation Chemistry of Gases, Reinhold, New York (1961) p.25.
93. P. Kriemler and S. E. Buttrill Jr., J. Amer. Chem. Soc., 92, 1123 (1970).
94. L. J. Puckett, M. D. Kregel and W. C. Lineberger, Phys. Rev., A, 21, 1659 (1971).
95. T. D. Mark, Int. J. Mass Spectrom. Ion Phys., 9, 387 (1972).
96. P. F. Knewstubb, Advances in Mass Spectrometry, Vol. 4, Institute of Petroleum, Elsevier, New York (1968).
97. R. N. Varney, J. Chem. Phys., 31, 1314 (1959).
98. R. N. Varney, Phys. Rev., 174, 165 (1968).
99. D. C. Conway, J. Chem. Phys., 50, 3864 (1969).
100. F. C. Fehsenfeld, E. E. Ferguson and D. K. Bohme, Planetary Space Sci., 17, 1759 (1969).
101. M. R. Arshadi and P. Kebarle, J. Phys. Chem., 74, 1483 (1970).
102. J. L. Moruzzi and A. V. Phelps, J. Chem. Phys., 45, 4617 (1966).
103. N. M. Rodiguin and E. N. Rodiguina, Consecutive Chemical Reactions - Mathematical Analysis and Development, D. Van Nostrand, Princeton, N. J. (1964).
104. D. C. Conway, J. Chem. Phys., 52, 1622 (1970).
105. D. K. Bohme, D. B. Dunkin, F. C. Fehsenfeld and E. E. Ferguson, J. Chem. Phys., 51, 863 (1969).
106. A. Good, Trans. Far. Soc., 67, 3495 (1971).
107. W. C. Gardiner, Jr., Rates and Mechanisms of Chemical Reactions, W. A. Benjamin, New York (1969).

108. J. L. Pack and A. V. Phelps, *Bull. Am. Phys. Soc.*, 16, 214 (1971).
109. A. V. Phelps, Aeronomy Report #48, COSPAR Symposium on D and E Region Ion Chemistry, Urbana, Illinois, July 1971. A. V. Phelps, private communication.
110. L. G. McKnight and J. M. Sawina, *Bull. Am. Phys. Soc.*, 15, 434 (1970).
111. D. S. Birch and R. Geballe, *Phys. Rev.*, 106, 188 (1957).
112. E. C. Beaty, L. M. Branscomb and P. L. Patterson, *Bull. Am. Phys. Soc.*, 9, 535 (1964).
113. L. G. McKnight, *Phys. Rev. A*, 2, 762 (1970).
114. V. I. Vedeneyev, L. V. Gurvich, V. N. Kontrat'yev, V. A. Medvedev and Ye. L. Frankevich, Bond Energies Ionization Potentials and Electron Affinities, Edward Arnold Ltd., London (1962).
115. J. E. Desnoyers and C. Jolicoeur, Hydration Effects and Thermodynamic Properties of Ions, a chapter in Modern Aspects of Electrochemistry, Vol. 5, Ed. J.O'M. Bockris and B. E. Conway, Plenum Press, New York (1969).
116. R. Yamdagni, private communication.
117. National Bureau of Standards Technical Note 270-3 U. S. Department of Commerce, Washington, D. C.
118. L. M. Branscomb, *Phys. Rev.*, 148, 11 (1966).
119. J. Berkowitz, W. A. Chupka and T. A. Walter, *J. Chem. Phys.*, 50, 1497 (1969).
120. D. B. Dunkin, F. C. Fehsenfeld and E. E. Ferguson, *Chem. Phys. Letters*, 15, 257 (1972).

121. C. Lifshitz, B. M. Hughes and T. O. Tiernan, Chem. Phys. Letters, 7, 469 (1970).
122. A. P. M. Baede, Physica, 59, 541 (1972).
123. J. Berkowitz, W. A. Chupka and D. Gutman, J. Chem. Phys., 55, 2724 (1971).
124. R. K. Curran, Phys. Rev., 125, 910 (1962).
125. S. J. Nalley, J. A. D. Stockdale and R. N. Compton, Bull. Am. Phys. Soc., 15, 418 (1970).
126. F. C. Fehsenfeld and E. E. Ferguson, Plant. Space Sci., 16, 701 (1968).
127. P. Warneck, Chem. Phys. Letters, 3, 532 (1969).
128. D. Vogt, Int. J. Mass Spectrom. Ion Phys., 3, 81 (1969).
129. M. McFarland, D. B. Dunkin, F. C. Fehsenfeld, A. L. Schmeltekopf and E. E. Ferguson, J. Chem. Phys., 56, 2358 (1972).
130. K. B. Yatsimirskii, Izvest. Akad. Nauk SSSR, Otdel. Khim. Nauk 411, 453 (1947); J. Gen. Chem. USSR 17, 2019 (1947).
131. J. I. Brauman and L. K. Blair, J. Amer. Chem. Soc., 92, 5586 (1970).
132. G. Choux and R. L. Benoit, J. Amer. Chem. Soc., 91, 6221 (1969).
133. R. Alexander, E. C. F. Ko, Y. C. Mac and A. J. Parker, J. Amer. Chem. Soc., 89, 3703 (1967).
134. R. Yamdagni and P. Kebarle, J. Amer. Chem. Soc., 93, 7139 (1971).

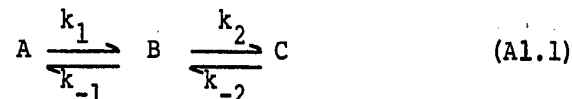
135. S. K. Searles, Ph.D. Thesis, University of Alberta (1968).
136. A. G. Harrison and J. C. J. Thynne, *Trans. Faraday Soc.*, 62, 2804 (1966).
137. M. A. Haney and J. L. Franklin, *J. Phys. Chem.*, 73, 4328 (1969).
138. W. P. Kraemer and G. H. F. Diercksen, *Chem. Phys. Lett.*, 5, 463 (1970).
139. P. A. Kollman and L. C. Allen, *J. Amer. Chem. Soc.*, 92, 6101 (1970).
140. M. D. Newton and S. Ehrenson, *J. Amer. Chem. Soc.*, 93, 4971 (1971).
141. P. Kebarle and E. W. Godbole, *J. Chem. Phys.*, 39, 1131 (1963).
142. L. J. Puckett and M. W. Teague, *J. Chem. Phys.*, 54, 2564 (1971).
143. C. E. Young, D. Edelson and W. E. Falconer, *J. Chem. Phys.*, 53, 4295 (1970).
144. M. DePaz, J. J. Leventhal and L. Friedman, *J. Chem. Phys.*, 51, 3748 (1969).
145. J. M. Williams and S. W. Peterson, *J. Amer. Chem. Soc.*, 91, 776 (1969).
146. R. Hackam, *Brit. J. Appl. Phys.*, 17, 197 (1966).
147. F. E. Niles and W. W. Robertson, *J. Chem. Phys.*, 42, 3277 (1965).

148. Chemical & Engineering News special report Chemistry and the Atmosphere (1966).
149. G. C. Reid, J. Geophys. Res., 75, 2551 (1970).
150. L. Thomas, J. Atmosph. Terr. Phys., 33, 157 (1971).
151. A. S. Dickinson, R. E. Roberts and R. B. Bernstein, J. Phys. B., 5, 355 (1972).
152. B. M. Smirnov, Sov. Phys. JETP, 24, 1180 (1967).
153. B. H. Mahan, J. Chem. Phys., 43, 3080 (1965).
154. F. E. Niles and W. W. Robertson, J. Chem. Phys., 43, 1076 (1965).
155. R. A. Gerber, G. F. Sauter and H. J. Oskam, Physica, 32, 2173 (1966).
156. D. C. Conway and G. S. Janik, J. Chem. Phys., 53, 1859 (1971).
157. K. J. Laidler, Chemical Kinetics, McGraw-Hill (1965) p.153.
158. F. Daniels and R. A. Alberty, Physical Chemistry, John Wiley & Sons, New York (1967).
159. T. M. Lowry and W. J. John, J. Chem. Soc., 97, 2634 (1910).

A P P E N D I X I

Analogue Computer Programmes

For the first order reversible reaction system



we may write the following differential equations

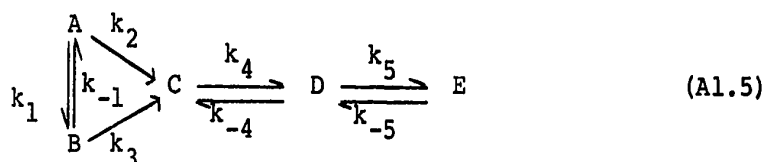
$$\frac{dA}{dt} = -k_1A + k_{-1}B \quad (\text{A1.2})$$

$$\frac{dB}{dt} = -(k_{-1} + k_2)B + k_1A + k_{-2}C \quad (\text{A1.3})$$

$$\frac{dC}{dt} = -k_{-2}C + k_2B \quad (\text{A1.4})$$

where A, B and C are the concentrations of the respective species. The analogue computer programme for solving the above set of differential equations with boundary conditions at  $t = 0$ ,  $A = 1$ ,  $B = C = 0$  is displayed in Figure (A1.1). This programme was used to generate the solutions to the kinetic systems in Chapters 5, 9 and 10.

For the somewhat more complex reaction system



the corresponding differential equations are



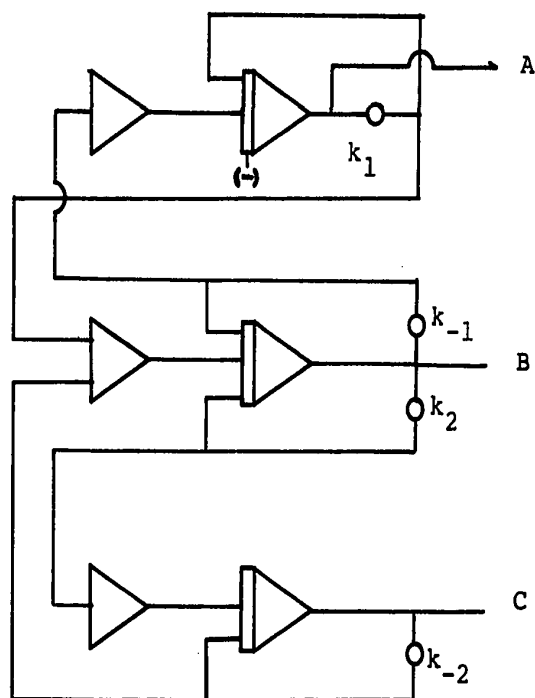


FIGURE (A1.1) Analogue computer programme for the kinetic system  $A \xrightleftharpoons[k_{-1}]{k_1} B \xrightleftharpoons[k_{-2}]{k_2} C$  with boundary conditions at  $t = 0$ .  
 $A = 1, B = C = 0$ .

$$\frac{dA}{dt} = -(k_1 + k_2)A + k_{-1}B \quad (\text{A1.6})$$

$$\frac{dB}{dt} = -(k_{-1} + k_3)B + k_1A \quad (\text{A1.7})$$

$$\frac{dC}{dt} = -k_4C + k_{-4}D + k_2A + k_3B \quad (\text{A1.8})$$

$$\frac{dD}{dt} = -(k_{-4} + k_5)D + k_4C + k_{-5}E \quad (\text{A1.9})$$

$$\frac{dE}{dt} = -k_{-5}E + k_5D \quad (\text{A1.10})$$

The analogue computer programme used to solve the above equations with boundary conditions at  $t = 0$ ,  $A = 1$ ,  $B = C = D = E = 0$  is displayed in Figure (A1.2). This programme was used in Chapter 4 in the study of the kinetics of hydration of  $O_2^-$ .

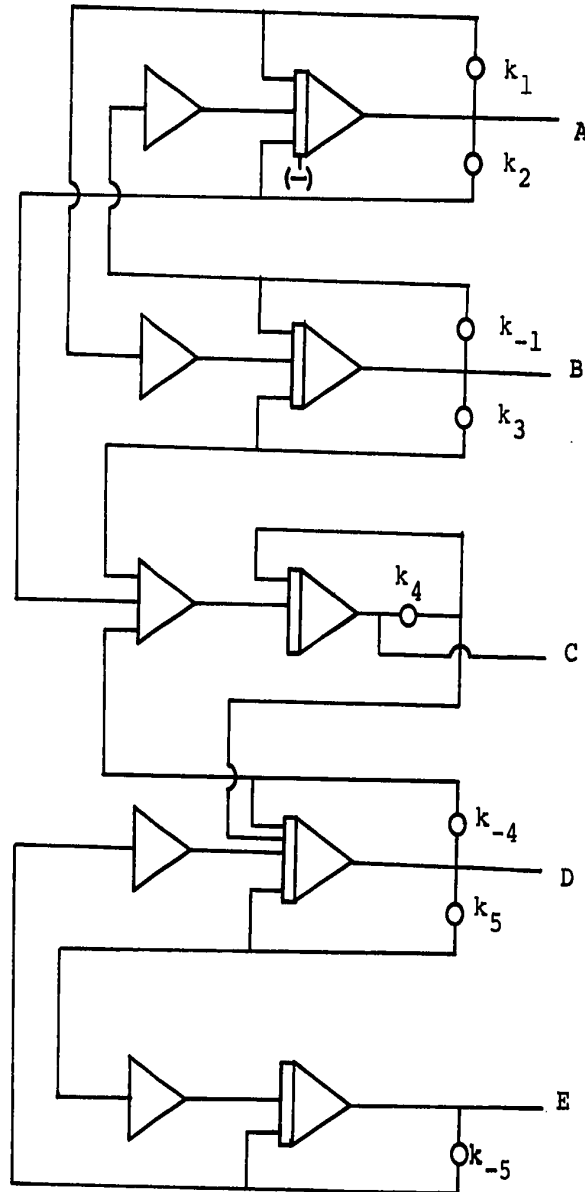
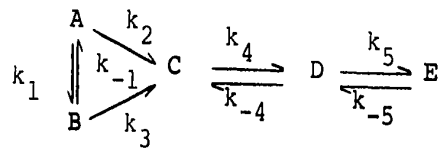


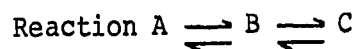
FIGURE (A1.2) Analogue computer programme for the kinetic system



with boundary conditions at  $t = 0$ ,  $A = 1$ ,  
 $B = C = D = E = 0$

A P P E N D I X    I I

A Mathematical Analysis of the Reversible First Order



For the simple first order reversible reaction



we may write the differential equation

$$\frac{dA}{dt} = -k_1A + k_2B \quad (A2.2)$$

which possesses the well known solution (158)

$$\ln(A - A_{eq}) = -(k_1 + k_2)t + \text{constant} \quad (A2.3)$$

where A is the concentration of A at time t and  $A_{eq}$  is the concentration of A at equilibrium. Thus a plot of  $\ln(A - A_{eq})$  versus time yields a straight line of slope  $-(k_1 + k_2)$ .

For the system



an expression similar to (A2.3) may be derived as is shown below. The differential describing (A2.4) are

314.

$$\frac{dA}{dt} = -k_1 A + k_2 B \quad (\text{A2.5})$$

$$\frac{dB}{dt} = -(k_2 + k_3) B + k_1 A + k_4 C \quad (\text{A2.6})$$

$$\frac{dC}{dt} = -k_4 C + k_3 B \quad (\text{A2.7})$$

Lowry and John (159) have shown that the solution to the above equations for A is

$$A = A_{\text{eq}} \left\{ -\frac{m_2}{m_2 - m_1} e^{-m_1 t} + \frac{m_1}{m_2 - m_1} e^{-m_2 t} + 1 \right\} + \frac{m_2 - k_1}{m_2 - m_1} e^{-m_1 t} + \frac{k_1 - m_1}{m_2 - m_1} e^{-m_2 t} \quad (\text{A2.8})$$

$$\text{where } A_{\text{eq}} = \frac{k_2 k_3}{k_2 k_3 + k_1 k_3 + k_1 k_4} \quad (\text{A2.9})$$

$$m_1 = \frac{1}{2} \left\{ (k_1 + k_2 + k_3 + k_4) - [(k_1 + k_2 + k_3 + k_4)^2 - 4(k_2 k_3 + k_1 k_3 + k_1 k_4)]^{\frac{1}{2}} \right\} \quad (\text{A2.10})$$

$$\text{and } m_2 = \frac{1}{2} \left\{ (k_1 + k_2 + k_3 + k_4) + [(k_1 + k_2 + k_3 + k_4)^2 - 4(k_2 k_3 + k_1 k_3 + k_1 k_4)]^{\frac{1}{2}} \right\} \quad (\text{A2.11})$$

On rearrangement equation (A2.8) yields

$$\begin{aligned}
 A - A_{eq} &= e^{-m_1 t} \left\{ \frac{m_2 - k_1 - m_2 A_{eq}}{m_2 - m_1} \right\} \\
 &+ e^{-m_2 t} \left\{ \frac{k_1 - m_1 + m_1 A_{eq}}{m_2 - m_1} \right\} \quad (A2.12)
 \end{aligned}$$

At equilibrium

$$\frac{dA}{dt} = 0 \quad (A2.13)$$

$$\begin{aligned}
 \therefore \frac{dA}{dt} &= -m_1 e^{-m_1 t} \left\{ \frac{m_2 - k_1 - m_2 A_{eq}}{m_2 - m_1} \right\} \\
 &- m_2 e^{-m_2 t} \left\{ \frac{k_1 - m_1 + m_1 A_{eq}}{m_2 - m_1} \right\} = 0 \quad (A2.14)
 \end{aligned}$$

or on rearrangement

$$e^{-m_1 t} \left\{ \frac{m_1 - k_1 - m_2 A_{eq}}{m_2 - m_1} \right\} = \frac{m_2}{m_1} e^{-m_2 t} \left\{ \frac{k_1 - m_1 + m_1 A_{eq}}{m_2 - m_1} \right\} \quad (A2.15)$$

Introducing (A2.15) into (A2.12) and rearranging we have

$$A - A_{eq} = e^{-m_2 t} \cdot \left[ \frac{k_1 - m_1 + m_1 A_{eq}}{m_2 - m_1} \right] \cdot \left[ \frac{m_2}{m_1} + 1 \right] \quad (A2.16)$$

or

$$\ln(A - A_{eq}) = -m_2 t + \text{constant} \quad (A2.17)$$

Upon expanding the term under the square root sign in (A2.11) and noting that the resultant is a perfect square it may be shown that

$$m_2 = k_1 + k_2 \quad (\text{A2.18})$$

Introducing (A2.18) into (A2.17) we find

$$\ln(A - A_{\text{eq}}) = -(k_1 + k_2)t + \text{constant} \quad (\text{A2.19})$$

Thus the relationship (A2.3) which held for the simple case (A2.1) also holds for the more complex case (A2.4).